PERI-TRANSPLANT CARDIOVASCULAR DYNAMICS IN AN OVINE MODEL OF HEART TRANSPLANTATION FOLLOWING 24-HRS DONOR BRAIN STEM DEATH

Mr Matthew A Wells

BExSc (Hons)

School of Medical Sciences

Griffith University

Submitted in fulfilment of the requirements of the degree of Doctor of Philosophy

25/09/2020

Abstract

Background

Heart transplantation (HTx) for end-stage heart failure is one of the most challenging complex health problems faced in intensive care units across the globe. This is partly due to the shortage of viable donor hearts and primary graft failure post-transplant. The mechanisms behind these shortfalls are diverse and arise from donor brain stem death (BSD), a significant stressor on the heart and the main pool from which donor hearts are sourced. A compromised myocardium is then preserved in cold preservation solution on ice (CSS), as per the current clinical standard, initiating significant ischaemia. The final stage of HTx is implantation in the recipient, which induces both warm ischaemia during the procedure and reperfusion injury. These multifarious injuries contribute to both non-viable donor hearts, reducing the number of available hearts, and graft dysfunction post-HTx. This doctoral project aims to utilise a clinically relevant model of transplantation to investigate 3 main aspects of cardiovascular function, 1) cardiac adrenergic excitation-contraction-coupling and perfusion, 2) mitochondrial function and 3) metabolic regulation.

Methods

Sheep were semi-randomised, influenced by blood group matching, into 2 main groups. Group A consisted of heart donors with confirmed BSD or sham operated controls (SHAM). Group B consisted of a separate group of heart donors both BSD (BSD-Tx) and SHAM (SH-Tx), which progressed through to CSS and consecutive HTx in a healthy recipient animal. The healthy recipient (HR) heart was excised and used as a healthy control following the establishment of cardio-pulmonary bypass (CPB). Heart collection occurred at end-points, defined as 24 hrs after BSD confirmation for Group A and 6 hrs after weaning the healthy recipient off CPB for Group B. Heart tissue was collected in ice cold oxygenated Krebs solution for in-vitro analyses, mitochondrial respiration and metabolic assessment.

In-vitro analyses: Briefly, left and right ventricular trabeculae were dissected and mounted on Blinks tissue blocks. Trabeculae were stimulated at 1 Hz intervals and the force of contraction was recorded over a concentration-effect curve to -(-)Noradrenaline. Potency at the β_1-adrenoceptor was determined and expressed as the concentration required to elicit a 50% maximum response in log units (pEC50).

Mitochondrial respiration: Tissue homogenate was injected into an Oroboros Oxygraph and respiration was measured using both carbohydrate and fatty acid substrates. Mitochondrial membrane potential (MMP) was measured fluorometrically. Respiration was measured during 3 respiratory states; LEAK state, non-phosphorylative oxygen utilisation, ATP producing Complex I oxidative phosphorylative state (OXPHOS) and Complex II OXPHOS. Tissue levels of 3-nitrotyrosine and the glutathione to reduced glutathione ratio (GSH:GSSG) were assessed using plate based assays.

Metabolomics: Biopsies were collected in a similar manner from similar regions as those used for mitochondrial respiration. Biopsies were pooled per ventricle prior to the detection of polar metabolites via LC/MS. Metabolites were extracted via MassHunter and statistical analyses were performed using MetaboAnalyst 4.0.

Results

Twenty-four sheep weighing on average 47 ± 6 kg were semi-randomised into the donor and transplant groups. There were 6 animals in each donor group, SHAM and BSD and 12 separate donors continued through to transplantation, 6 in each group, SH-Tx and BSD-Tx.

In-vitro analyses: Donor BSD caused a significant reduction in RV contractility, however β_1 sensitivity was unchanged. Post-transplanted hearts, regardless of donor BSD injury were characterised by bi-ventricular reductions in both contractility and pEC50 (SH-Tx: 0.59 p=0.04, and BSD-Tx: 0.62 p=0.02, mean difference).

Mitochondrial respiration: Following donor BSD, LEAK respiration in the RV was significantly elevated compared to HR (BSD: 0.11 ± 0.03 FCR, $p<0.01$). LV levels of 3-NT also trended upward, with a significant reduction in the GSH:GSSG ratio. CII OXPHOS in BSD using fatty acid substrates was significantly lower than HR hearts.

Post-transplantation however, there were bi-ventricular elevations in LEAK respiration and reductions in CII OXPHOS for both SH-Tx and BSD-Tx groups. These data were also in the presence of reduced MMP in LEAK and CII OXPHOS states. Transplantation was also characterised by significant increases in RV 3-NT levels and reduced LV GSH:GSSG ratios.

Metabolomics: Metabolically, BSD increased accumulation of myocardial amino-acids and glycolytic metabolites involved in oxidative and osmotic stress. Post-HTx, particularly in those exposed to donor BSD, there was a significant decrease in metabolites involved in mitochondrial respiration (eg. NAD, Acetyl-CoA) and accumulation of fatty acids and xanthine.

Conclusion

Using a clinically relevant model of HTx following donor BSD, this study focussed on cardiac contractility, mitochondrial function and metabolism in an effort to explain peri-transplant cardiac compromise. Based on these results it appears that donor oxidative stress, mitochondrial function and glycolytic metabolite build up are important determinants in cardiovascular dysfunction. Post-transplantation however, the mitochondrial, oxidative, metabolic and adrenergic systems are significantly impaired. Further research should investigate how best to support the donor heart outside of adrenergic agents, reduce oxidative stress and support metabolism. Whereas strategies to improve heart preservation and targetable mitochondrial/metabolic therapeutics may reduce reperfusion injury. Collectively, these approaches have the potential to increase the quality and quantity of HTx.

Statement of Originality

This work has not previously been submitted for a degree or diploma in any university. To the best of my knowledge and belief, the thesis contains no material previously published or written by another person except where due reference is made in the thesis itself.

(Signed)_____
Matthew A Wells

ALL PAPERS INCLUDED ARE CO-AUTHORED

Acknowledgement of Papers included in this Thesis

Section 9.1 of the Griffith University Code for the Responsible Conduct of Research ("Criteria for Authorship"), in accordance with Section 5 of the Australian Code for the Responsible Conduct of Research, states:

> To be named as an author, a researcher must have made a substantial scholarly contribution to the creative or scholarly work that constitutes the research output, and be able to take public responsibility for at least that part of the work they contributed. Attribution of authorship depends to some extent on the discipline and publisher policies, but in all cases, authorship must be based on substantial contributions in a combination of one or more of:
>
> - conception and design of the research project
> - analysis and interpretation of research data
> - drafting or making significant parts of the creative or scholarly work or critically revising it so as to contribute significantly to the final output.

Section 9.3 of the Griffith University Code ("Responsibilities of Researchers"), in accordance with Section 5 of the Australian Code, states:

> Researchers are expected to:
>
> - Offer authorship to all people, including research trainees, who meet the criteria for authorship listed above, but only those people.
> - accept or decline offers of authorship promptly in writing.
> - Include in the list of authors only those who have accepted authorship
> - Appoint one author to be the executive author to record authorship and manage correspondence about the work with the publisher and other interested parties.
> - Acknowledge all those who have contributed to the research, facilities or materials but who do not qualify as authors, such as research assistants, technical staff, and advisors on cultural or community knowledge. Obtain written consent to name individuals.

Included in this thesis are papers in Chapters 1 and 2 which are co-authored with other researchers. My contribution to each co-authored paper is outlined at the front of the relevant chapter. The bibliographic details papers including <u>all</u> authors, are:

(Where a paper(s) has been published or accepted for publication, you must also include a statement regarding the copyright status of the paper(s).

Chapter 1:

Wells, M. A., See Hoe, L. E., Heather, L. C., Molenaar, P., Suen, J. Y., Peart, J., McGiffin, D., & Fraser, J. F. (2020) Peritransplant Cardio-Metabolic and Mitochondrial Function The Missing Piece in Donor Heart Dysfunction and Graft Failure, *Transplantation*: June 22, 2020 - Volume Online First - Issue - doi: 10.1097/TP.0000000000003368

Copyright information:

Publication: Transplantation
Publisher: Wolters Kluwer Health, Inc.
Date: Jun 22, 2020

Chapter 2:

See Hoe, L. E., **Wells, M. A**., Bartnikowski, N., Obonyo, N. G., Millar, J. E., Khoo, A., Ki, K. K., Shuker, T., Ferraioli, A., Colombo, S. M., Chan, W., McGiffin, D. C., Suen, J. Y. and Fraser, J. F. (2020). *Heart transplantation from brain dead donors: a systematic review of animal models*. Transplantation, Publish Ahead of Print doi: 10.1097/tp.0000000000003217

Copyright information:

Publication: Transplantation
Publisher: Wolters Kluwer Health, Inc.
Date: Mar 5, 2020

Appropriate acknowledgements of those who contributed to the research but did not qualify as authors are included in each paper.

(Signed) _____ (Date) 13/09/2020

Name of Student: Matthew A Wells

(Countersigned) _____ (Date) 15/09/2020

Supervisor: Name of Supervisor

Acknowledgements

Firstly, I would like to thank Professor John Fraser for allowing me to work on this project. One of my aims starting this PhD was to grow as a scientist and I believe under his guidance and the fantastic network of scientists he has at the Critical Care Research Group (CCRG) I have done just that. My time working on this project under Prof. Fraser's tutelage has provided me with the personal and professional growth that will help provide an exciting academic career. I cannot imagine having the same experiences anywhere else, and I feel extremely privileged to be a part of the group. Where else can you interact with a leading cardiac surgeon regularly? To Professor David McGiffin, who flew from Melbourne to Brisbane and back fortnightly to complete a sheep heart transplant. Your constant sacrifice of time, that I'm sure you don't have, was extraordinary. I cannot express enough my enormous gratitude for this sacrifice.

To my second mum, Dr Louise See Hoe, I don't think I would have made it without you. You have provided one of the best experiences I could have hoped for. I count myself incredibly lucky to have worked with such a fantastic, accomplished scientist. Not only do you hold yourself to the highest of scientific standards, but you have shown me that you can achieve these standards in a supportive and fun environment. You are inspiring, I owe my future scientific success to you.

Thank you to Associate Professor Peter Molenaar. I would be lying if I did not say that at first, your lab was frightening. How could I manage to keep up with a man of your intelligence and scientific rigor? Thankfully, you are also extremely kind and an excellent teacher. You have taught me a great deal both scientifically and personally. An experience I will never forget. To Associate Professor Jason Peart, thank you for listening to my nagging. You have helped me enormously professionally and are always there when I'm panicking. One of the most exciting ventures was my conference in Beijing. You helped make this a reality and have opened doors to postdoctoral opportunities I could not dream of. Thank you! Thank you to Dr Jacky Suen, who helped me grow professionally, and taught me how to navigate the world of research.

This project was one of the most logistically complex and demanding experiments I have been a part of. We would begin the experiment on a Tuesday morning in the surgical unit at the MERF facility

(Queensland University of Technology), and I would not be complete in the laboratory at CCRG until Thursday morning. None of this would be possible without the dedicated staff at the CCRG. To the clinical staff who helped with the surgical procedures Charles McDonald, Lynnette James (it was magical watching you work), Lachlan Marshall, Arlanna Ross, Sacha Rozenwajg, Karin Wildi, Johnathan Miller, Sanne Pedersen, Obonyo Nchafatso, and many more, thank you. To the scientific staff who assisted with blood processing and data collection Mahe Bouquet, Kieran Hyslop, Margaret Passmore, Tristan Shuker, Alessandro Ferraioli, Olivia Zecovic, Gabriel Abbate, John Paul Tung, and many more, I am incredibly grateful.

I would like to thank Dr Barbara Kemp-Harper from Monash University for putting me up in her home while teaching me vascular reactivity assays. As a poor student, thank you. To Dr Nicole Bartnikowski, I would like to thank you for your constant support in the monumental effort that is managing the data collected from the surgical procedures. Thank you to Dr Meredith Redd and the Palpant lab from the Institute for Molecular Bioscience, University of Queensland, for providing cardiomyocytes for additional cell work. Thank you to Dr Haris Haqqani for taking the time out of your busy clinical schedule to perform electrophysiological mapping. Although this work didn't make it into my thesis, it is on-going and I'm excited to continue the work with you into the future.

This work would also not be a reality without the support of The Prince Charles Hospital Foundation. I was lucky enough to receive a New Investigator Grant to fund portions of this research. I am incredibly grateful for the support and for the experience of writing competitive grants. A skill I will carry further into my career.

Finally, I would like to thank my friends and family for your constant support and encouragement. Especially during the times when I was missing and presumed dead, but rather stuck in the lab.

This thesis is dedicated to my parents; I owe you everything and can never fully express my love and gratitude.

Table of Contents

CHAPTER 4 | PERI-TRANSPLANT CARDIAC MITOCHONDRIAL RESPIRATION

CHAPTER 5 | METABOLOMIC PROFILE OF THE DONOR AND TRANSPLANTED HEART

CHAPTER 6 | GENERAL DISCUSSION AND CONCLUSIONS

List of Figures

List of Tables

Abbreviations

2-methylcitric acid	2-MCA
3-nitrotyrosine modified proteins	3-NT
Amino acids	AA
Adenylyl cyclase	AC
Acetoacetate	AcA
Acetylcholine	Ach
Activated clotting time	ACT
Atrial fibrillation	AF
Adrenal insufficiency	AI
Protein kinase B	AKT
Adenosine monophosphate	AMP
AMP-activated protein kinase	AMPK
Analysis of Variance	ANOVA
One-way analysis of variance	ANOVA
Adenine nucleotide translocase	ANT
Australian and New Zealand Organ Donation Registry	ANZOD
Aldose reductase	ARase
Adrenergic receptors	Ars
Adenosine triphsophate	ATP
3(β)-aminoisobutanoic acid	BAIBA
Branched chain amino acids	BCAA
Branched chain α-keto acid dehydrogenases	BCKD
Bradykinin	BK
Baseline	BL
Brain stem death	BSD
Brain stem dead hearts/animals following transplantation	BSD-Tx
Cytosolic Ca^{2+}	$c[Ca^{2+}]$
Calcium	Ca^{2+}
Cyclic adenosine monophosphate	cAMP
Cardiac allograft vasculopathy	CAV
Coronary blood flow	CBF
Carbonyl cyanide m-chlorophenyl hydrazone	CCCP
Coronary flow reserve	CFR
Constricting factors	CFs
Cyclic guanosine monophosphate	cGMP
Carbohydrates	CHO
NADH dehydrogenase/Complex I	CI
Succinate dehydrogenase/Complex II	CII
Oxidoreductase/Complex III	CIII
Cytochrome oxidase/Complex IV	CIV
Carbon dioxide	CO_2
Coenzyme A	CoA
Cyclooxygenase	COX
Cardiopulmonary bypass	CPB

Cerebral perfusion pressure	CPP
Carnitine palmitoyltransferase 1	CPT1
Cross-sectional area	CSA
Cyclosporine A	CsA
Cold static organ storage	CSS
Cardiac troponin I	cTnI
Coefficient of variation	CV
Central venous line	CVL
Central venous pressure	CVP
Cytochrome c	Cyt c
Danger associated molecular patterns	DAMPs
Diastolic blood pressure	DBP
Dichloroacetate	DCA
Donation after circulatory death	DCD
DEA-NONOate	DEA
Electrocardiogram	ECG
Endothelial derived hyperpolarising factor	EDHF
End-diastolic pressure	EDP
Endothelium-derived relaxing factors	EDRFs
Enzyme linked immunosorbent assay	ELISA
Endothelial nitric oxide synthase	eNOS
Extracellular signal-regulated kinases	ERK
Endothelin-1	ET-1
Endothelin recptor A / B	ET_A / ET_B
End-tidal carbon dioxide	$ETCO_2$
Maximum electron transport system oxygen utilisation	ETmax
Electron transport system	ETS
Electron transport system	ETS
Fatty acid	FA
Flavin adenine dinucleotide	FADH2
FA oxidation	FAO
FA translocase	FAT/CD36
Flux control ratios	FCR
Inspiratory fraction of oxygen	FiO_2
Flavin adenine dinucleotide- linked respiration	F-linked
Flavin mononucleotide	FMN
Glucose-6-phosphate	G6P
Glycolic acid	GA
N-acetyl-glucosamine	GLcNAc
Glucose transporter 4	GLUT4
Glycerophosphocholine	GPC
G-protein coupled receptor	GPCR
G-protein coupled receptor kinase / 2	GRK / GRK2
Oxidised and reduced glutathione ratio	GSH:GSSG
G-stimulatory protein	Gαs
Hexoasamine biosynthetic pathway	HBP

High energy phosphate	HEP
Heart Failure	HF
Human-induced pluripotent stem cell-derived cardiomyocytes	hIPSC-CM
Hypothalamic-pituitary-adrenal	HPA
Healthy recipient hearts/animals	HR
High resolution respirometry	HRR
Hormone replacement therapy	HRT
Heat shock protein 90	Hsp90
Heart transplantation	HTx
Intracellular Ca^{2+}	$i[Ca^{2+}]$
3-isobutyl-1-methylxanthine	IBMX
Intracranial Pressure	ICP
Ischaemia reperfusion injury	IRI
International Society for Heart and Lung Transplant	ISHLT
Isoprenaline / isoproterenol	ISO
K+ depolarising solution	KPSS
Potassium depolarising solution	KPSS
Voltage gated potassium channel	KvC
Phosphorylative coupling ratio	L/P
Left anterior descending	LAD
Long chain fatty acids	LCFA
Liquid chromatography coupled with mass spectrometry	LC-MS
Left circumflex artery	LCX
Lactate dehydrogenase	LDH
Mitochondrial oxygen consumption with CI substartes and no ADP	LEAK
Left Ventricle	LV
LV maximum force development	LV dP/dT_{max}
LV minimum force development	LV dP/dT_{min}
Left ventricular ejection fraction	LVEF
Left ventricular systolic pressure	LVSP
Mitochondrial Ca^{2+}	$m[Ca^{2+}]$
Monoamine oxidases	MAO
Mean arterial pressure	MAP
Mitogen activated protein kinase	MAPK
Medium chain FAs	MCFA
Methionine sulfoxide	MeS
Metanephrine	MET
Mitochondrial permeability transition pore	mPTP
Omega 3 fatty acids	n-3 Fas
Sodium calcium channel	Na^+/Ca^{2+}
Sodium hydrogen exchanger	Na^+/H^+
Sodium potassium ATPase pump	Na^+/K^+ ATPase
Nicotinamide adenine dinucleotide	NADH
Nicotinamide adenine dinucleotide linked respiration	N-linked

Normetanephrine	NMET
Nitric oxide	NO
NADH oxidases 1/4	NOX 1/4
Oxalic acid	OA
Organ care systems	OCS
O-linked-β-linked-N-acetylglucosamine	O-GlcNAc
Oxidative phosphorylation	OXPHOS
Oxygen cost of ATP production per molecule	P/O
Arterial partial pressure of carbon dioxide	$PaCO_2$
Pooled quality control sample	pbQC
Phenoxybenzamine	PBZ
Principal component analysis	PCA
Phosphodiesterases	PDEs
Pyruvate dehydrogenase	PDH
Pyruvate dehydrogenase kinase	PDK
Effective concentration that elicits a 50% contractile response (beta-1-adrenoceptor sensitivity)	pEC_{50}
Positive end expiratory pressure	PEEP
Phosphofructokinase-2	PFK-2
PPAR gamma coactivator 1 alpha	PGC1α
Primary graft dysfunction	PGD
Phosphoinositide 3-kinase	PI3K
Protein kinase A	PKA
Polyol pathway	PoP
Peroxisome proliferator-activated receptor alpha	PPARα
Pentose phosphate pathway	PPP
Quadrupole time-of-flight mass spectrometer	QTOF MS
Reverse electron flow	RET
Ras homolog family member A guanosine triphosphatase	RhoA GTPase
Reactive oxygen species	ROS
Residual oxygen consumption	ROX
Respiratory rate	RR
Right ventricle	RV
Suppressors of site 1Q Electron Leak	S1QEL’s
Suppressors of site 3Q Electron Leak	S3QEL’s
Significance Analysis of Microarrays	SAM
Systolic blood pressure	SBP
Sarcoplasmic reticulum Ca^{2+}/ATPase	SERCA
Sham operated animals	SHAM
Sham operated animals/hearts following transplantation	SH-Tx
Succinate- linked respiration	S-linked
Sodium nitroprusside	SNP
Solid phase extraction	SPE
Oxygen saturation	SpO_2
ST elevated myocardial infarction	STEMI

Substrate-uncoupler-inhibitor titrations	SUIT
Systemic vascular resistance	SVR
Triiodothyronine	T3
Endothelin-1 receptor antagonist	TAK-044
Tricarboxylic acid	TCA
Tetramethylrhodamine methyl ester	TMRM
Uncoupling proteins	UCPs
Uridine 5’-diphosphate	UDP
Ultra-high performance liquid chromatography	UPLC
Very long chain fatty acids	VLCFA
Volcano plot	VP
Vasoplegic shock	VS
Vascular smooth muscle	VSM
D-xylulose-5, Phosphate	X5P
Alpha 1/2 adrenoceptor	α_1 - /α_2-AR
Beta 1/2/3 adrenoceptor	β_1- /β_2- /β_3-AR
β-adrenergic receptor kinase-1	βARK-1
β-adrenergic receptor kinase-1	βARK-1
β-arrestins	β-ARR
β-N-acetylglucosamine	βGLcNAc
β-hydroxybutyrate	βOHB
Proton motive force	Δp
Mitochondrial membrane potential	$\Delta\psi_m$
Omega-FAO	ω-FAO

STATEMENT OF CONTRIBUTION TO CO-AUTHORED PUBLISHED PAPER

This chapter includes a co-authored paper. The bibliographic details of the co-authored paper, including all authors, are:

See Hoe, L. E., **Wells, M. A**., Bartnikowski, N., Obonyo, N. G., Millar, J. E., Khoo, A., Ki, K. K., Shuker, T., Ferraioli, A., Colombo, S. M., Chan, W., McGiffin, D. C., Suen, J. Y. and Fraser, J. F. (2020). *Heart transplantation from brain dead donors: a systematic review of animal models*. Transplantation, Publish Ahead of Print doi: 10.1097/tp.0000000000003217

My contribution to the paper involved:

In the production of this paper I assisted with data search strategy, data extraction and review.

(Signed) _____ (Date)13/09/2020
Matthew Wells

(Countersigned) _____ (Date)15/09/2020
Corresponding author of paper: Louise See Hoe

(Countersigned) _____ (Date) 15/09/2020
Supervisor: Jason Peart

Chapter 1

Literature Review

Contents

1.0 | Introduction

Heart failure (HF) is a major global health problem affecting over 26 million people worldwide [1]. HF is described as a progressive decline in the ability of the heart to meet the metabolic demands of the body [2]. Despite a multimodal treatment approach, cardiac function will eventually deteriorate to end-stage heart failure. At this stage, one of the most effective treatments is heart transplantation (HTx) [3]. Unfortunately, HTx is not without complications. These complications manifest as both electrophysiological and contractile dysfunction causing significant recipient morbidity and mortality [4-6]. The mechanisms behind cardiovascular deterioration begin at donor brain stem death (BSD).

Currently, approximately 95% of heart donors are patients who have confirmed BSD [7]. However, BSD compromises cardiovascular function via a complex interaction between several physiological responses to brain death. These responses create physiological and biochemical chaos, which has no evolutionary benefit, causing cardiac injury, which in turn contributes to these potential donors being rejected for transplantation based on medical unsuitability. This BSD-mediated dysfunction however is reversible, implying that rejected donor hearts may be amenable to transplantation if the understanding and management of BSD-mediated dysfunction are improved.

Once a donor heart is identified as suitable, it must then endure injurious episodes of ischaemia during organ preservation and transport, and reperfusion injury upon re-establishment of circulation in the recipient. These events may lead to graft failure post-transplantation [8]. The deleterious events in the pathway to organ donation have been implicated in the development of graft dysfunction however [5, 8], the exact mechanisms by which this occurs are poorly understood. Our aim is to uncover these mechanisms by a thorough investigation of cardiovascular dynamics following BSD and subsequent transplantation. By doing so, this work will be instrumental in highlighting therapeutic strategies or targets to improve patient management and thus mortality and morbidity.

1.1 | The Brain Stem Dead Heart Donor

Relying on the BSD criteria cannot meet the demand for donor hearts. In 2017, the Australian and New Zealand Organ Donation Registry (ANZOD) [9] reported that only 25% of potential donor hearts progressed to transplantation, with an average of 72 HF patients on the waiting list every month. The main reason for this poor utilisation is medical unsuitability, accounting for approximately 48% of unused hearts. This is followed by donor age (22%), unsuitable recipient (17%) and logistical issues (4%) [9].

Since January 1989 to December 2015, seven conditions can explain 90% of the hearts rejected on medical grounds (Fig 1.1). The most prevalent of these is disease of the organ (48%) and approximately 28% relate to functional abnormalities (abnormal echocardiogram, electrocardiogram (ECG), inotropic support etc) [10]. Donor BSD however, has several well-recognised responses that can cause cardiac functional instability and therefore contribute to rejected donor hearts [11-13].

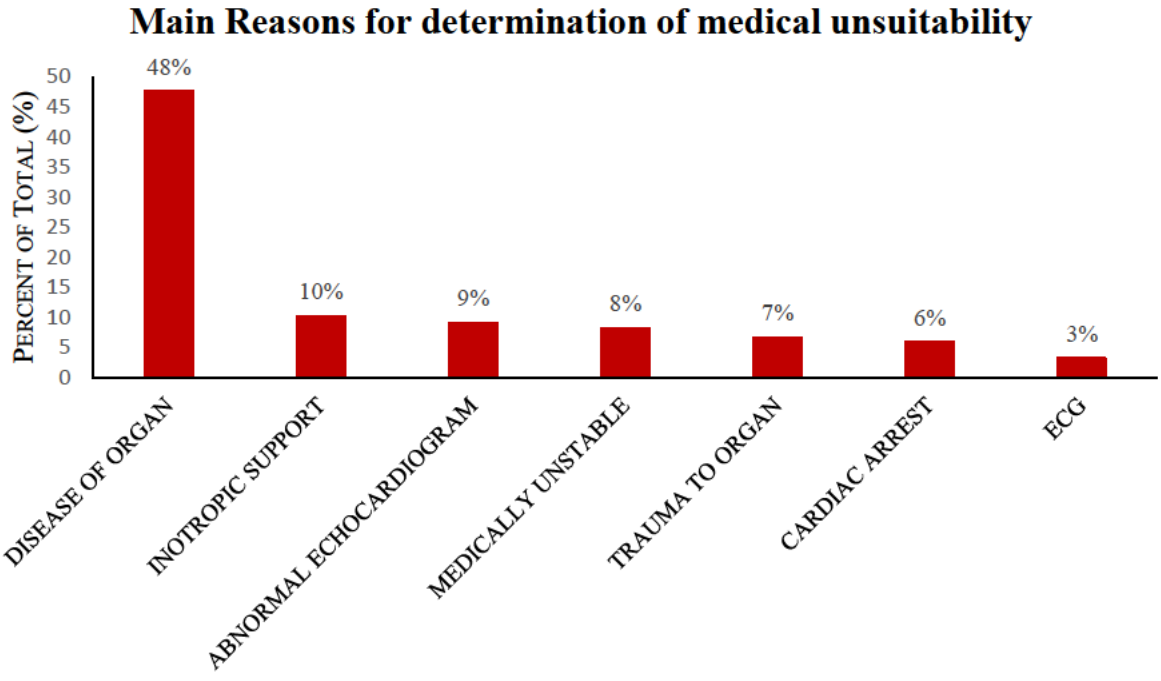

Figure 1.1. ANZOD data representing the contributing factors toward the determination of medical unsuitability for potential donor hearts. Data extrapolated from ANZOD Annual Report 2016, Supplement 1

1.1.1 | Cardiac Dysfunction Post-BSD

The leading cause of death in heart donors is intracranial haemorrhage, followed by cerebral hypoxia/ ischaemia and traumatic brain injury [9]. These mechanisms of injury cause several well characterised cardiovascular responses that result in poor cardiac function. Post-BSD cardiac dysfunction presents with, but not limited to, complement activation, endothelial dysfunction, inflammation, ECG abnormalities, arrhythmias, increases in cardiac enzymes (e.g. troponin I), ventricular systolic dysfunction, contraction band necrosis and even sudden death [11, 14]. These stress cardiomyopathy-like abnormalities however are reversible given enough time, usually within the first week, but may still contribute to the number of rejected donor hearts and may predispose the heart to development of graft dysfunction and allograft vasculopathy [8, 15, 16].

1.1.2 | Electrophysiological Disturbances Post-BSD

Cardiac rhythm disorders are frequently reported in patients suffering a stroke or traumatic brain injury. These conditions often progress to brain death and contribute to the BSD donor population, and therefore are relevant to consider. Arrhythmias occur in 25-80% of stroke sufferers, with a greater propensity associated with haemorrhagic stroke [17, 18]. Tachyarrhythmias are the most frequent, yet have variable reported incidence due to the mechanism of injury (e.g ischaemic/ haemorrhagic stroke) (Table 1.1).

Table 1.1 Incidence of cardiac arrhythmias post-acute stroke. Data extracted from Ruthirago *et al.,* 2016, Koppikar *et al.,* 2013 & Frontera *et al.,* 2007.

Tachyarrhythmia	**Incidence (%)**
Atrial Fibrillation	11-76
Atrial Tachycardia	3
Supraventricular Tachycardia	2-12
Ventricular Ectopy and Couplets	1-54
Sustained/ Non-sustained Tachycardia, Atrial Flutter	1-29
Bradyarrhythmia's	
Atrial Fibrillation with slow Ventricular Conduction	5
Mobitz Type II Second Degree Block	2-4
Asystole or Sinoatrial Block	2-16
Complete Atrioventricular Block	<1-4

These findings however are representative of a brain-injured population rather than a brain dead population. Khush and colleagues in 2012 investigated 980 ECGs from brain dead donors and reported a 97% rate of sinus tachycardia, with only rare occurrences of atrial or ventricular ectopy and conduction delays [19]. Additionally, Christè *et al.*, (2006) found no change in apical epicardial action potentials between brain dead and control pigs [20].

ECG waveform abnormalities are prolific in brain injury, occurring in 50-92% of acute stroke patients and 51% in ECGs from organ donors [17-19]. Over a 10 year period (2008-2017), ANZOD reported an average 22.4% of donors with abnormal ECG and 3% (1998-2015) donor rejection rate based on electrocardiographic grounds [10, 21-30]. The majority of ECG abnormalities appear during the repolarisation phase and include ST depression or elevation, abnormal T waves, U waves, left ventricular hypertrophy, pathological Q waves, increased QTc dispersion and QT/QTc prolongation (Table 1.2) [17, 19, 31-33]. These abnormalities arise in the

absence of pre-existing cardiac or coronary artery disease, are above the expected rate observed in age and sex-matched controls, but may also be transient, self-correcting with an increase in time from the initial injury [6].

Table 1.2. Published incidence rates for ECG abnormalities in both brain-injured and brain dead patients.

ECG Characteristic	Published Incidence Rates (%)	
	*Brain Injury	Brain Death
LVH	20	8
Q waves	8-10	7
ST Elevation	5-6	2
ST Depression	10-24	10
T Wave Inversion	19-25	12
Peaked	2.2	ND
Non-specific ST-T Segment abnormality	16-67	18
QT/ QTc Prolongation	16-71	36
U Waves	15	ND

*Brain Injury including intracerebral haemorrhage, traumatic brain injury, hypoxia, anoxia, ischaemic stroke and haemorrhagic stroke.*ND – no data. [19, 31, 32, 34, 35]

Elevation and depression of the ST segment and T wave inversions are indicative of myocardial injury, which is consistent with the finding of contraction band necrosis, and elevated troponin I and creatinine-kinase myocardial isoenzyme markers in brain-injured hearts [11, 36]. A prolonged QT interval reflects a longer period the heart is in a vulnerable state to dangerous ventricular arrhythmias [37]. Khush and colleagues however, in the presence of a prolonged QTc did not observe any dysrhythmias or decreases in allograft utilisation [19]. It is important to note

however that Khush *et al*., did not record specific reasons for allograft non-utilisation, and did not standardise the time between ECG capture and brain stem herniation, which may have influenced results.

Brain injury produces dynamic electrical disturbances that indicate both myocardial injury and negative lusitropy, both detrimental to haemodynamic performance and contributing to organ non-utilisation [17, 19]. The electrical consequences of BSD however, have not been studied beyond the ECG aside from Christè *et al.*, who measured apical action potential morphology [20]. Further research utilising more sophisticated technology, such as electroanatomical mapping, is required to thoroughly investigate the electrophysiological consequences of BSD.

1.1.3 | Haemodynamic Instability Post-BSD

The haemodynamic perturbations of BSD can be broken down experimentally into two phases; the hyperactive phase immediately following the initiation of brain injury and the depressed phase, encompassing the period following brain death. The two phases represent distinct haemodynamic changes that have been reproduced in several small and large animal studies and supported by clinical human data [13, 38]. Most animal studies have used a balloon catheter placed intracranially and inflated with saline to initiate brain injury and subsequently brain death [39]. This method is used to mimic the clinical scenario by increasing intracranial pressure (ICP) similar to that seen in brain-injured patients that progress to organ donation [39].

During the hyperactive phase, experimental observations reveal profound hypertension and increased heart rate, cardiac index, systemic vascular resistance (SVR), left ventricular systolic pressure (LVSP), end-diastolic pressure (EDP), central venous pressure (CVP) and coronary blood flow (CBF) [36, 40-42]. These changes are also accompanied by metabolic alterations evidenced by increases in serum lactate, glucose, fatty acid (FA), insulin, glucagon and tissue adenosine concentrations [43]. The increase in lactate concentration suggests a switch from myocardial aerobic to anaerobic metabolism [11]. Human studies examining metabolic profiles of traumatic brain injury and acute stroke patients have also shown elevated blood glucose, FAs

and insulin, and that these increases are associated with worse clinical outcomes [44-47]. Animal studies however have shown that this acute haemodynamic hyperactivity is short-lived upon the manifestation of brain death [13, 38].

The hyperactive phase reportedly lasts, between 3 min for rodent studies, up to 30 minutes in larger animals [38, 48]. After this period, mean arterial blood pressure, heart rate, LVSP, CBF, CVP and serum concentrations of lactate, FAs and glucose decrease to baseline levels [36, 38, 42, 43]. LVSP, LV maximum pressure development (LV dP/dT_{max}), CBF and SVR all have been shown to drop below baseline values 1-6 hrs post-BSD [38, 41, 48]. Several studies have also shown an increase in LV minimum force development (LV dP/dT_{min}), a measure of cardiac lusitropy, further supporting the negative lusitropic implications of a prolonged QTc interval [49]. Additionally, Herijgers *et al.*, [50] and a series of experiments by Szabò [13] showed that brain death was accompanied by altered loading conditions, specifically a pronounced decrease in afterload assessed by load-independent measures of contractility.

These dynamic changes in cardiac electrophysiology and haemodynamics in brain injury and subsequently brain death are similar to those observed in Tako-tsubo cardiomyopathy or stress cardiomyopathy, which suggests a common aetiology [36]. Moreover, these changes are also associated with allograft non-utilisation and poor post-transplant function [5, 8, 51]. It is crucial to fully understand the pathophysiological mechanisms in order to improve utilisation rates and potentially post-transplant function.

1.2 | Pathophysiology of Cardiac Dysfunction Post-BSD

The pathophysiological mechanisms of BSD-mediated cardiac dysfunction begin with an increase in ICP leading to brain stem herniation. Cerebral blood flow is determined by cerebral perfusion pressure (CPP), which in turn is associated with mean arterial pressure (MAP) and ICP. An increase in ICP reduces CPP and initiates the central nervous system ischaemic response, enhancing sympathetic outflow to maintain CPP and cerebral blood flow. The physiological

responses that follow can be explained by the 'catecholamine hypothesis', the 'Novitzky hypothesis' and endothelial activation (Fig 1.3, pg. 21).

1.2.1 | The Catecholamine Hypothesis

The increase in sympathetic outflow is referred to as the 'catecholamine storm'. As the term suggests, BSD induces a pronounced release of catecholamines at post-ganglionic nerve terminals and into the circulation. Plasma catecholamine concentrations can increase by up to 100-fold (approximately 300-4000 pg/mL for noradrenaline and 100- 750 pg/mL for adrenaline [52, 53]). The degree of catecholamine release and consequential cardiac dysfunction has been shown to positively correlate with the speed at which ICP increases [40]. In effect, the mechanism of BSD, in particular how quickly and the degree to which ICP rises in the initial minutes-hours of injury may induce variable levels of myocardial dysfunction [54].

Sympathetic stimulation, in turn, leads to activation of baroreceptors, thus increasing vagal activity to lower heart rate. It is this intense release of catecholamines and mixed sympathetic and vagal activity that induces the hyperactive haemodynamic phase and is referred to as the 'Cushing reflex' [2, 16]. Catecholamine levels peak after the initiation of injury and gradually decrease thereafter, returning to or below baseline 60-120 mins post-BSD. The paralleled trends in catecholamine release and the hyperactive phase led to the catecholamine hypothesis (Fig 1.3, pg. 21).

Catecholamines bind to alpha-1 adrenergic receptors (α_1-AR) on vascular smooth muscle and activate the inositol triphosphate 3 pathway which stimulates calcium (Ca^{2+}) release from the sarcoplasmic reticulum, activating protein kinase-C to produce vasoconstriction [55]. This effect can be observed by the large increase in SVR during the hyperactive phase of brain injury. Circulating catecholamines also bind to beta-adrenergic receptors (β-ARs), specifically β_1 and β_2 subtypes in the heart. α_2-ARs however, acting on pancreatic β-islet cells are involved in insulin suppression. Combined with stress-mediated insulin resistance, the donor heart is then subject to a precarious state of substrate utilisation, precipitating metabolic disturbance.

The β_1 subtype is the dominant β-AR subtype, with higher cardiac expression levels than β_2 [56]. β_1-ARs are coupled to G-stimulatory (Gαs) proteins which activate adenylyl cyclase which generates cyclic adenosine monophosphate (cAMP) to activate protein kinase-A (PKA). PKA then phosphorylates phospholamban, L-type calcium channels, ryanodine receptors, cardiac troponin I and myosin binding protein C to increase Ca^{2+} concentrations and contractility [57, 58]. Increases in blood pressure and LV dP/dT_{max} reflect this positive inotropic effect in the hyperactive phase. Additionally, in pacemaker cells cAMP binds to potassium/sodium hyperpolarization-activated cyclic nucleotide-gated channel 4 to enhance Ca^{2+} handling and increases automaticity. This is reflected by increases in heart rate and tachyarrhythmias [58]. However, the large levels of catecholamine release may also initiate the negative contractility observed after the peak hyperactive stage.

A widely accepted hypothesis is that the 'catecholamine storm' leads to toxicity negatively impacting cardiac performance. When the 'catecholamine storm' is blocked through adrenergic receptor antagonism or sympathectomy, BSD-mediated cardiac dysfunction can be ameliorated, particularly the hyperactive phase [53, 59]. Catecholamine toxicity can lead to intracellular Ca^{2+} overload and poor Ca^{2+} sequestration due to enhancements to pathological alterations in downstream phosphorylation processes. This produces myocardial hypercontracture and the development of contraction band necrosis, which leads to poor contractility and electrophysiology [11, 17]. However, since catecholamines remain elevated despite a decrease in cardiac performance after peak hyperactivity, several other mechanisms may also be involved.

Previous studies have also suggested desensitisation of β_1-ARs, leading to donor cardiac dysfunction [49, 60]. Beta-adrenoceptor desensitisation emerges from continued agonism of the receptor activating a family of G-protein coupled receptor kinases (GRKs), particularly GRK-2 (also known as β-adrenergic receptor kinase-1 (βARK-1)). Desensitisation begins with the translocation of GRK-2 to the plasma membrane where it phosphorylates agonist activated β-ARs. This leads to the recruitment of β-arrestins (β-ARR) promoting internalisation of the β-AR via endocytosis [57, 58]. Studies have also shown that GRKs, shown to be increased in BSD, can

localise to the mitochondria, promoting Ca^{2+} intolerance, cytochrome c release, increased apoptotic signalling and potentially affecting adenosine triphosphate (ATP) levels [61]. Desensitisation is believed to be a protective mechanism, alleviating catecholamine-induced stress and further injury, albeit at the expense of contractility. Adrenoceptor desensitisation however is a consequence of chronically elevated catecholamines, it is unclear whether the acute rise in catecholamines mediated by BSD elicits a strong enough stimulus to initiate desensitisation.

Bittner and colleagues investigated β-AR density and adenylyl cyclase levels in hearts from brain dead dogs. After 6 hours of BSD, Bittner found enhanced adenylyl cyclase activity and higher β-AR density compared to baseline [60]. Pandalai *et al.,* (2005) also showed no differences in β-AR density between brain dead pigs and sham-operated controls after 6 hours BSD, but did find a 3 fold increase in βARK-1 expression and a 2.5 fold increase in membrane βARK-1 activity [49]. BSD-mediated changes to adenylyl cyclase (AC) activity are also reportedly variable, showing either enhanced or reduced β-AR-AC coupling [60, 62, 63].

Similarly, White *et al.,* showed preserved β-AR densities, reduced β-AR-AC coupling and reduced right ventricular (RV) contractility in failing, non-utilised donor hearts [64]. These data were compared to non-failing hearts, also with BSD, indicating poor β-AR function may be a feature of donor heart dysfunction, but may not be a conserved effect of BSD. Increased adrenergic drive may also have influenced these findings, with the failing hearts receiving higher doses of dopamine (8.5 ± 6.4 $\mu g \cdot kg^{-1} \cdot min^{\cdot -1}$) for an extended period (17.2 ± 16.3 hrs) [64], whereas experimental animal models did not report the use of adrenergic support. Importantly, previous animal studies have also incorporated short post-BSD timeframes of 3-7 hrs. However, the average time taken for a BSD donor to progress to transplantation, in Australian centres, is approximately 21 hrs after BSD confirmation [22].

Another common theory is that the release of catecholamines exerts strain on myocardial oxygen demand and supply creating metabolic changes and potentially impacting mitochondrial ATP production [11, 65, 66]. In the face of coronary vasoconstriction, increased oxygen demand

potentiates metabolic changes. In response to increased oxygen demand, the body upregulates inefficient but oxygen-independent anaerobic metabolism, demonstrated by an increase in plasma and intracellular lactate concentration [11, 43, 66]. Human endomyocardial biopsies of donors that do not proceed to HTx for clinical reasons are sometimes used as a control group in studies examining the mitochondrial effects of HF. These studies have shown either preserved or higher mitochondrial respiration, particularly complex I driven state 3, or enzyme activities compared to HF patients [67-69]. Conclusions from these studies are under the assumption the BSD donor heart functions as a healthy control, however Holzem *et al.,* [67]suggested this assumption may be a limitation due to the physiological responses of BSD effecting the heart, and potentially the mitochondria. To date, one study has directly examined mitochondrial respiration post-BSD. Sztark *et al.,* permeabilised muscle fibres from the *peroneus longus* muscle of patients with BSD and found depressed phosphorylative oxygen consumption rates and respiratory control compared to controls [70]. Sztark concluded that the metabolic status of BSD donors should be evaluated for donor risk stratification in the form of lactate to pyruvate ratios, and highlights metabolism as a potential management strategy.

In addition to anaerobic switching, catecholamine-mediated Ca^{2+} overload may also cause increases in mitochondrial Ca^{2+} impacting oxidative phosphorylation and ATP production. A decrease in cellular ATP production, in turn, leads to a decrease in energy supply to the heart to fuel contraction and thus contributing to the well-known cardiac damage from BSD. Studies examining ATP concentrations after BSD however have reported preserved ATP content [71, 72]. This preservation may be due to the upregulation of all pathways leading to ATP production, a response that may cause further injury.

A common observation in patients with brain injury is hyperglycaemia and an increase in circulating FAs and receptors for FA sensing, trafficking and metabolism [43, 73]. These metabolic alterations are associated with worse clinical outcomes and severity in patients with acquired brain injury [73-75]. This heightened level of metabolic homeostasis however may cause further injury. The driving force of ATP production is mitochondrial respiration and increasing

intracellular concentrations of FAs can uncouple mitochondrial respiration. An uncoupled system detrimentally leads to energy crisis [76]. In response to oxidative stress, FAs also undergo lipid peroxidation, a consequence of anaerobic metabolism [77]. Due to the high abundance of lipids in cellular membranes, lipid peroxidation can cause membrane disruption and lead to inflammation and cell death, contributing to electrophysiological and contractile dysfunction [44, 77]. Neither cardiac mitochondrial respiration nor the cardiac metabolome has been studied in BSD.

Contradictory to the catecholamine hypothesis, Szabò and Herijgers interpreted the hyperactive phase differently [13, 38]. Whilst both agree that the catecholamine response contributes to the initial Cushing reflex observed during the hyperactive phase, they argue that BSD induces altered loading conditions that predispose the heart to reduce contractility. The emphasis was on the reduction in SVR that preceded reductions in contractility. Upon the evolution of BSD neural vascular tone is lost, thus decreasing SVR and therefore afterload, and causing intravascular hypovolemia leading to reductions in preload. A decreased afterload and preload then cause reductions in contractility via the Frank-Starling mechanism (reduced contractility due to reduced preload) and the Anrep effect (reduced contractility due to reduced afterload). This is due to a diminished Ca^{2+} affinity of contractile proteins, decreases in intracellular Ca^{2+}release, and activation of mechanosensitive Ca^{2+} channels [78].

Szabò also highlighted the importance of the coronary circulation, raising the theory that reduced afterload could also reduce CBF and thus decrease contractility via impaired perfusion. A vicious cycle could then ensue, involving reduced afterload initiating reductions in contractility and myocardial O_2 demand which leads to further reductions in CBF and contractility. However, BSD also causes endothelial activation, and reductions in flow may therefore be related not only to reduced afterload but endothelial dysfunction.

1.2.2 | Endothelial Activation

The coronary vascular network consists of three distinct structural compartments, the large conductive, pre-arteriolar (100-500 μm) and arteriolar (< 100 μm) vessels. Functionally, the conductive vessels store elastic energy at systole, during coronary filling, and convert this to kinetic blood movement during diastole to fill the smaller vessels that were constricted due to contraction. Each of these compartments are differentially regulated, the conductive and proximal pre-arterioles are most responsive to flow, distal pre-arterioles to pressure and the arterioles are regulated by myocardial metabolism [79]. The latter is to ensure that myocardial perfusion meets metabolic demands. Under normal conditions CBF can be upregulated by 3 times, referred to as coronary flow reserve (CFR). The main regulator of this CBF increase is the coronary vascular endothelium.

The vascular endothelium has four specific functions, i) an anticoagulant, ii) a trafficker of fluids and molecules, iii) vascular homeostasis and repair and iv) a regulator of vascular tone and hence blood flow. The endothelium regulates vessel tone by producing several vasoactive substances in response to various stimuli (Fig 1.2). The function of these substances is to induce vasodilation

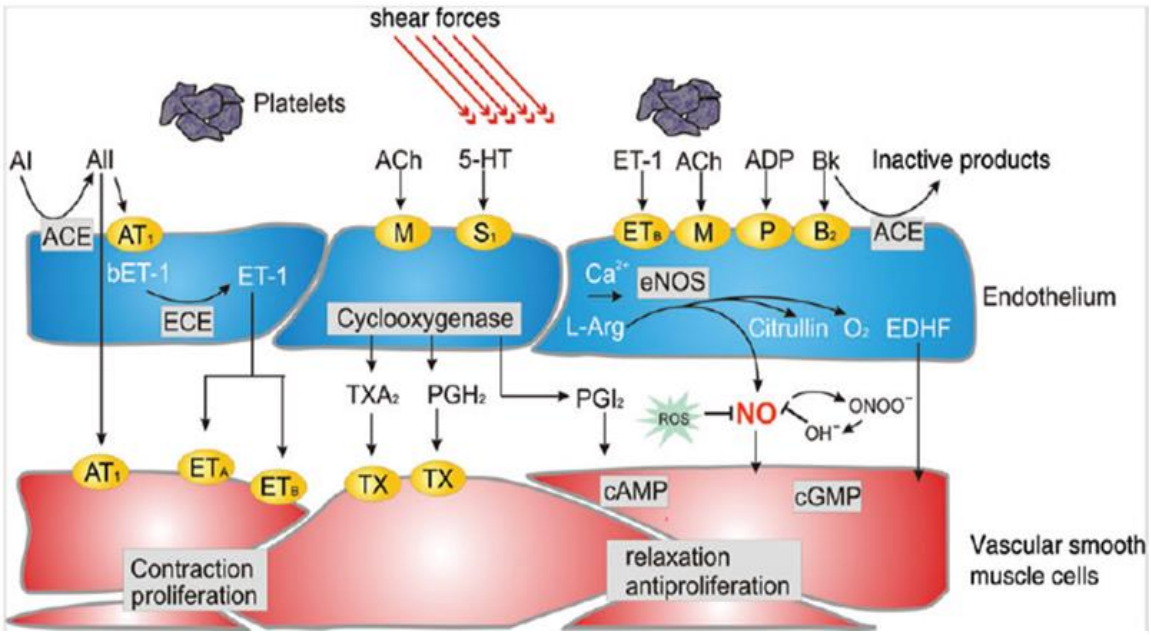

Figure 1.2. Endothelial regulation of vascular tone via vasoactive substances, figure extracted from Gutierrez *et al.*, 2013 [73]. Permission to reuse obtained 10/10/2020

or vasoconstriction. Endothelial dysfunction can therefore lead to poor metabolism perfusion matching and coronary blood flow, consequently leading to cardiac dysfunction [79, 80].

In 1988, Novitzky *et al.,* were the first to examine coronary vascular smooth muscle (VSM) in a baboon model of BSD [59]. Seventeen animals were subjected to BSD with 70% of these animals presenting with contraction band necrosis of coronary VSM. This effect was completely ameliorated after total cardiac sympathectomy and verapamil administration. These results highlight the importance of a catecholamine-mediated Ca^{2+} overload in VSM cell dysfunction post-BSD. Since then several studies have focused on the vascular endothelium, measuring coronary blood flow using endothelial-dependant and independent vasodilators, a summary of these studies is presented in table 1.3.

Table 1.3. Summary of studies examining coronary flow (CBF) and coronary flow reserve (CFR) using endothelial-dependant (Endo-D) and endothelial-independent (Endo-I) substances.

		Effect of BSD		
Paper		**General**	**Endo-D**	**Endo-I**
Seguin *et al.*, 2001 [42]	QLAD (CBF)	Initial increase Return to baseline after 40 mins	NM	NM
Szabo *et al.*, 2002 [81]	CBF	Initial Increase (LAD and LCX) Decline below baseline 180 mins Post-BSD	↓	↔
Oishi 2003 [82]	CBF	Increased initially remained elevated for 5 min post-BSD before decreasing below baseline 1-hr post	↓	↓
	CFR	Elevated 1-hr post	↑	↑
Herijgers *et al.*, 2004 [50]	Isometric tension	Serotonin induced vasoconstriction	↔	↑
Oishi *et al.*, 2005 [83]	CBF	Increased 5 min post Non-significant decrease below baseline 30 min post	↓	↓
	CFR	Reduced 30-60min after BSD	↓	↓

NM* not measured, BSD* Brain stem death, LAD* left anterior descending artery, LCX* left circumflex artery.

Data from these studies suggest that BSD leads to an initial increase in CBF during the catecholamine storm, followed by a reduction below baseline 40-60 mins post-BSD induction. The action of catecholamines on the vascular network is to vasoconstrict through α-ARs. However, on top of flow-mediated dilation and increased peripheral resistance, catecholamines also increase myocardial metabolism which releases metabolites such as adenosine, nitric oxide (NO), prostacyclin, bradykinin and carbon dioxide (CO_2) to induce vasodilation of coronary vasculature, thus leading to the observed increase in blood flow. As brain death progresses however, neural vascular tone is lost, peripheral resistance decreases and CBF falls. To delineate the endothelial-dependant and independent mechanisms of CBF changes, Szabo [81], Oishi [82] and Herijgers *et al.,* [50] utilised acetylcholine (Ach) as an endothelial-dependent vasodilator and serotonin (Herijgers *et al.,* [50]) or sodium nitroprusside (SNP) as an endothelial-independent vasodilator.

Ach acts on muscarinic receptors on endothelial cells to increase intracellular Ca^{2+} concentrations activating endothelial nitric oxide synthase (eNOS) via calmodulin to produce NO. NO then diffuses to the VSM cells to decrease intracellular Ca^{2+}, via activation of soluble guanylate cyclase and cyclic guanosine monophosphate (cGMP), thus promoting vasodilation. Both Szabo and Oishi found a reduction in CBF (Oishi *et al.,*) with paradoxical vasoconstriction after Ach administration [81, 82]. Herijgers *et al.,* on the other hand observed no change in flow across any time point after 60 min of BSD [50]. This however, may be due to methodological differences between studies, with Oishi and Szabo measuring *in vivo* flow after 1 and 3 hrs BSD, respectively. In comparison, Herijgers measured *in vitro* isometric tension after 60 mins BSD, only on large conductive vessels.

The vasoconstriction observed in previous studies indicates a dysfunctional endothelium (leading to direct Ach stimulation of VSM) or absence of NO production. To synthesise NO, eNOS requires l-arginine and a variety of other cofactors, the uncoupling of cofactors to NOS and competition for l-arginine can both reduce the bioavailability of NO. Arginase also utilises l-

arginine to produce l-ornithine and urea and in situations of hypoxia, inflammation and production of reactive oxygen species (ROS) can increase arginase activity and thus compete with eNOS. Whether arginase activity is upregulated or eNOS uncoupling is present post-BSD is unknown.

Sodium nitroprusside acts as a NO donor, which is liberated physiologically after reaction with sulfhydryl groups. Liberated NO then works via the same mechanism as Ach-mediated NO once localised to VSM. Oishi found a reduction in CBF and CFR post-SNP administration, whilst Szabo found no change in CBF [81, 82]. Both studies employed the same methodology for BSD induction and CBF measurement, however Szabo [81] measured CBF after 3 hours of BSD and Oishi after 1 hr. These results suggest either poor NO signalling in VSM post-BSD or highlight the importance of cardiac recovery post-BSD with increasing brain death time. Additionally, at baseline, animals in Oishi's study had on average, higher aortic pressure, heart rate and cardiac output and lower CBF.

In the study by Herijgers, administration of serotonin caused profound isometric contraction in the presence of normal Ach vasodilatory response, implying normal VSM NO signalling [50]. Herijgers concluded that this hypersensitivity to serotonin may be due to haemodynamic-induced endocrine, paracrine and inflammatory changes post-BSD; activating other pathways leading to Ca^{2+} sensitisation and vasospasm. Importantly, these previous studies did not take into account for the many other NO independent pathways that lead to vasoactive changes, such as endothelial-derived hyperpolarising factor, cyclooxygenase activity, prostanoid activity or soluble guanylate cyclase, cGMP dysfunction.

Endothelin-1 (ET-1) is a potent vasoconstrictor, synthesised in endothelial cells and binding to the Endothelin A and B (ET_A and ET_B) receptors on VSM. This constrictive effect is inversely proportional to vessel size with effective vasoconstriction occurring within the nanomolar range in human vessels [84]. Together, this suggests that only a small rise in ET-1 concentration is needed to produce a long-lasting vasoconstrictive effect, which will be more prominent in the coronary microvasculature. Previous studies have shown an increase in ET-1 post-BSD, which may then promote microvasculature contracture and lead to impaired CFR and cardiac function,

as observed by Oishi [82, 83]. Using the non-selective ET-1 receptor antagonist TAK-044, Oishi [83] showed improvements in both left ventricular function and CFR post-BSD and concluded that coronary flow was an important determinant in cardiac dysfunction post-BSD. Szabo also highlighted the importance of coronary flow on cardiac function [85]. By maintaining coronary perfusion pressure throughout BSD, both myocardial contractility and blood flow could be restored to pre-BSD levels.

These studies have emphasized the importance of the coronary vasculature by demonstrating endothelial-dependent and independent dysfunction leading to alterations in CBF and CFR. These alterations in turn, may then lead to the characteristic excitation and contractile dysfunction commonly observed post-BSD. Whether vascular dysfunction is causative of, or a symptom of poor haemodynamics and altered loading conditions after BSD is still debated.

1.2.3 | Endocrine Dysfunction

The significant insult of brain death leads to severe dysfunction of the hypothalamic-pituitary-adrenal (HPA) axis [12]. Early work by Novitzky in baboons and pigs revealed endocrine changes as a consequence of anterior/posterior pituitary failure [86]. The HPA axis is essential to adequate metabolic, inflammatory and immunological functioning. The identification of hormonal disturbance in BSD has led to the adoption of hormone replacement therapy (HRT) in donor management strategies. Recently however, the efficacy and safety of HRT have come into question.

Triiodothyronine (T3) depletion was one of the first described hormonal disturbances in BSD [48, 86]. It is characterised in animal models by a gradual decrease over time from ictus to suboptimal levels 3-6 hours following BSD. It was shown in early works that rescuing this depletion could reverse the metabolic changes, alleviate inotropic support and improve cardiac function [12, 86-88]. The cardioprotective effects of T3 are mediated by increasing the expression of sarcoplasmic reticulum Ca^{2+}/ATPase (SERCA), β_1-AR, sodium-potassium ATPase pump (Na^+/K^+ ATPase) and voltage-gated potassium channels [12, 89]. It is generally believed that T3 also increases

mitochondrial biogenesis, oxidative phosphorylation and prevents the opening of the mitochondrial permeability transition pore (mPTP) [90]. In a recent review by Rutiglioano *et al.*, (2017), the authors reported limited evidence of the latter which do not provide a cause-effect relationship. Moreover, James *et al.*, [91] showed that T3 administration increased voltage gated potassium channel (KvC) and SERCA expression, but not β_1-AR expression. The authors also found no association with T3 therapy and haemodynamic improvement.

Bugge *et al.*, [40] reviewed organ donor management strategies and highlighted that in patients with confirmed BSD, T3 levels varied with only 15% of patients reaching critically low levels. Two systematic reviews and meta-analyses [92, 93], reviews [12, 40, 94] and several research papers [95, 96] also concluded that T3 therapy was not beneficial in improving haemodynamics or procurement yield. The contradictory findings may be due to the heterogeneity in study design, poor controls, aggressive management and combination HRT. Most studies employed T3, vasopressin, insulin and corticosteroid therapy, essentially obscuring a cause-effect relationship. Notwithstanding, evidence for combination therapy although limited, also does not support improved graft function or utilisation rates. Corticosteroid inclusion stems from the association between BSD and adrenal insufficiency.

Adrenal insufficiency (AI) is reportedly present in up to 89% of brain dead patients and is characterised by poor responsiveness of the adrenal glands (particularly cortisol) to cortical regulation [97, 98]. Clinical data show no change in cortisol levels after stimulation with adrenocorticotropic hormone, revealing an impaired adrenocortical response resulting in diabetes insipidus and electrolyte disturbances [40]. Diabetes insipidus is present in up to 77% of brain dead patients, leading to hypovolemia, and if left untreated can cause haemodynamic instability [99]. Donor management guidelines suggest an immediate correction of hypovolemia in order to maintain adequate cardiac perfusion [100]. Hypovolemia may instigate hypernatremia, hypokalaemia, hypocalcaemia, and hypomagnesemia. Hypernatremia in some situations can be severe and has been associated with graft dysfunction post-transplant [101]. Electrolytes are important for regulation of cardiac contractility and rhythm. In an electrocardiographic study by

Khush, potential organ donors with a QTc >480 msec had a significantly lower serum potassium level than patients with a QTc <480 msec [19]. Management goals are aimed at correcting hypovolemia and maintaining normal electrolyte levels [99, 100].

Ancillary to the mentioned effects of AI, cortisol is also involved in the regulation of metabolism and inflammation. Cortisol is a well-known regulator of glucose metabolism, increasing utilisation and insulin release and at chronically high levels can cause hyperglycaemia and insulin resistance. This action is beneficial in the acute hyperactive phase of BSD, however once BSD ensues, cortisol levels decrease thus contributing to glycolytic unavailability. BSD also initiates a profound inflammatory response, increasing the levels of tumour necrosis factor-α, interleukin-1 and -6, C-reactive protein and procalcitonin [102, 103].

It's now well appreciated that there is a complex feedback regulation between inflammation and mitochondrial function. Danger associated molecular patterns (DAMPs) are endogenously produced and provoke numerous cell signalling cascades involved in changes to mitochondrial oxidative phosphorylation, dynamics (fission and fusion), ROS production, mitophagy and Ca^{2+} handling [104]. In turn, these changes in mitochondrial function and dynamics release further proinflammatory DAMPs. In the context of BSD, there exists a large inflammatory response which persists unabated in the presence of decreasing levels of cortisol. As mentioned, combined HRT including corticosteroids has not shown any haemodynamic benefits. Yeager and colleagues however, described a more complex relationship between cortisol and inflammation [105]. They suggest that cortisol acts more on a bell curve, permitting inflammation at low levels and suppressing inflammation at high doses. However, this is largely dependent on the physiological context, pharmacological interactions and responsiveness of receptors.

1.2.4 | Summary of BSD-Mediated Cardiac Dysfunction

Cardiovascular dysfunction post-BSD includes ECG abnormalities, decreased contractility, hormone depletion, electrolyte disturbances, endothelial activation and metabolic alterations. It is the complex interaction of all of the aforementioned mechanisms that act to induce BSD-mediated

cardiac dysfunction. Figure 1.3 outlines the cardiac dysfunction post-BSD and potential mechanisms. These pathophysiological mechanisms are not well understood and contribute approximately 30% to the donor hearts that are rejected on medical grounds. Further research is needed to thoroughly investigate these mechanisms in order to improve cardiac allograft utilisation and potentially improve post-transplant cardiac function, the end-stage in the donor heart journey.

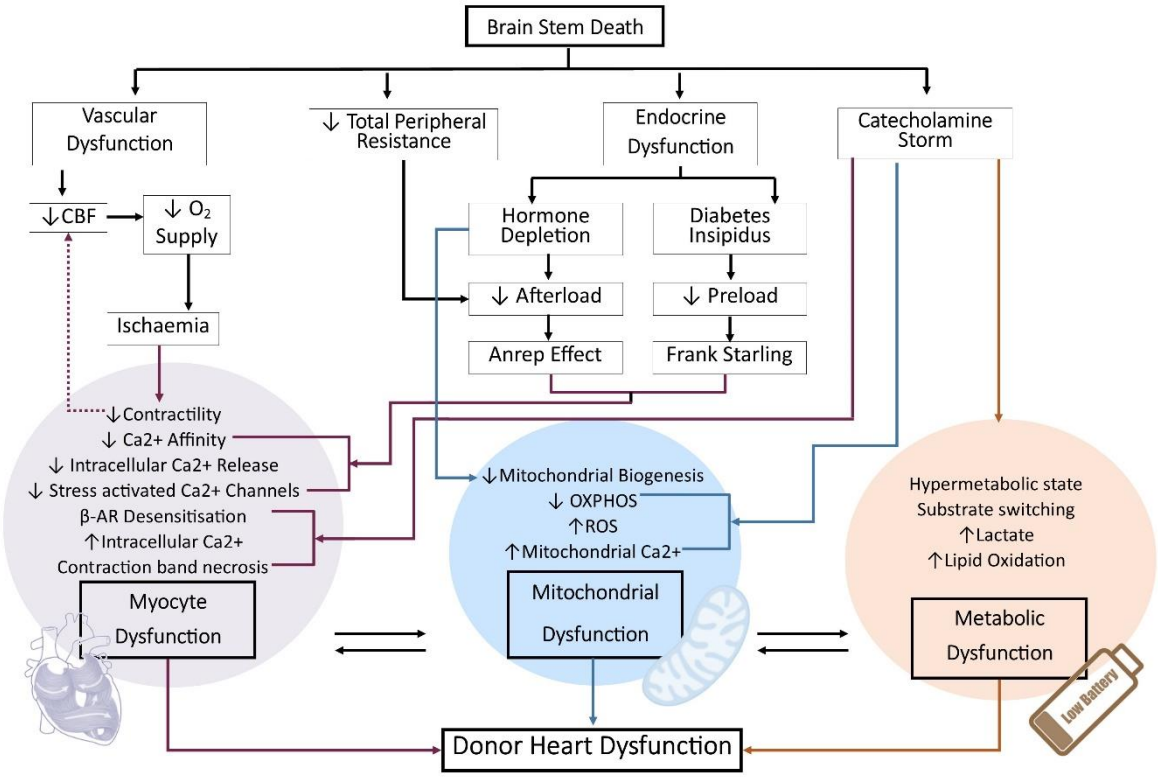

Figure 1.3. Schematic outlining the pathophysiological mechanisms behind BSD-induced cardiac dysfunction. *CPP- Cerebral Perfusion Pressure, OXPHOS- Oxidative Phosphorylation, ROS-Reactive Oxygen Species, β-AR – Beta-adrenergic receptor.*

1.3 | Donation after Brain Stem Death

Once a patient has confirmed BSD, consent has been obtained, the heart is determined viable and a suitable recipient is located, the heart can move to organ procurement. Following procurement, a donor must endure another two potentially injurious events on top of the dysfunction brought

forward from BSD. These events are organ preservation and transport and transplantation, specifically, reperfusion.

1.3.1 | Cold Static Organ Preservation

During organ procurement, the aortic cross-clamp is applied, marking the beginning of the ischaemic time frame. Explanted hearts are then stored in cold preservation solution on ice, referred to as cold static storage (CSS) which is the current gold standard and has remained unchanged for decades. The aim of CSS is three-fold, i) reduce myocardial metabolism, ii) maintain graft viability and reduce swelling and iii) reduce ischaemia reperfusion injury (IRI) injury by inhibiting ROS production and inflammation [106]. Hypothermic metabolic arrest, whilst capable of reducing metabolic rate 12-fold, does not prevent ATP consumption and metabolic changes completely [106, 107].

Intuitively, one would expect a decline in mitochondrial function proportionately to temperature, which is what is observed. In particular complex I driven state 3 respiration is significantly reduced at 6-12 hrs post-cold ischaemia, although 12 hr preservation was still characterised by reduced respiration [108-111]. This decline however can be dramatically improved up to 24 hrs post-cold ischaemia by improving the preservation solution [112]. Conversely, respiration has been shown to be elevated 12-140 hrs post-cold ischaemia, although this was mostly due to the increase in mitochondrial dyscoupling leading to oxygen wastage and not ATP production [113]. These previous data utilise either biopsies or whole heart preparations during storage, which are variably impacted by oxygen diffusion. Diffusion is enhanced for biopsies over an entire organ, which therefore impacts on the clinical utility of these long storage times. Nonetheless, cardiac mitochondria appear to be robust against cold ischaemia, assuming there the environment is properly optimised.

Despite hypothermia, CSS causes a depletion of high energy phosphates, enhancing anaerobic metabolism and acidosis [72, 114, 115]. Initially, strategies to improve CSS were centred on improving preservation solutions. An extensive review on preservation solutions is not within the

scope of this project, however their impact on cardiac performance is nonetheless crucial. Preservation solutions fall into one of 2 categories, intracellular (Na^+ < 70 mmol/L and K^+ between 30 and 125 mmol/L) and extracellular (Na^+ ≥ 70 mmol/L and K^+ between 5 and 30 mmol/L) solutions [106, 116]. Both types cause rapid myocardial depolarisation, cessation of electrical activity and by altering or adding components, reduce inflammation and prevent ROS production [116, 117]. In the United States alone, there are reportedly 167 different organ preservation solutions, 5 of which are used clinically worldwide. Currently, there are no clear distinctions regarding the most effective preservation solution for CSS [106, 117, 118].

Recently however, there has been a shift from halting metabolic rate, to supporting metabolism and aiding with waste product removal. The formulation of a new preservation solution, Somah [106, 116, 119] which contains several key metabolic substrates and ROS scavengers has shown promising experimental results. It was shown that Somah worked best at 21°C, challenging hypothermic preservation as a necessary feature of organ preservation. Further enhancing the bioenergetic properties of heart preservation, recent technological advances have prompted a revisit to perfusion assisted preservation, first utilised by Wicomb *et al.*, in 1984 [120]. Renewed market interest has sparked the advent of Organ Care Systems (OCS) designed to mechanically perfuse the heart in normothermia or hypothermia [121].

The utilisation of experimental machine perfusion has been shown to reduce lactate accumulation and improve energy dynamics compared to CSS by supplying the heart with oxygen and nutrients [121-124]. Hypothermic machine perfusion has also been shown to be beneficial in the preservation of the coronary endothelium, an often-forgotten system when approaching heart preservation [125]. The only OCS in clinical trials however is the Transmedics™ (TransMedics Inc., Andover, USA) system, the effectiveness of which was investigated in the PROCEED II trial comparing the OCS at 37°C to CSS. The results showed no difference between the OCS and CSS in terms of short-term patient outcomes [126]. More work on optimising these systems is necessary before they are to replace CSS in a clinical setting. Regardless of the preservation method, the heart is still subject to not only another bout of warm ischaemia during the transplant procedure, but also IRI upon re-establishment of coronary circulation.

1.3.2 | Heart Transplantation

Successful cardiac transplantation is determined by two important complications outside the immunological responses. These are primary graft dysfunction (PGD) and cardiac allograft vasculopathy (CAV), also referred to as transplant coronary artery disease as it specifically affects the coronaries of the donor heart. Both complications share common aetiologies and may be interrelated however, PGD is a leading cause of 30-day mortality whilst CAV is a determinant of long-term survival [16].

1.3.3 | Post-Transplant Cardiac Dysfunction

Electrophysiological disturbances post-transplant are common and recognised as affecting morbidity, quality of life and mortality. Arrhythmias include sinus bradycardia, conduction delays, atrial fibrillation (AF), atrial flutter, supraventricular tachycardia and sustained/non-sustained ventricular tachycardia (Table 1.4). Sinus bradycardia and conduction delays are most common in the early stages after transplantation alongside atrial fibrillation [6, 127, 128].

Table 1.4. Incidence rates for post-transplant arrhythmias.

Arrhythmia	**Incidence (%)**
Bradycardia	8-23
Conduction Delays	
Intraventricular Conduction Delay	50
Right Bundle Branch Block	10
AV Block	14
Pace Maker Dependence	5
Atrial Fibrillation	0.3-24
Atrial Flutter	2.8-30
Ventricular Fibrillation	10
Asystole	34

Persistent AF however, has been associated with episodes of rejection and if present 1-month postoperatively, is a strong indicator of higher long-term mortality. Atrial flutter is the most common sustained tachyarrhythmia and is associated with rejection, mortality and left ventricular (LV) dysfunction. Sudden cardiac death can occur in an estimated 25% of recipients as a consequence of ischaemia, rejection and LV dysfunction. Terminal rhythms in this population include asystole, pulseless electrical activity and a relatively low incidence of ventricular fibrillation.

Pickham *et al.,* [129] investigated 585 ECGs from 98 recipients and found that 99% were in sinus tachycardia, 69% presented with intraventricular conduction delays, and 64% ECG criteria for atrial enlargement, particularly the left side. Additionally, in this cohort of recipients, the QTc was >440 msec with significant gender differences, predisposing women to a longer QTc (458 msec). Moore *et al.,* investigated matched donor-recipient pairs and showed a significant increase in QRS duration and a decrease in QTc which was associated with hypokalaemia [130]. However, due to issues with follow up, the recipient population in this study consisted mostly of traumatic brain injured donors. Since the majority of donor hearts are procured from cerebrovascular accidents, Moore's recipient cohort may not be representative of the clinical scenario, and the time course of QTc for the two donors may be different. These electrophysiological changes relay important information regarding the haemodynamics of the heart.

Contractile dysfunction post-transplant is predisposed to the right ventricle and manifests secondary to pulmonary hypertension or without other causative factors, referred to as PGD. PGD develops as left, right or bi-ventricular contractile dysfunction in the absence of known causative factors, such as rejection. An estimated 7.4% of patients will develop PGD which accounts for 36% of deaths in the first 30 days post-transplantation. However, incidence rates are compromised due to the lack of a standardised PGD diagnosis criteria [8]. The International Society for Heart and Lung Transplant (ISHLT) in 2013 reached a consensus regarding PGD diagnosis and treatment. Table 1.5 shows these guidelines on the diagnostic criteria for both left and right PGD.

Table 1.5. Definition of Severity Scale for Primary Graft Dysfunction.

Ventricle	PGD **Severity**	**Criteria**
1. PGD-**LV**	Mild PGD-LV: One of the following criteria must be met:	LVEF ≤ 40 % by echocardiography, or Haemodynamics with RAP > 15 mm Hg, PCWP > 20 mm Hg, CI < 2.0 L/min/m^2 (lasting more than one hour requiring low dose inotropes
	Moderate PGD-LV: Must meet one criterion from I and another criterion from II:	I. One criteria from the following: LVEF ≤ 40 %, or Haemodynamic compromise with RAP > 15 mm Hg, PCWP > 20 mm Hg, CI < 2.0 L/min/m^2, hypotension with MAP < 70 mm Hg (lasting more than 1 hour) II. One criteria from the following: i. High-dose inotropes – Inotrope score > 10 or ii. Newly placed IABP (regardless of inotropes)
	Severe PGD-LV	Dependence on left or biventricular mechanical support including ECMO, LVAD, BiVAD, or percutaneous LVAD. Excludes requirement for IABP.
2.PGD-**RV**	Diagnosis requires either both I and ii, or iii alone	i. Haemodynamics with RAP > 15 mm Hg, PCWP < 15 mm Hg, CI < 2.0 L/min/m^2 ii. TPG < 15 mm Hg and/or pulmonary artery systolic pressure < 50 mm Hg iii. Need for RVAD

CI – cardiac index, LVEF – left ventricular ejection fraction, PCWP- pulmonary capillary wedge pressure, RAP- right atrial pressure, LABP- arterial balloon pump, ECMO- extracorporeal membrane oxygenation, LVAD- left ventricular assist device, BiVAD- Bi-ventricular assist device, TPG- transpulmonary pressure gradient, RVAD- right ventricular assist device. Table adapted from Kobashigawa *et al.*, 2013.

1.3.4 | Pathophysiology of Post-Transplant Cardiac Dysfunction

Recipient electrophysiological and contractile dysfunction may be explained by three interconnected mechanisms, donor BSD, ischaemic time (cross-clamp to reperfusion) and IRI. It is believed that the injury sustained from the consequences of BSD can be carried through to CSS and transplantation, where poor cardiac function is confounded by ischaemia and reperfusion

injury. Surprisingly, little is known about the transference of BSD-mediated cardiac dysfunction and PGD post-Tx. This may be due to the methodological difficulties in performing such a study.

The transplanted heart is denervated and as such has a higher resting heart rate and consequently higher metabolic demands. It has been shown that this denervation increases the sensitivity of the myocardium to catecholamines [131]. This is due to an absent noradrenaline reuptake mechanism, specifically uptake 1 which acts pre-synaptically [132]. Gilbert and colleagues showed downregulation of β-adrenoceptors in biopsies from human transplant recipients over time [132]. This data is in agreement with ischaemic models that show downregulated beta-adrenoceptors. The adrenergic concerns of donor grafts are mostly in the context of inotropic support and not the bio-energetic effects.

During the transplant procedure, the donor heart rests within the chest cavity as anastomoses are completed. During this time, the heart unavoidably warms and metabolism increases concomitantly, exhausting the remaining ATP and substrates for ATP generation left from CSS. Van Caenegem found that upon reperfusion after CSS, both the lactate concentration and the adenosine monophosphate (AMP)/ATP ratio increased, implying bio-energetic compromise [122]. Stoica also showed that energy status was not fully recoverable after reperfusion in human donor hearts and was associated with future cardiac dysfunction [72].

The most significant insult impacting successful transplantation is IRI. Upon re-establishment of blood supply, several biochemical responses act in unison to promote injury. The rapid restoration of pH activates the sodium hydrogen (Na^+/H^+) and sodium-calcium exchangers (Na^+/Ca^{2+}), the consequence of which are hypercontracture, myocardial cell death and opening of the mPTP [133].

Recently, Scheiber *et al.,* showed that compared to HF patients, mitochondrial respiration post-HTx was elevated [111]. Despite this, a decrease in mitochondrial respiration or gene activity has been associated with the degree of rejection [134], immunological response [135] and inflammatory response [136] post-HTx. Further, accumulation of succinate from CSS, at

reperfusion, is now used for OXPHOS. Succinate oxidation leads to increases in ROS production at Complex I, possibly by reverse electron transfer through the IQ site of electron leakage [137].

ROS targets are prolific throughout the myocardium and coronary circulation, resulting in metabolic and mitochondrial dysfunction, cell death and the initiation of a vicious cycle of ROS-induced ROS production [133]. Clinical trials utilising antioxidants however have not shown a conclusive improvement to cardiac function post-IRI. This may in part be due to the difficulty of antioxidants to enter the cell or their non-specific actions [138]. The mitochondria possess 11 sites of electron leakage which can lead to ROS production [139-141]. Initial trials with specific inhibitors of the IQ site of ROS production on respiratory complex I have shown promising results [142]. Lastly, mitochondrial re-energisation promotes mitochondrial Ca^{2+} overload and opening of the mPTP channel.

Animal models have shown that supplementation at the time of reperfusion with specific FAs, omega-3 FA's (n-3 FAs) can reduce IRI through multiple signalling mechanisms and potentially replenishing oxidised lipids from lipid peroxidation produced in the donor, thus repairing cellular membranes [46, 143]. This highlights the important role of metabolism and ATP dynamics in both contributing to cardiac injury and its potential to improve cardiac performance, highly relevant to PGD post-HTx. Metabolic alterations may also arise through necessary pharmacotherapy post-HTx that aims to reduce rejection.

Post-HTx, immunosuppression with calcineurin inhibitors to prevent rejection can induce dyslipidaemia and diabetes [144]. Post-HTx hyperlipidaemia has been associated with poor patient outcomes and the development of vasculopathy, a significant determinant of long-term mortality and morbidity [16]. In an animal model of auto transplantation, Drake-Holland *et al.*, (2001) found that chronic denervation (as in HTx) induced upregulation of FA metabolism [145]. Combined with a hyperlipidaemic state, it is possible that the transplanted heart may be subject to lipotoxicity-mediated damage, similar to that observed in diabetic patients [45]. Further metabolic studies are required in hearts post-transplant to determine the cardiac metabolome and its impact in cardiac dysfunction.

Proteomic biomarker discovery has been used in transplant recipient studies in order to identify early graft dysfunction. Lin *et al.*, (2017) recently used a heterotrophic HTx rat model in order to determine the metabolic profile in serum [146]. They found a panel of 4 metabolites, D-tagatose, choline, C16 sphinganine and D-glutamine could accurately diagnose early rejection. The authors also showed reductions in metabolites important in alleviating IRI, oxidative phosphorylation, immune function, and highlighted the interaction between immunosuppressive therapy and metabolic alterations. Additionally, they observed an increase in oxoglutaric acid, which plays a significant role in immune function, the rate of the tricarboxylic acid (TCA) cycle and amino acid production. The latter two functions were only briefly discussed. Given the accumulation of succinate and its role in ROS production, it seems likely that the increase in oxoglutaric acid may drive this and other functions, making it an important metabolic and immunological therapeutic target. However, this study was performed in rats with a known difference in metabolic regulation than humans.

Specific mostly to the electrophysiological disruptions, type of transplant procedure and cardiac denervation can leave the heart susceptible to arrhythmia. Atrial tachyarrhythmias can be generated as a consequence of the bi-atrial transplant procedure. The bi-atrial procedure involves donor to recipient atrial anastomoses, whereas the bi-caval procedure involves anastomoses at the vena cavae level. Bi-atrial procedures are associated with greater sinus node dysfunction and the suture line creates a conduction block. Partial healing across the isthmus creates re-entry loops, thus leading to arrhythmia which is amenable to ablation [6]. As a consequence, the bi-caval method is the most widely used method. Total cardiac denervation post-operatively induces a higher than average heart rate for most recipients. Partial heterogeneous re-innervation can also predispose the heart to arrhythmia by creating unbalanced sympathetic and parasympathetic regulation. Partial re-innervation has been associated with changes in the QTc interval, particularly sympathetic re-innervation [6].

A unique feature of the clinical course of HTx is a large cold and warm ischaemic time, which upon reperfusion may induce further ischaemic damage via the no-reflow phenomena [147, 148].

Characterised by a failure of the endocardial microvasculature following reperfusion, ischaemia induces endothelial dysfunction occluding vasculature and leading to more pronounced damage and swelling of the endothelium and leukocytic recruitment in distal vessels [147, 149]. Upon reperfusion, dysfunctional distal microvasculature prevent forward blood flow and thus promote ischaemia. Schramm *et al*, using a murine heterotropic transplant model and intravital microscopy, found a positive relationship between cold ischaemia and post-HTx no-reflow microvascular dysfunction [149]. In a series of 29 RV biopsies from human donor hearts, Koch *et al*, showed increasing endothelial swelling from cardioplegic arrest to 60 min post-reperfusion [150].

Microvascular spasms post-reperfusion also play an important role in no-reflow. It has been shown that microvascular tone can be regulated by activation of Ras homolog family member A guanosine triphosphatase (RhoA GTPase) [151]. Tuuminen *et al*, showed that inhibition of RhoA GTPase with simvastatin in the donor (pre-HTx) reduced post-HTx microvascular injury [151]. Further, inhibition of inflammation and leukocyte infiltration using an angiopoietin-1 analogue in the donor rat heart is reportedly protective for the post-HTx microvasculature, improving reflow and reducing acute rejection [152]. No-reflow is associated with pathological sequelae as a consequence of BSD [148], indicated by endothelial dysfunction outlined in section 1.2.2, and CSS which may contribute to the development of CAV.

CAV is characterised by a slowly developing, diffuse, concentric intimal thickening and remodelling of the affected vessel of the donor heart [16]. Due to the slowly developing nature of CAV, current diagnostic strategies can only detect 10-20% of CAV cases 1-year post-transplant, despite most of the hyperplasia occurring within the same timeframe. The development of CAV has been associated with multiple immunological mechanisms, but also non-immunological factors such as donor and recipient demographics, dyslipidaemia, endothelial activation (possibly transferred from donor BSD), donor hypertension, recipient history of cardiovascular disease, PGD and donor BSD [16, 153]. Vascular hyperplasia impedes the delivery of oxygen and nutrients to the myocardium potentially leading to graft failure, myocardial infarction, arrhythmia

and sudden cardiac death. It remains undetermined the specific contribution of transferred BSD cardiac damage, and whether CAV is causative of PGD or both CAV and PGD are symptoms of other immunological mechanisms.

Heart transplantation represents a unique set of events that unfortunately cause cardiac dysfunction, which opposes the main goal of curing end-stage heart failure. Events start at brain injury in the donor which creates a hyperactive haemodynamic state, progressing to a depressed haemodynamic state with impaired contractility and negative lusitropy subsequent to BSD. This may be due to catecholamine toxicity, endocrine changes, metabolic dysfunction and/or endothelial activation. Additionally, it is this dysfunction that hinders donor heart utilisation. This injured heart is then harvested and preserved statically in cold cardioplegia, where injury is exacerbated by depletions in energy and oxygen supply. These combined cardio-inhibitory effects are then transferred to the recipient, where further injury is added due to surgical procedures and reperfusion. It is pivotal to better understand the cardiovascular deterioration observed in the context of heart transplantation and the mechanisms behind this. A more detailed understanding of this area will lead to improved donor heart utilisation, subsequently increasing rates of transplantation, improving post-transplant cardiac function, ultimately decreasing mortality and morbidity and improving quality of life for end-stage heart failure sufferers.

1.4 | Aims and Hypotheses

Cardiac transplantation for end-stage heart failure is one of the most challenging complex health problems faced in intensive care units across the globe. This is partly due to the shortage of viable donor hearts and PGD post-transplant. The governing physiology behind these factors is still poorly understood, due to the logistical difficulties in modelling such a complex clinical scenario. This doctoral project aims to utilise a clinically relevant model of transplantation to investigate 3 main aspects of cardiovascular function, 1) cardiac adrenergic excitation-contraction-coupling and perfusion, 2) mitochondrial function and 3) metabolic regulation. By employing this ‘top-down’ approach, it is expected that a thorough investigation of cardiovascular function can be

determined. This systematic understanding may potentially serve the overarching clinical need to improve donor heart viability and consequently increasing the number of successful transplants.

1.4.1 | Aims

1. To develop a clinically relevant model of cardiac transplantation in sheep
2. Investigate the ventricular contractile response to (-)-noradrenaline in isolated trabeculae post-BSD and transplantation
    a. Investigate coronary vasculature endothelial and smooth muscle reactivity post-BSD and transplantation
3. Investigate mitochondrial respiration and membrane potential production post-BSD and transplantation
    a. Investigate ROS production post-BSD and transplantation
4. Profile the metabolomic consequences of BSD and transplantation

1.4.2 | Hypotheses

1. Ventricular contractile response to (-)-noradrenaline will be altered post-BSD and transplantation due to, β-adrenoceptor desensitisation and catecholamine toxicity
    a. BSD and transplantation will be characterised by poor endothelial and smooth muscle reactivity
2. Mitochondrial function will be altered post-BSD and transplantation, characterised by enhanced glucose oxidation capacity and higher ROS production
3. Metabolic regulation will be altered, with a preference toward glucose utilisation post-BSD and transplantation

STATEMENT OF CONTRIBUTION TO CO-AUTHORED PUBLISHED PAPER

This chapter includes a co-authored paper. The bibliographic details of the co-authored paper, including all authors, are:

Wells, M. A., See Hoe, L. E., Heather, L. C., Molenaar, P., Suen, J. Y., Peart, J., McGiffin, D., & Fraser, J. F. (2020) Peritransplant Cardio-Metabolic and Mitochondrial Function The Missing Piece in Donor Heart Dysfunction and Graft Failure, *Transplantation*: June 22, 2020 - Volume Online First - Issue - doi: 10.1097/TP.0000000000003368

My contribution to the paper involved:

In the production of this paper I was involved in the idea synthesis, data collection and synthesis and drafting.

(Signed) _____ (Date)13/09/2020
Matthew Wells

(Countersigned) _____ (Date) 13/09/2020
Corresponding author of paper: Matthew Wells

(Countersigned) _____ (Date) 15/09/2020
Supervisor: Jason Peart

Chapter 2

A SHEEP MODEL OF HEART TRANSPLANTATION FOLLOWING DONOR BSD

Contents

2.0 | Introduction

Disease states and their aetiology can only be fully understood if they are modelled in a realistic manner. The challenge in the context of HTx is the complexity of the clinical scenario. Currently, this scenario includes three main arms, donor heart identification, organ preservation and subsequent transplantation. Each arm in this process also has specific considerations that need to be met, further adding to the complexity of model development.

The current Australian National Health and Medical Research Council guidelines state an organ donor must be confirmed with irreversible brain injury, BSD; or irreversible cessation of circulation, donation after circulatory death (DCD) [154]. The majority of heart donors are retrieved from BSD donors (95%) as this pathway is more predictable and is currently associated with better transplant outcomes [154]. The main cause of death in these patients is haemorrhagic (39%), hypoxic/ischaemic (32%) or traumatic (16%) brain injury [155]. An important factor often overlooked in the context of modelling HTx studies is the duration of brain death. According to the ANZOD in the past 5 years, the average time from admission to brain death was 41.3 ± 2.7 hrs, and the time from BSD to organ donation was 21.2 ± 1.0 hrs [155].

Traditionally, the donor heart is preserved in cold preservation solution and placed on ice. This is referred to as CSS and has remained the gold standard for decades. The aim of CSS is three-fold, i) reduce myocardial metabolism, ii) maintain graft viability and reduce swelling, and iii) reduce IRI [106]. CSS however, cannot maintain graft viability for longer than 4-6 hrs from application of the aortic cross-clamp to reperfusion in the recipient, referred to as the ischaemic time [156]. This time limit often precludes the utilisation of donor hearts, especially in geographically vast countries such as Australia. CSS represents a significant period of time in the journey toward transplantation, and therefore is an important experimental feature.

Lastly, the donor heart journey ends with orthotopic HTx, meaning a HTx ‘in the natural position’. This is in contrast to heterotropic HTx where the donor heart is grafted in parallel with the native heart [157]. This procedure is widely used in studies investigating immunological rejection, often

not including a BSD donor or CSS period [157]. In humans, heterotropic HTx is seldom used except in specific circumstances [158]. Langendorff perfusion is a common strategy implemented in substitution to orthotopic HTx. This is suitable for functional analyses of grafts, however, it negates the physiology of the recipient.

Collectively, an appropriate model of HTx would include, i) a donor that has sustained irreversible brain injury and subsequently confirmed brain dead with a minimum of 20 hrs post-BSD time (as this is the average time from BSD to donation), ii) a cold static storage period between 4-6 hrs from cross-clamp to reperfusion and iii) orthotopic heart transplantation. Our group has previously developed a novel 24 hr model of ovine BSD which more closely resembles the current donor profile [159]. To extend on this model of 24-hrs BSD in sheep, we aimed to develop a HTx model that incorporated CSS and orthotopic HTx followed by a 6 hr monitoring period after weaning from cardiopulmonary bypass (CPB).

2.1 | Methods

All animal studies were conducted in accordance with the Australian Code for the Care and Use of Animals for Scientific Purposes. Ethical approval has been obtained through the Queensland University of Technology Animal Research Ethics Committee (approval #1600001109).

2.1.1 | Experimental Procedures

Twenty-four first-cross ewes, 47 ± 6 kg were semi-randomised into two main groups, influenced by blood cross-matching. Blood cross-matching was performed as previously described by Simonova et al [160]. Briefly, sheep were deemed compatible if no agglutination was observed over 4 tests; 1) two drops of saline, two drops of recipient sera and one drop 5% donor red blood cell (RBC) in saline, 2) as above, retested after 30 min incubation at room temperature, 3) Recipient serum and donor RBC incubated at 37°C for 30 min and 4) Sample from 3 was centrifuged (540 g for 1 min), supernatant removed, 10% albumin added and sample was re-examined for agglutination after 30 min at 37°C.

Group A consisted of heart donor animals that were exposed to brain stem death (BSD, n=6) or sham procedures (SHAM, n=6). Following either induction of BSD or SHAM, the animal was monitored for 24 hrs. Following the 24 hr monitoring period, Group A hearts were retrieved and underwent tissue analyses. Group B consisted of a separate group of donor hearts that progressed to orthotopic HTx into a healthy control sheep after the 24 hr donor monitoring period. The normal recipient heart was used as a biological control (HR, n=12). Both BSD and SHAM donor hearts progressed to transplantation. The donor heart was excised after cardioplegic arrest and preserved by CSS for ~100 mins. After transplantation and weaning from CPB, the animals were monitored for a further 6 hrs. Following this 6 hr period, transplanted hearts from BSD donors (BSD-Tx, n=6) and SHAM donors (SH-Tx, n=6) were retrieved and further tissue analyses undertaken. Figure 2.1 shows a schematic representation of the experimental design and timeline.

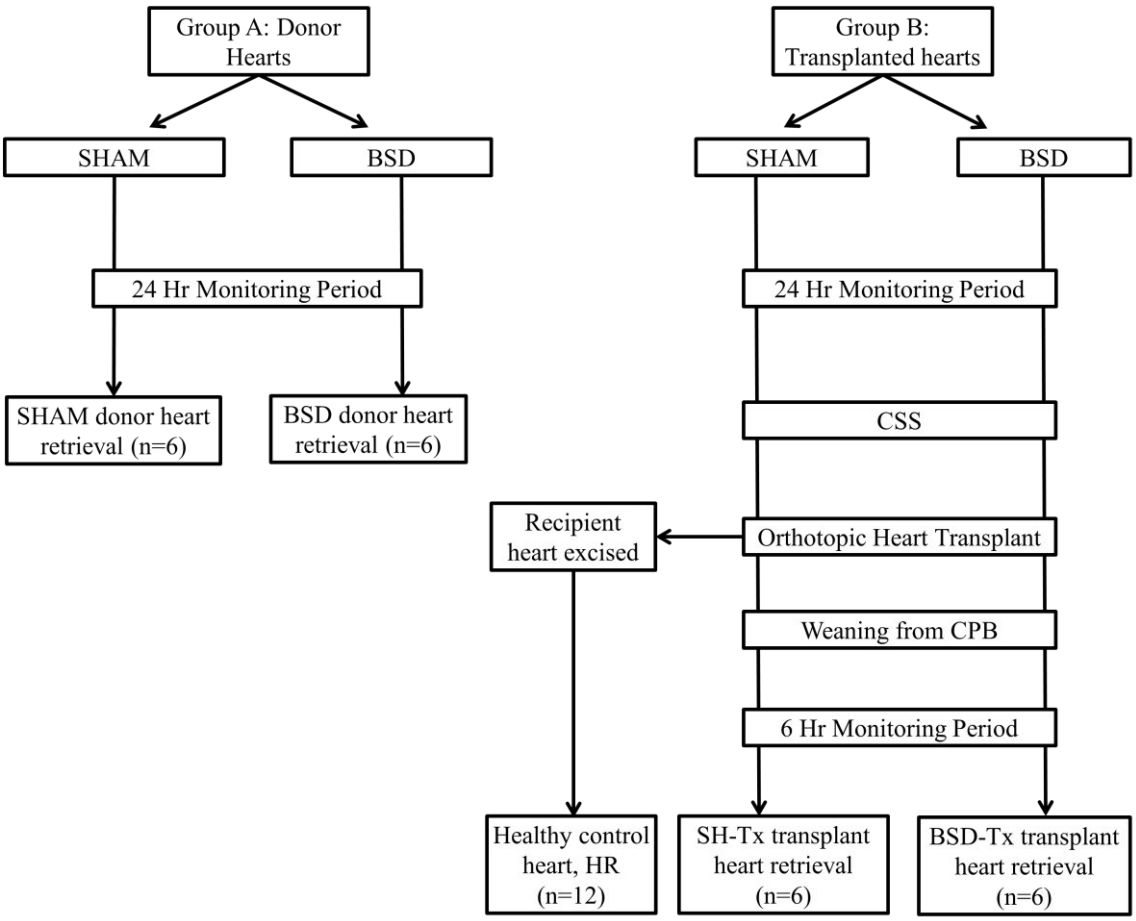

Figure 2.1. Flow diagram outlining experimental groups.

2.1.2 | Anaesthesia, instrumentation and monitoring

All sheep were fasted overnight prior to experimentation, with free access to drinking water. The animal was brought into the surgical theatre, local anaesthetic was administered (lidocaine 2%), and the external jugular veins were cannulated with a four-lumen 8.5 Fr central venous line (CVL; Arrow Int., Reading USA) and an 8 Fr venous sheath (Edwards Lifesciences, Irvine, USA). A baseline venous blood sample was collected. The animal was then induced with midazolam (0.5 mg/kg) and propofol (2.5-3 mg/kg), and antibiotics were administered (gentamycin 80 mg and cefazolin 2 g). The animal was then intubated with an 8-10 internal diameter endotracheal tube (Lo-Pro, Covidien, USA) and placed on the operating table in supine position. ECG, oxygen

saturation (SpO_2) and end-tidal carbon dioxide ($ETCO_2$) were continuously monitored. The animal was connected to a mechanical ventilator (Hamilton G5, Hamilton Medical, Switzerland) set as follows: tidal volume 8 ml/kg, positive end expiratory pressure (PEEP) 5 cmH_2O, respiratory rate (RR) adjusted to maintain arterial partial pressure of carbon dioxide ($PaCO_2$) at 40 ± 4 mmHg, and inspiratory fraction of oxygen (FiO_2) adjusted to maintain arterial partial pressure of oxygen (PaO_2) >60 mmHg. Anaesthesia and analgesia were maintained with continuous infusions of fentanyl (5 μg/kg/hr), midazolam (0.5-0.8 mg/kg/hr) and ketamine (2.5-7.5 mg/kg/hr). All animals received an initial i.v. bolus of 0.5-1 L Hartmanns (as guided by echocardiography and blood gas analysis to determine volume status), followed by a continuous i.v. infusion (1 mL/kg/hr) for the remainder of the experiment. A nasogastric tube and a yankuer cannula were placed into the stomach and the mouth, respectively, to continuously suction gastric and oropharyngeal secretions. Continuous infusion of potassium chloride (10-30 mmol/L/hr) was provided to maintain serum potassium at 4.0-4.5 mmol/L. The femoral artery was cannulated (3 Fr, Cook Medical, USA) for continuous arterial blood pressure monitoring and blood sampling. A pulmonary artery catheter (Swan-Ganz CCOmbo, Edwards Lifesciences, Irvine, USA) was inserted through the jugular introducer for continuous pulmonary pressures. A urinary catheter was then inserted to monitor urine output. Throughout experiments, fluid challenges and vasoactive support was provided to maintain haemodynamic stability, aiming at MAP ≥ 65 mmHg and urinary output ≥ 0.6 mL/kg/hr.

2.1.3 | Donor-specific procedures, induction of BSD and donor management

Following administration of vecuronium (0.1 mg/kg i.v.), a mini left thoracotomy was performed through the upper border of the 5th rib to cannulate the azygos vein drain with a 7 Fr 3-lumen central venous catheter (CVC; Arrow Int., Reading USA), which was then advanced approximately 3 cm to drain blood from the coronary sinus. The azygos vein was ligated over the catheter extra-pericardially. The distal lumen was used throughout the experiment for blood sampling from the coronary sinus.

Two burr holes (4.5 mm and 6 mm) were drilled into the skull [159]. Briefly, a midline incision on the skull was used to expose sagittal and lambdoid sutures. A burr hole was created 1.5 cm from and parallel to the sagittal and lambdoid sutures. A second burr hole was created in the same position, but on the contralateral side of the first burr hole. A 16 Fr Foley catheter (30 mL balloon) was placed in the right (6 mm) burr hole, and a 20-G intravenous cannula was inserted and secured into the left burr hole to monitor ICP. Once all the above procedures were complete, animals were rested for 1 hr.

In BSD animals, brain injury was developed by inflation of the Foley catheter with 10 mL sterile water every 5 mins (to a maximum of 60 mL) over 30 mins. In case of ST-segment elevation at the haemodynamic monitor, during the tachycardic and hypertensive response, 5 mg of metoprolol was administered intravenously every 2-3 min until ST-segment normalization. Brain death was confirmed by high ICP and continuous negative CPP (MAP-ICP), loss of haemodynamic response to ongoing Foley catheter balloon inflation, loss of pupillary and corneal reflexes and lack of respiratory efforts [159]. For sham donor animals, the Foley catheter was inserted, but not inflated, and these animals rested for an additional 30 minutes. Time 0 in the donor was designated at confirmation of BSD, or end of 30-minute additional monitoring for sham animals.

All donor animals were monitored for 24 hrs from Time 0. Arterial and coronary sinus blood, and urine samples were collected at regular intervals. Hormone resuscitation was administered 2 hrs following confirmation of BSD/sham. BSD animals received intravenously methylprednisolone 15 mg/kg, T3 4 μg bolus and 3 μg/hr thereafter, vasopressin 1.2 units/hr. Sham animals received same doses of methylprednisolone and T3, without vasopressin.

Following 24 hrs monitoring, the animal was placed supine position and a sternotomy was performed. A purse-string suture was placed in the ascending aorta for the cardioplegic needle. After full heparinisation, the superior vena cava was clamped, and the inferior vena cava was divided extra-pericardially to exsanguinate the animal. The ascending aorta was clamped and ice-cold St Thomas's cardioplegic solution (Baxter Healthcare Pty Ltd, NSW, AUS) [mmol/L; Na^+

120, Cl^- 160, K^+ 16, Mg^{2+} 16, Ca^{2+} 1.2, HCO_3^- 10] was infused into the aortic root (20 mL/kg bodyweight). The donor heart was then explanted by dividing the superior vena cava, pulmonary veins, ascending aorta and main pulmonary artery. Following explant the donor heart was preserved in an organ bag containing 1 L ice-cold St Thomas cardioplegia, and placed in an additional organ bag containing ice slush (0.9% Saline). The organ bag was then placed in an ice cooler containing ice slush for approximately 100 minutes.

2.1.4 | Recipient procedures and orthotopic heart transplantation

All recipients were prepared and instrumented as stated above (Section 2.1.2). Following administration of vecuronium (0.1 mg/kg i.v.), the animal was placed in supine position and the chest opened via median sternotomy. Purse-string sutures were placed in the ascending aorta, level with the take-off of the aortic arch, superior vena cava and inferior vena cava extra-pericardially within the pleural space. Caval tapes were placed around the superior and inferior vena cava. Prior to placement on CPB, lignocaine (1-2 mg/kg), amiodarone (5 mg/kg) and heparin (100-300 U/kg, to achieve ACT >400 sec) were administered intravenously. The CPB circuit was primed with 2-3 units of compatible ovine packed red blood cells [20]. After heparinization, the aorta was cannulated with a 16-Fr elongated one-piece EOPA® cannula (Medtronic, USA), and the superior and inferior vena cava were cannulated with a 24-Fr and 28-Fr right-angled cannulae (Medtronic, USA), respectively. The cannulae were then connected to the CPB circuit and CPB was commenced. The perfusate temperature was reduced to achieve a core temperature of 32°C. The azygos vein, which drains into the coronary sinus was ligated in the left pleural space. The ascending aorta was cross-clamped and the recipient heart was removed by transecting the ascending aorta, main pulmonary artery, and superior vena cava at the cavoatrial junction, dividing the inferior vena cava at the right atrial inferior vena cava junction. The heart was then transected to form the left atrial cuff through the atrioventricular groove, for the specific purpose of providing thicker muscle in the left atrial cuff and ensure that the left atrial suture line was quite haemostatic.

Once CPB was established and the recipient heart removed, standard orthotopic HTx was performed. The recipient left atrial cuff circumference formed by the atrioventricular groove tissue was smaller than if the cuff was fashioned by taking the excision line through the thin left atrial wall. Therefore, the left donor pulmonary veins were oversewn (5/0 Prolene) since incising the muscle between all of the pulmonary veins would have resulted in an excessively large donor left atrial cuff. The right sided pulmonary vein orifices only needed a small amount of enlargement to match the recipient left atrial cuff. Anastomoses were performed in the following order: left atrium (continuous 4/0 Prolene), inferior vena cava (continuous 4/0 Prolene), superior vena cava (continuous 5/0 Prolene), pulmonary artery (continuous 5/0 Prolene), ascending aorta (continuous 4/0 Prolene). Following completion of anastomoses, de-airing was performed with a needle vein in the ascending aorta and the aortic cross-clamp removed. If ventricular fibrillation occurred, internal defibrillation was performed (5-20 Joules) and 300 mg of amiodarone was administered based on need. The cardiac allograft was reperfused for 30 mins before attempting to wean from CPB. Venous return to the pump was ceased when the following criteria were achieved: spontaneous or pacing heart rate of 80 to 90 beats/minute; MAP > 60 mmHg without maximal vasoactive support (dopamine > 15 mcg/Kg/min or Epinephrine/Norepinephrine > 0.1 kg/min or vasopressin at any dose); adequate filling of the ventricles as observed through epicardial echocardiography. After complete separation from CPB, the venous cannula was removed and caval cannulation site pursestring sutures were tied. Blood remaining in the venous tubing was returned to the venous reservoir for transfusion back to the animal. Finally, the aortic cannula was removed, and the cannulation site repaired. If residual blood remained in the extracorporeal circuit reservoir, it was transfused through the CVL. Finally, anticoagulation was reversed with 20-25 mg of protamine. Animals were monitored for an additional 6 hrs following successful separation from CPB.

2.1.5 | Functional characterisation

Standard haemodynamic measures included systolic (SBP), diastolic (DBP) and mean arterial blood pressures, ECG abnormalities and arrhythmia incidence. Haemodynamics were calculated at baseline (BL), during BSD (BSD), at BSD confirmation (0 hr) and hourly thereafter. Post-HTx haemodynamics were calculated 30 mins (0.5), 1, 2, 3, 4, and 6 hrs after weaning from CPB. Haemodynamic measures were calculated from a rolling 5 min average over a 20 min period (10 min before and after) the indicated time-point using LabChart 8.0 (AD Instruments).

2.1.6 | Blood sample collection and processing

Arterial blood samples were collected at BL, 0 hr, 1 hr, 2 hr, 3 hr, 4 hr, 6 hr post-BSD and then every third hour thereafter (Fig 2.2). Post-Tx, blood samples were collected 0.5, 1, 2, 3, 4, and 6 hrs post-CPB. Samples were spun twice at 1500 x g for 15 mins at 4°C, snap frozen and stored at -80°C. Arterial plasma was assessed for levels of metanephrine (MET), normetanephrine (NMET) and cardiac troponin I (cTnI). cTnI was determined using an enzyme linked immunosorbent assay (ELISA) cat# CTNI-9-HSP (Life Diagnostics, Incorporated, Pennsylvania, USA), as per the manufacturers guidelines.

Plasma (EDTA) samples were sent to IDEXX Laboratories for external assessment of full blood counts, biochemistry and plasma free catecholamines (MET and NMET). Full blood counts were analysed on a Sysmex XT2000i-V haematology analyser, and assessment of blood biochemistry was undertaken using a Beckman Coulter AU680 ISE chemistry analyser as per standard manufacturers protocols. Plasma free MET and NMET were measured by an automated on-line Solid Phase Extraction (SPE) coupled to an ultrahigh performance liquid chromatographic system (UPLC). Plasma samples were diluted 1:1 with deuterated internal standards in a zinc sulfate/acetonitrile solution in 2 mL 96-well plates. After centrifugation, an aliquot of sample was injected into the on-line SPE equipped UPLC-tandem mass spectrometry (MS/MS) system. The purified extracts were eluted from the Mass Track Oasis WCX OSM cartridges onto the ACQUITY UPLC BEH Amide column, utilising a gradient of 100 mM ammonium formate, pH

3.0 and acetonitrile. Quantification was achieved by monitoring two transitions for each analyte on a Waters Xevo TQD mass spectrometer (Waters Corporation, MA, USA). The assay time between injections was 4.5 minutes. The analytical range of the assay was up to 100,000 pmol/L. The limit of quantitation (LOQ) with a coefficient of variation (CV) of 20% was 20 pmol/L for all analytes. The inter-run imprecision across 3 levels for the analytes were all < 8%.

2.1.7 | Heart Collection

For Group A, the donor heart was retrieved following the 24 hr monitoring time. Group B, post-transplanted hearts were retrieved at the end of the 6 hr monitoring time or earlier depending on clinical indications such as profound hypotension non-amenable to vasopressor treatment. After hearts from Groups A and B were excised, they were placed immediately in ice cold oxygenated Krebs solution [in (mM): Na^+ 125, K^+ 5, Ca^{2+} 2.25, Mg^{2+} 0.5, Cl^- 98.5, SO_4^{2-} 0.5, HCO_3^- 32, HPO_4^{2-} 1 and EDTA 0.04, pH 7.34-7.42, pO_2 >800 mmHg] and transported to the laboratory for further tissue analysis. Krebs solution was utilised as the transport solution to align with validated methods for *in vitro* contractile investigation, and to normalise across various organ bath experiments outline in subsequent chapters. Specific details of tissue collection for each tissue assay will be explained in the subsequent chapters.

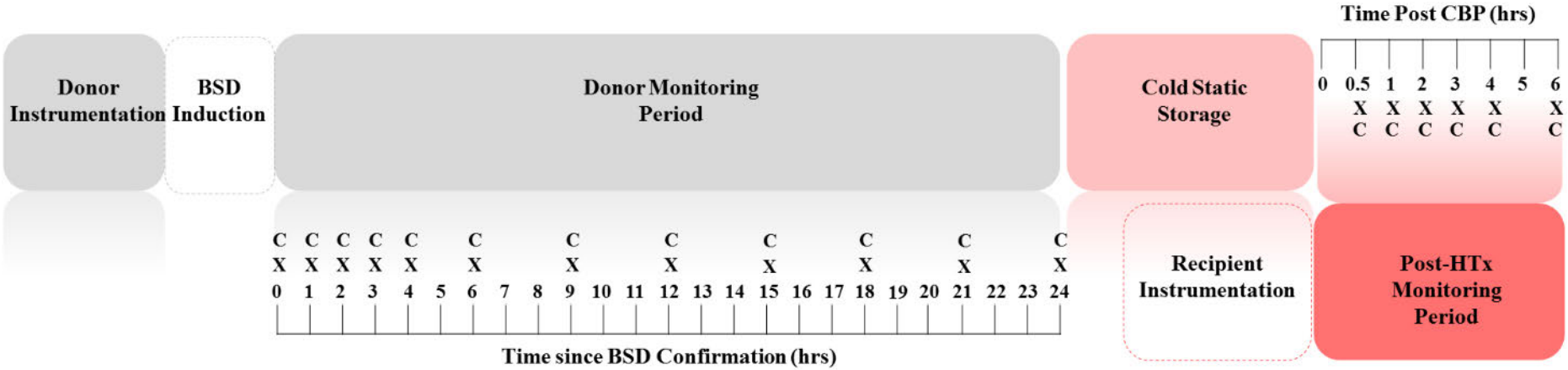

Figure 2.2. Schematic overview of HTx model timeline. C- Catecholamine analysis, X- blood sample

2.1.8 | Statistical Analysis

Statistical analyses were performed using GraphPad Prism version 8.0. Repeated measures analysis of variance (RmANOVA) was used to determine temporal differences in cardiac performance with Tukey's post-hoc analyses and multiple comparison correction. One-way ANOVA with Tukey post-hoc analyses were performed to assess between group effects. A $p<0.05$ was considered statistically significant.

2.2 | Results

During the donor period, all 24 animals including those that progressed through to transplant survived until the 24 hr end-point. There were no changes in baseline characteristics between any of the donor or recipient blood gas measurements, weights, or donor to recipient weight ratios (Table 2.1).

2.2.1 | Clinical outcomes following donor procedures

Total ischaemic times (aortic cross-clamp to reperfusion) were similar ($p=0.34$) for both BSD-Tx ($n=6$, 169.57 ± 11.7 mins) and SH-Tx ($n=5$, 169.67 ± 10.98 mins). Cold ischaemic time was also similar for both BSD-Tx (99.86 ± 9.4 mins) and SH-Tx groups (101.6 ± 7.3 mins). Post-CPB monitoring time varied for both groups and was non-significantly shorter for the SH-Tx group ((4.0 ± 0.89 hrs) compared to BSD-Tx (4.92 ± 0.68 hrs)).

All 6 BSD-Tx and 6 SH-Tx recipients were successfully weaned from CPB however, 25% [3/12 hearts; 1-BSD-Tx & 2-SH-Tx] were terminated prior to 6 hrs end-point due to consistently low MAP not amenable to inotropic support. All clinical data for these animals was included up until 2 hrs post-CPB and the heart was used for tissue analysis. One of the SH-Tx experienced vasoplegic shock, survived only 20 mins post-CPB. Consequently, this heart was not used for tissue analysis and therefore was excluded, due to the likelihood of significant cellular damage and to undergo a full autopsy in accordance with ethical guidelines. The final sample sizes per group are outlined in figure 2.3.

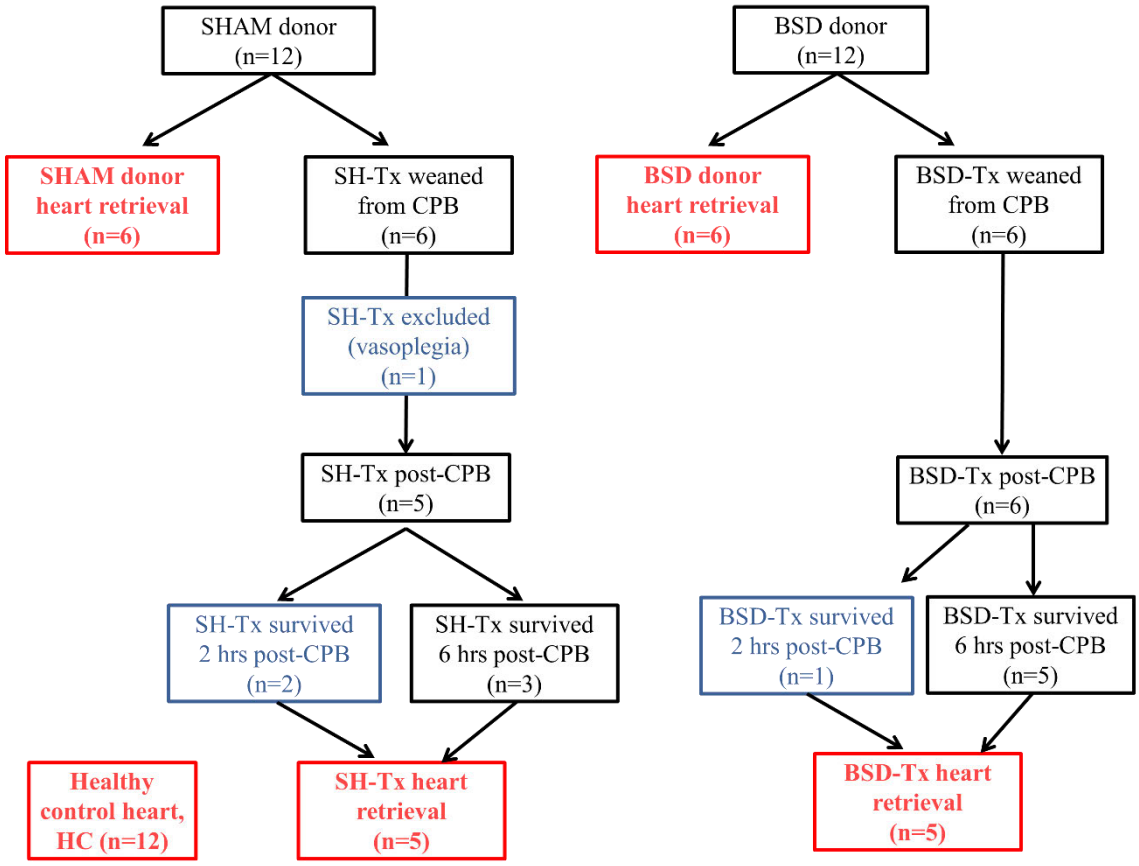

Figure 2.3. Flow diagram outlining final group numbers (red boxes) for tissue analysis (heart retrieval) and blood analysis (clinical data)

Table 2.1. Baseline characteristics between each group. Data are expressed as means (±SE)

	SHAM (n=6)	**BSD (n=6)**	**SH-Tx (n=5)**	**BSD-Tx (n=6)**	**HR (n=12)**
Weight	49.75 (2.78)	52.17 (1.76)	44 (2.16)	45 (3.25)	47.63 (1.95)
Donor-recipient weight ratio*	-	-	0.95 (0.06)	1.01 (0.11)	-
pH	7.43 (0.01)	7.42 (0.03)	7.42 (0.07)	7.46 (0.03)	7.44 (0.02)
pCO_2 (mmHg)	36.63 (1.33)	38.5 (2.84)	38.95 (6.16)	36.57 (1.72)	38.43 (3.04)
pO_2 (mmHg)	139 (16.82)	112.5 (9.93)	166 (27.53)	173 (28.9)	235.4 (11.82)
ctHb (g/dL)	8.78 (0.76)	8.02 (0.86)	8.98 (0.82)	8.82 (0.36)	8.46 (0.37)
Hct %	22.23 (6.75)	25 (2.59)	27.9 (2.48)	27.4 (1.10)	26.24 (1.12)
K+ ($mmolL^{-1}$)	3.2 (0.39)	3.07 (0.16)	2.93 (0.21)	3.02 (0.20)	3.19 (0.14)
Na^+ ($mmolL^{-1}$)	135.8 (1.32)	136.2 (1.40)	134 (2.48)	142.7 (3.34)	141.4 (1.10)
Ca^{2+} ($mmolL^{-1}$)	1.15 (0.03)	1.13 (0.01)	0.99 (0.06)	1.17 (0.09)	1.17 (0.01)
Cl- ($mmolL^{-1}$)	103.8 (1.25)	104.2 (1.45)	102.5 (2.60)	98.67 (5.38)	107.3 (0.80)
Glucose ($mmolL^{-1}$)	4.9 (1.56)	5.73 (1.53)	4.6 (0.79)	3.82 (0.27)	3.95 (0.27)
Lactate ($mmolL^{-1}$)	1.78 (0.53)	2.08 (0.35)	1.45 (0.28)	2.02 (0.48)	1.43 (0.48)

Data represents post-instrumentation measures, where animals were ventilated, *ISHLT guidelines suggest not using donor-recipient weight ratios <0.70 to avoid adverse effects [161].

2.2.2 | Vasoactive support

Donor vasoactive support included noradrenaline (SHAM and BSD) and dopamine (BSD only). Noradrenaline infusions were higher for BSD donors 1-3 hrs post-BSD confirmation, with the highest rate at 0.26 ± 0.07 μg·kg·min^{-1}, falling thereafter to a low requirement of 0.03 μg·kg·min^{-1} at 24 hrs. The same trend was observed for dopamine infusions with the highest rate at 3 hrs (3.13 ± 1.1 μg·kg·min^{-1}) falling to 0.33 μg·kg·min^{-1} at 18 hrs where infusions were ceased (Fig 2.4B). Post-Tx, both SH-Tx and BSD-Tx noradrenaline infusions steadily increased from ~0.18 at 30 mins post-CPB to 0.23 (SH-Tx) and 0.42 (BSD-Tx) at 6 hrs (Fig 2.4C). Adrenaline infusions for the SH-Tx group were highest 30 mins post-HTx after plateauing 2-6 hrs thereafter. For the BSD-Tx group, adrenaline infusions were stable at around 0.3 μg·kg·min^{-1} 30 mins-6 hrs post-CPB. Analysis by RmANOVA showed no significant differences in inotrope usage between SH-Tx and BSD-Tx groups from 0.5 – 2 hrs post-CBP. Statistical analyses were performed up to 2 hrs post-CBP as all animals in both groups (SH-Tx, n=5 and BSD-Tx, n=6) survived till this time. This reduces the impact differing sample sizes has on statistical power.

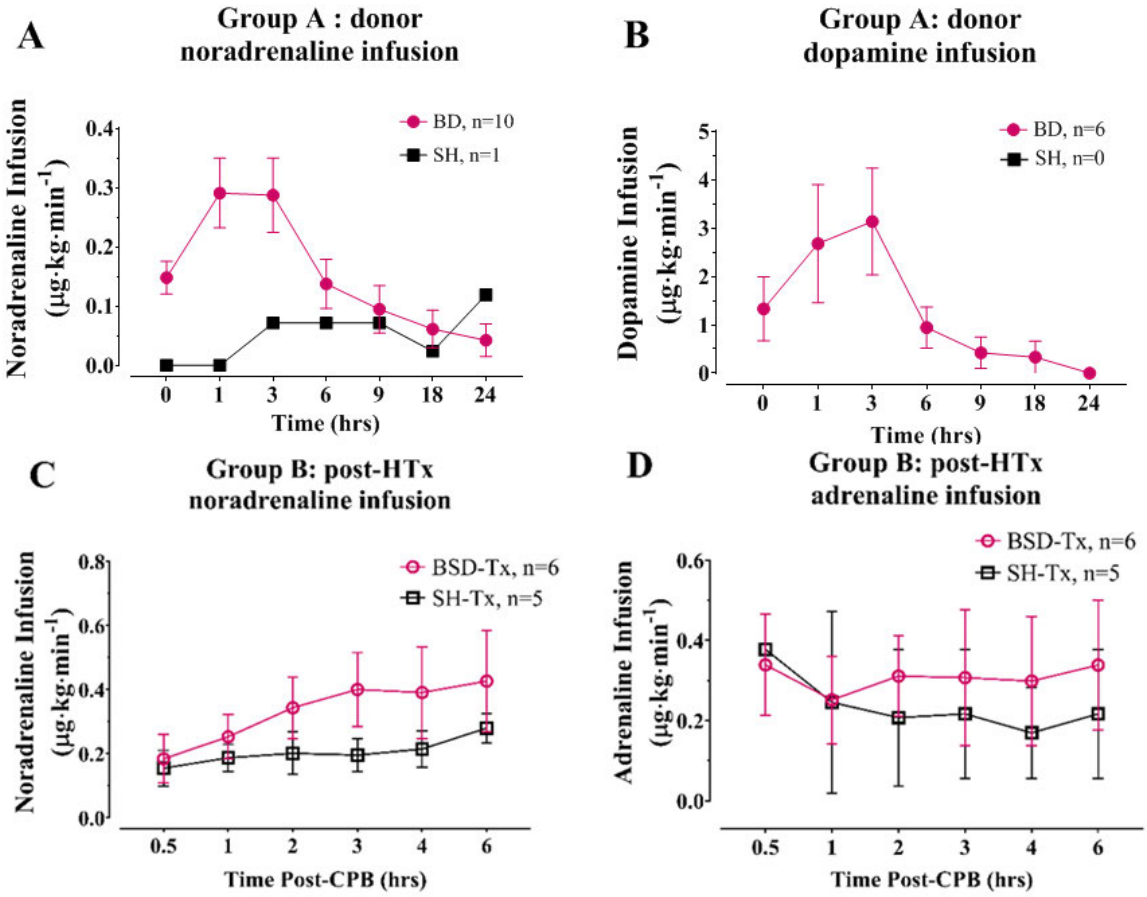

Figure 2.4. Vasopressor use for groups A and B. (A&B) pre-transplant donor period and (**C&D)** post-transplant period. Data represents means ±SE, sample size (n) values are representative of the animals that required vasopressor support not total group numbers.

2.2.3 | Donor Haemodynamics and Biochemistry

Electrocardiographic abnormalities were observed in all BSD and SHAM donors. The most common arrhythmia observed was sinus tachycardia, present in both SHAM and BSD donors. Sustained supraventricular tachycardia was present in only the BSD donors, 42.9% of the time ($p=0.01$, compared to incidence in SHAM, n=23 (all animals during the donor period)). Other ECG findings present in the BSD donor were inverted T-waves (75%), ventricular ectopy (75%), ST elevation/depression (33.3%) and atrial ectopy (25%). Initiation of BSD significantly increased heart rate [BL vs: BSD, $p=0.019$; 0, $p=0.012$; 1, $p=0.018$, n=23] (Fig 2.5B), before returning to baseline 2 hrs post-BSD. Following BSD, there was a trend toward reduced PR, QRS and QTc intervals. After BSD confirmation, all ECG measures returned to baseline and were not statistically different compared to SHAM donors.

Compared to SHAM animals, MAP in the BSD donor significantly increased during BSD [$p<0.0001$, n=23] and dropped immediately at BSD confirmation (0 hrs) (Fig 2.5A). MAP remained depressed up to 3 hrs post-BSD confirmation. There was no difference in MAP between BSD and SHAM donors 1-24 hrs post-BSD confirmation.

Donor BSD induced a significant release of cTnI, reaching a peak 3 hrs post-BSD [3 hrs:$p<0.0001$, 6 hrs:, $p<0.001$, 9 hrs: $p=0.0001$, 12 hrs: $p=0.003$, 15 hrs; $p=0.044$, n=23] and thereafter slowly falling until 18 hrs post-BSD where levels were similar to SHAM donors (Fig 2.5C). Plasma MET levels were significantly increased post-BSD [0 hr: $p=0.0071$, n=23] and fell to similar levels as SHAM donors after 1 hr post-BSD [1 hr: $p=0.0015$, n=23] (Fig 2.5D). Plasma NMET levels also significantly increased post-BSD [0 hr: $p=0.0001$, n=23], and remained elevated 9 hrs post-BSD [1 hr: $p=0.0031$, 3 hr: $p=0.0022$, 6 hr: $p=0.0012$, 9 hr: $p=0.0007$, n=23] until falling to SHAM levels (Fig 2.5D).

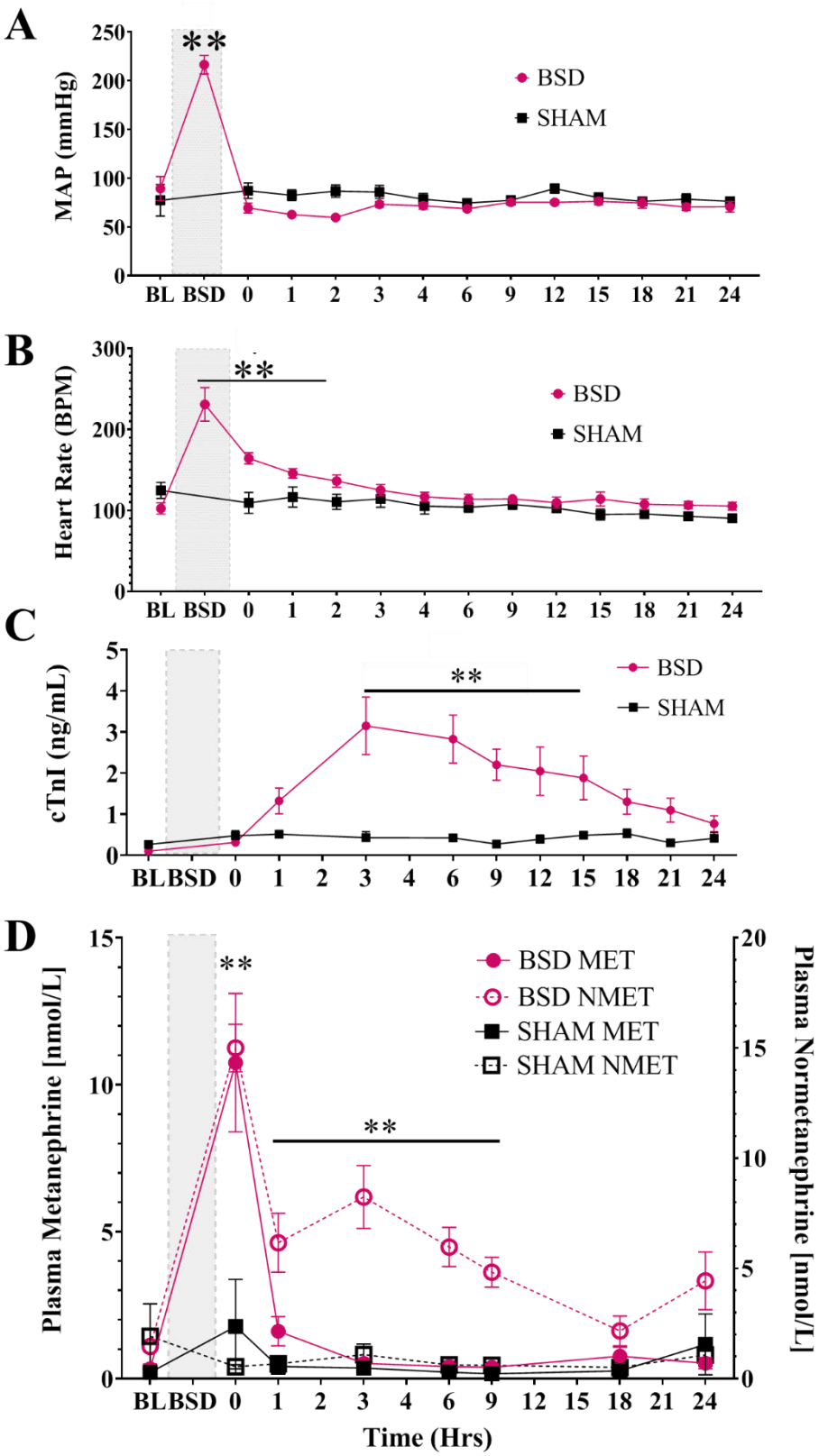

Figure 2.5. Cardiac biochemistry and haemodynamics across the 24hr donor time between BSD and SHAM donors. Indices recorded throughout care and included **A)** MAP, **B)** heart rate, **C)** cTnI and **D)** MET and NMET plasma levels. Shaded area indicates during BSD induction. ** significantly different from SHAM $p<0.01$

2.2.4 | Post-Engraftment Haemodynamics and Biochemistry

One SHAM donor heart experienced significant contractile dysfunction, progressed to ventricular fibrillation non-amenable to cardioversion or pharmacotherapy, and did not survive beyond 30 mins post-CPB. This heart was not used for *in vitro* or tissue-based assays due to the likelihood of significant cellular damage and in accordance with ethical guidelines. Since 25% of the transplanted hearts survived up until 2 hrs post-CPB, all clinical measures were statistically interrogated up until 2 hrs post-CPB as all animals (n=11) survived until this time point.

ECG abnormalities were observed in all post-Tx experiments regardless of donor type, with all animals in sinus tachycardia throughout the monitoring period. Transplants from both SHAM (SH-Tx) and BSD (BSD-Tx) donors experienced similar frequencies for ventricular tachycardia, T-wave abnormalities and ST depression/elevation. The QRS interval trended toward shortening (105-60 ms), 30 min to 6 hrs post-CPB in SH-Tx. For BSD-Tx, QRS interval trended toward lengthening (59-89 ms), 30 min to 6 hrs post-CPB. The QTc was significantly prolonged in SH-Tx throughout the monitoring period compared to BSD-Tx. No significant trends were observed within groups for the QTc interval.

MAP was depressed (<70 mmHg) throughout post-CPB time for both BSD-Tx and SH-Tx (Fig 2.6A). There were no significant changes within groups during this time. cTnI for BSD-Tx animals, 30 mins to 6 hrs post-CPB was 3-5 times greater than the donor period, trending upward to 14.94 ng/mL. For SH-Tx animals, cTnI was significantly elevated 30 min to 2 hrs post-CPB above BSD-Tx levels (Fig 2.6C). This was due to very high levels, above the maximum concentration assessable (200 ng/mL) in 2 experiments where the animal died thereafter. Levels of cTnI 3-6 hrs post-CPB for SH-Tx were similar to BSD-Tx (Fig 2.6C).

There were no significant differences within or between recipient groups for plasma MET or NMET (Fig 2.6D). SH-Tx MET levels were elevated 10 times greater than pre-Tx donor period 30 min to 2 hrs post-CPB before falling to pre-Tx levels. NMET levels remained stable and similar to pre-transplant donor levels. For BSD-Tx, both MET and NMET levels began to elevate 2 hrs

post-CPB and were approximately 10 times greater at 4 hrs post-CPB compared to pre-transplant donor period (during BSD).

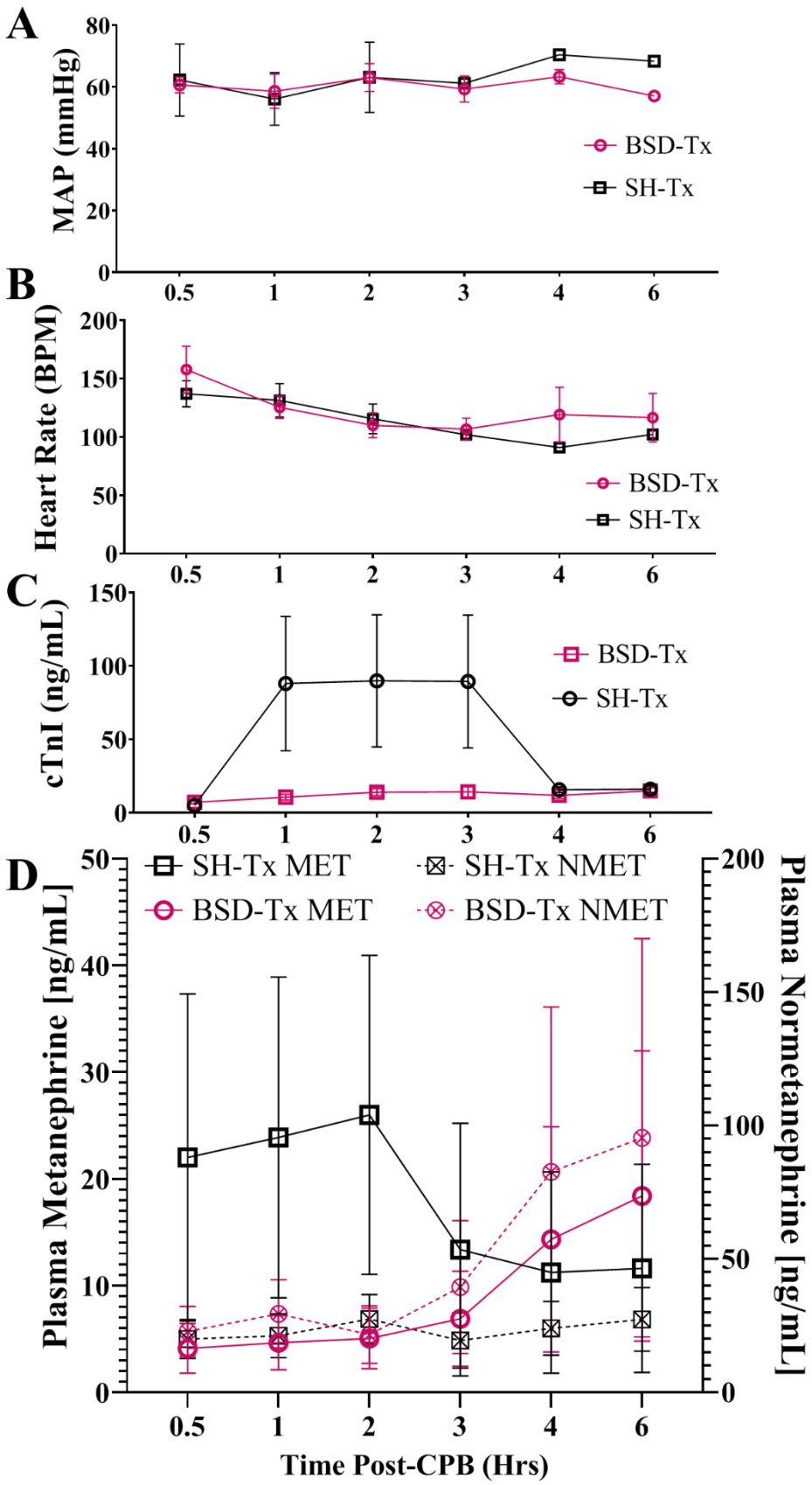

Figure 2.6. Cardiac biochemistry and haemodynamics 6 hrs post-CPB for SH-Tx and BSD-Tx recipient groups. Indices recorded throughout care and included **A)** MAP, **B)** heart rate, **C)** cTnI and **D)** MET and NMET plasma levels.

2.3 | Discussion

Our group has built upon an established 24 hr model of BSD in sheep by successfully transplanting both BSD and SHAM operated donor hearts. The BSD donor animals showed the characteristic profile of brain injury and subsequently BSD. The majority of donor hearts were successfully weaned from CPB, although post-transplant cardiac function was heterogeneous for both groups.

2.3.1 | The Donor

Sheep heart anatomy and haemodynamics share similarities with that of the human, and sheep have been shown to be an appropriate species to model human cardiovascular physiology [162]. We have successfully replicated the average heart donor, both in BSD aetiology, its physiological consequences and medical management of the donor. This approach closely matches the clinical scenario by capturing donor cardiac dysfunction due to brain injury, and the possible effects of medical management. The pathophysiology of BSD presented here is similar to other animal models of BSD showing the characteristic catecholamine storm, ECG changes, cardiac enzyme release and haemodynamic response [13, 38, 66, 85]. The hyperdynamic response, tachycardia and hypertension was prominent and lasted 1 hr post-BSD confirmation. The hypodynamic phase included hypotension and was observed up to 3 hrs post-BSD confirmation, thereafter elevating to normal levels in response to vasoactive management which began 2 hours post-BSD confirmation.

2.3.2 | Post-Transplant

In this series of transplantations, hearts procured from SHAM donors generally performed worse than BSD donor hearts, with only 50% reaching the 6 hr endpoint. These SH-Tx procedures were complicated and terminated at 2 hrs, generally due to vasoplegic shock. VS is a low systemic resistance in the presence of a normal cardiac output precipitating hypoperfusion. This is clearly demonstrated by the release of cTnI, hyperlactaemia and prolonged QTc in the SH-Tx group. VS is usually treated with catecholamines, contributing to the large plasma catecholamine profile observed for SH-Tx.

Clinically, VS can complicate 5-25% of cardiac surgery cases, where a randomised control trial found vasopressin to be an effective treatment for VS in this population [163-165]. Post-HTx rates of vasoplegia syndrome are believed to be slightly higher, found in ~31% of recipients [166]. As surgical procedures were matched, VS should therefore equally affect both transplantation groups. Elevated cTnI, hyperlactaemia and prolonged QTc were also observed in the BSD-Tx group, albeit at lower levels. A limitation relevant towards VS is the exclusion of the SH-Tx heart that did not survive past 20 mins post-CPB. Tissue analysis may have provided useful insight into the mechanisms of VS. Further, histological analysis of these post-HTx hearts, nor donor hearts was performed and therefore the degree of tissue ischaemia was not evaluated.

Donor BSD may, paradoxically, offer a level of cardioprotection prior to transplantation leading to enhanced cardiac function and therefore improved vasoplegia response. There is a large body of evidence that shows pre-ischaemic β-adrenoceptor stimulation can improve outcomes following ischaemia-reperfusion injury by reducing infarct size [167]. Other factors may also initiate VS, including the release of DAMPs, ROS and catecholamine resistance [165]. DAMPs are well-known to be involved in feedback mechanisms involving mitochondria, mitochondrial DNA being a well-known DAMP [168]. Although a heart transplant from a non-BSD or brain-injured donor is unlikely clinically, identifying specific perturbations between groups may help to improve the viability of the BSD donor heart.

2.4 | Conclusion

The first aim of this project was to replicate the steps involved in human HTx with a clinically relevant 24 hr sheep model of BSD recently developed by our group. We have shown that BSD induction in our model results in a haemodynamic and biochemical profile similar to that observed in clinical cases of BSD and previous animal models. Following this, we simulated organ preservation via CSS, the standard clinical approach, and progressed to successful orthotopic HTx including an off by-pass monitoring time. By incorporating these steps, we have very closely re-created the clinical journey of the donor heart. Using this model, hearts from both the donor period and post-transplant period can be assessed for determinants of cardiac function. The

following chapters will explore cardiac function with a focus on β_1-adrenoceptor-mediated contractility, mitochondrial function and metabolism. This mechanistic approach is expected to elucidate aberrant physiological processes that contribute to poor cardiac function post-BSD and post-transplant observed here

CHAPTER 3

IN VITRO CONTRACTILITY AND CORONARY VASCULAR REACTIVITY IN BSD AND HTX

Contents

3.0 | Introduction

The shortage of viable donor hearts is a global problem facing HTx. A major contributor to this shortage is the sad fact that ~48% of hearts offered for HTx are rejected for medical reasons [9]. Approximately one-third of these hearts are rejected due to poor contractile function [10]. The majority of donor hearts are received from patients who have sustained irreversible BSD, which is frequently accompanied by variable degrees of poor cardiac contractile function.

The primary focus of this chapter is to address the hypotheses that BSD-mediated pathophysiology, cold organ preservation and transplantation induce 1) contractile dysfunction, 2) altered adrenergic signalling and 3) vascular dysfunction. Previous work has highlighted the significance of these two physiological responses in important models, albeit utilising shorter BSD time-frames. The work hereafter will demonstrate whether these changes are valid in a longer model of BSD leading to HTx.

3.0.1 | Normal adrenergic signalling

In the context of adrenergic signalling, the most important catecholamines are adrenaline and noradrenaline which act on adrenergic receptors (ARs), members of the G-protein coupled receptor (GPCR) family. Two classes of ARs are present in the heart; alpha-ARs subdivided into three α_1-ARs (α_{1a}, α_{1b}, α_{1d}) and three α_2-ARs (α_{2a}, α_{2b}, α_{2c}) and beta-ARs, subdivided into β_1-, β_2 and β_3-ARs [57]. α_1-ARs are primarily expressed in the vasculature and are critical in controlling blood flow via vasoconstriction, whereas α_2-ARs are expressed in presynaptic nerve endings and control the reuptake of noradrenaline in a negative feedback [169, 170]. The β-ARs are highly expressed in the heart and regulate heart rate (chronotropy), force of contraction (inotropy) and rate of relaxation (lusitropy). The β_1 subtype is the predominant subtype, expressed ~60% higher than that of β_2s and important in the context of HTx [170].

β_1-ARs generate a cellular response by coupling to Gαs proteins which activate adenylyl cyclase, generating cAMP to PKA (Fig 3.1 extracted from [171]) [57]. Activation of PKA is the major effector involved in β_1-ARs cellular response, due to the phosphorylation and regulation of

multiple sites, predominantly involved in intracellular Ca^{2+} concentration ($i[Ca^{2+}]$). Increases in $i[Ca^{2+}]$ result from the phosphorylation of L-type Ca^{2+} channels and ryanodine receptors located on the sarcoplasmic reticulum. Phosphorylation of phospholamban by PKA enhances the uptake of $i[Ca^{2+}]$ into the sarcoplasmic reticulum via SERCA after contraction, which enhances the bioavailability of Ca^{2+} for the next contraction. PKA also mediates positive lusitropy by binding to troponin I and myosin binding protein C, reducing their sensitivity to Ca^{2+}; in conjunction with phospholemman phosphorylation alleviating its inhibition of the Na^{+}/K^{+}-ATPase pump and enhancing relaxation [57]. Additionally, in pacemaker cells, cAMP binds to potassium/sodium hyperpolarization-activated cyclic nucleotide-gated channel 4 to enhance Ca^{2+} handling and increases automaticity (positive chronotropic effect). To prevent deleterious cellular effects of sustained agonism, the β_1 receptor, like many GPCRs, is negatively regulated through heterologous and homologous desensitisation [169, 170].

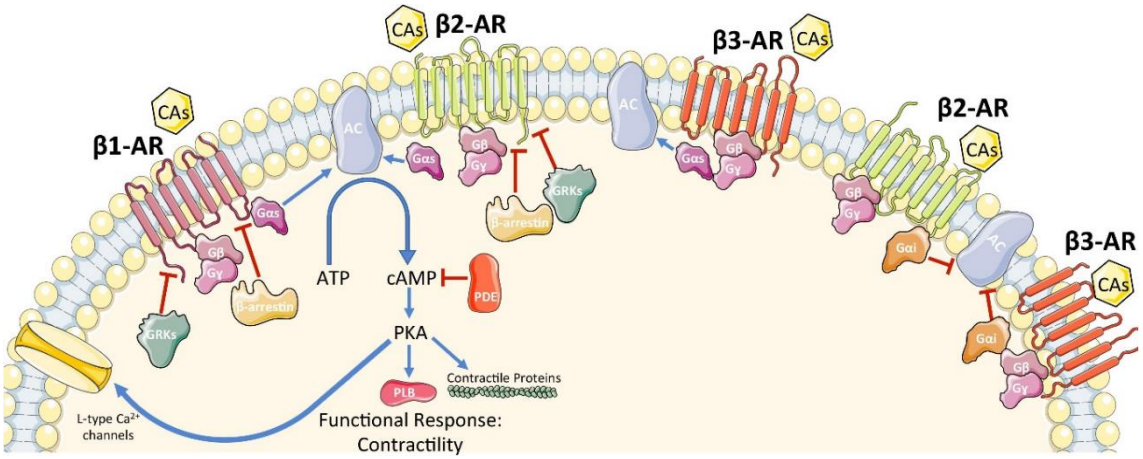

Figure 3.1. Schematic overview of β-adrenergic receptors and their signalling pathways in the heart extracted from Lucia *et al.*, 2018. Upon activation by catecholamines (CAs), beta 1 and 2adrenoreceptors (β1/2-AR) activate receptor coupled G-proteins (Gα/β/γ) to activate adenylyl cyclase (AC), in turn activating cyclic AMP (cAMP) and protein kinase A (PKA) signalling. This cascade results in a contractile response in cardiomyocytes. Chronic overactivation may lead to the inhibition of cAMP by phosphodiesterases (PDE) and/or the deactivation and internalisation of the β-AR's by β-arrestin and g-protein coupled receptor kinases (GRKs) (discussed in section 3.3).

3.0.2 | Normal vascular function

The coronary vascular network can be divided structurally and functionally into 3 compartments, the conduit (500 um-5 mm), prearteriolar (100-500 μm) and arteriolar (< 100 μm) compartments [79]. Functionally, the conduit vessels are responsive to flow and store elastic energy during systole, which is converted to kinetic energy during diastole, allowing myocardial perfusion [79]. The prearteriolar vessels are most responsive to pressure and regulate arteriolar pressure, which in turn is regulated by myocardial metabolites [79, 172]. Metabolite regulation of arteriolar tone permits the matching of myocardial oxygen demand to supply. To achieve these actions, VSM tone is tightly regulated by the vascular endothelial layer via endothelial-dependent and independent mechanism of VSM tone.

Vasodilation can be achieved via the release of endothelium-derived relaxing factors (EDRFs) in response to endothelium-dependent vasodilators or via direct stimulation of VSM by endothelium-independent vasodilator substances. Endothelium-dependent vasodilators include a wide range of substances that promote the endothelial-dependent release of NO, prostacyclin or NO-independent hyperpolarisation and thus VSM relaxation [172, 173]. Table 3.1 summarises the common endothelium-dependent vasodilators, their receptor targets and mechanism of action. The majority of these substances stimulate the release of NO from the endothelium, which then diffuses to the VSM and activates soluble guanylyl cyclase, leading to an increase in intracellular cGMP and relaxation [173]. Direct stimulation of VSM β_2-AR however, stimulates the classical Adenylyl cyclase-PKA-cAMP pathway inducing endothelial- and NO-independent vasodilation [174].

Table 3.1. Well-known EDRF substances that mediate endothelial-dependent/NO-dependent vasodilation

EDRF	Receptor target	Mechanism
Shear Stress	NA	i. Increased eNOS ii. Endothelial GPCR sensitisation iii. Activation of KCa channels, increasing NO release iv. Activation of TRP receptors, increasing eNOS
VEGF	VEGFR	i. PI3k-Akt-Ca^{2+}, increasing eNOS ii. Increasing eNOS mRNA iii. PPA2-PLCγ-PKC activation of prostacyclin
Bradykinin	B2	
Purines	P2Y	Gq-HSP90-Ca^{2+} activation, increasing eNOS
Histamine	H2	
Adrenaline/Noradrenaline	α2-AR	
Endothelin-1	ET_B	Gi-HSP90-Ca^{2+} activation, increasing eNOS
5-HT	5-HT1D	
Thrombin	PAR	
Ca^{2+}	Ca^{2+} ion channel	Activates CAM, increasing eNOS activity
Acetylcholine	M3	
Arachidonic Acid	IP (VSM)	Production of prostacyclin, increases PKA-cAMP in VSM, leading to vasodilation

EDRF – endothelium-derived relaxing factor, NA- not applicable, eNOS-endothelium-derived nitric oxide synthase, GPCR- G-protein coupled receptor, KCa – potassium-calcium channel, NO- nitric oxide, TRP – transient receptor potential, PI3k-Akt-Ca^{2+}- Phosphoinositide 3-kinase- protein kinase B-calcium pathway, VEGFR- vascular endothelial growth factor receptor, PPA2-PLCγ-PKC- protein phosphatase 2-Phosphoinositide phospholipase C-gamma- Protein kinase C pathway, B2- bradykinin 2 receptor, P2Y- purinergic receptor, H2- histamine 2 receptor, 5-HT – serotonin receptor, Gq-HSP90-Ca^{2+}-Gq coupled receptor-heat shock protein 90-calcium pathway, α2-AR- alpha 2 adrenoceptor, ET_B-endothelin B receptor, PAR- protease activated receptor, Gi- Gi-coupled receptor, CAM- calmodulin, IP- prostanoid receptor, VSM- vascular smooth muscle, PKA- protein kinase A, cAMP- cyclic AMP.

In the presence of a dysfunctional endothelium, many of these endothelium-dependent vasoactive factors can lead to the release of endothelium-derived constricting factors (CFs), including vasoconstrictor prostanoids [173]. Endothelial-derived constricting factors largely rely on the activity of cyclooxygenase (COX) enzymes. In pathological settings, these enzymes increase vasoactive prostanoids activating VSM thromboxane receptors and promoting vasoconstriction. The balance between endothelial-dependent vasoconstriction and dilation are regulated, to a large extent, by NO bioavailability [175]. Inhibiting NO synthase has been shown to enhance endothelial-derived CFs and conversely, increases in CFs can suppress EDRF-mediated relaxation [173]. Direct VSM vasoconstriction occurs via activation of the α_1-AR-Gαq-PLC pathway increasing Ca^{2+} and leading to vasoconstriction. α_1-ARs have a high affinity for noradrenaline, and moderate affinity for adrenaline, whilst the β_2-AR has a low affinity for noradrenaline and high affinity for adrenaline [176]. In times of stress, the overall vascular response to circulating catecholamines is vasoconstriction due to these affinities [176].

3.0.3 | Catecholamine-mediated contractile dysfunction

The ‘catecholamine storm’ is often attributed to donor cardiac dysfunction, due to the significant elevations in circulating levels and known toxicity [11, 33]. This results in substantial increases in blood pressure, heart rate, arrhythmias and contraction band necrosis [11, 36]. Following this ‘hyperactive phase’ haemodynamic performance deteriorates and catecholamines return to baseline, referred to as the hypoactive phase. Animal experiments have shown that when the catecholamine storm is blocked through adrenergic receptor antagonism or sympathectomy, BSD-mediated cardiac dysfunction can be ameliorated, particularly the hyperactive phase [36, 53].

During the hyperactive phase, several mechanisms may be acting in unison to induce cardiac dysfunction. Under intense catecholamine stimulation, intracellular Ca^{2+} increases dramatically, causing hypercontracture. Together, this creates a state of localised hypoxia due to poor myocardial perfusion in a hypercontracted state. Further, alongside $i[Ca^{2+}]$ increases, mitochondrial Ca^{2+} also increases, promoting mitochondrial swelling, poor oxidative

phosphorylation, ROS production and opening of the mPTP. Collectively, Ca^{2+} overload, hypoxia and mitochondrial dysfunction lead to cardiomyocyte apoptosis and necrosis evidenced by histological findings of contraction band necrosis post-BSD [11, 14, 59].

During the hypoactive phase, catecholamine levels reduce, however they are replaced exogenously by adrenergic agents to combat waning haemodynamics [177]. This further aggravates the Ca^{2+}-ischaemia-mitochondrial dysfunction processes that may occur during the hyperactive phase. Traditionally, high donor inotrope use has been considered a contraindication to HTx, likely through these cardiotoxic effects, leading to poor donor heart utilisation. Chronic administration of catecholamines may also induce receptor desensitisation, uncoupling cardiac excitation to contraction.

Homologous desensitisation develops from continued agonism, activating a family of G-protein coupled receptor kinases, particularly GRK2. Prolonged agonist activation initiates the translocation of GRK2 to the plasma membrane allowing phosphorylation of the agonist occupied β_1-AR. This leads to the recruitment of β-ARR promoting G protein uncoupling (functional desensitisation) and internalisation (downregulation) via clathrin-mediated endocytosis. From here, the internalised receptor is either recycled to the membrane or undergoes lysosomal degradation [57, 170, 178].

Previous studies investigating β-AR signalling in the context of the BSD heart have focussed primarily on protein activity (membrane fraction) on short, 6 hr models of BSD. The findings of these studies are outlined in table 3.2, and suggest β-AR desensitisation, but not internalisation. The major limitation of these previous studies, which will be addressed in this chapter, is the unknown effect of a longer BSD timeframe on β-AR signalling. Further, changes in isolated membrane protein activity may not completely reflect potential functional deficits in excitation-contraction-coupling, and therefore, this chapter will explore β-AR signalling on a functional level.

Table 3.2. Summary of studies examining cardiac β-AR signalling following BSD

Study	BSD time (hrs)	Species	β-AR density	AC activity*	GRK2 activity
Bittner *et al.*, [60]	6	Dog	↑ns	↑	NM
D'Amico *et al.*, [63]	3	Pig	↔	↓§	NM
Van Trigt *et al.*,	6	Dog	↑ns	↑	NM
†White *et al.*,	NK	Human	↑ns	↓	NM
Pandalai *et al.*, [49]	6	Pig	↔	↓/ ↔‡	↑

NM- not measured, * based on isoproterenol stimulated response, AC – Adenylyl Cyclase, GRK2- G-protein coupled receptor kinase 2, ns- non-significant, §- Same effect for Sodium Fluoride and Forskolin stimulation. NK- Not known, † compared non-utilised, failing (based on Echocardiography) BSD hearts to non-failing donor hearts, non-utilised for logistical reasons. ‡- Sodium fluoride stimulated AC activity

3.0.4 | Vascular dysfunction post-BSD

Chapter 1 (pg. 14) discussed the vascular consequences of BSD from histological to *in vivo* findings. A summary of those findings will be discussed here. The first evidence of vascular dysfunction in BSD was presented by Novitzky in the '80s who suggested changes in myocardial metabolism, implying reduced O_2 supply [86]. This was substantiated by observing VSM contraction band necrosis 12 hrs post-BSD, which could be completely reversed by sympatholytic techniques [59].

During the hyperactive phase of BSD, a rise in contractility and blood pressure induces a significant increase in CBF. In the presence of immense catecholamine release, vasoconstriction should reduce CBF. To overcome this, flow-mediated dilation, increases in peripheral vasoconstriction, and metabolites released from the myocardium (adenosine, NO, prostacyclin, bradykinin and CO_2) work in concert to increase CBF. Conversely, Li *et al.*, showed that during

the same phase, myocardial extraction of oxygen was depressed and did not return to pre-BSD levels [52]. The same trend was observed for CBF, reducing to below baseline levels 40-60 min post-BSD (hypoactive phase), in conjunction with a loss of neural vasomotor tone [38, 42, 81, 82].

Reductions in CBF are associated with endothelial dysfunction, evidenced by paradoxical acetylcholine vasoconstriction during *in vivo* percutaneous techniques [81, 82]. *In vitro* testing of conduit vessels however, has shown intact endothelial function [50]. Novitzky highlighted VSM damage during the hypodynamic phase [59]. This may be true for models employing BSD times of 1 hr however, 3 hrs post-BSD was not associated with VSM dysfunction, evidenced by no changes in dilation with the endothelium-independent vasodilator SNP [81]. These data are consistent with reduced myocardial oxygen extraction during the hyperactive phase, precipitating ischaemic injury and thus poor function in the hypoactive phase. Mechanistically, this would suggest VSM damage or poor NO signalling early in BSD which is recoverable.

Adding to the possible endothelial and VSM dysfunction, BSD causes a large release of ET-1. ET-1 is a potent vasoconstrictor causing microvasculature contracture and leads to impaired coronary flow reserve (CFR) and cardiac function, as observed by Oishi [82, 83]. Using the non-selective ET-1 receptor antagonist TAK-044, Oishi [83] showed improvements in both left ventricular function and CFR post-BSD.

In agreement with the aforementioned data, Szabo further highlighted the importance of CBF on the generation of BSD-mediated cardiac dysfunction. The authors showed that if loading conditions (and CBF) were kept constant, cardiac function in the hypoactive phase was preserved, despite the usual hyperactive phase [13, 85] (Fig 3.2A). Therefore, post-BSD cardiac depression reflects a parallel decrease in ventriculo-arterial coupling with maintained mechanical efficiency, through the Anrep and Frank-Starling mechanisms. These data suggest decreased coronary perfusion pressure as an important and independent mechanism initiating donor cardiac dysfunction, regardless of the catecholamine storm. Whether dysfunction of the endothelium or vascular smooth muscle contributes further to this is still under investigation.

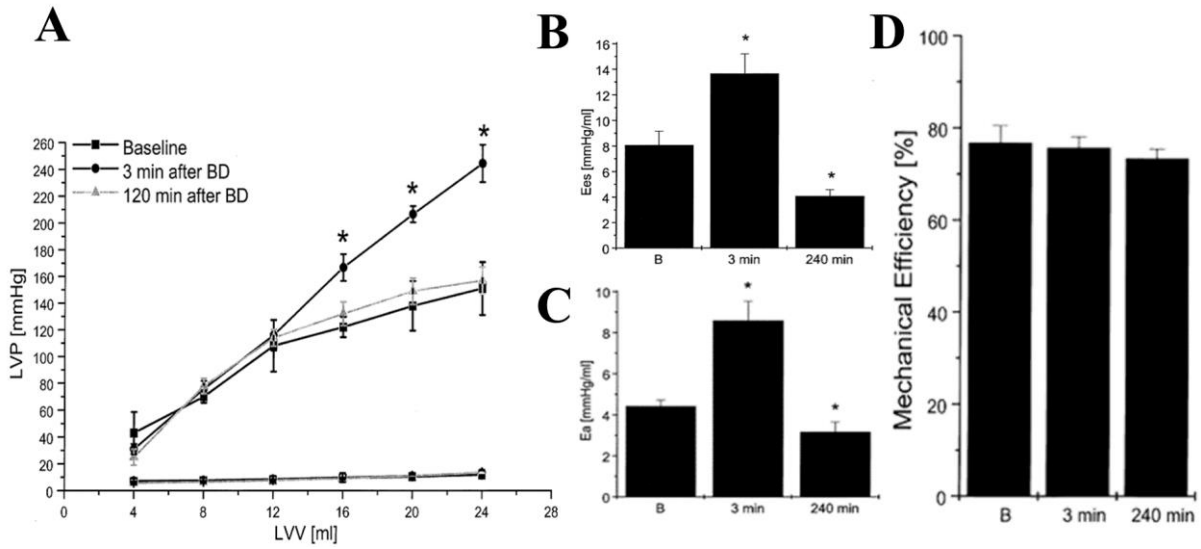

Figure 3.2. BSD-mediated changes in loading conditions described by Szabo *et al.*, [30,31]. A. LV pressure volume relationship at baseline, 3 and 120 min post-BSD. Maintaining loading conditions prevented decreases in LVP (top circles) compared to baseline despite the usual hyperactive reaction (3 min post). No changes in end diastolic pressure volume relationship was observed (bottom line, 3 time points superimposed). B. & C. Shows parallel changes in end systolic pressure volume relationship (B) in BSD without maintenance of loading conditions and arterial elastance (C). These parallel decreases were in the presence of maintained mechanical efficiency (D) which suggests BSD mediated damage is load dependant.

Another largely understudied contributor to vascular tone in the context of BSD is co-transmission of vasoactive substances from the autonomic nervous system. Pertinent to BSD, sympathetic NA release can be coupled with both ATP and neuropeptide Y (NPY) causing potent vasoconstriction and NPY can stimulate leukocyte adhesion [179, 180]. The sympathetic storm through the actions of ATP and NPY may then contribute to microvascular dysfunction (no-reflow) through vasoconstriction and activation of immune and inflammatory cascades [179]. After brain stem herniation, autonomic tone is lost, thus the antagonistic effects of the parasympathetic system reducing cardiac workload, and reducing the inflammatory response [179] may also be lost. Additionally, central sympathetic tone is lost, however local vasoactive substances such as bradykinin (BK) may activate the release of NA from sympathetic nerve terminals, thus promoting a level of vasoconstriction [181, 182].

3.0.5 | HTx-mediated dysfunction

The most significant factor affecting 30-day patient mortality is PGD [51]. PGD develops as uni- or bi-ventricular reductions in contractility, requiring inotropic or mechanical support [8]. Donor factors associated with the development of PGD are, age, ischaemic time, BSD, mechanism of BSD (intracranial haemorrhage) and inotrope use, all of which can alter adrenergic and vascular function [183-185]. Additional to these retrospective risk factors, the immediate concern in the acute stage of HTx is IRI.

During CSS, the heart is placed into a cold preservation solution and transported on ice, which has been the standard for decades. CSS imposes a significant ischaemic insult involving a switch to anaerobic metabolism, increasing lactate production, thus lowering cytosolic pH which in conjunction with $i[Ca^{2+}]$ overload initiates mitochondrial and contractile dysfunction [133]. The vascular endothelium experiences a similar injury via reductions in pH, increased ROS production, eNOS dysfunction and potassium channel/transient receptor potential channel activation [186].

Upon re-establishment of coronary circulation in the recipient, lactate is washed out and intracellular pH is rapidly restored. Activation of the Na^+/H^+ and Na^+/Ca^{2+} exchangers produces hypercontracture via Ca^{2+} overload [133, 138]. Ca^{2+} overload also initiates the production of ROS and thus mitochondrial damage, further aggravating Ca^{2+} overload leading to cell death [138]. Post-HTx haemodynamic instability is usually treated with sympathomimetics, which may potentially worsen IRI by exacerbating Ca^{2+} overload and increasing oxygen demand.

Reductions in pH inhibit endothelial uptake of Ca^{2+} and activate caspases, leading to the reduction in EDRFs and apoptosis [186]. Increased ROS from cardiomyocytes, vascular endothelium and inflammatory cells activate nuclear factor kappa-B, causing an upregulation of proinflammatory and vasoactive substances [186]. Arginase activation, eNOS dysfunction and activation of ion channels on the endothelium result in uncoupling of eNOS to NO production and the generation of hyperpolarising factors which are important in the microvasculature [186]. Collectively,

endothelial ischaemic injury propagates myocardial ischaemic injury by downregulated CBF, leading to poor perfusion.

It has also been shown that the transplanted and consequently denervated heart is supersensitive to circulating catecholamines [132]. Originally it was thought that the transplanted heart therefore must have an increased β-AR density [132]. However, Gilbert and colleagues showed downregulation of β-ARs and an absent noradrenaline uptake-1 mechanism, concluding that the observed supersensitivity was presynaptic in origin [132].

By simulating the steps involved in human HTx, with a clinically relevant 24 hr sheep model of BSD, we sought to investigate myocardial contractility and adrenergic signalling in conjunction with vascular reactivity, to further understand the consequences of BSD, CSS and HTx. We assessed contractility of left and right ventricular trabeculae, and vascular reactivity of the left anterior descending artery taken from hearts to mimic 1. BSD injury and, 2. Transplantation after cold static storage. Post-transplanted hearts were maintained for up to 6 hours and explanted with corresponding time-matched controls. The heart from the recipient sheep (into which the donor heart was transplanted) was used for further comparison. The methods for studying contractility in sheep ventricular trabeculae in this study were established for human heart ventricular trabeculae [187-189].

3.1 | Methods

Following a) 24 hrs post-BSD confirmation or b) 6 hrs after weaning off CBP for the BSD/SHAM and SH-Tx and BSD-Tx groups, respectively, the heart was excised, stored immediately in ice-cold oxygenated Krebs solution and transported to the laboratory. The healthy recipient heart (HR) was also excised and used as a healthy non-medically treated control. Left and right ventricular trabeculae and the left anterior descending (LAD) artery were dissected under continuous oxygenation. Conduit vessels were isolated from a second-order branch of the left anterior descending artery, and resistance type vessels were isolated from a branch of the first diagonal of the LAD [190].

3.1.1 | *In Vitro* Contractility

Left and right ventricular trabeculae were dissected under continuous oxygenation, clamped to Blinks electrode blocks in a 50 mL tissue bath and attached to Swema SG4-45 strain gauge transducers [191, 192]. Trabeculae were stimulated with 5ms square wave pulses at a frequency of 0.2 Hz (1 beat per 5s). The length of the trabeculae was set at L_{max}, the length giving the greatest developed force. The Krebs solution [in (mM): Na^+ 125, K^+ 5, Ca^{2+} 2.25, Mg^{2+} 0.5, Cl^- 98.5, SO_4^{2-} 0.5, HCO_3^- 32, HPO_4^{2-} 1 and EDTA 0.04, pH 7.34-7.42, pO_2 >800 mmHg] in the tissue bath was exchanged for Krebs solution supplemented with Na^+ (15 mM), fumarate (5 mM), pyruvate (5 mM), L-glutamate (5 mM) and glucose (10 mM) at 37 °C.

To selectively activate the β_1-AR, β_2-AR were blocked with 50 nM ICI 118,551 and α-AR, extraneuronal and neuronal uptake irreversibly blocked with 5 μM phenoxybenzamine (PBZ) [188, 192]. After 90 min incubation, the incubation solution was exchanged to remove unbound PBZ and ICI 118,551 re-added. Upon stabilisation of contractility, the pacing frequency was increased to 1 Hz (60 beats per minute). A cumulative concentration-effect curve for (-)-noradrenaline was then established using ½ log increments in concentration, commencing at 2 nM until 200 μM. Experiments were concluded by the addition of 200 μM (-)-isoprenaline and 9.25 mM Ca^{2+} [188, 191, 192].

In some experiments, high concentrations of (-)-noradrenaline used in the concentration-effect curve caused a reduction in contractile force. To determine whether (-)-noradrenaline induced reductions in contractile force were due to activation of β_3-AR [193, 194] trabeculae were incubated with the β_3-AR antagonist L748,337 for 60 min [195-197]. To determine whether the reduction in contractile force was due to metabolism of cyclic AMP by phosphodiesterases (PDEs), trabeculae were incubated with non-selective PDE inhibitor 3-isobutyl-1-methylxanthine (IBMX) 10 μM, incubated for 20 min prior to construction of a concentration-effect curve to (-)-noradrenaline.

Both sympathomimetic usage and plasma catecholamines are highly relevant to the investigation of β_1-AR-mediated contractility. Therefore, the data from Chapter 2 are re-presented here for

convenience (Fig 3.3 & 3.4). However, for plasma catecholamine concentrations, the time course data was converted from pmol/mL to ⁻log Molar concentrations to facilitate comparisons with the generated concentration-effect curves to (-)- noradrenaline (Fig 3.4 [198]).

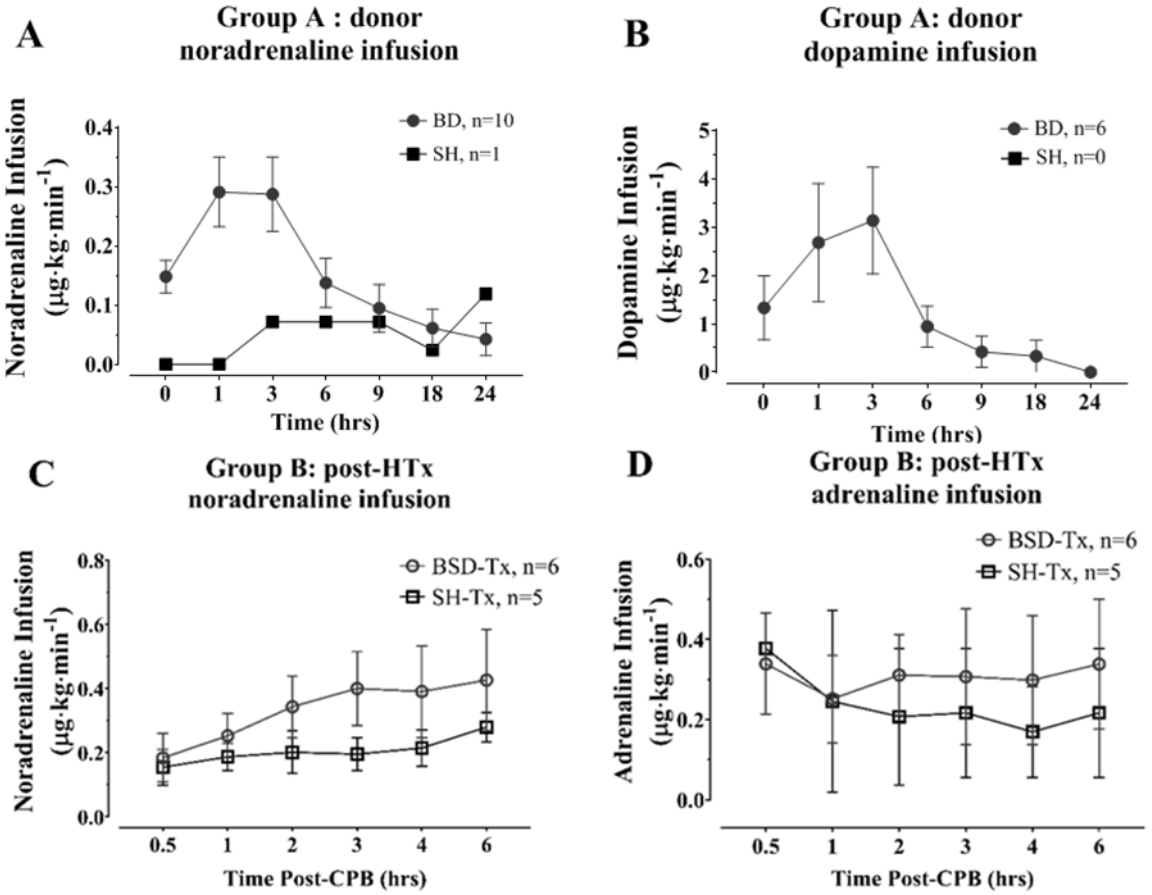

Chapter 2, Figure 3.3. Adrenergic support throughout the pre transplant A and B, and post-transplant periods C & D between BSD and SHAM donors.

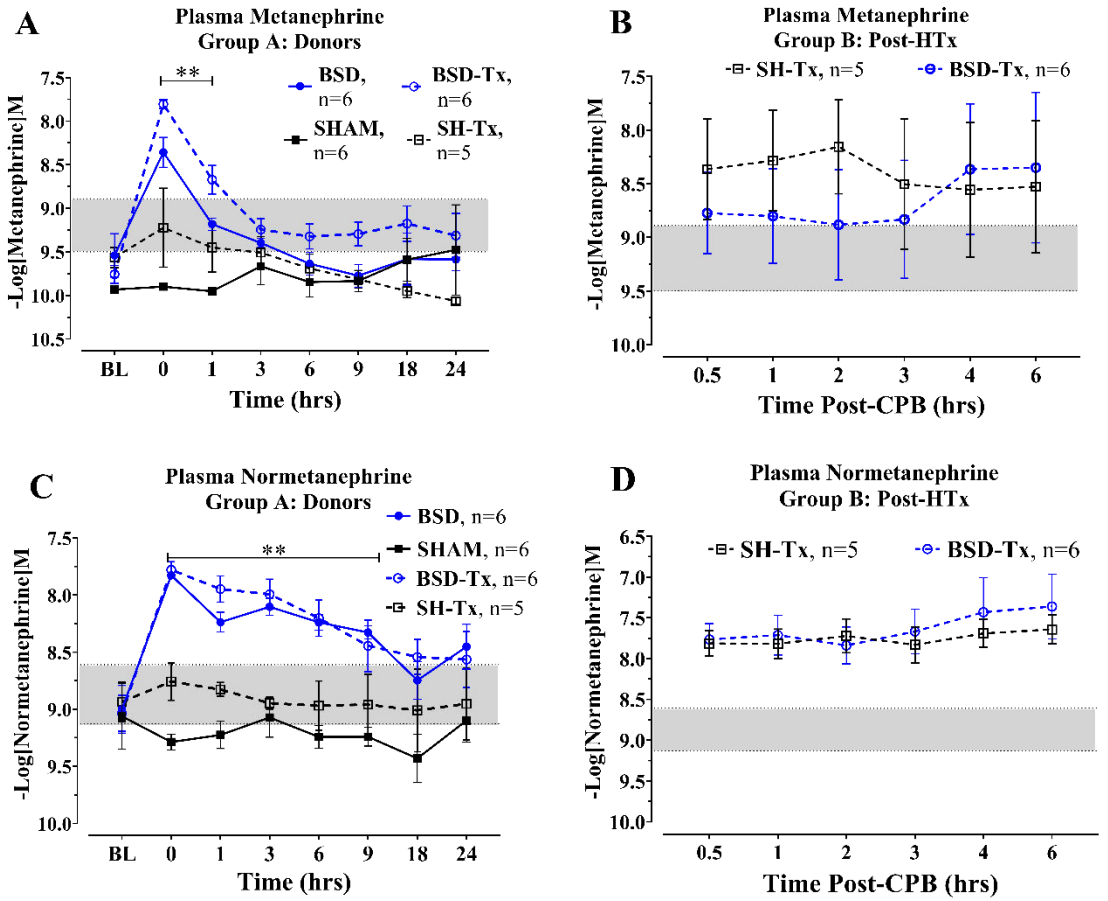

Chapter 2, Figure 3.4. Metanephrine and Normetanephrine concentrations in donor and recipient plasma. A. BSD mediated increase in plasma MET levels. B. Elevated MET post-transplant in both SHAM and BSD transplanted hearts. C. Profound increase in nMET levels after BSD induction compared to SHAM/SH-Tx donors. D. Elevated nMET post-transplant in both SHAM and BSD transplanted hearts. Data has been converted to –Log Molar units here for ease of comparison to pEC_{50} results. Shaded areas represent normal ranges by Green *et al.*, [51].** Significantly different compared to SHAM $p<0.05$

3.1.2 | Vascular Reactivity

After isolation, arteries were cut into 1-2 mm segments and mounted on a 4-channel wire myograph (Danish Myo Technologies), which measures isometric force via a force transducer with 5 mL of physiological saline solution (PSS) (mmol/L: NaCl 114, KCl 4.7, KH_2PO_4 0.8, $MgCl_2$ 1.2, D-glucose 11, $NaHCO_3$ 25, $CaCl_2$ 2.5, EDTA 0.026, bubbled with 95 % O_2 and 5 % CO_2, pH 7.4). For conduit vessels, this was achieved by placing the parallel wires of the myography through the lumen of the vessel and increasing the distance between the two wires to secure the vessel position. For resistance vessels, a 20 µm wire was first threaded through the lumen of the vessel and secured to one side of the myography. A second wire was then threaded through the lumen in parallel and secured to the opposite side. Again, the distance between the two wires was increased to add tension.

Once mounted, all vessels were normalised to a force equivalent to 100 mmHg using the Laplace relationship between wall tension and internal vessel circumference [190]. To assess maximal contraction, the bath contents were replaced with K^+ depolarising solution (KPSS (mmol/L: KCl 123, $MgSO_4$ 1.17, KH_2PO_4 2.37, CaCl 22.5, D-glucose 11.1, EDTA 0.026, bubbled with 95 % O_2 and 5 % CO_2, pH 7.4)) twice, rinsed and allowed to recover. A single dose of the thromboxane mimetic U46619 (0.1 µM) was added to contraction vessels, followed by the vasodilator bradykinin (0.1 µM) to test endothelial integrity. Vessels were then pre-contracted to ~50% of the maximum KPSS contraction in the presence of the non-selective COX inhibitor indomethacin (10 µM) for vascular reactivity assessment.

Vascular reactivity was assessed via consecutive endothelial-dependent, endothelial-independent and NO-independent cumulative concentration-effect relationships. For endothelial-dependent vasodilation, bradykinin was administered in ½ log increments from 10 nM-1 µM. Endothelial-independent vasodilation was assessed using the NO donor DEA-NONOate in ½ log increments from 1 nM-1 µM. To assess NO- endothelium-independent action and therefore VSM function, the non-selective β-AR agonist isoproterenol was administered in ½ log increments from 0.03

nM-1 µM. Methods for vascular reactivity of ovine vessels were performed as described elsewhere and at 37°C [190, 199].

3.1.3 | Analysis and Statistics

Trabeculae were measured and weighed for force correction against cross-sectional area. The force produced after each (-)-noradrenaline titration was measured using LabChart version 8.0 (ADI Instruments). A stable period between titrations representing the largest force produced was chosen, and the absolute change in force was measured.

Maximum VSM contraction was measured from the response to KPSS and expressed as force corrected to vessel diameter. Vascular reactivity data will be expressed as cumulative concentration-effect curves of the per cent relaxation to a given vasodilator.

The effective concentration that elicits a 50% contractile or relaxation response (pEC_{50}) for (-)-noradrenaline, bradykinin, DEA-NONOate and isoproterenol will be determined by non-linear curve fitting using the Hill function with variable slopes in GraphPad Prism 8.0. Significant differences in contractility and pEC_{50} were determined using a one-way ANOVA with Tukey post-hoc tests. A significance threshold of 0.05 was used. Where normality was violated, data other than pEC_{50} were log-transformed to facilitate statistical analysis. Unless otherwise stated, data represent means ± standard error (SE) of the mean.

3.2 | Results

A total of 21 donor hearts were included, 4 SHAM and 6 BSD hearts were collected at the end of the 24 hr post-BSD monitoring time. 5 SHAM donors and 6 BSD donors progressed to transplantation, SH-Tx (n=5) and BSD-Tx (n=6), respectively.

3.2.1 | *In vitro* muscle mechanics

The mean width and cross-sectional area (CSA) of the left trabeculae was 1.24 ± 0.1 mm width; 2.48 ± 0.25 mm^2 CSA and right trabeculae was, width 1.44 ± 0.1 mm; CSA 2.73 ± 0.22 mm^2. There were no differences in CSA of trabeculae in different groups (Table 3.3). Basal contractility was weakly, inversely correlated with CSA in LV of HR hearts (R=-0.472, p=0.03, n=12) but not in all other groups or ventricles. There was no difference between left and right ventricular basal contractility from HR hearts (p = 0.53, n=12). Right ventricular trabeculae from BSD, BSD-Tx and SH-Tx hearts exhibited lower basal contractility than RV trabeculae from HR (Fig 4B), but transplantation of BSD hearts (BSD-Tx) did not further reduce RV contractility (Fig 3.5B). Unlike RV, LV trabeculae were unaffected by BSD or transplantation (Fig 3.5A & C). This pattern of absolute contractility was maintained for maximal (-)-noradrenaline induced contractility (Fig 3.5C & D).

Table 3.3. **Group characteristics for trabeculae geometry.** Data represent means (±SE)

Group	**HR**		**SHAM**		**BSD**		**SH-Tx**		**BSD-Tx**	
	n=12		n=4		n=5		n=5		n=6	
	LV	**RV**	**LV**	**RV**	**LV**	**RV**	**LV**	**RV**	**LV**	**RV**
Width (mm)	1.3 (0.26)	1.14 (0.18)	1.11 (0.28)	1.55 (0.70)	1.23 (0.22)	1.40 (0.24)	1.13 (0.14)	1.48 (0.23)	1.44 (0.26)	1.65 (0.21)
CSA	2.51 (0.44)	2.15 (0.33)	2.33 (0.83)	2.93 (0.53)	2.53 (0.43)	2.36 (0.36)	2.05 (0.40)	3.44 (0.59)	2.96 (0.74)	2.76 (0.53)

CSA- cross sectional area, LV- left ventricle, RV- right ventricle

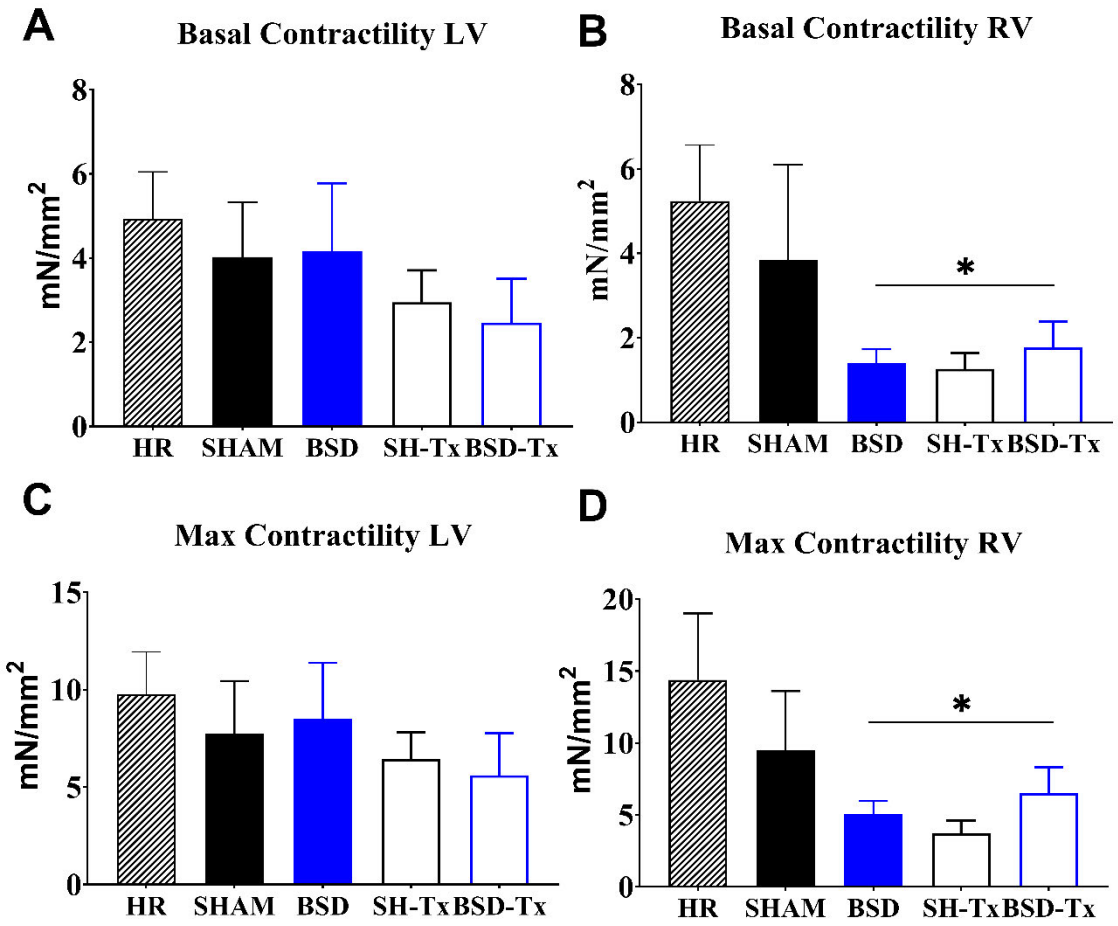

Figure 3.5. Basal and maximal (-)- noradrenaline induced contractility in ventricular trabeculae expressed as force/CSA (mN/mm^2). ***A&C.*** Downward trend of basal (**A**) and maximal (**C**) ***LV*** contractility observed in trabeculae from SH-Tx and BSD-Tx. ***B& D.*** Reduced basal (**B**) and maximal (**D**) ***RV*** contractility in trabeculae from BSD, SH-Tx and BSD-Tx compared to HR group. *Statistically significant compared to HR, [**B**: BSD vs HR p=0.028, SH-Tx vs HR p=0.015, BSD-Tx vs HR p=0.041] and [**C**: BSD vs HR p= 0.014, SH-Tx vs HR p=0.001, BSD-Tx vs HR p=0.008]. CSA – cross sectional area

(-)-Noradrenaline caused concentration-dependent increases in contractile force through activation of β_1-AR. In some (~ 58 ± 5%) left and right ventricular trabeculae from all groups, the maximal (-)-noradrenaline-induced contractility was not maintained with further increases in concentration of (-)-noradrenaline, causing reductions in contractility (Fig 3.6). (-)-Noradrenaline-induced reductions in contractility at high concentrations were not prevented by the β_3-AR antagonist L748 337 (100 nM) (Fig 3.7A & B) or the non-selective PDE inhibitor IBMX (Fig 3.7B); excluding the involvement of β_3-AR and PDEs in the depressant effects at high (-)-noradrenaline concentrations (Fig 3.7 A & B).

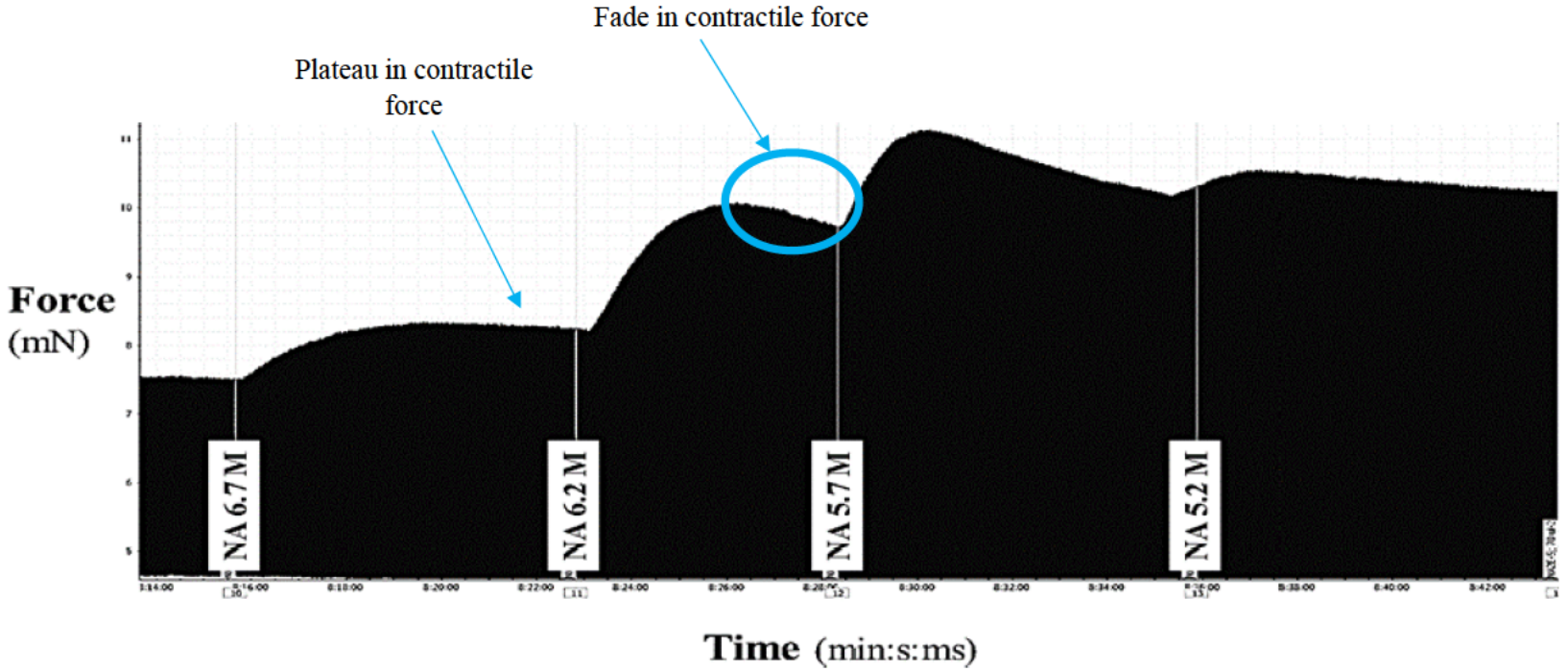

Figure 3.6. Original representative trace from *in vitro* recording of a transplanted BSD donor heart (BD-HTx) showing a decrease in contractility at higher doses of (-)-Noradrenaline. NA- (-)-Noradrenaline, NA concentrations are in Log molar concentrations.

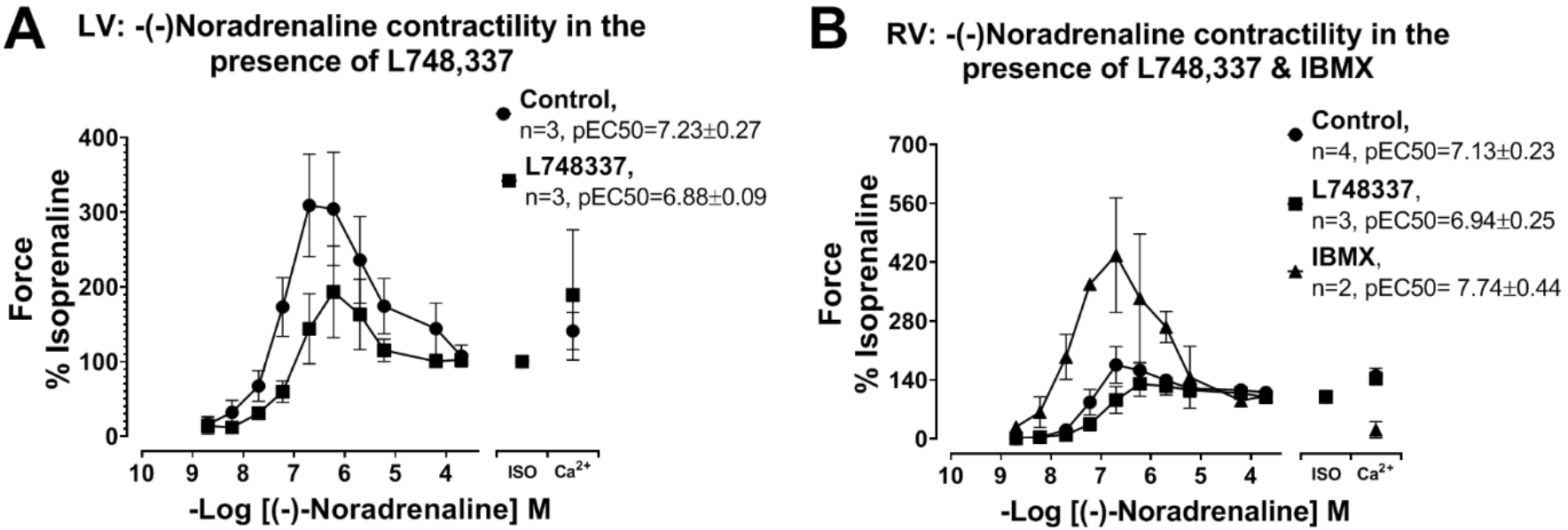

Figure 3.7. Dose-response curves to (-)-noradrenaline in the presence of the β_3 antagonist L748,337 (100 nM) and the non-selective PDE inhibitor IBMX (10 µM) in left (A) and right (B) isolated trabeculae. Data is normalised to isoprenaline induced maximum β-AR induced contractile response and is expressed as means ±SE.

For BSD donors, pEC_{50} values were slightly reduced compared to the HR (LV p=0.30, RV p=0.065, BSD: n=5, HR: n=12) and SHAM (LV p=0.57, RV p=0.94, SHAM: n=4) groups (Fig 3.8A & C). For the LV, (-)-noradrenaline potencies were reduced for the SH-Tx (0.59 mean difference, p=0.04, SH-Tx: n=5) and BSD-Tx (0.62 mean difference, p=0.02, BSD-Tx: n=6) groups compared to HR group (Fig 3.8 B). There were significantly reduced RV potencies for the SH-Tx (0.56-pEC_{50} difference, p=0.03) and BSD-Tx (0.71-pEC_{50} difference, p=0.005) groups compared to the HR group (Fig. 3.8 D).

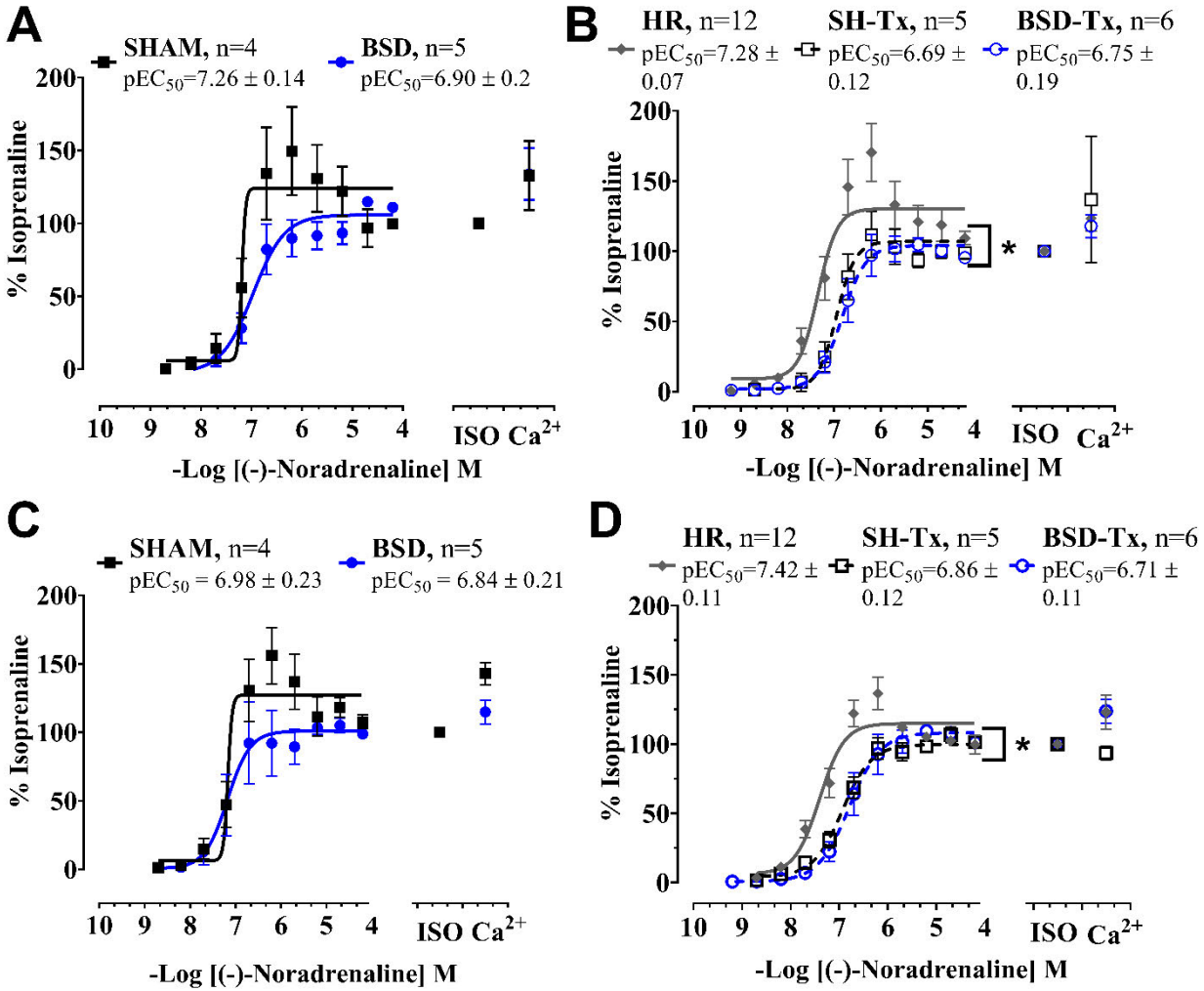

Figure 3.8. β_1-mediated (-)- noradrenaline concentration effect curves for SHAM and BSD donors (A & C) and HR, SH-Tx and BSD-Tx (B & D). A&C Preserved sensitivity for BSD compared to all groups in both LV and RV. B&D Right shift in BSD-Tx and SH-Tx concentration effect curves compared to HR in both LV and RV. * statistically significant change compared to HR group $p<0.05$

3.2.2 | Spontaneous Contractions

Spontaneous contractions were classified as individual contractions which occurred outside the 1 Hz stimulation frequency. These contractions were present in both ventricles and all groups. Basally, there was a greater propensity for spontaneous contractions in the RV in the SHAM, BSD and SH-Tx groups compared to other groups ($p>0.05$) (Fig 3.9 B). For the LV, 1/6 hearts in the BSD group and 1/4 hearts in the SHAM group presented with spontaneous contractions (Fig. 3.9A). No post-HTx or HR LV trabeculae presented with spontaneous contractions basally.

To statistically analyse if the incidence of spontaneous contractions were significantly higher between groups, contingency tables were created which reflected the number of dose-response curves where spontaneous contractions were observed compared to the dose-response curves where no spontaneous contractions were observed. A Fisher's exact test was performed to determine any differences in proportions of curves that contained spontaneous contractions or not between groups.

Fisher's exact test showed that the RV developed a higher incidence of spontaneous contractions in SHAM (63.64%, $p<0.0001$) and BSD (42.22%, $p=0.0009$) than the HR and SH-Tx and BSD-Tx (Fig 3.9D). There were no significant differences in the incidence of spontaneous contractions between groups for the LV (Fig 3.9C). The occurrence of spontaneous contractions in the presence of (-)-noradrenaline was concentration-dependent in LV. Spearman's correlation test were performed on the incidence of contractile fade compared to the incidence of spontaneous contractions across all concentrations of (-)-noradrenaline. Correlation analysis showed a significant association in all groups for the LV between spontaneous contractions and the decrease in contractility observed at high concentrations of (-)-noradrenaline (mean $R=92.6$, $p< 0.01$) (Table 3.4). The same association was observed for the RV (mean $R=93.8$, $p<0.01$) except for the BSD group ($R=38.4$, $p=0.24$). This may suggest that dose-dependent decreases in contractility are potentially associated with arrhythmic mechanisms.

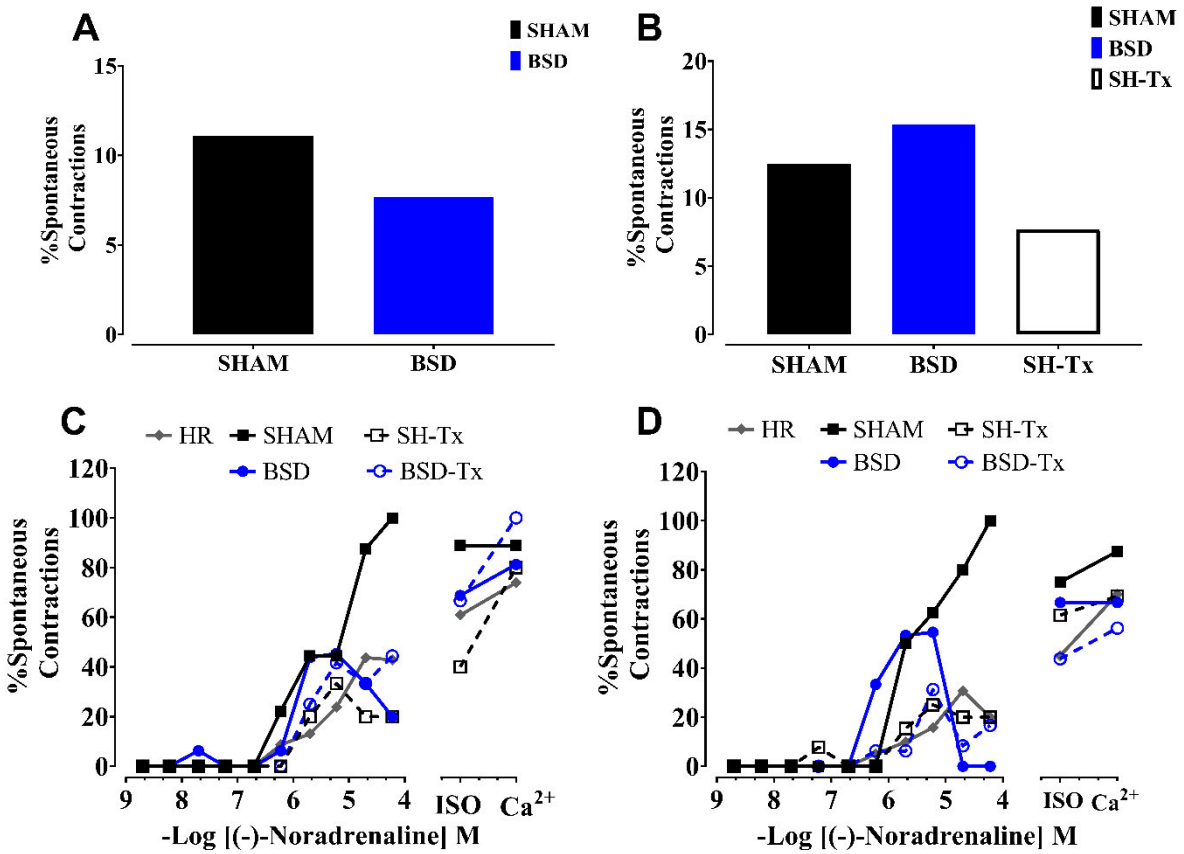

Figure 3.9. Incidence of spontaneous contractions in LV (A&C) and RV (B&D) per group. A&B There was a non-significant preponderance of spontaneous contractions basally in the SHAM, n=1, BSD, n=1 and SH-Tx, n=1 groups. **C&D** incidence of spontaneous contraction for **(C)** RV were higher for SHAM and BSD compared to HR, BD-Tx and SH-Tx. There were no differences in spontaneous contraction incidence between groups in the LV **(D).**

Table 3.4. Correlation analysis between the dose-dependent incidences of reduction in contractility vs spontaneous contractions per group.

Group Incidence of contractile fade vs Incidence spontaneous contraction	**Spearman's R LV**	**Spearman's R RV**
HR	0.964 [a]	0.965 [f]
SHAM	0.997 [b]	0.931 [g]
BSD	0.846 [c]	0.384
SH-Tx	0.891 [d]	0.899 [h]
BSD-Tx	0.932 [e]	0.955 [i]

a- p= $6.61e^{-5}$, b- p=1.32e-4, c- p=0.006, d- p=0.004, e- p=0.001, f- p=0.001, g- p=0.001, h- p=0.002, i- p=0.001

3.2.3 | Diastolic Force

Increases in diastolic forces were most prevalent in the BSD group and in the RV. For BSD, 80% (4/5 experiments) showed diastolic drift, whereas only 1 heart from other groups (16%) showed diastolic drift. Figure 3.10 shows the diastolic drift as a function of (-)- noradrenaline.

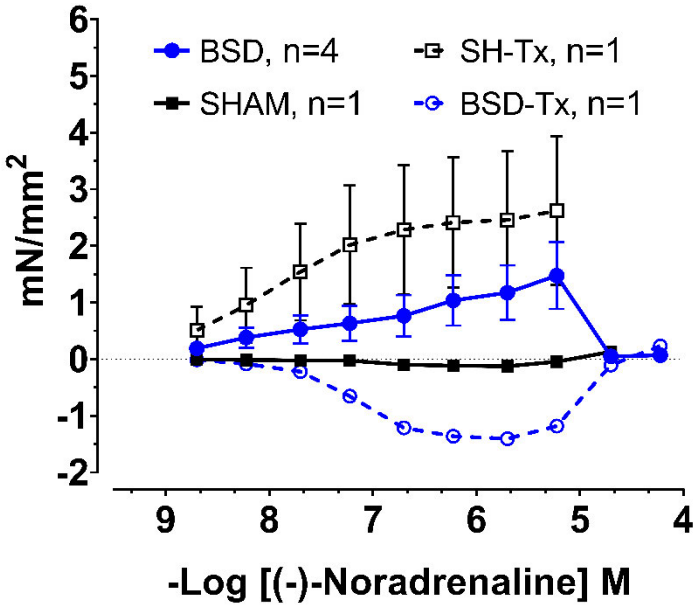

Figure 3.10. Absolute changes in diastolic force produced corrected for CSA (±SE) as a function of (-)- noradrenaline dose. CSA – Cross Sectional Area. n= the number of experiments where diastolic drift was evident.

3.2.4 | Vascular Reactivity

Due to difficulties in optimising the *in vitro* techniques, data presented here represent preliminary findings. Sample sizes varied between vascular indices, therefore sample size is reported accordingly. Where more than one vessels segment was used for a particular heart, the measures are reported as a mean. Samples sizes are reported as individual sheep.

All conduit vessels were of similar diameter ($p=0.87$, $n=19$), with no change in maximum force produced (Table 3.5). Bradykinin induced a complete endothelial-dependent relaxation in vessels for all tested groups. There appeared to be a higher potency in the BSD and BD-Tx groups (Fig. 3.11A) where a 1 nM concentration of bradykinin-induced a ~50% relaxation. Pre-contraction levels with U46619 were similar for HR and SH-Tx groups, and slightly lower for the BSD and BD-Tx groups (Table 3.5). DEA-NONOate and ISO produced a full endothelial-independent and NO-independent (respectively) relaxation in all groups (Fig 3.11B & C). There were no obvious changes to potency between the groups.

Table 3.5. Conduit vessel geometry, max KPSS produced force and pre-contraction efficiency prior to commencement of concentration-effect curves.

	HR (n=4)	SHAM (n=3)	BSD (n=6)	BD-Tx (n=3)	SH-Tx (n=3)
Diameter (µm)	1570 (218.4)	1579 (345.7)	1813 (278.6)	1654 (447.4)	1977 (75.5)
Max KPSS (mN/µm)	0.014 (0.003)	0.018 (0.003)	0.015 (0.003)	0.017 (0.004)	0.012 (0.003)
Pre-contractions (%KPSSmax)					
BK	63.73	NA	37.29 (6.89)	32.07	63.15
n	*2*		*3*	*1*	*2*
DEA	45.28	33.98	45.53 (3.22)	32.12	54.84
n	*2*	*1*	*4*	*1*	*2*
ISO	23.92	19.97	31.16 (6.19)	NA	51.23
n	*2*	*1*	*4*		*2*

Data represent means ±SE where n>2, BK- Bradykinin, DEA- DEA-NONOate, ISO- Isoprenaline

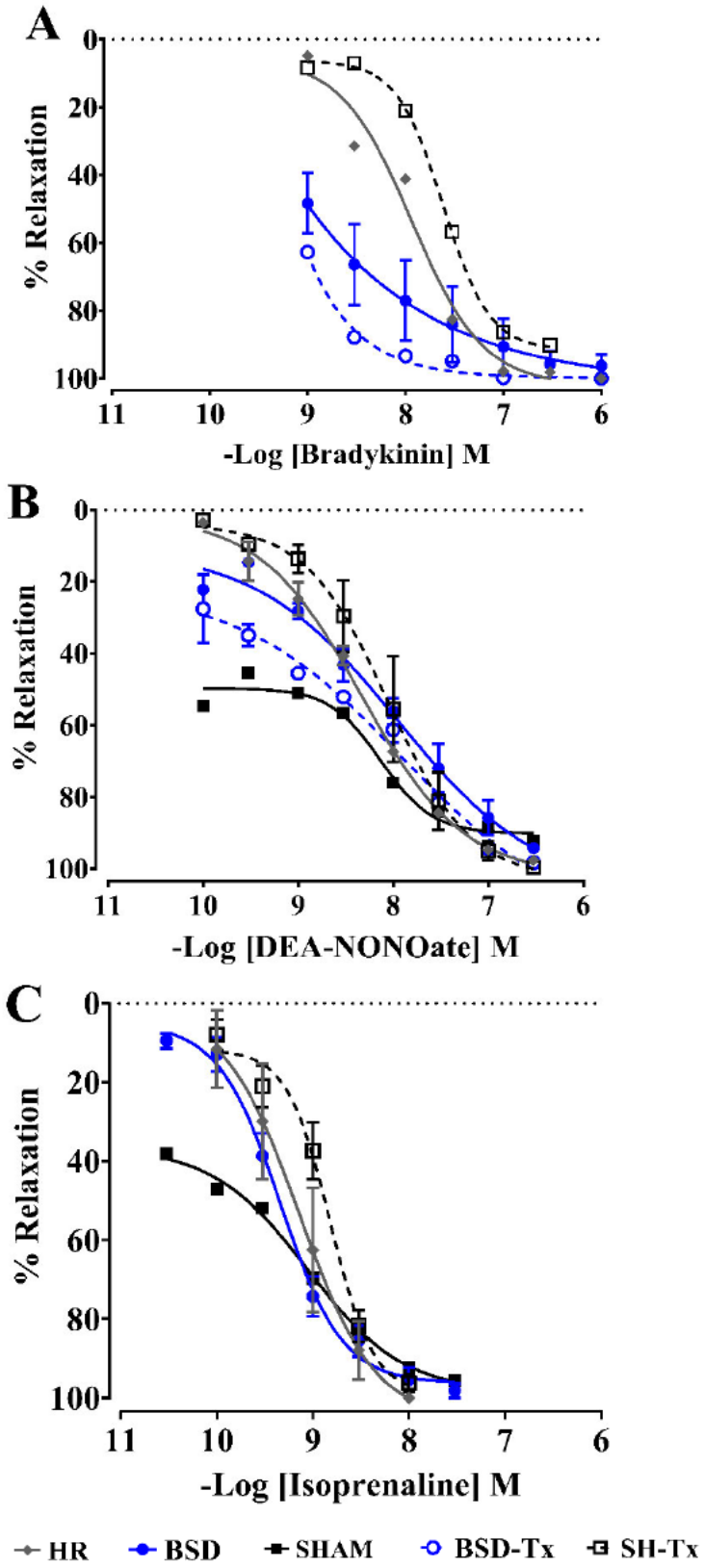

Figure 3.11. Conduit vessel concentration effect curves to A. Bradykinin B. DEA-NONOate and C. Isoprenaline. A. Apparent increase in bradykinin potency for the BSD and BSD-Tx groups. **B&C.** No change in potency or efficacy for DEA-NONOate or Isoprenaline between any groups tested. **A)** HR n= 2, BSD n= 3, SHAM n= 0, BD-Tx n=1, SH-Tx n=2, **B)** HR n= 2, BSD n= 4, SHAM n= 1, BD-Tx n=1, SH-Tx n=2, **C)** HR n= 2, BSD n= 4, SHAM n= 1, BD-Tx n=0, SH-Tx n=2

All resistance vessels were of similar size (p=0.98, n=15) (Table 3.6) with similar maximal contractile responses, except the BSD group with a 0.011 mN/μm reduction in maximal force compared to SHAM only (p=0.02) (Fig 3.12A) Concentration-effect curves for resistance vessels were pre-contracted with 30 mM K^+ to negate the effects of endothelial hyperpolarising factor (EDHF) and examine NO-mediated vasodilation. Bradykinin induced a concentration-dependent relaxation between 70-80% of pre-contraction, with no change in potencies between groups (Fig 3.12 B). DEA and ISO followed this same trend with a 70-97% relaxation, with no change in potencies between any groups (Fig 3.12 C &D). For ISO, the BSD group appeared to have a higher potency, showing a 0.39 and 0.46 log concentration shift to the left compared to SH-Tx and HR groups respectively.

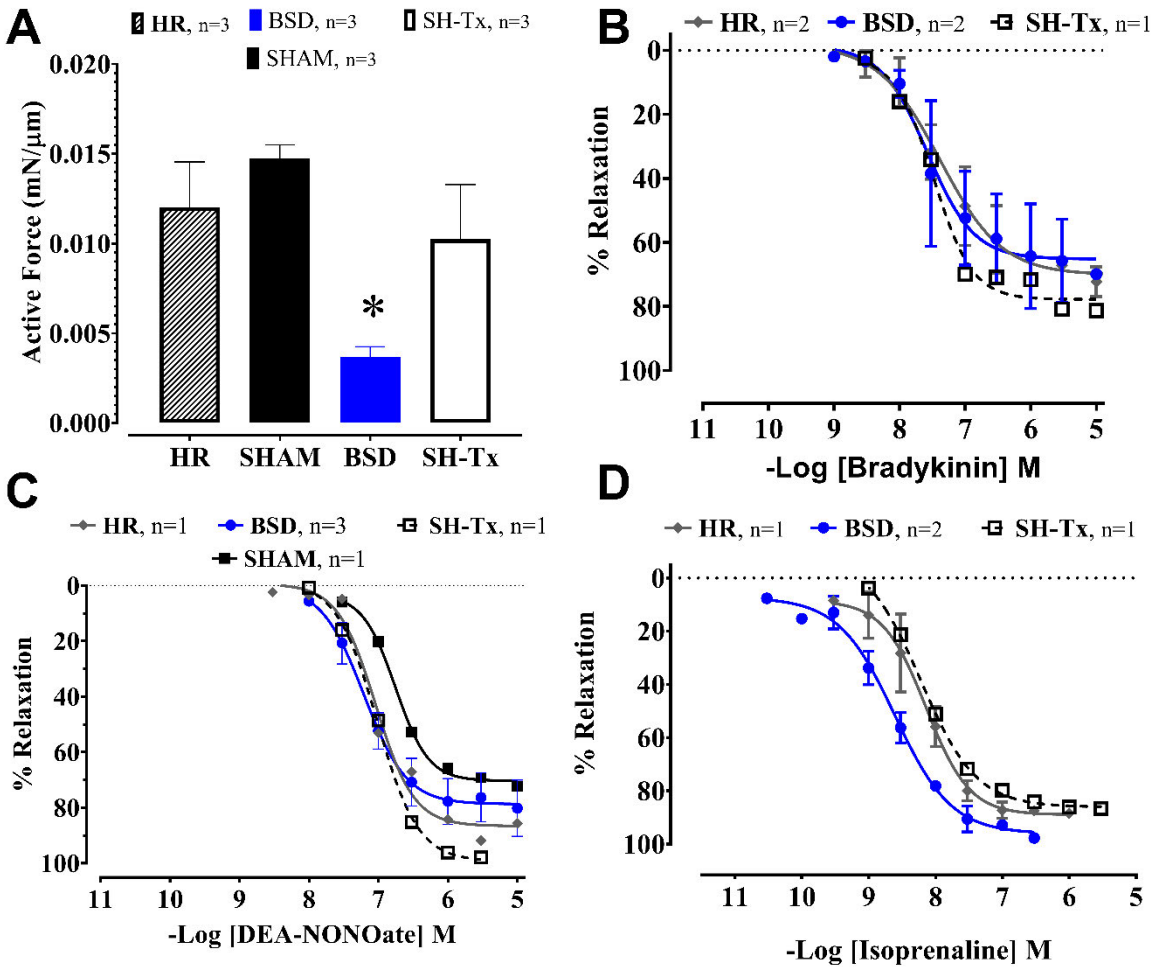

Figure 3.12. Resistance vessel contractile response and concentration effect curves. A. Maximum KPSS contractions were reduced for BSD group compared to the HR group. **B&C** No obvious changes in potency or efficacy for bradykinin or DEA-NONOate concentration-effect curves. **D** Apparent increase in isoprenaline concentration for the BSD group compared to HR and SH-Tx groups. * Significantly different compared to HR

Table 3.6. Resistance vessel diameters and maximum KPSS contractions per group

	HR (n=3)	SHAM (n=3)	BSD (n=3)	BD-Tx (n=3)	SH-Tx (n=3)
Diameter (µm)	451.9 (133)	415.7 (27.6)	419.3 (4.4)	NA	413.3 (79.7)
Max KPSS (mN/µm)	0.012 (0.003)	0.015 (0.001)	0.004 (0.001)	NA	0.010 (0.003)

Data represent means ±SE where n>2

3.3 | Discussion

The *in vitro* cardiac contractile and vascular function was examined in our novel sheep model of cardiac transplantation following 24 hrs BSD. The main findings were 1) a blunted β_1-AR-mediated basal and maximal contractile response following BSD and transplantation from both BSD and SHAM donors, and 2) transplantation regardless of donor type is characterised by β_1-AR desensitisation to (-)- noradrenaline. Preliminary data also suggest enhanced endothelial-dependent vasodilatory response in conduit vessels and increased potency of the VSM to β-AR-mediated vasodilation.

Impaired right ventricular contractile performance is a well-recognised phenomenon in BSD donor hearts [11, 156]. One hypothesis to explain this observation is desensitisation of myocardial β-ARs due to the catecholamine storm. Our data however, have shown preserved sensitivity at the β_1-AR in donor hearts to (-)-noradrenaline after BSD (BSD vs SHAM). These data suggest that factors outside β-AR sensitivity may be involved in contractile dysfunction following donor BSD. Previous works have identified multiple other factors which may contribute to contractile dysfunction including catecholamine-mediated cardiotoxicity, alterations in loading, vascular dysfunction, neurohumoral changes, metabolic alterations (Chapter 5) and oxidative stress [12, 65].

Catecholamine toxicity may be evident here, evidenced by a greater propensity for dose-dependent increases in diastolic force for the BSD group. The higher propensity of diastolic drift in the BSD group may suggest poor Ca^{2+} handling [200]. Prolonged β_1-AR stimulation increases $i[Ca^{2+}]$, which can increase PKA-dependent phosphorylation of ryanodine receptors, phospholamban, troponin I and myosin binding protein C, which work in concert to increase $i[Ca^{2+}]$, leading to hypercontracture and poor cardiac relaxation [200]. These β-AR-independent mechanisms can induce necrotic damage, a common finding in histological studies, thus leading to poor cardiac performance [11, 36, 201]. Together, these data suggest that BSD is characterised

by a preserved β_1-AR sensitivity, but reduced efficacy potentially due to β-AR-independent mechanisms.

A general theory in the context of HTx is that these pathophysiological effects of BSD are associated with PGD [51]. Our data shows that post-HTx, basal and maximal produced forces are reduced in both SH-Tx and BSD-Tx RV compared to healthy recipient controls. This contractile dysfunction was also in the presence of a ~3 fold desensitisation to (-)-noradrenaline at the β_1-AR. Post-transplant graft dysfunction therefore, may be attributed to deficiencies in both β_1-AR-dependant and β_1-AR-independent pathologies. These data suggest that the deficiency in β_1-AR function appears to stem from mechanisms following donor heart procurement rather than BSD itself, since no changes in potencies were observed in BSD hearts and both SH-Tx and BSD-Tx exhibited similar cardiac dysfunction.

Our data is in agreement with that of Gilbert and colleagues who showed reductions in β-AR densities in human heart post-HTx [132]. An important difference in Gilbert's study is that the β-AR densities were measured 25-93 days post-HTx, corresponding to a more chronic change over months, rather than up to 6 hrs in this study. Decreases in β-AR densities have also been shown 6 hr following cardiac arrest in a pig model, highlighting the acute impact of ischaemia on adrenergic signalling [202]. Vettel and colleagues found a blunted cAMP response to isoprenaline stimulation in a model of CSS utilising isolated neonatal rat cardiomyocytes [203]. This model however, implemented a cold storage period of 12 hrs, 3 times that of acceptable clinical standards for HTx and did not report measures of potency or pre-intervention serum starvation [203]. Alterations in β-AR densities post-HTx may then arise from 2 sources, overstimulated receptors via absent noradrenaline reuptake and inotropic support, and cold storage-mediated reduction.

A significant detriment to cardiac performance results from ischaemia caused by CSS and subsequent reperfusion injury. During CSS, oxygen delivery is substantially reduced, precipitating apoptotic and necrotic cell death, decreases in pH and depletions in high energy phosphates [72, 133, 204]. At reperfusion, pH is rapidly restored and initiates a sequela of

pathological signalling mechanisms, ultimately leading to cardiac dysfunction [133]. Therefore, IRI alone can induce significant contractile dysfunction in conjunction with reduced βAR-mediated excitability. Other mechanisms involved in the IRI cascade such as mitochondrial function and metabolic regulation will be discussed in further chapters.

We have also reported a dose-dependent increase in the frequency of spontaneous contractions for all groups. This can be attributed to the well-known pro-arrhythmic effects of (-)-noradrenaline [205]. Increased leak of Ca^{2+} from the sarcoplasmic reticulum as a result of enhanced β_1-AR agonism and PKA signalling, activates the Na^+/Ca^{2+} exchanger thus causing depolarisation in phase 4 of the action potential leading to what is referred to as a delayed afterdepolarisations. Delayed afterdepolarisations are the mechanism behind triggered activity leading to arrhythmias, which are prolific in brain-injured patients [183, 206, 207].

These spontaneous contractions were also strongly associated with the novel finding of dose-dependent fade in contractility. Interestingly, this association was not present in the RV of the BSD group. However, 4/5 of these hearts exhibited increases in diastolic force as described previously. Although only a correlation is presented, the incubation of IBMX and dose-response curve to Mirabegron suggests phosphodiesterases (PDEs) and β_3-ARs are not involved. The later experiments however are representative of small sample sizes. Further experiments to eliminate PDEs and β_3-ARs, as well as the addition of antiarrhythmics or Ca^{2+} sensitisers, are needed to thoroughly explain the dose-dependent fade in contractility.

Our data showed that conduit vessels from BSD hearts appeared to have a higher sensitivity to bradykinin, which is in contrast to previous data showing endothelial dysfunction [81]. This may highlight the reversible nature of cardiac dysfunction from BSD with increasing time from the initial injury. Other possible factors include ischaemic injury and activation of inflammation and coagulation cascades. In the hyperactive phase, decreased perfusion induces myocardial ischaemia, which has been shown to upregulate bradykinin-1 & -2 receptors, therefore increasing bradykinin signalling [208]. Further, the kallikrein-kinin and coagulation systems are all upregulated post-BSD or traumatic brain injury [209, 210]. A common regulatory point in these

cascades is factor XIIa, activating intrinsic coagulation and the formation of kallikrein, leading to the production of bradykinin and its metabolite des-Arg9-bradykinin (Fig. 3.13). Thus, the upregulation of bradykinin and its receptors promotes vasodilation, endothelial permeability, inflammation and oedema, contributing to cardiac dysfunction. Additionally, bradykinin release may stimulate sympathetic NA, ATP and NPY release which can promote vasoconstriction, and leukocyte infiltration leading to vascular dysfunction [180, 182]. Further work should investigate the autonomic influence on endothelial and vascular function as a consequence of both BSD and HTx.

In resistance vessels, we observed that bradykinin did not induce a full endothelial-dependent relaxation. This is not unexpected, since the vessels were pre-contracted with KPSS, the high K^+ concentration closes K^+ channels and negates the effect of EDHF, which is the most important regulator of pre-arteriolar vessels. Isoprenaline however, appeared to have a greater potency on BSD resistance vessels, enhancing dose-dependent vasodilation in the presence of a reduced contractile response compared to the HR and SH-Tx groups (Fig. 3.12D). One possible explanation for this may be supplementation with T3 in the donor period, which was used in our study for both BSD and SHAM donors. T3 acts largely on a genomic level to increase the expression of β-ARs and voltage-gated K^+ channels, both important mediators of isoprenaline-induced vasodilation [89].

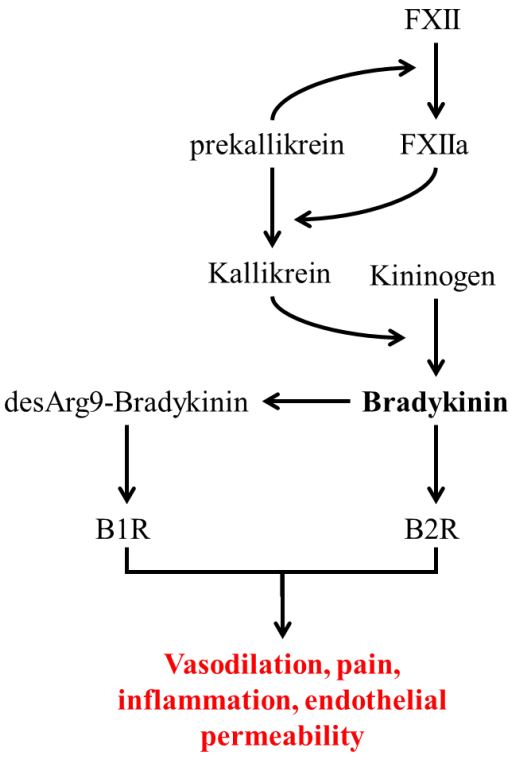

Figure 3.13. **Schematic diagram of the production of bradykinin via simultaneous activation of the coagulation system at the level of FXIIa**. FXIIa promotes kallikrein production which in turn cleaves kininogen to form bradykinin. Bradykinin is then metabolised quickly to desArg9-bradykinin. Bradykinin and desArg9-bradykinin bind to B2 and B1 receptors, respectively to promote vasodilation, inflammation and increases in endothelial permeability. *Figure extracted from Albert-Weissenberger et al., 2014. FXIIa – coagulation factor 12 a*

Donor BSD is also characterised by a significant pro-inflammatory cascade, which can affect vascular smooth muscle and endothelial function [103]. In our study, vessels were pre-incubated with indomethacin to negate the effects of vasoactive prostanoids via COX antagonism. Inhibiting these effects may have skewed our results in favour of enhanced vasodilation, and therefore may not be representative of true *in vivo* vascular function.

3.3.1 | Clinical Significance

As the gap continues to grow between acceptable donors and the need for transplantation, so too has the utilisation of marginal donors. High donor inotrope usage, defined as dopamine/dobutamine infusions >10 $\mu g \cdot kg^{-1} \cdot min \cdot^{-1}$ and noradrenaline infusions >0.05 $\mu g \cdot kg^{-1} \cdot min^{-1}$ has long been considered as an important factor in donor heart selection [211, 212].

Reconsideration of the non-use of marginal hearts based on high inotropic dosage has arisen owing to growing evidence that inotrope usage >0.4 $\mu g \cdot kg^{-1} \cdot min^{-1}$ is not associated with an increase in 1-year post-transplant mortality, and frequently does not appear in multivariate donor risk scores even in the presence of necrotic damage [213-215]. In conjunction with our data, high donor plasma catecholamine levels were not associated with alterations in β-AR signalling. Consequently, high adrenergic support may then signify an alternate underlying pathology of the cardiomyocyte.

Perioperative management of the recipient necessitates the use of adrenergic agents to support haemodynamics in the implanted heart [216]. Transplantation however, is thought to increase the sensitivity of the heart to circulating catecholamines due to denervation and perhaps increases in β-AR densities [217]. Contradictory to this hypothesis, we have shown a slight decrease in sensitivity of the β_1-AR. Plasma NMET concentrations post-HTx for both SH-Tx and BSD-Tx were significantly higher than normal ranges (max 7.5 M) but similar to the pEC_{50} of (-)-noradrenaline (average LV and RV pEC_{50} = 7.2 M). Consistent adrenergic support may in part explain the reduced sensitivity of β_1-ARs however, plasma MET levels were within the therapeutic range and therefore may not be the prime driver of desensitisation.

Our data support previous studies that have reported decreases in myocardial β-AR densities and upregulated GRK2 levels in ischaemia-reperfusion and BSD models [49, 60, 218, 219]. Additionally, CSS and subsequent reperfusion injury may facilitate contractile dysfunction downstream of β-AR signalling, in part explaining the decrease in efficacy of (-)-noradrenaline on contractility shown here. An important question relevant to both donor heart management and post-HTx adrenergic use is, to what degree these agents contribute to cardiac dysfunction. It may be advantageous to consider the utilisation of other pharmacological (eg. Ca^{2+} sensitisers/omecamtiv mecarbil) or non-pharmacological (eg. mechanical assist devices) means to haemodynamically support the donor and recipient outside of β-AR agonists [220].

RV failure poses a significant clinical complication for both the donor heart and post-HTx graft function [221]. Our data has also shown greater cardiac dysfunction in the RV than the LV of

BSD donors and hearts post-HTx, regardless of donor BSD. It appears that this RV dysfunction may be independent of β-AR signalling when considering mechanism of donor heart dysfunction. This may be an effect of altered loading conditions [85], poor bioenergetics [72], vascular dysfunction [81] and/or hormonal disruption [59, 86, 222] either independently or collectively initiating RV dysfunction. A compromised RV then progresses to CSS and transplantation, where significant ischaemia and reperfusion injuries may worsen contractile function. RV contractile function was more greatly affected by transplantation than the LV, however both experienced a significant decrease in β_1-AR sensitivity to (-)-noradrenaline. Therefore, contractility post-HTx may in part, be due to alterations in β-AR signalling.

3.3.2 | Limitations

The short post-HTx monitoring period utilised in this study may render these data relevant to the immediate perioperative period and may not persist to induce clinically relevant longer-term consequences. Although a 6 hrs monitoring period is short, it is still longer than most large animal studies of HTx [39]. Additionally, the β-AR and bradykinin receptor densities were not directly examined, therefore any changes in their expression remain speculative, although based on functional data. GPCRs are well known to undergo G-protein switching under different cellular environments, therefore our observations may be due to alterations in cellular signalling rather than decreases in membrane receptor number [58]. This is evident in Tako-Tsubo cardiomyopathy which is characterised by Gαs-Gαi (inhibitory G-protein) switch resulting in the characteristic Tako-Tsubo phenotype [223]. BSD-mediated cardiac dysfunction shares functional similarities, such as regional hypokinesis, with Tako-Tsubo and therefore it is likely that changes in coupling may be present. A contributing factor to the low sample size for vascular studies was the variability in pre-contraction efficiency using the thromboxane-A mimetic U46619. Pre-contractions to 50% KPSS were difficult to achieve, especially for the resistance vessels, and therefore may have affected results. This is particularly relevant for the conduit vessels.

3.4 | Conclusion

The conservatism concerning organ donor selection for heart transplantation represents a growing worldwide concern that requires immediate attention. Clinical use of marginal donors has shown favourable outcomes and potentiated the reconsideration of some donor rejection criteria. We have shown decreases in contractility particularly for the RV in both the donor and post-HTx, consistent with clinical observations. Further, these data suggest that this contractile dysfunction is not due to β_1-AR desensitisation following donor BSD. However, following transplantation β_1-AR desensitisation may contribute to contractile insufficiency. Factors outside β-AR signalling should be considered to explain donor heart dysfunction, and a greater focus should be placed on improving donor heart preservation and recipient haemodynamic support. Some of these extra-adrenergic mechanisms such as mitochondrial function and metabolic derangement will be discussed in the following chapters.

CHAPTER 4

PERI-TRANSPLANT CARDIAC MITOCHONDRIAL RESPIRATION

Contents

4.0 Introduction

In the previous chapter, we showed that changes in β_1-AR function cannot wholly explain the reduction in contractility post-BSD, but rather may subsequently be involved in post-HTx contractile dysfunction. In this chapter, we explore alterations in mitochondrial function as a possible mechanism for poor donor heart function that may continue through to and adversely affect cardiac function post-HTx. Mitochondria have the important role of providing ATP to the cell and are thus essential to excitation-contraction coupling and cardiac performance. The donor heart must traverse the perilous journey from brain injury through to reperfusion in the recipient, with a multitude of potential injurious events during this process where mitochondrial damage may occur.

4.0.1 | Mitochondrial Respiration

Mitochondria utilise the stored energy in macronutrients such as fats and carbohydrates (CHO), to produce energy for the cell in the form of ATP [224]. Glycolysis breaks down glucose in the cytosol to form pyruvate, whereas FAs (dependent on their carbon length) are first activated in the cytosol to form fatty acyl-CoA [225-227]. Both pyruvate and fatty-acyl-CoA within the mitochondrial matrix enter into the TCA cycle. Two important products of the TCA are reduced nicotinamide adenine dinucleotide (NADH) and flavin adenine dinucleotide ($FADH_2$). NADH and $FADH_2$ are essentially electron carriers, which are oxidised by mitochondrial respiratory enzymes in a process called oxidative phosphorylation (OXPHOS) [224].

OXPHOS utilises four inner membrane-bound proteins to oxidise NADH and $FADH_2$, with a terminal reduction of molecular oxygen, the mechanism of which is referred to as the chemiosmotic theory [228-230]. This process starts at NADH dehydrogenase or Complex I (CI), where NADH is oxidised by CI to form NAD+ and a hydrogen ion (H^+). NAD is returned to the NAD pool where it can be reduced again in the TCA. Simultaneously $FADH_2$ is oxidised by succinate dehydrogenase or Complex II (CII), leaving FAD and a H^+. The 2 electrons (e-) liberated by CI and CII are now passed onto ubiquinone with two H^+ ions thus reducing it to

ubiquinol. This convergent electron flow toward ubiquinone is referred to as the Q-junction, and causes $4H^+$ to move from the matrix into the intermembrane space via CI only [231].

Ubiquinol then shuttles these 2e- to cytochrome c (Cyt c) oxidoreductase or Complex III (CIII), a process that pumps 2 more H^+ into the intermembrane space. These 2e- then take two paths, the first reducing Cyt c, the second reducing Cytochrome b forming a semi-quinone molecule. A second Ubiquinol binds to CIII, thus pumping another $2H^+$ and transferring 2 more e-, which repeat the cycle. The second pair of e- again bind Cyt c and b, this time further reducing semi-quinone to form a ubiquinol molecule which is returned to the ubiquinol pool. This ubiquinone-dependent electron cycling is referred to as the Q-cycle. Cyt c then shuttles the 2e- from two ubiquinol to cytochrome oxidase or Complex IV (CIV), reducing CIV and pumping 2 H^+. Finally, the 2e- are then used to reduce molecular oxygen to form water [231]. Figure 4.1 shows a graphical representation of the oxidative phosphorylation process.

The pumping of H^+ into the intermembrane space creates a potential difference between the matrix and the intermembrane space. This mitochondrial membrane potential ($\Delta\psi_m$) is utilised by ATP synthase, an enzyme that transfers the force of H^+ moving down its gradient or proton motive force (Δp) to generate ATP [231, 232]. The proton motive force is a function of both the charge potential and the pH (concentration gradient) difference between the matrix and the intermembrane space. At 37°C the Δp can be expressed using the equation, $\Delta p = \Delta\psi_m - 60\Delta pH$, where $\Delta\psi_m$ = 150 mV and ΔpH= -0.5 units, resulting in a Δp of approximately 180 mV [232]. Under normal circumstances the Δp can range from 180-220 mV, with the largest contributor being the $\Delta\psi_m$, contributing 150-180 mV and the ΔpH contributing the remaining 30-60 mV [232]. The continued maintenance of Δp by OXPHOS drives the production of approximately 65 kg ATP per day needed for a resting heart [233].

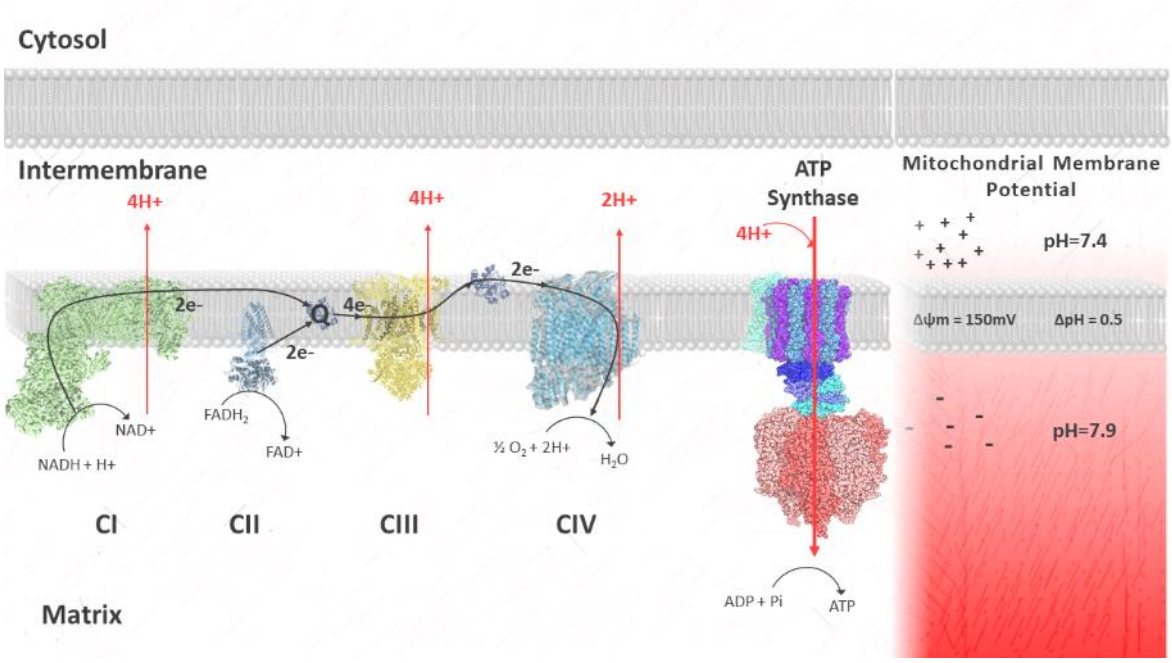

Figure 4.1. Graphical representation of oxidative phosphorylation and membrane potential. Convergent electron flow from oxidation of NADH and $FADH_2$ at CI & CII, respectively, reduce ubiquinone to ubiquinol QH, i.e the Q junction. QH then shuttles 2e- from CI and 2e- from CII to CIII in 2 consecutive cycles, referred to as the Q-cycle. Electrons then flow from CIII to Cyt c and subsequently to CIV. Electrons from CIV are then used to reduce molecular oxygen to form water. Shuttling of e- from complex to complex provides the energy required to pump H^+ into the intermembrane space to create a membrane potential. Components of the membrane potential include the charge potential ($\Delta\psi m$) and the concentration gradient or pH gradient. Combined these components create a proton motive force of ~180 mV. ATP synthase then uses the proton motive force of intermembranous H^+ to produce ATP.

4.0.2 | Mitochondrial Function and BSD

There is limited empirical evidence of mitochondrial disturbance after donor BSD. To date, only one study has directly examined mitochondrial respiration post-BSD. In permeabilised muscle fibres from the *peroneus longus* muscle of the lower limb of patients with BSD, Sztark *et al.*, [70] found that phosphorylative oxygen consumption rates and respiratory control were depressed compared to non-BSD patients. The authors concluded that this depressed phosphorylative control was due to 1) the catecholamine surge, 2) metabolic switch, and 3) depletions in T3 hormone.

An effective strategy to increase cardiac work is to increase the rate of ATP synthesis. This is achieved physiologically via catecholamines, acting through adrenergic receptors to increase intracellular Ca^{2+}, which in turn activates the TCA cycle [226]. Consequently, higher metabolic demand increases oxygen requirements, leading to physiological increases in ROS. Oxygen delivery in the context of BSD however is compromised [52], causing ischaemia and pathological increases in Ca^{2+} and ROS. Both Ca^{2+} overload and ROS can disturb mitochondrial respiration, and in severe cases, lead to the opening of the mPTP [234]. Opening of the mPTP leads to mitochondrial swelling and mitophagy, effectually compromising cardiac bioenergetics [234, 235].

Reducing oxygen supply in the presence of high metabolic demand prompts a switch from FA utilisation and oxidation to anaerobic CHO utilisation [226, 236]. The metabolic consequences of BSD and HTx are discussed further in the following chapter. Briefly, this metabolic switch increases intracellular levels of lactate, reducing pH, and initiating cellular apoptosis [236]. A hallmark of this process is the uncoupling of glycolysis to glucose oxidation in the mitochondria. Glycolytic uncoupling has been shown to contribute to the progression of HF [236].

T3 depletion was one of the first described hormonal disturbances in BSD [48, 86]. It is characterised in animal models by a gradual decrease over time from ictus to suboptimal levels 3-6 hours post-BSD [12, 48]. On a mitochondrial level, T3 is believed to regulate mitochondrial biogenesis, oxidative phosphorylation and some evidence suggests that T3 prevents the opening of the mPTP [89, 90]. Recent evidence suggests that T3 therapy does not improve cardiac function post-BSD and may worsen patient outcomes [40, 91]. Regardless, T3 therapy remains a standard of care in potential cardiac donors and as such is included in the care of our sheep model.

In Chapter 3 (pg. 80-81), it was shown that BSD does not cause functional desensitisation, however contractile performance was compromised. The mechanisms influencing mitochondrial function explained thus far may contribute to reduced contractile performance. Excessive catecholamine stimulation has been reported to promote mitochondrial dysfunction via increasing ROS, intracellular Ca^{2+}, and altering metabolism [201]. In the context of BSD, altered

mitochondrial function may play an important role in both donor heart and post-transplant graft function. Aside from desensitisation, the molecular machinery involved in the process also acts on important signalling pathways [57].

Of specific interest to BSD, the profound catecholamine storm increases GRK2 activity and may influence GRK2 translocation to the mitochondria. Studies have shown that increases in ROS activate the MAPK-ERK pathway to phosphorylate GRK2, allowing the association with heat shock protein 90 (Hsp90) [237]. Hsp90 acts as a chaperone of GRK2, translocating it to the mitochondria, where GRK2 influences mitochondrial respiration [238]. As a consequence of the catecholamine storm, increases in cardiac GRK2 have been shown in BSD models up to 6 hrs post-injury [49, 60]. Whether mitochondrial GRK2 levels increase as a consequence of BSD is unknown.

4.0.3 | Mitochondrial Function and Cold Static Storage

The main strategy for organ preservation is CSS, the aim of which is to reduce metabolism and maintain graft viability [106]. However, as stated in Chapter 1, ATP consumption during CSS is not completely arrested, giving rise to the potential of energetic compromise [106, 112]. To overcome the cold ischaemic damage imposed on the donor heart, numerous preservation solutions have been developed, along with perfusion technologies that aim to increase graft viability. These aspects of CSS are beyond the scope of this project, and have been discussed in Chapter 1. This project will focus on previous works which have examined energetics during the traditional CSS period.

During CSS, activation of the Na^+/H^+ exchanger increases intracellular Na^+ ions in the presence of dysfunctional Na^+/K^+ATPase. This causes the reverse action of the Na^+/Ca^{2+} exchanger, leading to Ca^{2+} overload and further inhibiting mitochondrial function. The manifestation of these responses is mitochondrial dysfunction and reduction in high energy phosphate (HEP). Both animal and human studies have identified reductions in HEPs during CSS [72, 114, 115]. Table 4.1 summarises the reported effects of CSS on myocardial HEP levels. Generally, most studies

reported reduced HEP levels during CSS, except for Stoica *et al*., who reported a replenishment of HEP during CSS compared to pre-explantation. In the study by Stoica, HEP compromised was evident during warm ischaemia and reperfusion. The differences between the studies may be due to methodological differences in HEP detection, where each study employed a different technique.

Table 4.1. Summary of studies investigating the effect of CSS on myocardial HEP levels

Study	BSD (Yes/No)	CSS Duration (hrs)	Species	HEP effect	HEP Detection
Van Caenegem *et al.*, [122]	No	4	Pig	↑AMP/ATP ratio ↓PCr/Cr ratio	HPLC
Biagioli *et al.*, [115]	Yes	1.46 ± 0.87	Human	↓ATP, GTP, ATP/ADP ↑AMP, GMP, IMP, Ado, Hyp	CE
Bruinsma *et al.*, [239]	Yes	17	Cat	Depleted PCr at 6 hrs (BSD and control) ↑ Pi at 4 hrs – greater increase in control animals Gradual decline in γATP for both groups	^{31}P MRS
Stoica *et al.*, [72]	Yes		Human	↑ ATP and EC during CSS compared to pre-explanation	Chemiluminescence

AMP- adenosine monophosphate, ADP- adenosine diphosphate, ATP- adenosine triphosphate, PCr- Phosphocreatine, Cr- Creatine, GTP- Guanosine triphosphate, GMP- guanosine monophosphate, IMP- inosine monophosphate, Ado- adenosine, EC- energy charge (given by ATP + 0.5ADP/ATP + ADP +AMP), HPLC- high performance liquid chromatography, CE – capillary electrophoresis, ^{13}P MRS- phosphorus-31 magnetic resonance spectroscopy, chemiluminescence – via luciferin-luciferase

4.0.4 | Mitochondrial Function Post-Transplantation

The next stage in the HTx timeline is implantation, where the heart experiences a period of warm ischaemia, whilst anastomoses are completed, and reperfusion injury. Both Stoica and Van Caenegem found that at the time of reperfusion, energy status was not fully restored highlighting energetic compromise [72, 122]. This compromise was also associated with future cardiac dysfunction in human hearts [72]. Exacerbating bio-energetic dysfunction, the transplanted heart is also subject to the classical IRI cascade involving hypercontracture, metabolic dysfunction, mitochondrial succinate build-up, ROS production, and mPTP opening [133, 138, 240]. IRI as a pathologic diagnosis was present in 48% of autopsied PGD hearts, highlighting its involvement in PGD development [5, 8].

This study aimed to examine cardiac mitochondrial respiration, membrane potential, and ROS production after 24 hrs BSD and cardiac transplantation. Further, we developed a cellular model of BSD utilising human induced pluripotent stem cell-derived cardiomyocytes (hIPSC-CM). Using this model we investigated if the catecholamine storm and subsequent β-AR stimulation with isoprenaline (ISO) can induce the translocation of GRK2 to the mitochondria. A cellular model was used to ascertain the direct consequences of β-AR stimulation alone without any confounding factors of the donor management process.

4.1 | Methods

Following the 24 hr donor monitoring period, or 6 hr monitoring period post-HTx, the heart was excised and placed immediately into cold oxygenated Krebs solution and transported to the laboratory (Chapter 3). Approximately 10 mg biopsies were taken with a biopsy gun at the base, mid and apical regions of both ventricles. These biopsies were placed in cold respiration buffer (MiR05, Oroboros Instruments) containing: EGTA (0.5 mmol/L), $MgCl_26H_2O$ (3 mmol/L), K-lactobionate (60 mmol/L), Taurine (2 mmol/L), KH_2PO_4 (10 mmol/L), HEPES (20 mmol/L), sucrose (110 mmol/L), FA free bovine serum albumin (1 g/L) at pH 7.1. An equal amount of each biopsy (~7 mg per ventricle) was pooled together to mitigate regional variations in mitochondrial

respiration and obtain a more accurate representation of mitochondrial respiration for the entire ventricle. Samples were homogenised using the PBI-Shredder SG3 (Oroboros Instruments) in 500 µL MiR05 (20 mg/mL) for 10 sec in position 1 and 5 sec in position 2. To yield a 1 mg/mL chamber concentration, 50 µL of the 20 mg/mL homogenate was injected into each 2 mL respiratory chamber of the O2k-oxygraph (Oroboros Instruments, Innsbruck, Austria), followed by respirometry and fluorometry measures.

4.1.1 | General methods for High-Resolution Fluoro-Respirometry

High-resolution fluoro-respirometry (HRR) is assessed using the Oroboros Oxygraph (O2k) combined with the addition of substrates, uncouplers, and inhibitors of the electron transport system (ETS). Mitochondrial preparations (tissue homogenate or intact cells) are injected into 1 of 2 chambers of an O2k. This chamber contains MiR05, a magnetic stirrer, and an injector port or stopper which is elevated to create a gas phase with the atmosphere and allow oxygen diffusion and calibration. Before the sample is added, the stopper is depressed into the chamber to remove the gas phase (Fig 4.2). Removing this gas phase prevents further oxygen diffusion and therefore any changes in oxygen concentration, measured via oxygen sensors, are due to mitochondrial oxygen utilisation.

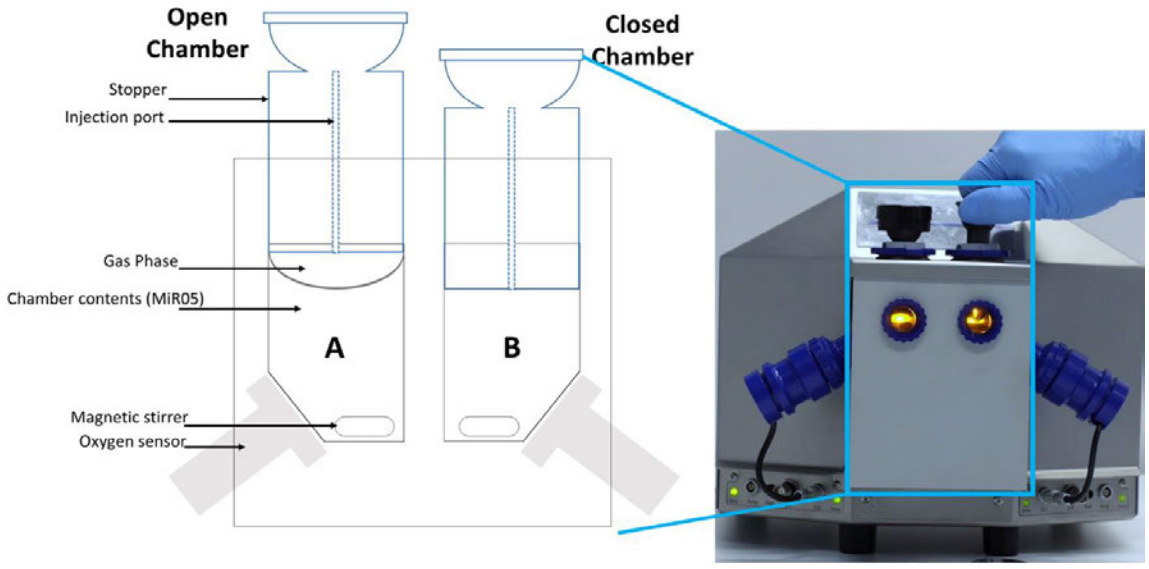

Figure 4.2. The Oroboros Oxygraph (right) and a schematic diagram of the highlighted region (left). Mitochondrial preparations were suspended in the chamber containing MiR05 with the stopper depressed closing the system. Any changes in oxygen concentration therefore are dependent on mitochondrial utilisation for oxidative phosphorylation. The open configuration with a gas phase is used to calibrate the oxygen signal to atmospheric air.

Respiratory complex-specific function can be determined via sequential substrate-uncoupler-inhibitor titrations (SUIT) protocols. Substrates for OXPHOS are added that, via the TCA cycle, create NADH (N-linked, CI), $FADH_2$ (F-Linked) substrates, or succinate (S-linked) for succinate-dehydrogenase (CII). The addition of these substrates in the absence of ADP is referred to as LEAK respiration. LEAK is oxygen utilisation that compensates for proton slip and is not involved in the generation of ATP, but is influenced by the production of ROS as a consequence of proton and electron slip [241]. Next, the addition of saturating concentrations of ADP allows the formation of ATP via oxidative phosphorylation, traditionally referred to as state 3 respiration, hereafter referred to as OXPHOS. By adding ADP after substrates for CI, CI-mediated OXPHOS capacity can be determined and likewise after Succinate, CII OXPHOS capacity can be determined.

OXPHOS capacity in living systems rarely functions at maximum capacity. There is an excess capacity imposed by the phosphorylation system caused by coupling or the dependence of electron input at one point from an upstream source, ie CIII requires electrons from the Q-junction [241]. Experimentally, maximum capacities can be obtained by uncoupling respiration using a protonophore, a substance that allows H^+ to move from the intermembrane space to the matrix. The partial collapse of the $\Delta\psi_m$ uncouples the phosphorylation system allowing the ETS to operate at maximum capacity (ETmax) [241].

Other oxidative reactions that do not contribute to phosphorylation occur within the mitochondria and their oxygen consumption must be accounted for. To achieve this, specific inhibitors of the phosphorylation system are added sequentially. Once inhibition of the phosphorylation system is achieved, the remaining or residual oxygen consumption (ROX) can be accounted for [241]. The respirometry parameters used in this study to compare mitochondrial function between groups are described in table 4.2.

Table 4.2. Parameters calculated from high resolution respirometry with a brief description [113, 241]

Parameter	Description	Substrates Added [Final concentration]
LEAK	A measure of mitochondrial coupling. High LEAK represents high oxygen wastage.	P [5 mM]/Pal [20 mM]+ M [2/5 mM] + G [10 mM]
CI OXPHOS	Isolated Complex I phosphorylative state (ATP producing)	PMG + ADP [2.5 µM]
L/P	A measure of OXPHOS coupling calculated as the ratio of LEAK to CI OXPHOS. Elevated L/P represents lower OXPHOS coupling	NA
Cyt C	Oxygen consumption measured after exogenous Cyt c titration during CI OXPHOS	PMG+ADP+Cyt c [10 µM]
CII OXPHOS	Isolated Complex II phosphorylative state, corrected for CI OXPHOS	PMG+ADP+Cyt C+Succ [10 mM] +ADP
ETmax	A measure of maximum mitochondrial oxygen utilisation following experimental uncoupling with CCCP.	PMG+ ADP+ Cyt C+ Succ+ ADP+ CCCP [0.5-2.5 µM]
ROX	Residual oxygen consumption after ETS inhibition	Total ETS + Rot [0.5 µM] + MnA [5 µM] + AmA [2.5 µM]

P – Pyruvate, Pal – Palmitoylcarnitine, M- Malate [2mM for CHO SUIT and 5mM for FA SUIT], G- Glutamate, ADP-adenosine diphosphate, Cytc C- Cytochrome C, Succ- Succinate, OXPHOS- oxidative phosphorylation, CCCP- Carbonyl cyanide m-chloro phenyl hydrazone, Rot- Rotenone, MnA- Malonic acid, Ama- Antimycin A, ETS- Electron transport system ETmax- Electron transport system capacity. NA-Not applicable

4.1.2 | Sheep Heart High-Resolution Fluoro-Respirometry

Two SUIT protocols were performed to determine HRR in tissue homogenate from donor and post-HTx hearts. SUIT1 measured HRR in the presence of carbohydrate substrates and SUIT2 utilised β-oxidation in the presence of FA substrates (Table 4.3). After the addition of N-linked substrates, ADP was added to obtain CI-mediated OXPHOS capacity. For SUIT2, palmitoyl carnitine produces both N- and F-linked substrates and therefore required further N-linked support from malate [241]. Cyt c was titrated to assess mitochondrial outer membrane integrity. This was followed by the addition of succinate and ADP to determine CI+CII-mediated OXPHOS capacity. Uncoupler titrations with carbonyl cyanide m-chlorophenyl hydrazone (CCCP) were applied to determine maximum CI+CII ETmax capacity. Serial titrations of rotenone, malonic acid, and Antimycin A were added to inhibit CI, II, and III respectively, to induce ROX state. All oxygen consumption rates are corrected against ROX as this state reflects oxygen consumption that does not contribute to OXPHOS, but side reactions [241].

Mitochondrial membrane potential was quantified fluorometrically using the LED2 module and the fluorophore Tetramethylrhodamine methyl ester (SUIT3, TMRM) (Excitation: 548 nm, Emission: 574 nm). TMRM accumulates in energised mitochondria proportional to membrane potential, quenching the fluorescent signal. Depolarisation causes the release of TMRM and an increase in fluorescence at 574 nm. After calibration of the fluorometry signal to a final concentration of 2 μM, 1 mg/mL of tissue homogenate was injected into the chamber. Membrane potential was determined using CHO substrates.

Table 4.3. SUIT protocols 1-3, in order of titration (top to bottom) and the respective final bath concentration for each compound

SUIT 1		SUIT 2		SUIT 3	
Substrate	**[Final]**	**Substrate**	**[Final]**	**Substrate**	**[Final]**
Catalase	280 U/mL	Catalase	280 U/mL	Catalase	280 U/mL
Pyruvate	5 mM	Malate	5 mM	TMRM	0-2 µM
Malate	2 mM	Glutamate	10 mM	Pyruvate	5 mM
Glutamate	10 mM	Palmatoylcarnitine	20 µM	Malate	2 mM
ADP	2.5 mM	ADP	2.5 mM	Glutamate	10 mM
Cytochrome c	10 µM	Cytochrome c	10 µM	ADP	2.5 mM
Succinate	10 mM	Succinate	10 mM	Cytochrome c	10 µM
ADP	2.5 mM	ADP	2.5 mM	Succinate	10 mM
CCCP	1-2.5 µM	CCCP	1-2.5 µM	ADP	2.5 mM
Rotenone	0.5 µM	Rotenone	0.5 µM	CCCP	1-2.5 µM
Malonic Acid	5 µM	Malonic Acid	5 µM	Rotenone	0.5 µM
Antimycin A	2.5 µM	Antimycin A	2.5 µM	Malonic Acid	5 µM
Ascorbate	2 µM	Ascorbate	2 µM	Antimycin A	2.5 µM
TMPD	0.5 µM	TMPD	0.5 µM	Ascorbate	2 µM
Azide	100 mM	Azide	100 mM	TMPD	0.5 µM
				Azide	100 mM

CCCP - carbonyl cyanide m-chlorophenyl hydrazone, TMPD - N,N,N′,N′-tetramethyl-p-phenylenediamine. Dose regimes [Volume/stock concentration]; SUIT 1: catalase [5 µL/112000IU/mL], pyruvate [5 µL/2 M], malate [5 µL/0.8M], glutamate [10µL/2M], ADP [4µL/1.25M], cytochrome c [5µL/4mM], succinate [20µL/1M], CCCP [1µL/1mM], rotenone [5µL/1mM], malonic acid [5µL/2M], antimycin A [1µL/5mM], ascorbate [5 µL/0.8M], TMPD [5 µL/0.2M], Azide [50µL/5M], SUIT 2: Dosages the same as SUIT 1 except malate [12.5µL/0.8M], palmitoylcarnitine [4µL/10mM], SUIT 3: Dosages the same as SUIT 1 including TMRM [4µL/0.2mM].

4.1.3 | HRR Data Analysis

Mitochondrial oxygen consumption was corrected for ETmax capacity and expressed as flux control ratios (FCR) calculated as per Gnaiger *et al* [241]. Three respiratory states were compared, i) LEAK (PMG), ii) CI-mediated OXPHOS (PMG + ADP), and CII-mediated OXPHOS (Succinate + ADP corrected for CI). For membrane potential using TMRM, data were expressed in absolute units (AU) as described by Chowdhury *et al* [242]. The magnitude change between states was used to isolate the effects at the same respiratory states mentioned above. For this calculation, membrane potential produced in LEAK state was calculated as the magnitude change in AU_{TMRM} between the addition of tissue homogenate and N-linked substrates (PMG). CI-mediated depolarisation capacity was calculated as the change in fluorescent signal between LEAK and CI (PMG + ADP). The CII contribution to $\Delta\psi_m$ was calculated as the difference in fluorescent signal between succinate titration and CII (Succ + ADP). Utilising FCR and AU corrects for any changes in mitochondrial density or morphology [241]. Table 4.4 shows the calculations used to determine HRR and $\Delta\psi_m$.

Table 4.4. Calculations used to determine i) respiratory activity, corrected for maximum capacity (ETmax) and ii) mitochondrial membrane potential. Respiratory activity and membrane potential were measured in LEAK, CI OXPHOS and CII OXPHOS states. [241, 242]

Parameter	Calculation
LEAK	$LEAK\ (FCR) = \frac{\text{PMG (Oxygen flux [pmol} \cdot \text{s}^{-1} \cdot \text{mg}^{-1}\text{])} - ROX}{ETS}$
Complex I OXPHOS	$CI\ (FCR) = \frac{\text{PMG + ADP (Oxygen flux [pmol} \cdot \text{s}^{-1} \cdot \text{mg}^{-1}\text{])} - ROX}{ETS} - LEAK\ (FCR)$
Complex II OXPHOS	$CII\ (FCR) = \frac{\text{PMG + succ + ADP(Oxygen flux [pmol} \cdot \text{s}^{-1} \cdot \text{mg}^{-1}\text{])} - ROX}{ETS} - CI\ (FCR)$
$\Delta\psi_m$ (LEAK)	$\Delta\psi\text{m (LEAK)} = Thom\ \Delta\psi\text{m}\ (AU_{TMRM}) - \text{LEAK}\ (AU_{TMRM})$
$\Delta\psi_m$ (Complex I)	$\Delta\psi\text{m (CI)} = CI\ [PMG + ADP](AU_{TMRM}) - \text{LEAK [PMG]}\ (AU_{TMRM})$
$\Delta\psi_m$ (Complex II)	$\Delta\psi\text{m (CII)} = CII\ [Succ + ADP]\ (AU_{TMRM}) - \text{Succ}(AU_{TMRM})$

FCR- flux control ratio, $\Delta\psi_m$ – mitochondrial membrane potential, Thom- tissue homogenate, PMG- pyruvate, malate, glutamate, ADP- adenosine diphosphate, Succ- succinate, TMRM- Tetramethylrhodamine, methyl ester, CI- complex I, CII- complex II

4.1.4 | Tissue ROS Assays

Tissue levels of 3-nitrotyrosine modified proteins were assessed using a competitive ELISA (Abcam CAT #ab113848). Initial optimisations showed that; i) a higher initial sample concentration (20 mg/mL) was needed compared to the manufacturer's protocol (5 mg/mL) and ii) an overnight incubation at 4°C was required to obtain a reliable result. All other steps were completed as per the manufacturer's protocol. The tissue levels of oxidised and reduced

glutathione (GSH:GSSG) was assessed using a fluorometric-green assay (Abcam CAT #ab138881). The assay was performed according to the manufacturer's protocol with no alterations.

4.1.5 | hIPSC-CM Cell Culture

Human-induced pluripotent stem cell-derived cardiomyocytes (hIPSC-CM) were obtained as 14-day old cell suspensions from the Institute of Molecular Bioscience, University of Queensland (courtesy of Dr. Meredith Redd). Cells were diluted with RPMI-1640 media supplemented with, 1X B27 supplement (Life Technologies), 5% FBS, 0.1% Rho kinase inhibitor (ROCKi – to inhibit replating-derived apoptosis) (Y-27632, Stem Cell Technologies) and 1% Penicillin-Streptomycin. The diluted cell suspension was then plated in 5 ug/mL Vitronectin (Stem Cell Technologies) coated 35 mm dishes at 10^6 cells/dish and incubated overnight (37°C, 5% CO_2), to allow adherence. After overnight incubation, the media was changed and the cells were allowed to mature for 7 days, with media changes every second day, until a beating monolayer was observed under the microscope.

4.1.6 | hIPSC-CM Treatment

Cells were separated into 3 experimental groups based on catecholamine stimulation; 1. Control (no stimulation), 2. Chronic ISO stimulation and 3. Acute ISO stimulation. The chronic group was stimulated with 100 nM ISO for 24 hrs with media changes every 6 hrs to replace degraded ISO. The acute group was stimulated with 100 nM ISO for 1 hr to simulate BSD-mediated catecholamine response, followed by washout and replacement with ISO-free media, and further culture for 24 hrs.

These groups were further subdivided based on antagonism into; 1. No inhibition, 2. β-AR inhibition, 3. GRK2 inhibition and 4. β-AR/GRK2 inhibition. Antagonists were added to complete media 90 mins before ISO stimulation, in addition to 100 nM Prazosin hydrochloride (Praz) to inhibit α_1-receptor for all groups. Propranolol (Prop, 100 nM) was administered to inhibit β-ARs, while Compound 101 (CMPD101, 30 μM) was administered to inhibit GRK2. Following the 24 hr stimulation protocol, cells were dissociated and prepared for western blotting. Figure 4.3 shows a schematic diagram of the grouping for hIPSC-CM experiments.

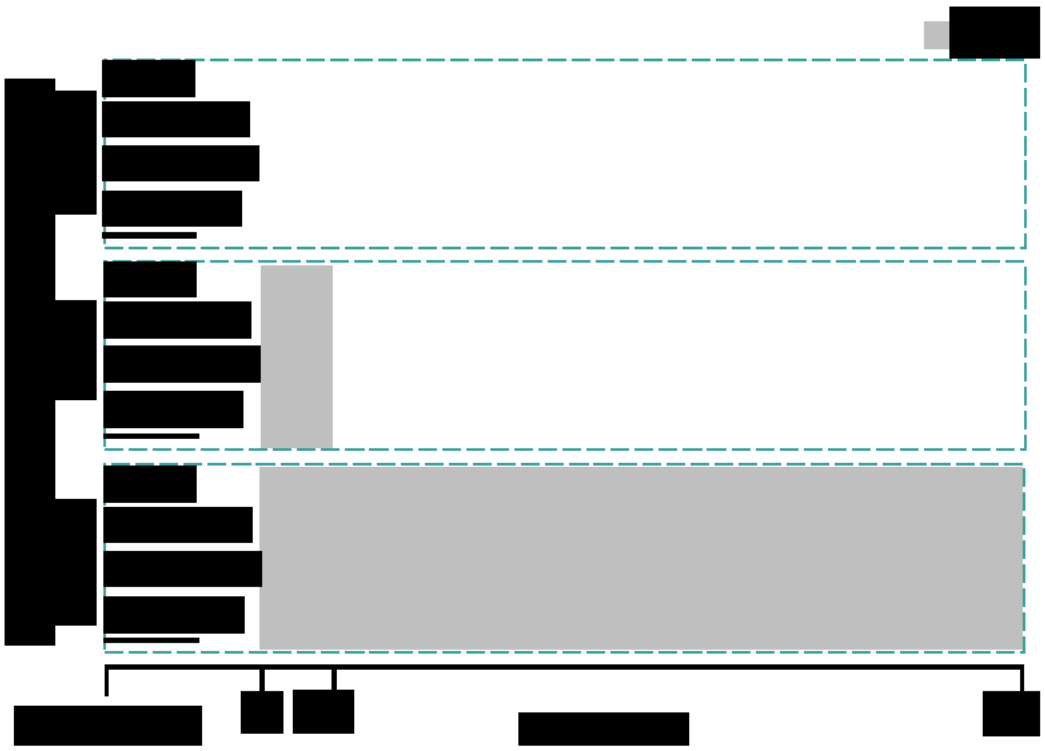

Figure 4.3. Schematic diagram of the time-course and experimental groups for hIPSC-CM experiments.

4.1.7 | Western Blotting

Western blotting for mitochondrial GRK2 was performed using isolated mitochondrial fractions from 1.8 x 10^6 cells. Cells were washed in isolation buffer (mM; 70 Sucrose, 190 Mannitol, 20 HEPES, 0.2 EDTA), centrifuged at 1000 RPM for 5 mins, the pellet resuspended in isolation buffer and incubated on ice for 10 min. After incubation, cells were lysed with an ice-cold pellet pestle, and the suspension was centrifuged at 600 x g for 10 mins. The supernatant was collected and centrifuged at 10, 000 x g for 10 mins to isolate the mitochondrial pellet. The mitochondrial

pellet was then resuspended in radioimmunoprecipitation assay (RIPA) lysis buffer with 1% Protease/Phosphatase Inhibitor Cocktail (Thermo-Fisher). The mitochondrial fraction was then homogenised with a Polytron Homogeniser followed by 100% ethanol precipitation to concentrate proteins.

Approximately 5 μg of protein/well was loaded onto an 8% Bis-Tris gel for SDS-Page. Samples were loaded in duplicate across a total of 6 gels. Proteins were transferred using the iBLOT system (Thermo-Fisher) to a polyvinylidene difluoride (PVDF) membrane. The membrane was probed for GRK2 with a rabbit anti-GRK2 (#3982, Cell Signalling Technologies, 1:1000) and a rabbit anti-Hsp60 (ab46798, Abcam, 1:20, 000). Secondary antibody staining followed with goat anti-rabbit horseradish peroxidase (HRP) conjugated secondary (A16110, 1:2000). Protein was detected using enhanced chemiluminescence (ECL) detection (Amersham) and visualised using the ImageQuant 350 Phosphorimager (GE Life Sciences). Densitometry was measured using ImageJ software for GRK2 (~80kDa) and corrected for Hsp60 (~60kDa) expression. Hsp60 normalisation was performed to decrease the variation in mitochondrial content across samples.

4.1.8 | Statistics

All data were expressed as means ± SE unless otherwise stated. A one-way ANOVA with Tukey's post-hoc analyses was used to determine statistically significant changes. Where normality is violated, non-parametric Kruskal-Wallis tests with Dunn's post-hoc analyses were used. Statistical significance was determined if $p<0.05$.

4.2 | Results

Ventricular biopsies were taken from 6 SHAM, 6 BSD donor animals and 9 HR, 4 SH-Tx, and 5 BSD-Tx hearts for mitochondrial respiratory tests using CHO substrates (SUIT 1). For the membrane potential (SUIT 3) and FA (SUIT 2) protocols, some tissue was lost to optimisation experiments, reducing the sample size. Table 4.5 summarises the sample sizes for each group across each SUIT protocol.

Table 4.5. Sample size distribution for each group across each SUIT protocol

	HR	SHAM	BSD	SH-Tx	BSD-Tx
SUIT 1 – CHO Substrates	9	6	6	4	5
SUIT 2 – FA Substrates	7	3	3	4	4
SUIT 3 – Membrane Potential	8	6	6	3	4

SUIT- Substrate Uncoupler Inhibitor Titration, HR- Healthy Recipient, SHAM – Sham operated donor hearts, BSD – Brain stem dead donor hearts, SH-Tx – SHAM donor hearts that have been transplanted, BSD-Tx- BSD donor hearts that have been transplanted

4.2.1 | Mitochondrial Respiration

Overall, there were no differences in FCRs at any level of the ETS between CHO or FA substrates for any group. Maximum uncoupled respiration (ETmax) was depressed post-HTx in the LV for the BSD-Tx group compared to SHAM for N-linked substrates (BSD-Tx (n=5): 23.13 ± 6.95 pmol· s^{-1}· mg^{-1} vs SHAM (n=4): 71.61 ± 8.81 pmol·s-1·mg-1, p=0.02). For all other groups and FA substrates, ETmax capacities were highly variable and not different between groups (Table 4.6).

4.2.2 L/P Ratios and Cyt c FCR in Donor Hearts – SHAM & BSD

In the presence of CHO substrates, the L/P (phosphorylative coupling) ratio was elevated post-BSD compared to SHAM and HR (p>0.05) and significantly elevated in the LV between BSD and HR (BSD (n=6): 0.46 ± 0.10, HR (n=9): 0.14 ± 0.02, p=0.01) (Table 4.6). This trend was similar for F-linked substrates although statistical significance was not reached. There were no changes in Cyt c FCR post-BSD for either ventricle (Table 4.6).

4.2.3 L/P Ratios and Cyt c FCR in Transplanted Hearts – SH-Tx & BSD-Tx

Post-HTx L/P ratios were similar between the two groups (BSD-Tx and SH-Tx) but trended higher compared to control groups (HR and SHAM, p>0.05) (Table 4.6). Cyt c FCR was moderately reduced for both ventricles, groups, and substrates compared to SHAM and HR, but

reached statistical significance for BSD-Tx compared to SHAM in the LV only (BSD-Tx (n=5): 0.35 ± 0.10 vs SHAM (n=6): 0.58 ± 0.02, =0.03) (Table 4.6).

Table 4.6. Group means ± SE for maximum CHO and β-oxidation-mediated electron transport capacity (ETmax), complex I phosphorylation coupling (L/P) and exogenous Cyt c stimulation (Cyt c FCR).

	HR, n=9 (±SE)	SHAM, n=6 (±SE)	BSD, n=6 (±SE)	SH-Tx, n=4 (±SE)	BSD-Tx, n=5 (±SE)
SUIT 1- CHO					
Left Ventricle					
ETmax	61.96 (11.18)	71.61 (8.81)	59.39 (7.96)	30.81 (3.63)	23.13 (6.95)[b]
L/P FCR	0.14 (0.02)	0.20 (0.02)	0.46 (0.1)[a]	0.3 (0.12)	0.36 (0.11)
Cyt c FCR	0.55 (0.03)	0.58 (0.02)	0.53 (0.05)	0.38 (0.06)	0.35 (0.1)[c]
Right Ventricle					
ETmax	42.97 (8.97)	58.41 (8.35)	30.57 (6.05)	40.09 (7.64)	22.75 (7.86)
L/P FCR	0.43 (0.32)	0.17 (0.03)	0.57 (0.2)	0.31 (0.11)	0.37 (0.12)
Cyt c FCR	0.55 (0.07)	0.48 (0.06)	0.59 (0.07)	0.28 (0.08)	0.38 (0.1)
SUIT 2- FA	**HR, n=7 (±SE)**	**SHAM, n=3 (±SE)**	**BSD, n=3 (±SE)**	**SH-Tx, n=4 (±SE)**	**BSD-Tx, n=4 (±SE)**
Left Ventricle					
ETmax	39.21 (6.02)	49.93 (8.52)	35.47 (6.84)	57.22 (21.37)	32.08 (5.04)
L/P FCR	0.29 (0.05)	0.28 (0.06)	0.76 (0.34)	0.42 (0.13)	0.55 (0.10)
Cyt c FCR	0.48 (0.08)	0.47 (0.12)	0.50 (0.18)	0.32 (0.11)	0.23 (0.10)
Right Ventricle					
ETmax	36.29 (9.66)	36.29 (6.72)	41.88 (6.75)	52.82 (18.75)	27.14 (2.96)
L/P FCR	0.32 (0.05)	0.17 (0.03)	0.66 (0.17)	0.44 (0.16)	0.50 (0.09)
Cyt c FCR	0.46 (0.06)	0.48 (0.12)	0.42 (0.08)	0.37 (0.04)	0.25 (0.07)

a-statistically different compared to HR(p=0.01, BSD), b-significantly different compared to SHAM (p=0.02), c- significantly different compared to SHAM (p=0.03)

4.2.4 | LEAK Respiration

Using CHO substrates, LEAK post-BSD was moderately increased in the LV and significantly elevated in the RV compared to HR, suggestive of higher mitochondrial uncoupling (BSD (n=6): 0.11 ± 0.03 FCR vs HR (n=9): 0.03 ± 0.01 FCR, $p<0.01$) (Fig. 4.4A). No changes in LEAK respiration were evident in SH-Tx hearts compared to donor (SHAM or BSD) or HR hearts. BSD-Tx, showed a bi-ventricular elevation in LEAK above controls (HR and SHAM) (Fig 4.4A).

Mitochondrial membrane potential production in LEAK was similar for both donor groups. The RV for the SH-Tx group did not develop a similar $\Delta\psi_m$ compared to HR (p=0.04, n=13). Reduced RV $\Delta\psi_m$ was also observed in the BSD-Tx group compared to HR (p=0.006, n=14), SHAM (p=0.04, n=15) and BSD (p=0.02, n=15) groups (Fig. 4.4B). This trend toward increased LEAK was also observed post-BSD and transplantation using FA substrates, but was not significant (Fig 4.7 A&D).

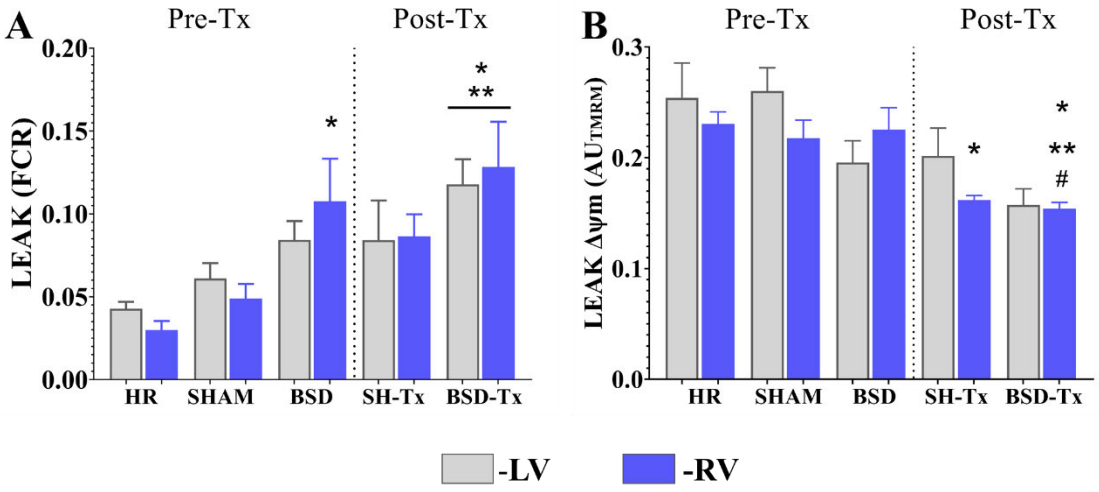

Figure 4.4. Mitochondrial respiration and Δψm in LEAK state using CHO substrates (SUIT 1). A. Oxygen utilisation, corrected for maximum activity (FCR). **B.** Δψm production. *significantly different compared to HR, ** significantly different compared to SHAM, # significantly different from BSD

4.2.5 | Complex I Respiration

Both SHAM and BSD hearts showed similar CHO-mediated CI activity (Fig. 4.5A). Post-HTx, CI activity for SH-Tx and BSD-Tx was moderately (although not significantly) elevated above HR and donor levels (Fig. 4.5A). There were no obvious trends in CI-mediated $\Delta\psi_m$ for either donor group (Fig. 4.5B). Post-HTx $\Delta\psi_m$ depolarisation capacity moderately (but not significantly) declined, particularly for BSD-Tx (Fig 4.5B). Using FA substrates, CI FCR was moderately elevated post-BSD in the LV and both ventricles in both post-transplant groups, however this trend did not reach significance (Fig 4.7 B&E).

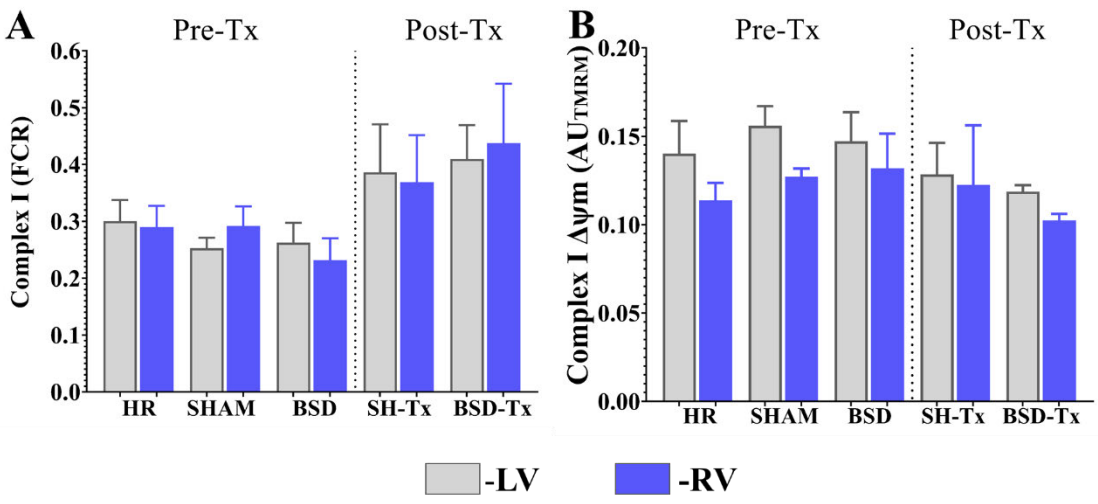

Figure 4.5. Mitochondrial respiration and Δψm in Complex I-mediated OXPHOS using CHO substrates (SUIT 1). A. Oxygen utilisation, corrected for maximum activity (FCR). **B.** Δψm production.

4.2.6 | Complex II Respiration

CII-mediated phosphorylation using CHO substrates showed similar bi-ventricular function for HR and both donor groups. Post-HTx, there was a significant, bi-ventricular depression in CII FCRs for both groups compared to HR [LV, SH-Tx: p=0.03, n=13 & BSD-Tx: p=0.024, n=14], [RV, SH-Tx: p=0.043, n=13 & BSD-Tx: p=0.003, n=14] (Fig 4.6A). Compared to SHAM, RV CII FCRs were reduced for both transplant groups [SH-Tx: p=0.04, n=10 & BSD-Tx: p=0.003, n=11]. BSD-Tx hearts were characterised by even further depression in CII function compared to hearts from BSD donors [LV, p=0.002, RV, p=0.002, n=11]. Compared to HR and SHAM, there was a bi-ventricular reduction in $\Delta\psi_m$ depolarisation capacity post-HTx for both SH-Tx [LV: HR, p=0.042, n=13 & SHAM, p=0.033, n=10 & RV: HR, p= 0.044, n=13 & SHAM, p=0.039, n=10] and BSD-Tx [LV: HR, p=0.038, n=14 & SHAM, p=0.018, n=11 & RV: HR, p= 0.014, n=14 & SHAM, p=0.013, n=11] hearts. There were no changes in CII-mediated $\Delta\psi_m$ between donors.

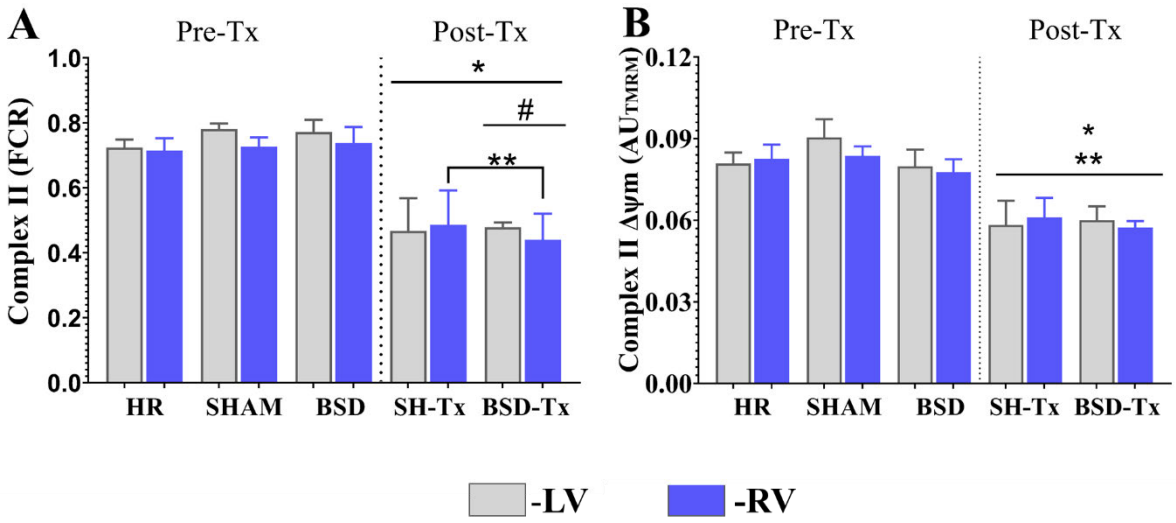

Figure 4.6. Mitochondrial respiration and Δψm in Complex II-mediated OXPHOS using CHO substrates (SUIT 1). A. Oxygen utilisation, corrected for maximum activity (FCR). **B.** Δψm production. *Significantly different from HR, ** significantly different from SHAM, # significantly different compared to BSD

For FA substrates, post-BSD, bi-ventricular CII-mediated phosphorylation was significantly depressed compared to SHAM [LV: p=0.013 & RV: p=0.055, n=6] and HR [LV: p=0.018 & RV: p=0.024, n=10] (Fig 4.7C&F). This depression remained post-HTx in both SH-Tx [LV: HR, p=0.009, n=11 & SHAM, p=0.008, n=7 & RV: HR, p=0.002, n=11 & SHAM, p=0.01, n=7] and BSD-Tx [LV: HR, p=0.013, n=11, SHAM, p=0.011, n=7 & RV: HR, p=0.011, n=11 & SHAM, p=0.034, n=7] groups (Fig 4.7C&F).

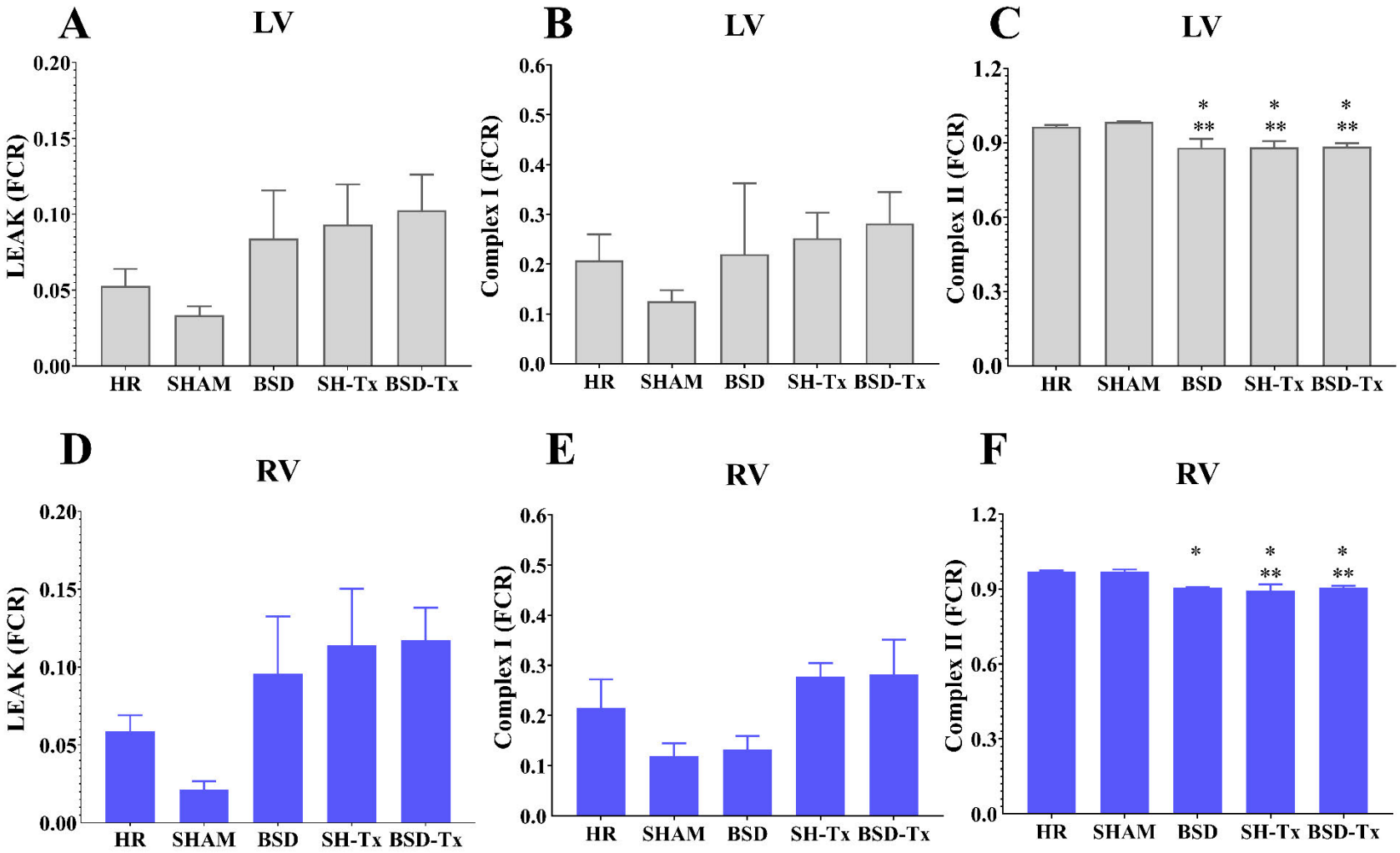

Figure 4.7. Mitochondrial respiration during LEAK, Complex I and II-mediated OXPHOS using FA substrates (SUIT 2). Left ventricle (**A-C**) and right ventricle (**D-F**) in the presence of fatty acid substrates. **A&D** LEAK respiration in the LV and RV. **B&E** CI mediated OXPHOS in the LV and RV. **C&F** CII mediated OXPHOS in LV and RV. *Statistically different compared to HR, ** Statistically different compared to SHAM.

4.2.7 | Tissue ROS Production

Myocardial oxidative stress was elevated with BSD and HTx, with clear elevations in 3-NT modified proteins observed. There appeared to be a greater accumulation of 3-NT in the RV for both SH-Tx ($p=0.0002$, $n=10$) and BSD-Tx ($p=0.0007$, $n=11$) groups compared to BSD and HR [SH-Tx, $p<0001$, $n=13$ & BSD-Tx, $p<0.0001$, $n=14$] (Fig. 4.8A&C). The GSH:GSSG ratio was also substantially reduced for BSD and both transplant groups, particularly for the LV (Fig. 4.8B). There was also a modest reduction ($p>0.05$) in RV GSH:GSSG for both the BSD and BSD-Tx groups compared to SHAM (Fig. 4.8D). The RV of SH-Tx hearts appeared to have preserved glutathione oxidation capacity above that of the SHAM control. There were no differences between ventricles within groups, except for the SHAM group, where the GSH:GSSG ratio was significantly lower in the RV ($p<0.01$).

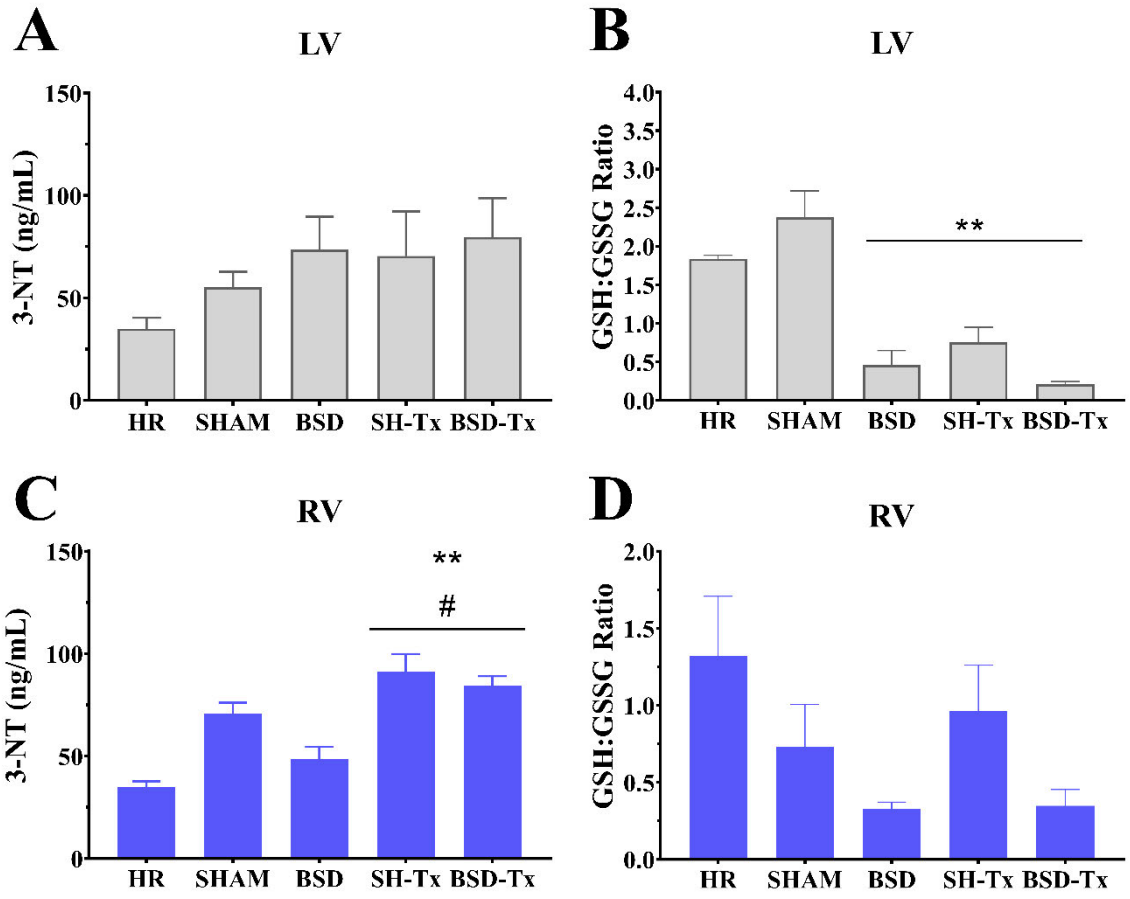

Figure 4.8. Tissue concentration of 3-NT modified proteins in the LV **A**, and RV **C**. Tissue GSH:GSSG ratios in the LV **B** and RV **D**. **statistically different compared to SHAM, #statistically different compared to BSD.

4.2.8 | hIPSC-CM Mitochondrial GRK2 Expression

Antagonism of either the β-ARs or GRK2 appeared to reduce the mitochondrial GRK2 content for the acute ($p>0.05$, n=3) and the chronic groups ($p=0.025$, n=3) compared to no inhibition (Fig. 4.9B & C). Chronic ISO treatment appeared to be associated with slightly reduced mitochondrial GRK2 content compared to acute ISO treatment (Fig. 4.9D).

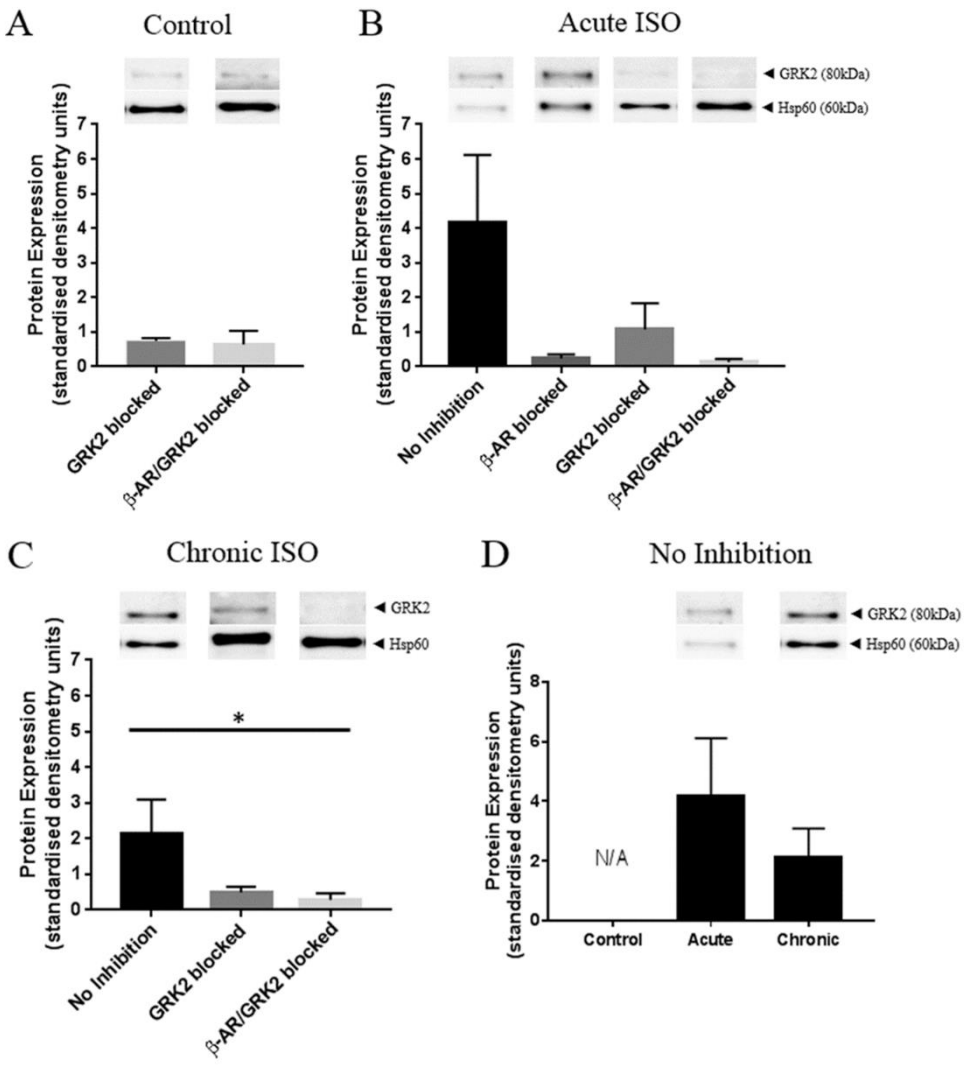

Figure 4.9. **Mitochondrial GRK expression (n=3) corrected for Hsp60 expression in non-ISO stimulated control cells A, Acute ISO stimulated cells B and Chronic ISO stimulated cells C.** A. GRK2 blocked and dual β-AR/GRK2 blocked effects on mitoGRK2 in the absence of ISO stimulation. B. Effect of no antagonism, β-AR, GRK2 and dual β-AR/GRK2 blockade on mitoGRK2 expression after acute ISO stimulation. C Effect of no antagonism, GRK2 and dual β-AR/GRK2 blockade on mitoGRK2 expression after chronic ISO stimulation. D. Comparison of mitoGRK2 for acute and chronic ISO stimulated cells without antagonism. *statistically different compared to no antagonism, $p<0.05$

4.3 | Discussion

Changes to mitochondrial function in both the donor heart and transplanted heart are largely understudied. We examined mitochondrial respiration and membrane potential in the ventricles from sheep exposed to 24 hrs BSD and subsequent transplantation. The results demonstrate that donor BSD is associated with higher RV proton slip, deficits in CII-mediated β-oxidation, and higher ROS production. Post-HTx, regardless of donor type, showed increased LEAK respiration, particularly for BSD-Tx, decreased CII respiration for both β-oxidation and CHO, reduced CII membrane potential, and higher ROS production. Preliminary data have also shown that β-AR stimulation is involved in the translocation of GRK2 to the mitochondria.

4.3.1 | The Donor Heart

Overall, we found no significant difference in the rates of β-Oxidation compared to CHO oxidation between any experimental groups, except for the BSD group. Oxygen flux in BSD at CII was reduced using FAs, but not for CHO substrates. Alterations in β-oxidation or FA transport via the Carnitine palmitoyltransferase I (CPT1) transporter, may limit the production of $FADH_2$, the electron carrier for CII. Reducing β-oxidation in our system would increase the reliance on the N-linked substrates pyruvate+malate (PM). Oxidation rates with PM is to a small degree supported by CII due to the high malate concentration [241]. High malate supports the 4:1 equilibrium between malate and fumarate, thus inhibiting flux through succinate and increasing the production of oxaloacetate, an inhibitor of CII [241]. This may explain the BSD-mediated reduction in CII respiration in the presence of FAs observed here. These data support the hypothesis that BSD mediates a metabolic switch from FA utilisation to CHO utilisation [86, 102].

Sztark *et al.,* found that in the *peroneus longus* muscle of BSD patients, total state 3, or phosphorylative respiration was reduced compared to healthy controls [70]. In contrast to this, our data reports enhanced oxygen consumption in LEAK state with preserved CI and CII activity. This discrepancy may be due to important differences between the two studies, Sztark *et al.,* i)

measured mitochondrial respiration at 30°C, ii) utilised glutamate (10 mM) and an unknown concentration of malate as N-linked substrates for CI, and most importantly, iii) utilised skeletal, rather than cardiac muscle [70].

Initially, mitochondrial respiratory analysis was performed at 30°C and corrections were made by assuming increases in temperature-dependent mitochondrial activity based on the Q10 effect [243]. Placing this assumption on tightly regulated enzymatic activity and metabolic flux however may produce erroneous findings. Additionally, skeletal muscle state 3 respiration and citrate synthase activity are reportedly lower than that of cardiac muscle fibres [244]. The increases in respiratory capacity observed in our study may be due to tissue differences in mitochondrial physiology.

Winkler-Stuck *et al.,* showed that the N-linked substrate combination pyruvate-malate-glutamate increases human skeletal respiratory capacity over that of pyruvate-malate or glutamate-malate alone [245]. If cytosolic malate concentrations are low, 2-oxoglutarate efflux decreases and the malate-aspartate shuttle cannot transport NADH into the mitochondria [241]. Therefore respiratory fluxes in Sztark's study may be limited by electron flow through CI, depending on malate concentrations that were not defined.

Another potentially confounding variable is changes to mitochondrial dynamics, addressed in our study by correcting oxygen consumption to the total respiratory capacity of the system in the uncoupled state. One direct comparison that can be made between our study and that of Stzark's, is CI-mediated LEAK-OXPHOS coupling control ratio (L/P ratio). This is given by respiration at LEAK as a function of ADP-stimulated OXPHOS. L/P ratios between studies show a similar increasing trend for the BSD group compared to the respective study controls (Fig 4.10). These similarities support BSD-mediated decreases in CI phosphorylation capacity due to increases in LEAK.

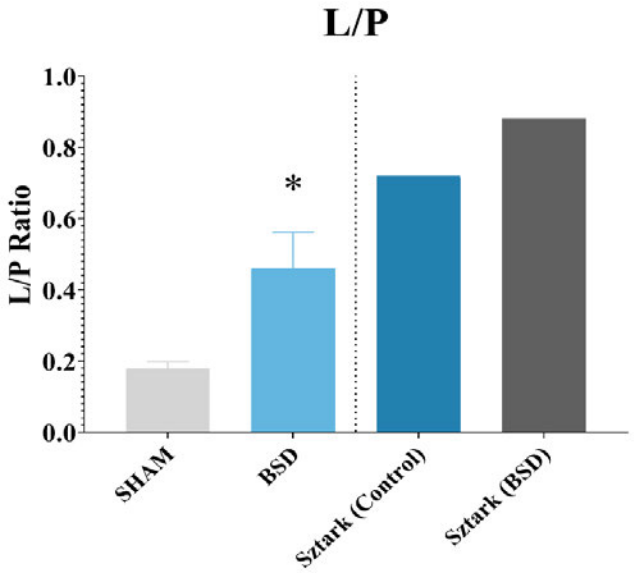

Figure 4.10. Comparison between L/P ratios in this study, with calculated L/P ratios in the study by Sztark [3]. L/P ratios are a measure of coupling of the oxidative phosphorylation system. Increased proton slip induces a reciprocal increase in oxygen consumption in order to maintain a membrane potential, thus LEAK increases. Increases in LEAK thus impact on the phosphorylation capacity P. *statistically different compared to SHAM

Therefore, based on these similarities, a common feature of BSD is the dyscoupling of mitochondrial respiration at the level of Complex I. This site-specific defect is further supported by evidence of preserved CII FCRs and no change in membrane potential compared to SHAM or HR. In the presence of a higher proton leak, the BSD heart may increase substrate oxidation in order to maintain a membrane potential [246]. A significant side effect of this is increased ROS production evidenced by elevated 3-NT modified proteins and reduced GSH:GSSG ratios in cardiac tissue. A feedback loop then begins whereby increased ROS generation increases proton leak via membrane-bound uncoupling proteins (UCPs) or adenine nucleotide translocase (ANT) [246-248].

Synergistically, catecholamines are involved in the upregulation of substrate oxidation and the generation of ROS. By increasing cytosolic Ca^{2+} levels, mitochondrial Ca^{2+} levels also rise which

is a positive regulator of TCA dehydrogenases, consequently upregulating substrate oxidation rates [249]. Under physiological stress mitochondrial Ca^{2+} overload can activate ANT, contributing to the feedback loop [250, 251]. Mitochondrial Ca^{2+} overload can also lead to the opening of the mPTP, leading to mitochondrial swelling and cellular apoptosis [234, 252]. Evidence of contraction band necrosis in BSD hearts supports Ca^{2+} overload, leading to cardiomyocyte ischaemia and cell death [11].

This mitochondrial uncoupling may also be protective, referred to as the "uncoupling to survive" hypothesis [248]. "Uncoupling to survive" states that increases in cellular ROS, promotes proton leakage through UCPs and ANT, which reduces further ROS production [253]. Further, proton conductance through ANT has been associated with higher OXPHOS rates, increasing ANT concentrations and protection against ROS-mediated cell damage [248, 253]. Our data have shown that in the presence of increased ROS generation, BSD hearts maintain phosphorylative capacities and membrane potential, supporting the "uncoupling to survive" hypothesis.

In summary, the BSD donor heart is characterised by significant RV mitochondrial uncoupling. This may be due to increases in oxidative stress which initiate mechanisms that enhance proton slip, to reduce ROS production in a stressed heart (Fig. 4.11). Right ventricular dysfunction in the donor heart is a common finding [221], and this data represents the first empirical evidence of RV mitochondrial pathology which may predispose donor heart dysfunction. This is particularly relevant in the context of cardiac transplantation, where post-HTx RV failure is a common clinical problem affecting 30-day mortality [221].

The LV of the donor heart appears to be, in the short term, relatively spared of mitochondrial dysfunction, aside from the deficiency in β-oxidation. Altered upstream FA metabolism or transport may impose a limit on $FADH_2$ production. Reducing FA transport in our system would increase the reliance on the substrates glutamate+malate (GM). Oxidation rates with GM is to a small degree supported by CII due to the high malate concentration [241]. High malate supports the 4:1 equilibrium between malate and fumarate, thus inhibiting flux through succinate and increasing the production of oxaloacetate, an inhibitor of CII [241]. This may explain the BSD-

mediated reduction in CII respiration in the presence of FA observed here. These data may suggest altered FA transport or metabolism post BSD but will require a direct metabolic assessment to determine the mechanism.

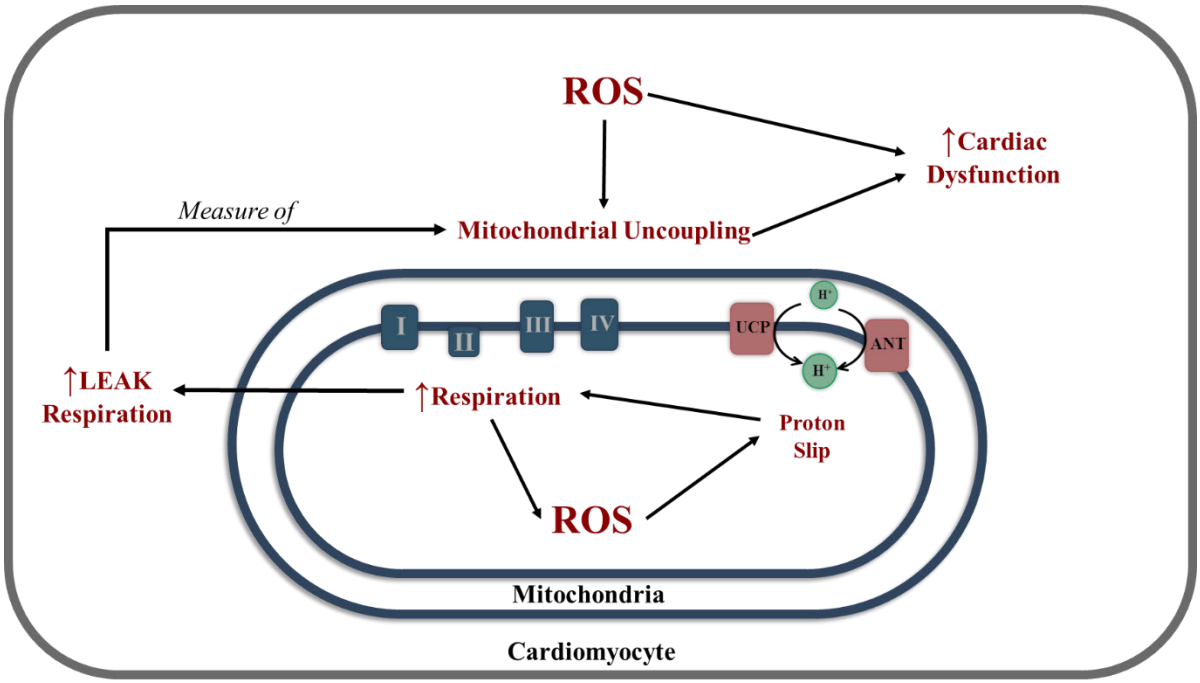

Figure 4.11. Schematic overview of mitochondrial dysfunction, particularly RV dysfunction, in the BSD donor heart. Increases in oxidative stress lead to increased proton and potentially electron slip, which in turn stimulate higher respiratory activity, promoting higher ROS production. In turn ANT levels increase in an effort to reduce ROS production whilst maintaining $\Delta\psi m$.

4.3.2 | Cardiac Mitochondrial Function Post-HTx

We observed significant mitochondrial dysfunction post-HTx using both SHAM and BSD donor hearts. Compared to BSD alone, mitochondrial dysfunction appears to worsen after CSS and subsequent reperfusion injury. Data also showed increased LEAK respiration for both ventricles and substrates post-HTx, with the greatest effect observed following HTx using BSD donor hearts (ie. the most clinically relevant group). The same mechanisms involved in higher proton slip may be operating post-transplant, however, this higher LEAK is in the presence of higher CI (Fig. 4.5,

pg. 121) and lower CII OXPHOS (Fig 4.6A, pg. 122), and reduced mitochondrial membrane potential (Fig 4.6B, p. 119).

Higher dyscoupling has been observed in mitochondrial preparations as a consequence of CSS. Lemieux showed that Custodiol preservation of human ventricular biopsies increased OXPHOS capacities and LEAK respiration after 12-140 hrs cold storage [113]. Although this preservation time is considerably longer than clinical guidelines (max 6 hrs) [254], Lemieux stated that this preserved oxidative capacity up to 12 hrs preservation may be due to a reduction in total ischaemia [113]. When storing a myocardial biopsy, O_2 diffusion is not limited by tissue dimensions, whereas storing an entire organ imposes a significant reduction in O_2 diffusion and therefore higher ischaemic damage.

These paradoxical increases in LEAK and OXPHOS capacities are in response to higher proton and electron slip. As with the BSD donor in order to maintain a membrane potential, OXPHOS capacities are increased, reducing the inherent excess capacity. Post-HTx however, we see a decreased CI membrane potential, suggesting that these higher capacities cannot overcome the proton and electron slip. These results agree with those from reperfusion injury, where uncoupling, specific CI damage, Cyt c release, and ROS production were significantly associated with reduced myocardial contractile function [110].

Exogenous administration of Cyt c increases OXPHOS rates by replacing lost Cyt c due to injury [241]. It is important to note that in the study by Kuznetsov *et al.,* [110] Cyt c release was heterogenous post-reperfusion in a rat model of transplantation after 10 hrs CSS. We also observed a large variation in OXPHOS stimulation by Cyt c post-transplantation. Of relevance to our data, Kuznetsov also found that OXPHOS stimulation with Cyt c, when supplied with only N-linked substrates was reduced, and this reduction was associated with the severity of contractile dysfunction [110]. This is in line with our data showing reduced Cytc response after the addition of pyruvate, malate, and glutamate, highlighting specific CI limitation on oxidative phosphorylation (Table 4.6, p.116).

Our data also shows significantly reduced CII capacities, for both types of donor, substrate, and ventricle. Chouchani *et al.*, explained a "unifying mechanism" in which IRI may cause the production of ROS and thus the changes in oxidation capacities presented here [137]. Central to this mechanism is reverse electron transfer (RET) through CI, mediating increases in matrix peroxide levels. During ischaemia, CSS in this case, there is a rise in intracellular succinate concentration often assumed to arise from the inhibition of the TCA cycle [255]. Succinate accumulation, subsequently driving reperfusion injury was comprehensively shown by Martin *et al.*, in a mouse HTx model, and a tissue model of ischaemia reperfusion utilising mouse, pig and human tissue [256]. However, data suggests that succinate dehydrogenase (CII) acts in reverse, converting fumarate to succinate [41]. Matrix succinate is then exchanged for cytosolic malate, thus creating more fumarate. Reverse CII function is supported by ischaemic increases in NADH and reductions in GTP and Coenzyme A, inhibiting succinyl-CoA formation [137]. In essence, succinate accumulation creates an electron sink during ischaemia, decreasing electron input into the electron transport system from CII.

Upon reperfusion, high succinate levels then drive an increase in succinate oxidation in the presence of ROS. This increase in succinate oxidation supports RET through CI by maintaining the Q-pool in a reduced state [137]. Complex I contains 2 sites in which electrons can be transferred, the I_F and I_Q sites [140]. RET preferentially increases electron flow via the I_Q site, elevating matrix superoxide which is converted to peroxide via superoxide dismutase, and subsequently detoxified by the glutathione system [137, 140]. Additionally, the formation of peroxide and higher LEAK may decrease mitochondrial pH, which further supports RET by increasing reverse proton motive force.

Given this potential mechanism in the context of HTx, during CSS the heart accumulates succinate and ROS increases due to ischaemia. ROS then increases CI LEAK respiration to maintain a membrane potential. However, during reperfusion, succinate oxidation increases dramatically, enhancing RET and thus reducing the capacity of CII to generate a membrane potential. RET increases the production of peroxide via the I_Q site in the presence of a higher

LEAK at the expense of membrane potential. The glutathione system then attempts to detoxify enhanced peroxide production evident by the reduction in tissue GSH:GSSG ratios (Fig 4.8, pg. 125) [257]. Figure 4.12 represents a schematic diagram of the potential mechanisms inducing poor cardiac function due to alterations in OXPHOS.

Our analyses of flux control ratios correct for changes in mitochondrial dynamics, i.e density and morphology [241]. This correction may have obscured the effects of altered mitochondrial dynamics, which have been reported following cardiac stress and IRI [258]. Total ETmax capacities trended lower for both transplant groups, significantly for the LV in the BSD-Tx group. This may suggest altered mitochondrial dynamics after CSS and reperfusion as a consequence of IRI.

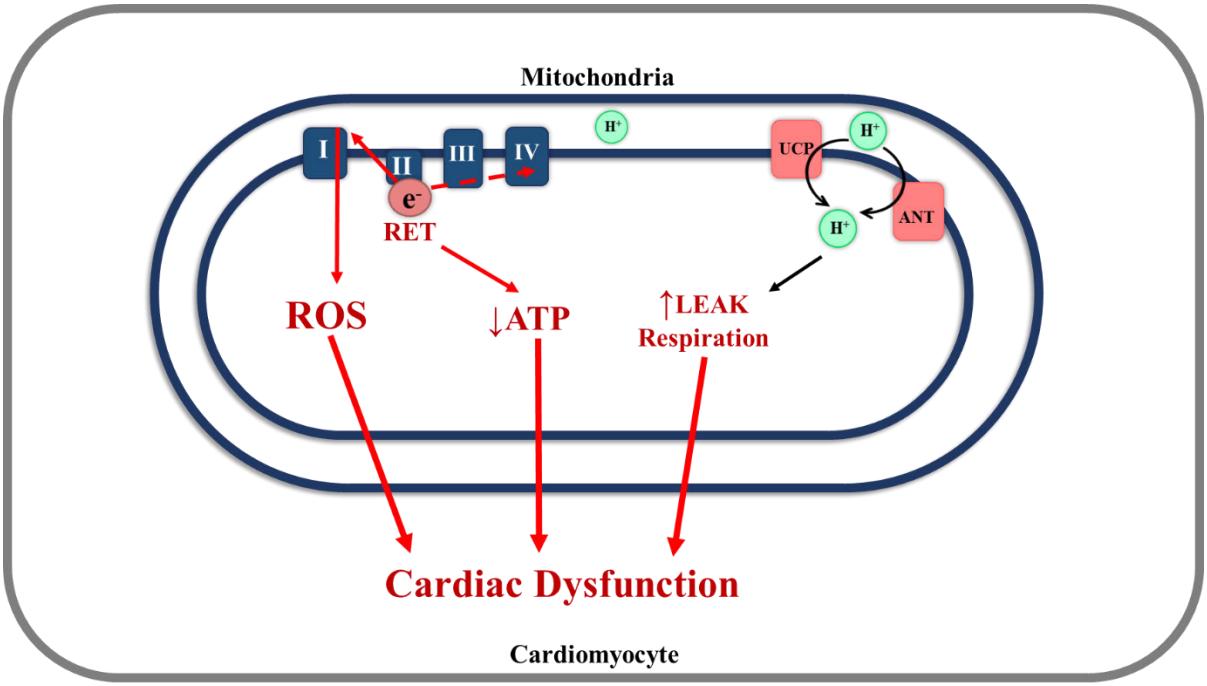

Figure 4.12. Schematic overview of mitochondrial dysfunction, particularly RV dysfunction, in the post-transplanted heart. Increased complex II activity increases reverse electron flow to complex I thereby reducing oxygen consumption at complex IV by decreasing the electron flow through to the Q-junction which is kept in a reduced state. Reduced electron flow causes reductions in CII-mediated $\Delta\psi m$ production.

4.3.3 | Preliminary hIPSC-CM data

One of the largest physiological stressors in the context of HTx is catecholamines, both endogenous release at BSD, and exogenous administration via vasopressor support [66, 215]. Preliminary data from our hIPSC-CM model of BSD suggest that β-AR activation is an important stimulus in GRK2 translocation. Inhibiting β-ARs and/or GRK2 showed a large reduction in the mitochondrial GRK2 content.

Chen *et al.*, were the first to describe the translocation of GRK2 to the mitochondria [237]. The authors showed that in response to ischaemia or elevated ROS, ERK activation leads to the phosphorylation of GRK2 at residue Ser670, allowing Hsp90 association and thus mitochondrial translocation. Further works by Sato *et al.*, demonstrated that increased levels of mitochondrial GRK2 decreased FA utilisation and oxidation [238]. Post-BSD we have also demonstrated a

reduced FA utilisation, the mechanisms of which might be increased mitochondrial GRK2 as a consequence of catecholamine toxicity.

A limitation to the translation of these studies to the sheep or human scenario is the immaturity of hIPSC-CM's. hIPSC-CM's have less organised sarcomeres, lower contractile performance, absent T-tubules and rely largely on glycolysis for energy production [259]. The mitochondrial distribution and morphology also differ in immature cardiomyocytes. Culturing up to 100 days has shown a more mature morphology, but respiratory enzyme capacity remains unchanged [260]. Importantly, β-AR receptor signalling, expression and regulation are reportedly closer to the adult cardiomyocyte in terms of cardiotoxicity and downstream signalling after 90 days of culture [261]. Therefore, our data is significantly confounded by the age of our myocytes (21 days).

4.3.4 | Clinical Implications

We have shown that donor RV mitochondrial uncoupling may potentially compromise the myocardium prior to continuation to CSS and subsequent transplantation. Post-reperfusion, the reported mitochondrial impairment in this study coincides with other data pertaining to IRI [137, 141]. RV dysfunction post-HTx is a common clinical observation [221]. We have shown for the first time, in a clinically relevant model of transplantation, that mitochondrial deterioration both carried forward from the donor, and as a consequence of IRI, may be an important factor affecting graft dysfunction. Targeting the mitochondria in the context of HTx may then be a promising new strategy for improving patient outcomes. Numerous therapeutic targets affect mitochondrial function. Upstream drugs, that target substrate utilisation or transport, and drugs acting at the level of the mitochondria themselves altering respiration (CoQ, Idebenone, Succinate, Cyclosporin A, Nortriptyline) [262] or preventing mitophagy. Strategies altering metabolic flux will be discussed in the following chapter.

Reducing oxidative stress in both the donor and recipient would alleviate mitochondrial dyscoupling by reducing proton LEAK. Antioxidant lowering drugs however have not been successful in improving cardiac function in *in vivo* studies [263]. This is due mostly to their non-specific actions and difficult entry into the cell. Specifically targeting the generators of ROS may

be a more appropriate approach in reducing oxidative stress. Catecholamines for example are a significant effector of cardiac ROS in the context of HTx. This is partially due to their degradation by monoamine oxidases (MAO) located on the outer mitochondrial membrane, producing hydrogen peroxide, aldehydes and ammonia [264]. Selective inhibition of MAOs in the context of IRI and pressure overload-induced heart failure has shown promising results [265].

There are 11 sites on the respiratory chain in which electron slip can occur, creating ROS [140, 141]. *In vivo*, the I_F and I_Q sites on CI and the III_{Qo} site on CIII have the largest capacity to produce ROS [140]. Specific inhibitors of these sites, suppressors of site 1Q Electron Leak (S1QEL's) and suppressor of site 3Q Electron Leak (S3QEL's) have been developed that successfully block the ROS generation and do not interfere with oxidative capacities, as with rotenone [142]. The use of these agents has proven beneficial in IRI models at reducing infarct size and improving haemodynamics [142]. Another potential target that may work synergistically with I_Q blockade is the reduction of mitochondrial transport of succinate. This would effectively reduce the high succinate oxidation rates that promote RET and ROS production.

The accumulation of GRK2 in cardiac disease has been considered detrimental and associated with the progression of HF [61, 266]. The use of β-blockers in HF is standard practice and mitigates the activation of GRK2 [267]. However, in the context of HTx, inotropic support via β-ARs is required, and therefore blocking these receptors is contraindicated. Strategies that specifically block GRK2 have been shown to improve cardiac function in HF [61]. Specific inhibition of GRK2 may be advantageous in this setting, allowing inotropic support but reducing the negative effects of GRK2 on mitochondrial and cellular functions, as described by Sato *et al.*, [238].

The introduction of immunosuppression in HTx greatly improved the long-term mortality of patients and the overall success of HTx. Immunosuppression is initiated immediately post-operatively and aggressively, often with calcineurin inhibitors [268]. Cyclosporine A (CsA) has a dual action of immunosuppression and is also a potent inhibitor of the mPTP [269]. CsA then may prove beneficial in HTx by reducing IRI injury and thus improving graft function [269].

Controversially, the use of CsA prior to percutaneous coronary intervention for ST elevated myocardial infarction (STEMI) in 395 patients did not improve clinical outcomes [270]. This contrasts with animal models and preclinical studies showing an improvement in cardiac function [271, 272]. An important difference between STEMI and HTx is the ischaemic insult itself. STEMI is characterised by an often-unknown amount of time in warm ischaemia, whereas HTx has a significant cold ischaemic insult and therefore may be less developed than STEMI. Further studies should specifically examine whether pre-operative CsA is beneficial in the context of HTx, either added to cardioplegic solutions or a feature of recipient management.

4.3.5 | Limitations

A significant limitation is the low sample sizes, particularly for the β-oxidation and $\Delta\psi_m$ protocols (n=3) for the post-transplant groups. Modelling cardiac transplantation represents unique logistical and experimental difficulties, resulting in loss of data due to human error and optimisation studies. Additionally, specifically examining mitochondrial function in the left and right ventricle imposed a constraint on the number of assays that could be run promptly across 3 oxygraph machines.

Anaesthetic agents have shown variable pro-survival and anti-survival effects via mitochondrial regulation. Volatile anaesthetics (not used here) and opioids (Fentanyl 5 μg/kg/hr used here), have shown cardioprotective properties through activation of mu, delta, kappa and potassium channels, preventing Ca^{2+} overload [273, 274]. Ketamine (2.5-7.5 mg/kg/hr) and midazolam (0.5-0.8 mg/kg/hr) have no effect on potassium channels and depending on their concentration have been shown both cardiodepressant and cardioprotective effects [275]. Midazolam is a well-known complex I, inhibitor and can inhibit complexes II and III even at clinical concentrations [275, 276]. Propofol primarily inhibits fatty acid utilisation and in vitro studies show comparatively lower inhibitory effect on respiratory complexes [273, 275]. Anaesthetic agents used here therefore, may have influenced mitochondrial parameters. However, all animals received the same anaesthetic combination and hence the overall impact on these data may not be significantly

large. Future studies should be aimed at reducing the potential effects of anaesthetic-mediated reductions in mitochondrial function.

Vasopressin was administered to all groups except the HC group, potentially impacting mitochondrial function. Vasopressin has been shown to cause mitochondrial swelling, potentiated by GSH. In IRI [277] and haemorrhagic shock [278], vasopressin has shown to be cardioprotective, restoring CI and CII respiratory capacities, reducing infarct size and inhibiting the MPTP. Since vasopressin was absent in the HC group, this may partly contribute to the differences in respiratory patterns and membrane potential observed for HC and SHAM controls.

The protocols utilised in this study were not optimised to directly assess CIII or CIV function. Complex III is an important site of ROS production, and impaired CIII activity in ischaemic hearts has been shown to correlate with the level of reduced contractile function [279]. Future research should determine the association between CIII function in the context of peri-transplant cardiac function.

The Oroboros is capable of determining real-time ROS production which would have provided greater insight into distinguishing cardio-protective vs pro-apoptotic increases in LEAK present in BSD donors, and the extent to which RET induced CI-mediated ROS production. Due to instrument limitations, real-time ROS measurements were not possible. Mitochondrial UCP and ANT are also indicated in the physiology of proton leak and may contribute to ROS formation, uncoupling and LEAK respiration. Analysis of UCP and ANT expression patterns between groups would have further informed the mechanisms behind increased LEAK respiration. Further, western blot analysis of mitochondrial GRK2 translocation in sheep tissue would've provided important information on this process as governed by the *in vivo* environment and the consequences of BSD and subsequent transplantation.

Further, assessing membrane potential in the presence of FA substrates may have aided in determining the cause of the observed CII reduction in O_2 consumption. We suggested that the

N-linked substrates used, limited electron flow and could inhibit CII function, whether this had a significant effect on membrane potential should be determined in future studies.

We have shown significant increases in RV mitochondrial LEAK following donor BSD. However, BSD donors were also administered exogenous adrenergic agents for vasoactive support. Catecholamines are known to induce mitochondrial dysfunction [201]. It is difficult to ascertain whether the results we have shown are primarily a consequence of adrenergic support, or the consequences of BSD itself. Clinically, BSD donors are administered similar adrenergic agents. This implies that whether our results are an effect of BSD or vasoactive support, they are still relevant in the clinical context. However, in the face of reduced RV contractility (Chapter 3, Fig 3.5, pg. 77) it may be advantageous to explore the use of non-adrenergic donor support. These strategies may include therapeutics to improve Ca^{2+} handling (levosimendan), increase myofilament contraction (Omecamtiv Mecarbil), inhibit PDE's, activate NO signalling, target metabolism (outlined in Chapter 5) or therapeutics that improve mitochondrial function as outlined above. These potential therapeutics are detailed in Table 6.2.

4.4 | Conclusion

Using a large pre-clinical model of 24 hrs donor BSD, followed by heart transplantation, we have, for the first time, described mitochondrial respiration with respect to the heart donor and post-transplanted heart. Donor hearts are characterised by mitochondrial dyscoupling which may be a protective mechanism to reduce oxidative stress. Transplanted hearts however, regardless of exposure to BSD or not showed significant mitochondrial dyscoupling, reducing effective membrane potential production. These data have highlighted respiratory CI as a potential therapeutic target in post-transplanted hearts to reduce ROS production. Further, mitochondrial succinate transport and GRK2 blockade may also reduce IRI post-transplantation. Targeting mitochondrial function in the context of HTx may help to increase viable donor heart numbers and post-transplant graft function.

CHAPTER 5

METABOLIC PROFILE OF THE DONOR AND TRANSPLANTED HEART

Contents

5.0 | Introduction

The heart is the most mechanically active organ in the body. As such, it leverages the inherent flexibility of several metabolic pathways for bio-energetic gain. Metabolic alterations are also important regulators of cardioprotective and pro-apoptotic signalling pathways. In the context of donor BSD and HTx, cardiac metabolism remains largely understudied. In the previous chapter we observed significant alterations in mitochondrial function, which relies on the proper functioning of upstream metabolism. This chapter will explore the cardiac metabolic profile following BSD and subsequent transplantation.

5.0.1 | Normal Cardiac Metabolism

In one day, the heart generates ~65 kg of ATP, with a complete turnover of the myocardial ATP pool every 10 seconds [227, 233]. To achieve this enormous energetic feat, the heart acts as a metabolic ‘omnivore’. The most significant contributors to energy production in the heart are from glucose and FA oxidation within the mitochondria [236, 280]. The heart can also leverage ATP from glycolysis, lactate, ketone bodies and amino acids (AA) [226, 281]. In fact, the relative contribution of each may change according to energetic requirements and the cellular environment, i.e oxidative stress. Figure 5.1 outlines the relative contributions of each substrate group under normal myocardial metabolic conditions [225, 236, 282, 283].

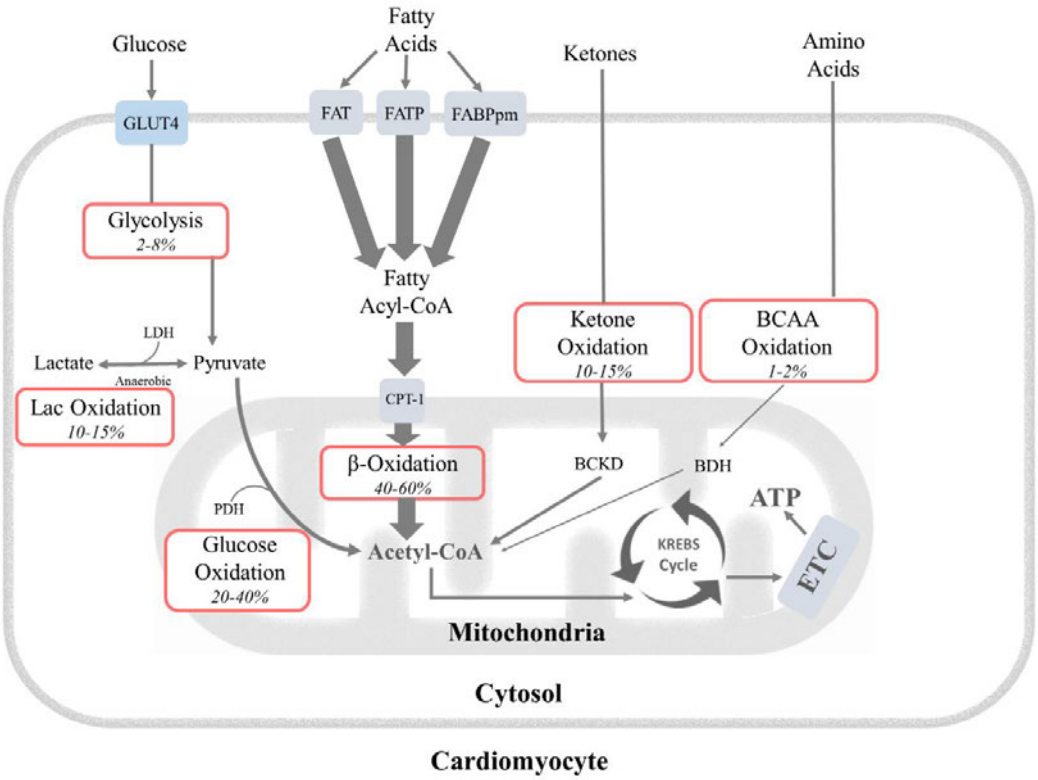

Figure 5.1. Schematic overview of inherent cardiac metabolic flexibility and the relative contribution of each pathway to ATP production, in percentages. Adult cardiomyocytes prefer β-oxidation, but will switch to glucose oxidation in times of increased metabolic demand. Ketone and lactate oxidation contribute a small proportion to ATP production, whilst glycolysis (in the presence of adequate levels of O_2) and BCAA oxidation contribute the least. GLUT4, glucose transporter-4; FAT, fatty acid transporter; FATP, fatty acid transporter protein; FABPpm, plasma membrane associated fatty acid binding protein; BCAA, branched chain amino acids; LDH, lactate dehydrogenase; Lac, lactate; PDH, pyruvate dehydrogenase; BCKD, branched chain α-keto acid dehydrogenase; BDH, β-hydroxybutyrate dehydrogenase;ETC, electron transport chain. Information extracted from [3, 6-8]

5.0.2 | Fatty Acid Utilisation

FA metabolism and subsequent β-oxidation is the preferred metabolic pathway to myocardial energy production under normal conditions. FA supply to the heart is through albumin bound free FAs or released from triacylglycerol [227]. FA uptake into the myocyte occurs through passive diffusion or receptor-mediated transport. These transporters include, FA translocase (FAT/CD36), plasma membrane isoform of FA binding protein (FABPpm) and FA transport

protein (FATP) 1/6 [284]. The largest contributor to FA uptake is FAT/CD36, providing 50-60% of the cellular FA content [227, 284].

Upon uptake, FAs are first activated in the cytoplasm by conversion to long-chain acyl CoA esters. These long chain acyl-CoAs may then be used for lipid synthesis or conversion to long-chain acylcarnitine for mitochondrial transport [227, 285]. This conversion is catalysed by the outer mitochondrial membrane bound CPT1 enzyme. Carnitine acyl translocase then shuttles acylcarnitine into the mitochondrial matrix, where it is converted to acyl-CoA by CPT2 [285]. Mitochondrial acyl-CoA is then β-oxidised in a 4 step process to n-2 acyl-CoA and acetyl-CoA, producing NADH and $FADH_2$ [227, 285]. Acetyl-CoA is then metabolised through the TCA cycle for further production of NADH and $FADH_2$ which are utilised by complex I and II, respectively, in the mitochondrial electron transport system.

Despite being the preferred substrate for energetics, FA oxidation (FAO) is less efficient than glucose in regard to the oxygen cost of ATP production per molecule, i.e the P/O ratio. Palmitate (a common FA) produces 105 ATP molecules from 46 O_2 molecules (P/O 2.33), whereas glucose generates 31 ATP from 12 O_2 molecules (P/O 2.58) [227]. This is mostly due to the higher reduced state of FAs compared to glucose, which require consumption of ATP and O_2 for activation prior to their oxidation for ATP production [227]. Therefore, in times of elevated energetic demand, FA metabolism is usually downregulated in favour of glucose utilisation.

5.0.3 | Glucose Utilisation

The majority of glucose uptake in the heart is via the glucose transporter 4 (GLUT4) and to a lesser extent GLUT1 [286]. Upon entry into the cell, glucose is rapidly phosphorylated to glucose-6-phosphate (G6P), trapping it within the cell. G6P enters many cellular pathways, but under normal circumstances, the majority of G6P is metabolised through glycolysis [286]. Glycolysis generates 2 NADH and 2 ATP in coupled reactions to produce pyruvate [287]. In situations of hypoxia, pyruvate is reduced to lactate via lactate dehydrogenase (LDH), contributing to the hypoxic decrease in intracellular pH levels [286, 287].

Both lactate and pyruvate can be oxidised within the mitochondria, although the contribution of pyruvate to energy production is up to 2.5 times that of lactate (Fig 5.1). Conversion of pyruvate to acetyl-CoA is the main route of glucose oxidation and represents the functional coupling of glycolysis to glucose oxidation and subsequent ATP production [288]. Acetyl-CoA is then entered into the TCA cycle for formation of NADH and $FADH_2$. The ratios of acetyl-CoA:CoA and NAD+:NADH are important regulators of glucose metabolism, upregulating and downregulating glycolytic flux in response to demand or pathology [240, 289].

Glucose may also be utilised in neighbouring glycolytic pathways including the pentose phosphate pathway (PPP), the polyol pathway (PoP) and the hexosamine biosynthetic pathway (HBP) [287]. Under normal conditions, glucose flux through these pathways is minimal. These alternate routes act as metabolic sensors of oxidative stress, energetic compromise and substrate availability to reduce myocyte injury and contribute to anaplerosis (TCA replenishment via metabolic intermediates), but may also contribute to the progression of cardiac dysfunction [236].

5.0.4 | Ketone utilisation

Myocardial ketone metabolism is proportional to the delivery of two main circulating ketones, β-hydroxybutyrate (βOHB) and acetoacetate (AcA) [281]. These ketone bodies are produced via hepatic ketogenesis which is upregulated in situations of reduced glucose availability (starvation), impaired insulin signalling and increased rate of lipolysis. Myocardial uptake of ketones occurs via the monocarboxylate transporters 1/2, followed by conversion of βOHB to AcA within the mitochondria [236, 281]. Succinyl-CoA:3-oxoacid-CoAtransferase is the rate limiting step of ketone metabolism, converting AcA to acetoacetyl-CoA [236]. The final step is conversion of acetoacetyl-CoA to acetyl-CoA and entry into the TCA cycle.

In regard to myocardial efficiency, ketone body metabolism has a P/O ratio of 2.5, making it more efficient than FA, but less efficient than glucose oxidation in terms of energy production [236]. The majority of cardiac metabolism-focussed research is concerned with glucose and FA flux. Relatively little is known about ketone metabolism. Recently however, interest has grown as

evidence toward enhanced ketone metabolism has emerged in the setting of diabetes and heart failure [281, 290]. Whether enhanced ketone utilisation is cardioprotective is still under debate.

5.0.5 | Amino Acid Utilisation

Lastly, a small amount of AAs, under normal conditions, are used to generate ATP. There are three main groups of AAs when considering end-point energetics, glucogenic, ketogenic and branched chain AAs (BCAA) (Fig 5.1) [291]. The majority of research on cardiac AA is concerned with BCAA utilisation. Each BCAA is broken down by specific branched chain α-keto acid dehydrogenases (BCKD) to acetyl-CoA [292]. Glucogenic AA can be catabolised to either pyruvate, oxaloacetate, α-ketoglutarate or succinyl-CoA and therefore support TCA activity in an anaplerotic manner [291]. Ketogenic AA catabolism functions similarly, instead creating ketone bodies for TCA input [291].

Relatively little is understood on the regulation and consequences of myocardial AA metabolism. Reportedly, BCAAs have signalling implications, such as mammalian target of rapamycin, and histone acetylation cascades regulating insulin signalling, cell growth and proliferation, and enhancing transcriptional activity [292]. Defects in BCAA oxidation have been implicated in the pathogenesis of heart failure [291, 292]. Free AA metabolism flux has been shown to increase during ischaemia and may offer the advantage of non-oxygen consuming substrate level ATP production. Although this ATP contribution is minor. AAs may also reduce oxidative stress via the biosynthesis of glutathione [291].

5.0.6 | Metabolic Dysfunction Post-BSD

There has been considerable investigation into characterising the physiological responses to donor BSD. These studies have led to the improvement of patient management and the realisation of important mechanisms behind donor cardiac dysfunction. These mechanisms are closely linked to metabolism, which to date remains largely understudied (Table 5.1). Investigating these metabolic alterations may provide alternative strategies to improve both patient outcomes and donor heart function.

Table 5.1. Summary of Cardio-Metabolic Considerations for the donor.

	Presentation	Metabolic Effects
Catecholamine Storm	Increased NA, A and Dopamine [14, 38, 42, 43] Increased GRK2 expression [49, 60]	Hypermetabolism Substrate switch Ca^{2+} overload→Mitochondrial dysfunction
Endothelial/Vascular Dysfunction	Vasoconstriction VSM Ca^{2+} overload [59] Endothelial activation [50, 81, 83]	Poor lactate clearance Decreased O_2 delivery initiating ischaemia
Endocrine Changes	Decreased T3 Decreased Insulin Decreased Cortisol [12, 48]	T3-mediated decrease in mitochondrial respiration and metabolism Inflammation precipitating mitochondrial dysfunction

NA-Noradrenaline, A-Adrenaline, GRK2-G-protein receptor kinase 2, VSM- vascular smooth muscle, T3-triiodothyronine

Novitzsky and colleagues in the 1980's described metabolic alterations in a baboon model of brain death [86, 222, 293]. These seminal works described a switch to anaerobic respiration, evidenced by reductions in labelled glucose, pyruvate and palmitate utilisation and increases in lactate [86]. These findings were substantiated in further works measuring blood metabolites [42, 66]. However, to our knowledge there has been no direct, thorough investigation of metabolic derangement beyond plasma metabolites.

Novitzky suggested that these metabolic alterations lead to depleted energy stores, i.e., HEPs [86]. However, despite an initial drop in HEP during the autonomic storm, studies have found that HEP concentrations remain conserved thereafter [60, 114, 294]. This result is consistent throughout species and analytical methods. Two studies found that the RV post-BSD, was susceptible to a

drop in HEP; however, these results failed to reach statistical significance [60, 72]. There are several perturbations of BSD that precede metabolic dysfunction but are inexorably linked. These include the catecholamine storm, vascular/endothelial dysfunction and endocrine dysfunction, and will be discussed in more detail below.

5.0.7 | Catecholamine Storm

The non-haemodynamic actions of catecholamines are rarely studied in relation to the organ donor. This is particularly important when considering the management of both the potential organ donor and recipient. Inotropic support of donor heart dysfunction is most frequently provided by sympathomimetics such as adrenaline, noradrenaline and/or dopamine. High inotrope use defined as dopamine/dobutamine infusions >10 $\mu g \cdot kg^{-1} \cdot min \cdot^{-1}$, and noradrenaline infusions >0.05 $\mu g \cdot kg^{-1} \cdot min^{-1}$ are believed to be a relative contraindication for cardiac transplantation [211, 212]. This notion has recently been contested with both experimental and retrospective studies (examining relative risk) demonstrating clinical acceptability of donor hearts from patients with high inotropic support [215].

5.0.8 | The hyperdynamic phase of BSD

The hyperdynamic phase is the focus of most BSD studies trying to ascertain mechanisms for the development of the hypodynamic phase. The hypothesis generated by Novitzky's studies states a metabolic shift to anaerobic metabolism as a consequence of endocrine changes (discussed below) [86]. Catecholamines however, are important regulators of cardiac metabolism in situations of stress and therefore, are involved in anaerobic metabolism and its deleterious consequences [201].

Activation of adrenergic receptors activates several key signalling molecules and metabolic enzymes. Firstly, β-AR agonism increases cAMP levels, a positive regulator of glycogen phosphorylase, which increases glucose 1-phosphate [226, 295]. This allows fast substrate access to the glycolytic pathway to increase ATP. In addition, cAMP activation of PKA, which increases cytosolic Ca^{2+} ($c[Ca^{2+}]$) activates Phosphofructokinase-2 (PFK-2) [226]. PFK-2 then stimulates PFK-1, an important enzyme in the irreversible production of Fructose 1,6-bisphosphate [226].

Collectively, catecholamines can quickly increase glycolysis through cAMP-PKA for energy production.

Increases in lactate observed by many in the context of BSD is interpreted as an anaerobic shift. However, increases in glycolytic rate are usually accompanied by physiological increases in lactate formation, which the heart can utilise. Lactate reportedly contributes 10-15% to energy production via the catalytic conversion of lactate to pyruvate via lactate dehydrogenase (LDH) [290]. The formation of pyruvate couples glycolysis with glucose oxidation in the mitochondria. The uncoupling of glycolysis with glucose oxidation is a hallmark of heart failure and contributes to the progression of the disease [236, 288, 290]. Increases in ROS, mitochondrial dysfunction and ischaemia may initiate glucose uncoupling [288, 296].

BSD-mediated catecholamines may facilitate ROS production, mitochondrial dysfunction and ischaemia, and thus promote uncoupling. Catecholamines have been shown to increase the production of ROS by increasing mitochondrial rate, auto-oxidation and deamination via monoamine oxidases [201]. Ischaemia develops from vascular α_1-AR-mediated vasoconstriction and increases in $c[Ca^{2+}]$. Intracellular Ca^{2+} overload promotes hypercontracture, thus reducing diastolic time, the period in which myocardial perfusion takes place [200]. Evidence of this has been demonstrated via reductions in myocardial O_2 extraction in a porcine model of BSD [52].

β-AR-mediated increases in $c[Ca^{2+}]$ correspondingly increase mitochondrial Ca^{2+} ($m[Ca^{2+}]$), effectively matching energy supply with demand [249]. This is achieved by $m[Ca^{2+}]$ activation of TCA cycle dehydrogenases to increase rates of oxidative phosphorylation [249, 297]. Evidence of contraction and coagulation band necrosis post-BSD is attributed partially to $c[Ca^{2+}]$ overload as a consequence of elevated β-AR agonism [36, 298, 299]. Increased $m[Ca^{2+}]$ uptake, however, activates the mPTP, leading to mitophagy, energy depletion and consequently decreased contractility. Ultimately these catecholamine-mediated actions may increase acetyl-CoA:CoA and NADH:NAD+ ratios, negatively regulating pyruvate dehydrogenase (PDH), causing glucose uncoupling [240, 289]. This results in increased lactate and proton production, which contributes to a decrease in intracellular pH and thus cardiomyocyte function.

Direct assessment of glucose oxidation in the context of BSD has not been conducted outside of lactate production. Indeed, there are increases in glycolytic rates; however, HEPs remain unchanged in the face of high energetic demand. Given the brief, yet intense catecholamine signal and reductions in myocardial oxygen extraction it is difficult to ascertain, i) if glycolytic uncoupling is present, ii) how much this contributes to cardiac dysfunction and iii) how long metabolic dysfunction persists post-BSD and thus closer to donation. Identification of glycolytic uncoupling would open new avenues to therapeutic intervention, i.e. 'metabolic resuscitation'. Improvements in efficiency of glucose oxidation via inhibition of pyruvate dehydrogenase kinase (PDK) and thus, activation of PDH, has been shown to be associated with increased cardiac function and efficiency in settings of heart failure and myocardial ischaemia [290, 300].

In opposition to elevated in glycolytic rate, catecholamines can also increase activities in pathways involved in the inhibition of glycolytic rate. In periods of ischaemia, AMP levels rise, which stimulates the activity of AMP-activated protein kinase (AMPK) [240, 301]. AMPK relieves the inhibition of malonyl-CoA on CPT1 via acetyl-CoA carboxylase inhibition [240, 302]. CPT1 is a rate-limiting step in FAO (β-Oxidation), therefore, AMPK acts to increase rates of β-Oxidation [240, 301]. Moreover, combined β_1/β_2 or selective β_2-AR stimulation increases the rate of β-oxidation and lipid accumulation [303-305]. Lipid accumulation in the setting of oxidative stress also predisposes the heart to lipid toxicity and mitochondrial uncoupling, triggering cardiomyocyte damage and contributing to electrophysiological changes [44-46]. Enhanced β-oxidation results in substrate competition between FFA and glucose utilisation where upregulation of one inhibits the other, referred to as the '*Randle Cycle'* [306].

Given this reciprocal relationship, reducing β-Oxidation rates, thus improving glucose oxidation is of therapeutic interest. Inhibitors of CPT1 (etomoxir, perhexiline) have been shown to increase glycolytic rate and improve cardiac energetics and function in preclinical HF models [290, 307]. However, their use is also associated with hepatoxicity and neurotoxicity, and may produce rebound energetic dysfunction via uncompensated energetic demand through glycolytic pathways [290, 307, 308]. Inhibiting long-chain 3-ketoacyl-CoA thiolase (e.g., Trimetazidine) can provide

equal benefits as CPT1 inhibitors without hepatoxicity. Trimetazidine use in HF is also associated with a reduction in HF class, hospitalisation rate and mortality [309, 310].

Non-cardiac actions of catecholamines also have disparate metabolic activities. Catecholamine activation of pancreatic α_2-ARs produces a potent suppression of insulin release [311]. Whereas α_1/β-ARs promote hepatic glycogenolysis, adipocyte lipolysis and increased insulin secretion upon stimulation [311]. The donor heart is therefore subject to a precarious state of substrate delivery in combination with altered utilisation, a situation referred to as '*futile cycling'* [240]. Determining the changes in metabolic flux in the context of BSD could potentially uncover important mechanisms of donor cardiac dysfunction and open up exciting new avenues for therapeutic regulation. Figure 5.2 outlines the potential cardiac metabolic alterations induced by BSD-mediated catecholamine release.

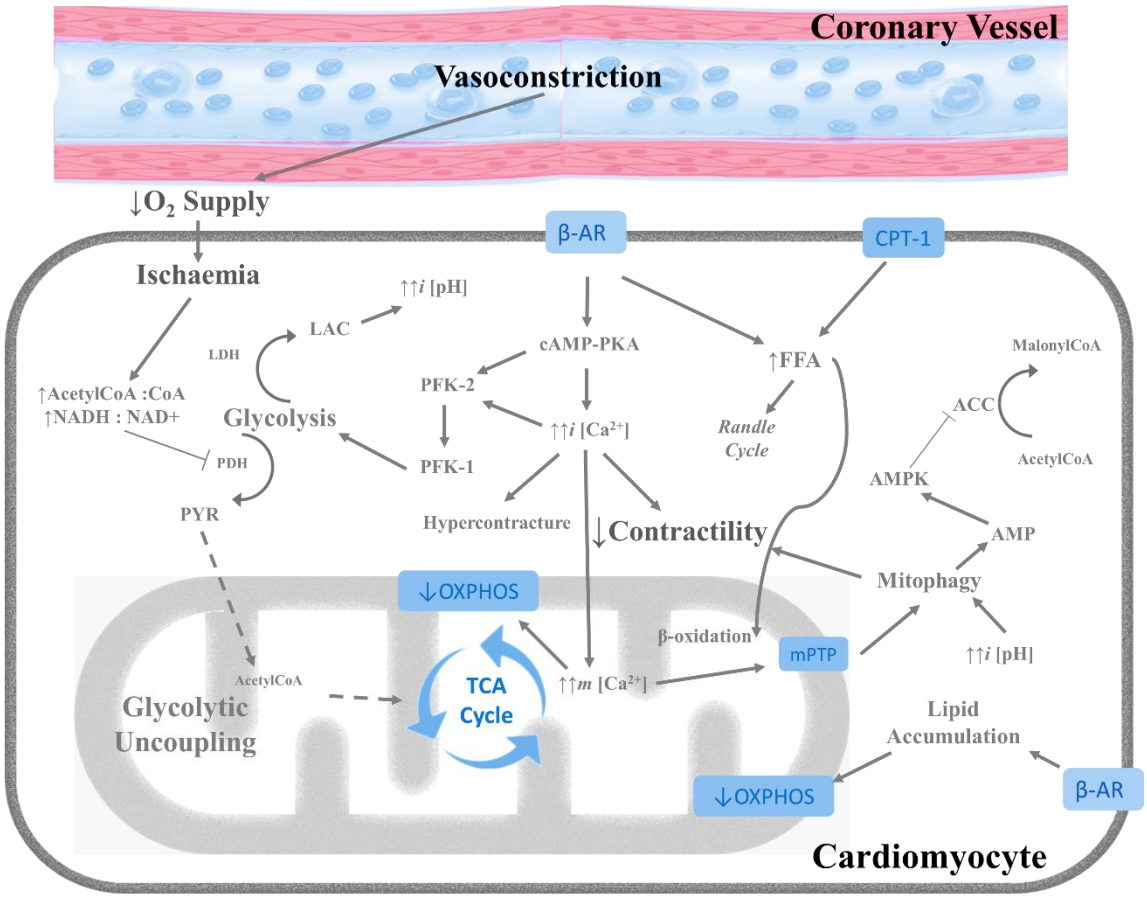

Figure 5.2. Mechanisms of catecholamine induced cardiac dysfunction during the hyperactive of BSD. In the hyperactive phase CATs cause vasoconstriction, Ca^{2+} overload, increased uptake of FFA and glucose, and an increase in glycolysis. Vasoconstriction causes a decrease in O_2 supply leading to an anaerobic switch via glycolytic uncoupling, thus increasing lactate concentrations and lowering cellular pH, which consequently leads to cardiomyocyte death. Increases in $i[Ca^{2+}]$ leads to hypercontracture and increases in $m[Ca^{2+}]$. $m[Ca^{2+}]$ build-up then leads to mPTP opening, mitophagy, decreases in ATP production, cell death, and thus decreases in contractility. cAMP-cyclic adenosine monophosphate, PKA-Protein kinase A, LAC-Lactate, OXPHOS-oxidative phosphorylation, mPTP-mitochondrial permeability transition pore, PYR- Pyruvate , PDH-pyruvate dehydrogenase, LDH- lactate dehydrogenase, AMP- adenosine monophosphate, AMPK-adenosine monophosphate kinase, ACC- acetyl-CoA carboxylase, CPT-1 - carnitine palmitoyl-transferase I, FFA- Free fatty acids, Ca^{2+}-calcium

5.0.9 | The hypodynamic phase of BSD

The hypodynamic phase of BSD is of clinical interest as this is the time where potential donor hearts are assessed for adequate function. This phase is also vital in terms of patient management, specifically inotropic support in the form of sympathomimetic agents. Exogenous catecholamines during this phase, therefore, may exacerbate the metabolic dysfunction carried forward from the hyperdynamic phase. The catecholamine '*profile*' between the two phases are discrete, an intense,

acute signal during the first phase, and a smaller, more chronic profile (inotropic support) for the hypodynamic phase.

The metabolic influence on insulin signalling may also play a key role in substrate selection and therefore, utilisation. Chronic β-AR activation can reduce GLUT4 levels, as well as fatty acid and insulin stimulated glucose metabolism [312, 313]. This process may involve GRK2 and β-ARR upregulation, increasing PI3K-Akt signalling, resulting in phosphorylation of insulin receptor-β [314, 315]. Mangmool *et al.*, proposed that this is a β_2-mediated response, which is supported by evidence of greater apical metabolic dysfunction [314]. The justification behind this is β_2-AR densities are highest at the apex and decline toward the base [316]. These regional differences share similarities with that of Tako-Tsubo cardiomyopathy, sometimes referred to as stress cardiomyopathy given its occurrence after elevations in catecholamine levels. BSD-mediated dysfunction also shares these similarities, and the same mechanisms are likely involved [36].

Historically, catecholamine excess in the potential organ donor was considered a contraindication for transplantation. Due to increasing demand, the clinical need has widened the acceptable donor criteria to those donors who have received high inotropic support [213]. This has successfully increased the amount of available hearts with no adverse post-HTx outcomes, even with the presence of donor ischaemic injury [214]. The cardio-metabolic interaction with catecholamines gives further insight into donor heart dysfunction, and may introduce new therapeutic targets within patient management to further increase viable donor numbers.

5.0.10 | Endothelial and vascular dysfunction

In 1988, Novitzky *et al.*, were the first to examine coronary VSM in a baboon model of BSD [59]. Further works by Szabo and Oishi suggested endothelial and VSM dysfunction in short models of BSD, i.e <3 hrs post-BSD. Metabolism plays an important role in vascular function particularly NO signalling. To synthesise NO, eNOS requires l-arginine and a variety of other cofactors. The uncoupling of cofactors to NOS and competition for l-arginine can both reduce the bioavailability of NO [317]. Arginase also utilises l-arginine to produce l-ornithine and urea, and in situations of hypoxia, inflammation and production of ROS can increase arginase activity and thus compete

with eNOS [318, 319]. Whether arginase activity is upregulated or eNOS uncoupling is present in hearts following BSD is unknown. Adrási and colleagues showed altered NO metabolism in the renal vasculature of BSD donors, causing poor vascular function and increases in nitrogenous ROS [320]. These effects were mitigated with l-arginine supplementation. However, NO metabolism in the heart has not been studied in the context of BSD.

Vascular dysfunction as a consequence of BSD may reduce myocardial perfusion, thereby causing the established ischaemic responses such as contraction band necrosis and metabolic switch. In agreement, Szabo found no cardiac dysfunction or evidence of metabolic compromise post-BSD if loading conditions (and CBF) were kept constant, despite the usual hyperactive phase [85]. Therefore, post-BSD cardiac depression reflects a parallel decrease in ventriculo-arterial coupling with maintained mechanical efficiency, through the Anrep and Frank-Starling mechanisms [85]. These data position decreased coronary perfusion pressure as an important mechanism initiating donor cardiac dysfunction and thus cardio-metabolic and mitochondrial dysfunction.

5.0.11 | Endocrine Changes

Endocrine changes as a consequence of BSD were highlighted in Chapter 1 (p.18). To summarise, early investigations revealed reductions in T3 and adrenal insufficiency in the majority of BSD patients. These findings, particularly T3 depletion, lead to the inclusion of hormone replacement therapy as standard medical management of the BSD donor. T3 therapy was originally thought to rescue metabolic dysfunction and improve haemodynamics since T3 has been indicated in metabolic regulation, mitochondrial biogenesis and increasing oxidative phosphorylation. Whereas corticosteroid administration (usually high doses) helps to reduce inflammation and improve haemodynamics by mimicking the actions of cortisol. Cortisol is a well-known regulator of glucose metabolism, increasing utilisation and insulin release, and at chronically high levels can cause hyperglycaemia and insulin resistance [321]. Whether hormone replacement therapy is beneficial for the BSD donor is questionable, with studies reporting both positive, negative and non-effects, usually on haemodynamics or organ utilisation rate. The metabolic effects of hormone therapy or lack thereof is unknown.

5.0.12 | Metabolic Dysfunction Following CSS

As mentioned in Chapter 1, aim of CSS is three-fold, i) reduce myocardial metabolism, ii) maintain graft viability and reduce swelling, and iii) reduce IRI by inhibiting ROS production and inflammation [106]. However, hypothermic metabolic arrest (such as CSS), while capable of reducing metabolic rate up to 12-fold, does not prevent ATP consumption completely [106, 107, 112].

During CSS, activation of the Na^+/H^+ exchanger increases intracellular Na^+ ions in the presence of dysfunctional Na^+/K^+ATPase. This causes the reverse action of the Na^+/Ca^{2+} exchanger, leading to Ca^{2+} overload, and further inhibiting mitochondrial function. Despite hypothermia, CSS causes a depletion of HEPs, enhancing anaerobic metabolism and acidosis [72, 114, 115]. Depletions in HEP also increases intracellular AMP and as mentioned above, increases the activity of AMPK leading to enhanced, yet oxygen inefficient β-oxidation.

5.0.13 | Metabolic Dysfunction Post-Transplantation

The metabolic consequences of cardiac transplantation have not been widely studied. Chapter 1 (pg. 28) outlined the physiological consequences and pathophysiology of the transplanted heart. The major disturbances include adrenergic failure, endothelial/vascular dysfunction, IRI and pharmacotherapy. The physiological manifestation of these disturbances, and their potential metabolic effects are outlined in table 5.2.

Table 5.2. Summary Cardio-Metabolic Considerations for the recipient.

	Actions	Metabolic Effects
Adrenergic failure	Downregulated β-ARs	Catecholamine-mediated mitochondrial dysfunction
	Hypersensitivity to CATs	Increased lactate production
	High inotrope usage	Deficiencies in upregulating metabolic rate to meet demand
Endothelial/Vascular Dysfunction	CAV	Poor metabolite delivery and lactate clearance
		Decreased O_2 delivery initiating anaerobic respiration
		Ischaemic damage
IRI	Rapid pH restoration	Mitochondrial Dysfunction
	Ca^{2+} overload	Succinate build-up
	ROS production	Increased ROS induced mitochondrial damage
Pharmacological Treatment	Immunosuppression	Lipotoxicity

β-AR- beta-adrenoceptor, CAT-catecholamines, CAV-cardiac allograft vasculopathy, ROS-reactive oxygen species

Adrenergic failure manifests as supersensitivity to circulating catecholamines due to an absent presynaptic noradrenaline reuptake mechanism [132]. This mechanism increases synaptic noradrenaline levels and may contribute to the desensitisation of β-ARs to noradrenaline observed in Chapter 3. Further, this supersensitivity may also contribute to mitochondrial dysfunction, observed in Chapter 4, via catecholamine-mediated toxicity. Combined, these effects then lead to well documented contractile dysfunction, predisposing the transplanted heart to primary graft dysfunction.

Ischaemia and subsequent reperfusion injury is a significant stressor in the transplant process. Van Caenegem *et al.,* [122] and Stoica *et al.,* [72] showed that the HEP depletions during CSS

are not fully restored at reperfusion, reporting elevated lactate concentrations and increased AMP/ATP ratio. As a consequence, β-oxidation predominates as the primary energetic pathway following reperfusion, which decreases glycolytic coupling leading to increases in lactate, acidosis and ionic disturbances [240, 290]. Supplementing at reperfusion with n-3 FAs has been shown to reduce IRI, by repairing cellular membranes and decreasing lipid peroxidation [46, 143].

Proteomic biomarker discovery has been used in transplant recipient studies to identify early graft dysfunction. Lin *et al.*, recently used a heterotrophic HTx rat model to determine the metabolic profile post-BSD in serum [146]. They found a panel of 4 metabolites, D-tagatose, choline, C16 sphinganine and D-glutamine could accurately diagnose early rejection. Additionally, they observed an increase in oxoglutaric acid, which plays a significant role in immune function, the rate of the TCA cycle and AA production [146]. Given the accumulation of succinate and its role in ROS production, it seems likely that the increase in oxoglutaric acid may drive this and other functions, making it an important metabolic and immunological therapeutic target. A caveat in this study however, was that this study was performed in rats with known difference in metabolic regulation compared to humans.

The aim of this chapter was to characterise the cardiac metabolome following BSD and post-HTx. We utilised a metabolomic platform, liquid chromatography coupled with mass spectrometry (LC-MS), to investigate metabolite changes. Given the aforementioned cardiac effects of BSD, CSS and HTx, we hypothesised that the BSD and post-HTx myocardium would experience energetic failure, particularly post-HTx, and preference glycolytic substrates.

5.1 | Methods

Following 24 hr monitoring time for the donor and 2-6 hrs post-HTx, the heart was placed immediately in cold oxygenated Krebs solution and transported to the laboratory. Ventricular samples were collected using a biopsy gun from the apical, mid and basal regions under continuous oxygenation in Krebs solution. This was performed for 4 hearts from each group. All 3 samples per ventricle were then placed into an Eppendorf tube and snap frozen in liquid

nitrogen. Samples were stored at -80°C before transport to Metabolomics Australia, University of Melbourne. Figure 5.3 outlines the metabolomics workflow utilised in this study.

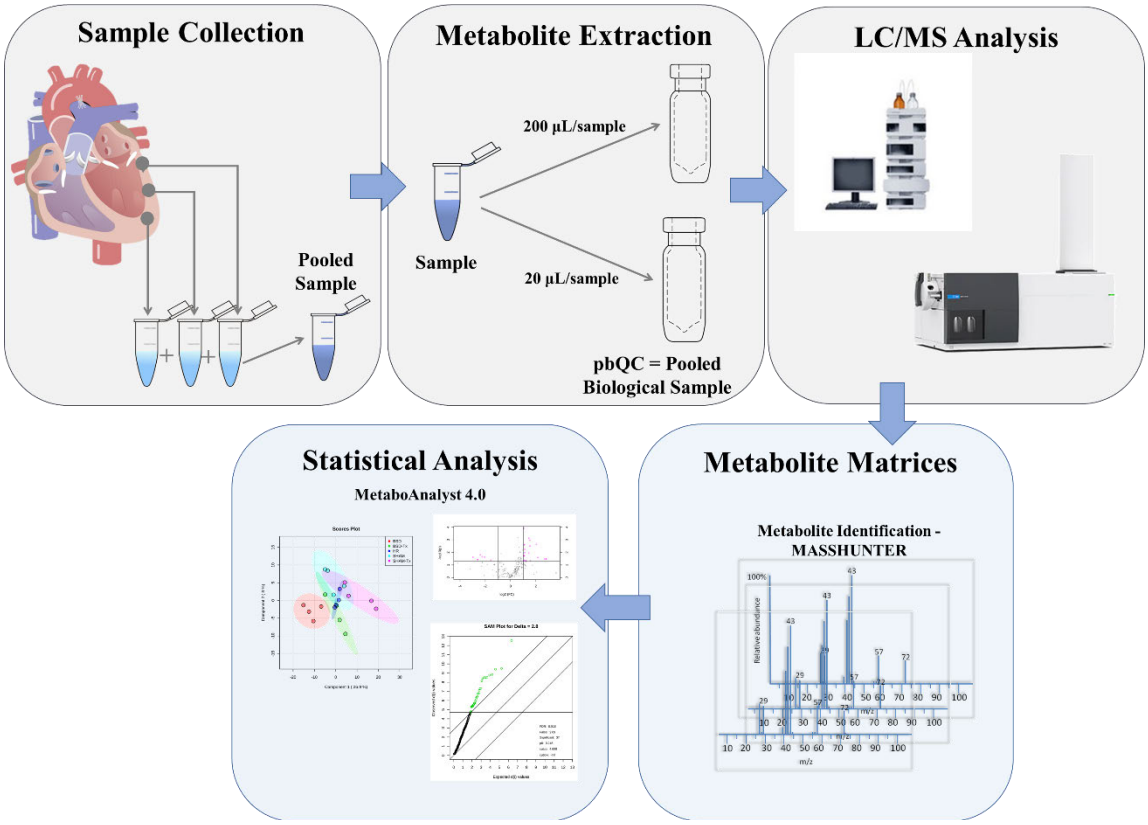

Figure 5.3. Metabolomics workflow from sample collection to statistical analysis. Ventricular biopsies were collected in 3 discreet regions of the myocardium, i) apex, ii) mid and iii) basal. Biopsies were snap frozen and pooled and remained at -80°C until transport. Metabolites were extracted and a portion of each sample pooled for quality controls (pbQCs). Polar metabolites were detected via LC/MS. Metabolites were identified using MassHunter and statistical analysis was performed using MetaboAnalyst 4.0.

5.1.1 | Quenching and extraction of polar metabolites

The excised sample tissues were first washed with phosphate buffer saline (PBS) and quenched using liquid nitrogen. The tissues were weighed in pre-weighed cryomill vials (MPS Biomedicals) to around 20-30 mg. The samples were kept on ice for the extraction. Polar metabolites were extracted using Acetonitrile:Methanol:Milli-Q water (2:2:1 v/v/v, 500 µl) containing internal standards ($^{13}C_{10}$,$^{15}N_5$-AMP, ^{13}C,^{15}N-UMP, $^{13}C_6$-Sorbitol and $^{13}C_5$, ^{15}N-Valine) at 2 µM

concentration per sample. The tissues were homogenised using a homogeniser (Precellys®24 and the Cryolys® cooling) unit at 6800 rpm at 3 x 30 sec pulses with 45 sec intervals between the pulses at < -10°C (pre-chill with liquid nitrogen). The tissues were normalized by adding additional extraction solvent to normalize the weights to 25 mg. The homogenate from cryovials were transferred to an Eppendorf microcentrifuge tube and vortexed. The homogenate was incubated for 10 mins at 4°C on the thermomixer to ensure lysis of all cell membranes and then centrifuged to maximum speed 14000 rpm at 4°C to remove the cell debris. Around 200 µl of the clear supernatant was transferred into a HPLC vials with inserts for LC-MS analysis. For pooled biological samples, 20 µl of the clear supernatant was pooled from all the samples.

5.1.2 | LC-MS analysis of polar metabolites:

Polar metabolites were analysed by LC-MS. Analysis was performed on an Agilent 1200 series LC system (Agilent Technologies). Samples were stored in an autosampler at 4°C. Metabolite separation was performed by injecting a 7 µl sample onto a SeQuant ZIC-pHILIC column (150 mm×4.6 mm, 5 µm, Merck Millipore) maintained at 30 °C using Solvent A (20mM $(NH_4)_2CO_3$, pH 9.0, Sigma-Aldrich) and Solvent B (100% Acetonitrile, Hypergrade for LCMS LiChrosolv, Merck) at a flow rate of 300 µl min^{-1}. The gradients used were: time (t)=0 min, 80% B; t=0.5 min, 80% B; t=15.5 min, 50% B; t=17.5 min, 30% B; t=18.5 min, 5% B, t=21.0 min, 5% B; t=23 min, 80% B, t=33 min, 80% B.

The mass spectrometry analysis was performed on an Agilent 6545B series quadrupole time-of-flight mass spectrometer (QTOF MS) (Agilent Technologies). The LC flow was directed to an electrospray ionisation source (ESI), where metabolite ionisation in negative mode was performed with a capillary voltage of 2500 V, a drying gas (N2) pressure of 20 psi with a gas flow rate of 10.0 L.min−1, a gas temperature in the capillary of 300 °C and fragmentor and skimmer cap voltages of 125 V and 45 V, respectively. Data was collected in centroid mode with a mass range of 60–1200 m/z and an acquisition rate of 1.5 spectra sec−1 in all-ion fragmentor (AIF) mode, which included three collision energies (0, 10 and 20 V). Prior to analysis, mass calibration was performed for negative mode to 0.5 ppm accuracy of the m/z value. Internal mass calibration was

performed using Agilent ESI-TOF Reference Mass Solution containing purine (119.036320) and hexakis (1H,1H,3H-tetrafluoropropoxy) phosphazine (981.99509) (API-TOF Reference Mass Solution Kit, Agilent technologies), which was continuously infused into the ESI source at a flow rate of 200 μl min^{-1}.

Targeted data matrices were generated using MassHunter Quantitative Analysis software (version B.09.00, Agilent Technologies) with metabolite identification (Metabolomics Standard Initiative (MSI) level 1) based on the retention time and molecular masses matching an authentic standard [322].

5.1.3 | Statistical Analysis

Data quality and instrument performance was tested using internal standards and quality control samples derived from pooled ventricular samples (pbQC). Detection of internal standards and pbQCs were assessed via the coefficient of variation (CV), where CV<20% is considered acceptable.

5.1.3.1 | Data Normalisation

Statistical analyses were performed using MetaboAnalyst 4.0, a web-based platform for the statistical and functional analysis of metabolomic data. Data matrices are first checked for integrity (missing values), median normalised and transformed via general logarithm. Normalisation removes variability from non-biological sources such as instrument performance. There is much debate over the correct normalisation method, however a consensus is sample normalisation must be performed [323]. Metabolite concentrations can be highly variable both between and within groups for any one biological sample [323]. To reduce this variation in spectrum values and to allow statistical analysis, data are transformed usually via log_2 transformation. Log_2 normalisation however, tends to inflate low (near zero) variances and decrease high variances [324]. Generalised log transformation reduces the error associated with low variance, bringing the error close to homoscedastic (error equal across all values) and therefore, is a more robust normalisation method [324].

5.1.3.2 | Multivariate analysis

After data normalisation and transformation, statistical tests can be performed to determine important metabolic differences between groups. Principal component analysis (PCA) is a common multivariate method for metabolomic feature identification [325]. However, as the sample size per group is small, PCA is an inappropriate method to identify important metabolic differences. Instead, it was used here to initially visualise data and assess general variation in metabolic profile between ventricles and groups. Assessment of metabolite differences between all groups included ANOVA and Significance Analysis of Microarrays (SAM). SAM is a supervised method of feature identification that utilises moderated t-tests via non-parametric assessment of important metabolites based on repeated permutations.

5.1.3.3 | Univariate Analysis

Although multivariate testing highlights important metabolic differences between all groups, it is important to consider biological questions. The questions that will be addressed here are, i) what are the metabolic consequences of BSD?, ii) what are the metabolic differences post-HTx between hearts with and without pre-transplant BSD injury?, and iii) how does the metabolic profile of the donor heart compare to the post-HTx profile?, i.e BSD vs BSD-Tx.

To interrogate these questions, univariate analysis was conducted comparing i) donors only (BSD vs SHAM), ii) post-HTx hearts (SH-Tx Vs BSD-Tx) and iii) donor hearts to post-HTx hearts (BSD Vs BSD-Tx). These univariate tests included volcano plots (VP) and SAM. For VP analysis, a fold change threshold of 2.0 was used to assess significance. For all statistical tests a p-value less than 0.05 was considered statistically significant.

5.2 | Results

A total of 221 metabolites were detected with the majority (90%) resolving well with a coefficient of variation (CV) below 10%. Internal standards in pbQCs and all samples were detected with a CV<20% indicating optimal extraction efficiency and instrumental performance.

5.2.1 | Metabolic differences between ventricles

Multivariate PCA analysis showed close clustering of ventricular samples within each group (Fig. 5.4 & 5.5), although the spread of the data (size of the cluster) was variable. This appeared to be more common for the BSD and BSD-Tx groups. Post-hoc volcano plots showed no more than 5% of metabolites were significantly different within each group between ventricles (Table 5.3).

Further statistical tests examined LV and RV samples independently due to the differences in metabolite deviations between samples and the presence of altered metabolite intensities. Additionally, in the context of HTx, ventricular differences in dysfunction (particularly the RV) are well-recognised and are used in the categorisation of PGD. Therefore, to elucidate the potential metabolic contribution to PGD, ventricular metabolic profiles were analysed separately.

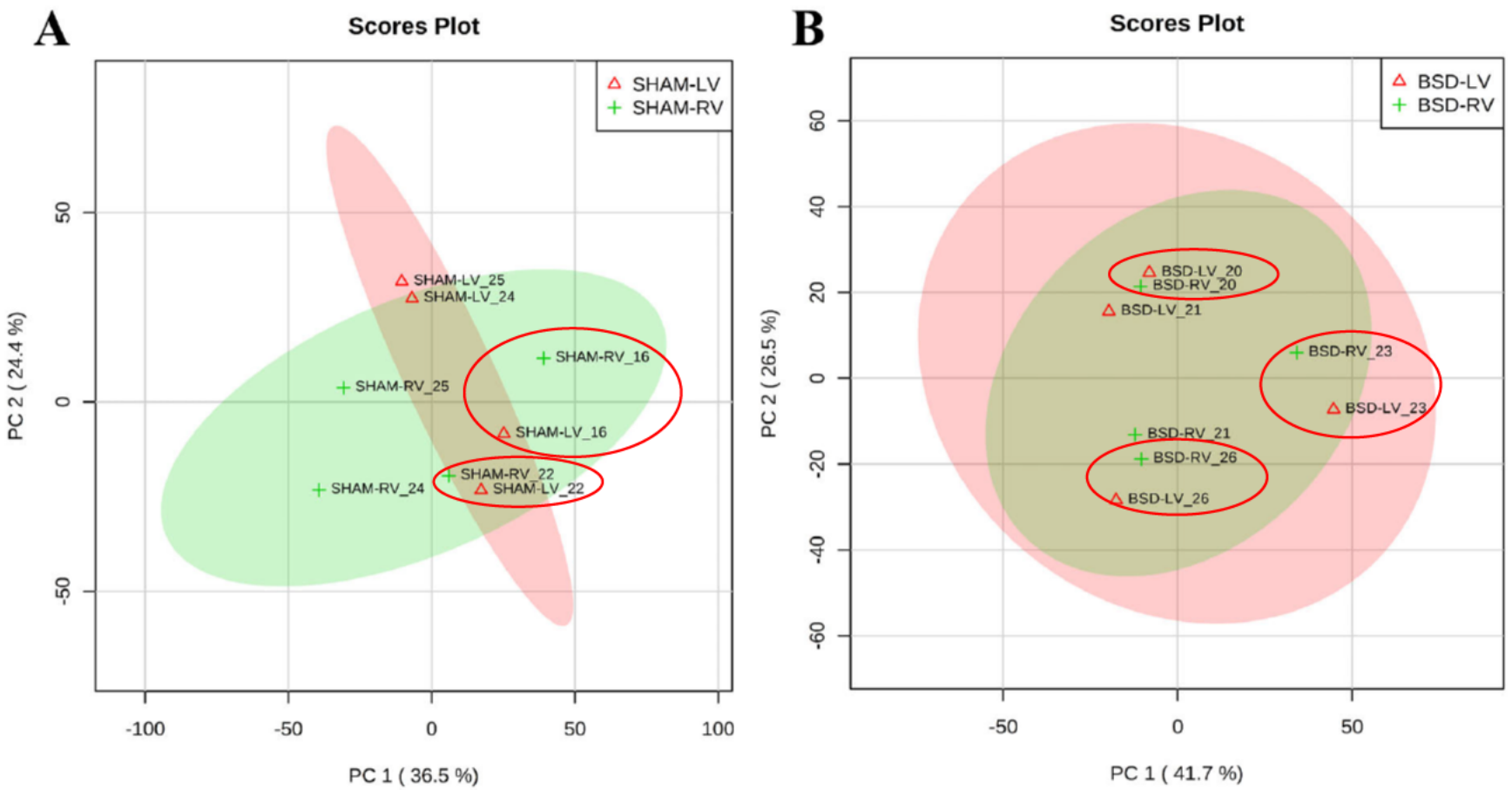

Figure 5.4. PCA analysis showing close clustering of metabolites between ventricles for donor groups. A SHAM group PCA **B,** BSD group PCA. Red circles highlight the LV & RV for the same sample. BSD group appeared to show closer clustering of metabolites between the ventricles of the same animal SHAM donors. n=4 for all groups

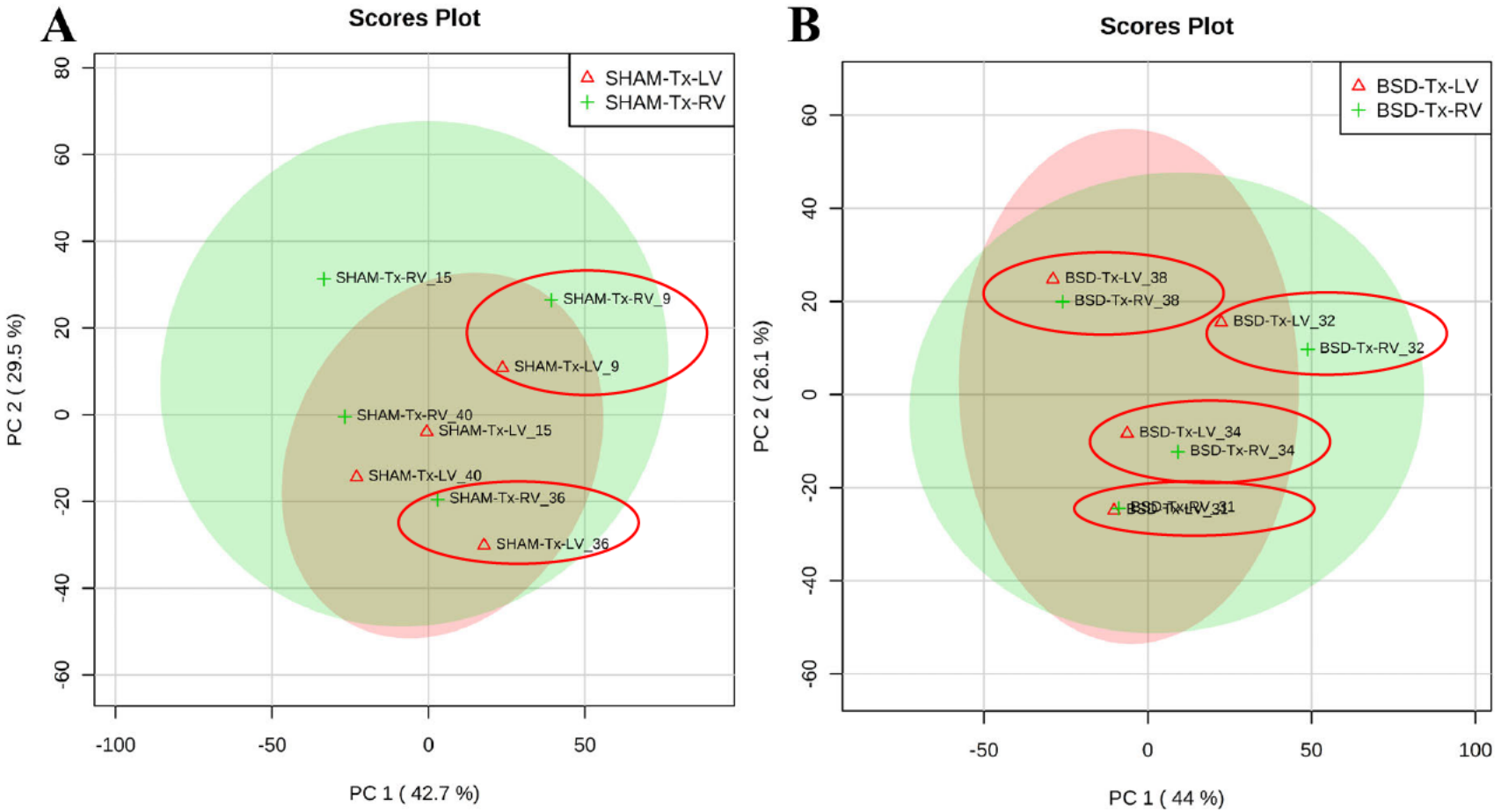

Figure 5.5. PCA analysis showing close clustering of metabolites between ventricles for post-HTx groups. A SH-Tx group PCA **B,** BSD-Tx group PCA. Red circles highlight the LV & RV for the same sample. BSD-Tx group appeared to show closer ventricular metabolic profiles than SH-Tx donors.

Table 5.3. Statistically significant metabolite differences between left and right ventricles of each group. Fold changes >1 indicate higher metabolite content in LV compared to RV

Group	Metabolite	Fold Change	-log10 p-value
HR	Behenic acid	0.39	2.78
	Hydrocinnamic acid	0.48	2.52
	3-Methylphenylacetic acid	0.47	2.52
	Dimethylglycine	0.09	2.24
	N-Acetylglutamine	0.38	1.76
	D-Glucurono-6,3-lactone	0.19	1.71
	Flavin Mononucleotide	3.18	1.25
	D-Glucuronic acid	0.38	1.20
	Fructose 1,6-bisphosphate	2.24	1.10
	Hydroxyisocaproic acid	0.46	1.09
SHAM	Fructose 1,6-bisphosphate	2.92	2.63
	Caproic acid	0.46	2.36
	Flavin Mononucleotide	5.88	2.10
	Caprylic acid	0.44	1.83
	Alpha-Tocopherol	5.52	1.52
BSD	Citraconic acid	2.24	1.94
SH-Tx	Pentadecanoic acid	0.43	2.44
	Oxoglutaric acid.1	2.00	2.02
	D-Glucurono-6,3-lactone	0.42	1.67
	Alpha-Tocopherol	3.06	1.60
	Flavin Mononucleotide	5.78	1.52
	Octadecanedioic acid	0.46	1.44
BSD-Tx	Octadecanedioic acid	0.45	3.06
	Linoleic acid	0.36	2.98
	Undecanoic acid	0.45	1.99
	Retinol acetate NPS	0.42	1.91
	Valeric Acid	0.46	1.75
	Caproic acid	0.48	1.58
	Alpha-Tocopherol	3.93	1.54
	Alpha-Linolenic acid	0.41	1.52
	Nonadecanoic acid	0.45	1.43
	Stearic acid	0.44	1.12
	Palmitic acid	0.48	1.01

5.2.2 | Overall metabolic differences between all groups

Initial data visualisation using PCA revealed a close association of metabolism between groups (Fig 5.6). The largest differences appeared to be between donor and transplanted groups for both ventricles. For the LV, 2 component PCA explained 26.8% of the variation in the data and 24.1% for the RV.

ANOVA for the LV across all groups identified 16 significantly altered metabolites, 3 of which were also identified by SAM analysis (Fig 5.7 A). These metabolites were dimethylglycine, sorbitol and 3-aminoisobutanoic acid. For the RV, 20 metabolites were identified by ANOVA, 14 of which were also identified by SAM analysis (Fig 5.7 B). ANOVA alone identified alanine AA derivatives, sarcosine, FAD, L-arginine and oxalic acid compared to SAM. Whereas SAM also identified (S)-3-hydroxyisobutyric acid and α-hydroxyisobutyric acid, pimelic acid and methionine sulfoxide as significantly altered. These results suggest that alterations in AA metabolism, PoP activity (sorbitol), mitochondrial energetics (CoA), oxidative stress and glycosylation are likely to be important in peri-transplant metabolic function.

A potential drawback when making multiple comparisons across a large dataset, such as in metabolomics, is the potential to make a type II error. That is, disregarding potentially important metabolite changes. In the context of transplantation, the changes stated here, may not fully elucidate i) cardiac dysfunction in the donor heart, ii) cardiac dysfunction post-HTx and iii) metabolite changes from the donor to post-HTx. It is prudent then, to interrogate a subset, i.e SHAM vs BSD, of the data to reduce multiple comparisons.

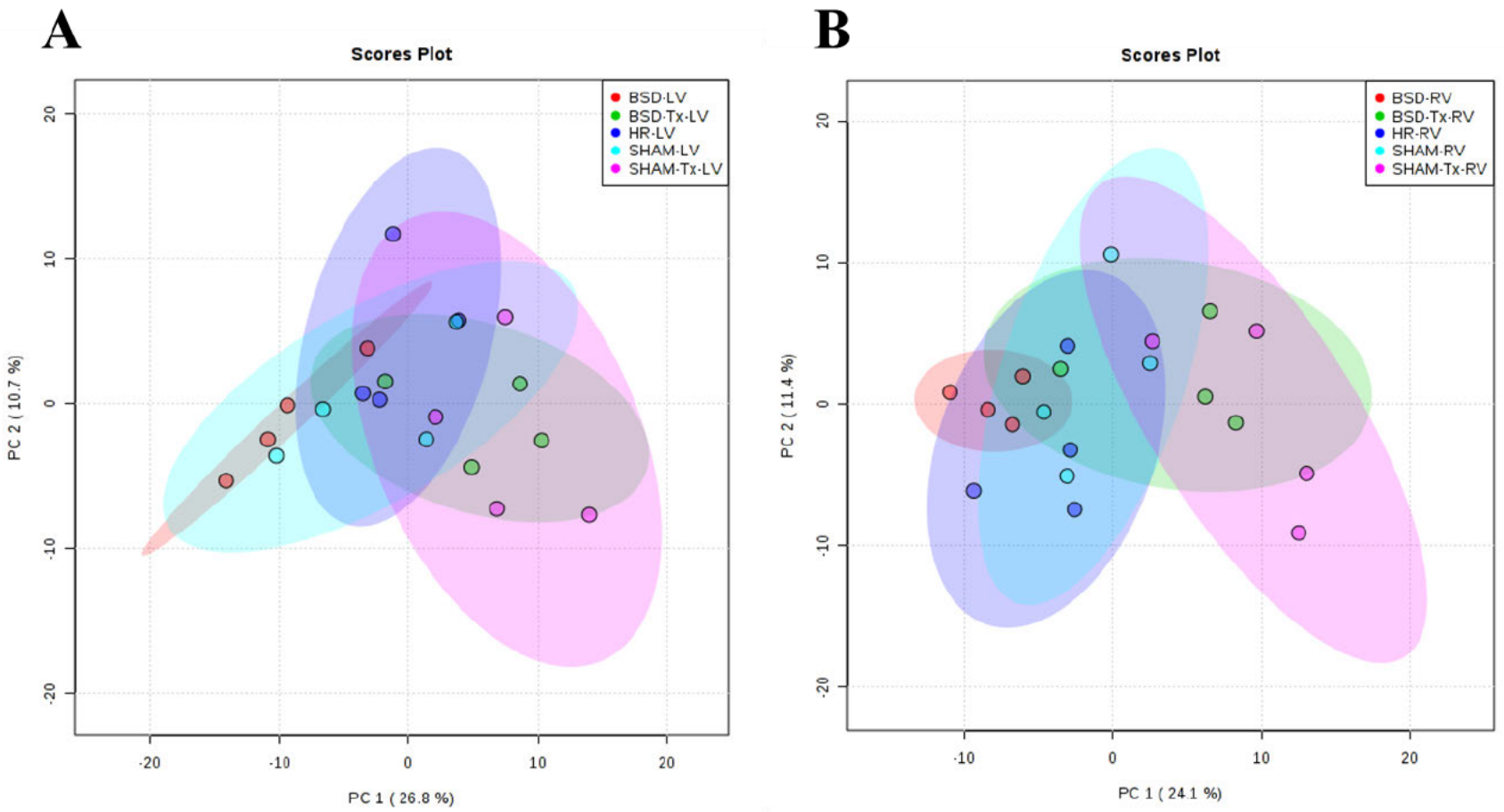

Figure 5.6. PCA analysis showing close clustering of metabolites between all groups per ventricle. A left ventricle PCA **B.** Right ventricle. 2 component PCA was able to explain 26.8% and 24.1% of the variance between LV (A) and RV (B), respectively. The most significant differences appeared to be between donor and post-HTx groups.

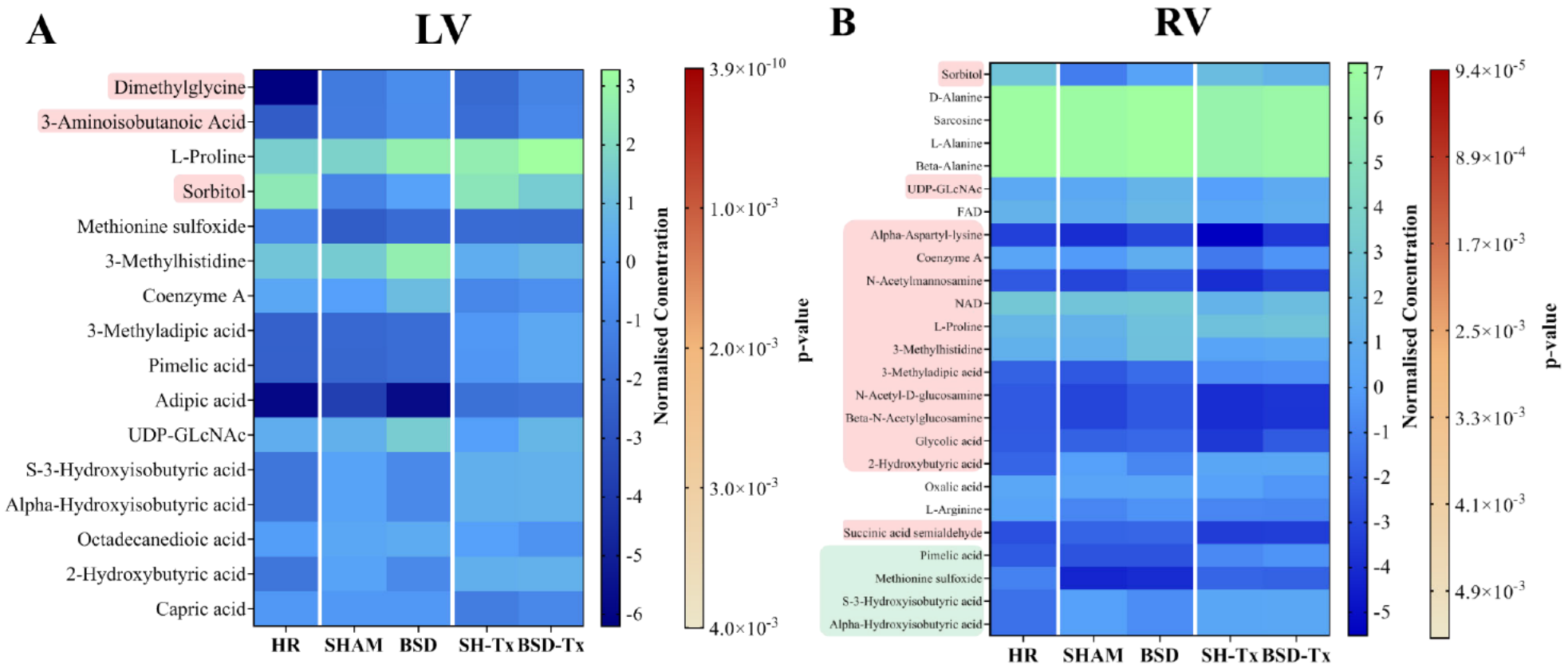

Figure 5.7. Heatmaps of significant metabolites identified via ANOVA in the left ventricle (A) and right ventricle (B). Red highlighted metabolites represent those metabolites that were identified by both ANOVA and SAM analysis. Green highlighted metabolites represent metabolites only identified by SAM analysis. Heatmap colour gradient represents average normalised log concentrations of metabolites between groups. The p-value range for ANOVA is represented by a simplified heatmap to the right of each map.

5.2.3 | Metabolic Consequences of BSD

For the LV, VP plots showed a BSD-mediated elevation in 3-methylhistidine, AA metabolites, R-lipoic acid, 2-methylcitric acid and caprylic acid (C8:0) (Fig 5.8 A). BSD hearts also had lower levels of D-glucuronic acid, galacturonic acid, L-tryptophan and adipic acid. SAM analysis identified reductions in the metabolites D-glucuronic and adipic acid as important features. VP analysis for the RV revealed an upregulation of AA metabolites, sorbitol, R-lipoic acid, 2-methylcitric acid (2-MCA), and gluconolactone and compounds involved in mitochondrial energetics (CoA and flavin mononucleotide (FMN)) (Fig 5.8 B). Only D-glucuronic acid was downregulated in the RV of BSD hearts. SAM for RV metabolites however, identified only CoA and FMN as significant.

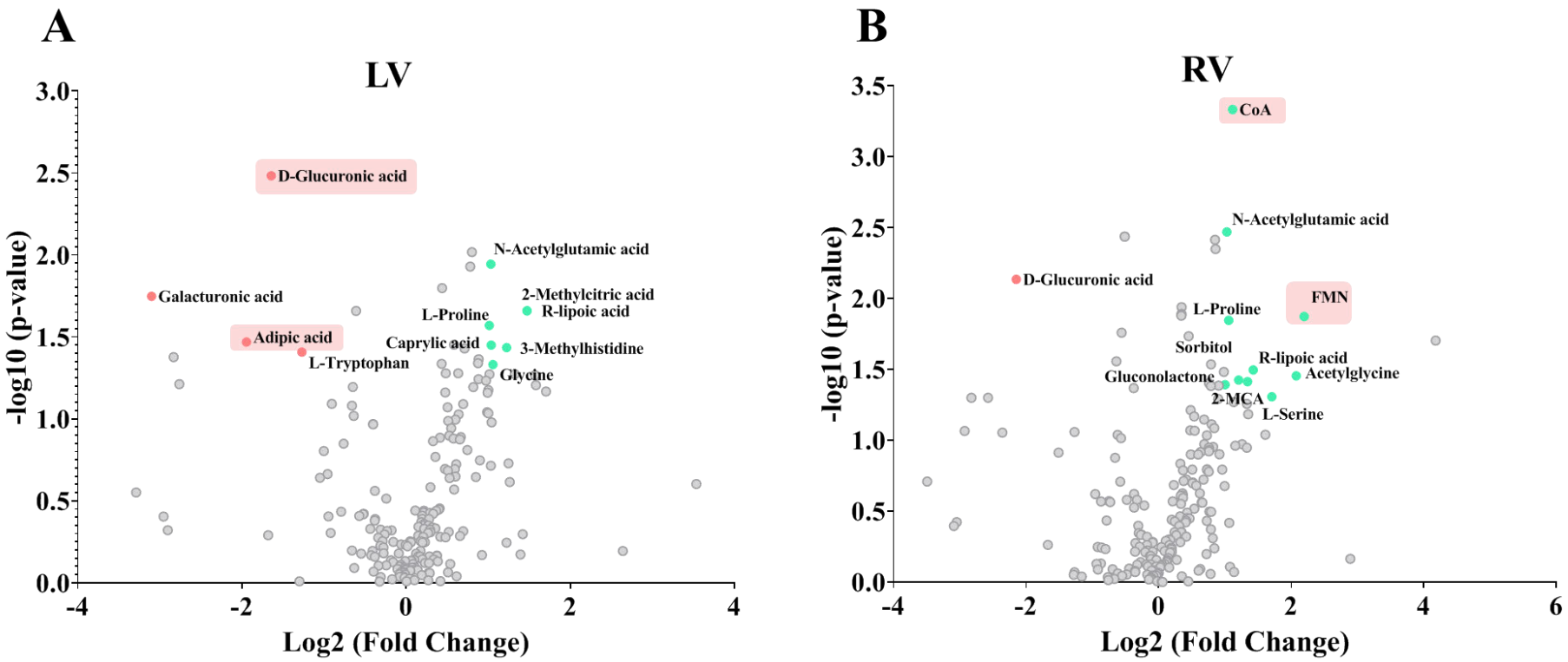

Figure 5.8. Volcano plot of significantly altered metabolites comparing SHAM to BSD hearts for the left ventricles (A) and right ventricles (B). Green symbols represent metabolites upregulated in BSD hearts (vs SHAM). Red symbols indicate metabolites downregulated in BSD hearts. Red highlighted metabolites indicate metabolites that were identified by both VP and SAM analysis.

5.2.4 Metabolic Consequences of Transplantation

For the LV, BSD-Tx hearts showed upregulated uridine 5'-diphosphate (UDP), glycine, dimethylgycine and 3-aminoisobutanoic acid according to VP analysis. Both SAM and VP analysis identified lower levels of citraconic acid (methyl-branched FA of citric acid) in BSD-Tx compared to SH-Tx (Table 5.4). VP for the RV showed increased levels of alpha-aspartyl-lysine, glycolic, glutathione and glycerophosphocholine in BSD-Tx. SAM only identified lower levels of oxalic acid in BSD-Tx compared to SH-Tx (Table 5.4).

Table 5.4. Significantly altered metabolites comparing BSD-Tx with SH-Tx hearts.

		VP		SAM	
	Metabolite	**Fold Change**	**p-value**	**d.value**	**p-value**
Left Ventricle	Citraconic Acid	0.15	0.008	2.79	0.002
	3-Aminoisobutanoic Acid	2.01	0.008		
	Dimethylglycine	2.09	0.012		
	Glycine	2.56	0.019		
	UDP	4.70	0.041		
Right Ventricle	Alpha-Aspartyl-Lysine	3.19	0.009		
	Glycolic acid	2.4	0.012		
	Glutathione	2.19	0.028		
	Glycerophosphocholine	2.17	0.033		
	Oxalic acid			4.43	0.006

A fold change >1 indicates upregulated metabolites in BSD-Tx hearts. UDP- uridine 5'diphosphate

Univariate comparisons between the BSD donor and BSD-Tx showed that, post-HTx, there was a bi-ventricular reduction in N-acetyl-glucosamine (GLcNAc) derivatives (N-acetyl-D-glucosamine and β-N-acetylglucosamine), CoA, glycyl-L-Leucine and 3-methylhistidine, with accumulation of 3-methyladipic acid (Fig 5.9 A). Isolated to the LV, there were post-HTx reductions in inositol derivatives, the FAs C11:0 and itaconic acid, gluconolactone and metabolites involved in mitochondrial energetics and AA metabolism. Elevated LV metabolites post-HTx included dicarboxylic acids, L-isoleucine and orotidine. SAM also identified 7 of the 21 metabolites identified by VP. In addition, SAM identified reductions in purine in the LV of hearts from BSD-Tx group. For the RV, succinic semialdehyde and L-Serine were decreased with an accumulation of D-glucuronic acid, D-xylitol, ribitol and xanthine post-BSD-Tx (Fig 5.9 B). SAM identified 2 of the 12 metabolites identified by VP.

Comparing SHAM donors with SH-Tx hearts, VP showed a bi-ventricular increase in sorbitol, pimelic acid and 3-methyladipic acid with a reduction in glycolic acid NAD and acetyl-CoA for the SH-Tx group (Fig 5.10 A). Specific to the LV of SH-Tx hearts, levels of glucose-6-phosphate, 3-methylhistidine, ADP, glutathione, citicoline and UDP were significantly decreased compared to SHAM. Whereas, D-Fructose acetyl-cysteine, D-glucuronic acid and 2-MCA were elevated. For the RV, the FAs C8:0 and C9:0, N-alpha-acetyllysine, succinic acid semialdehyde, alpha-aspartyl-lysine, UDP-glucose and NADH were elevated in SH-Tx group (Fig 5.10 B). RV tissue from SH-Tx also contained significant accumulation of L-proline, adipic acid, methionine sulfoxide and N-acetyl-L-alanine. SAM identified the same metabolites that were elevated in the LV of SH-Tx, with the addition of behenic acid (C22:0). SAM for RV metabolites also identified the post-SH-Tx elevated metabolites sorbitol, pimelic acid and 3-methyladipic acid.

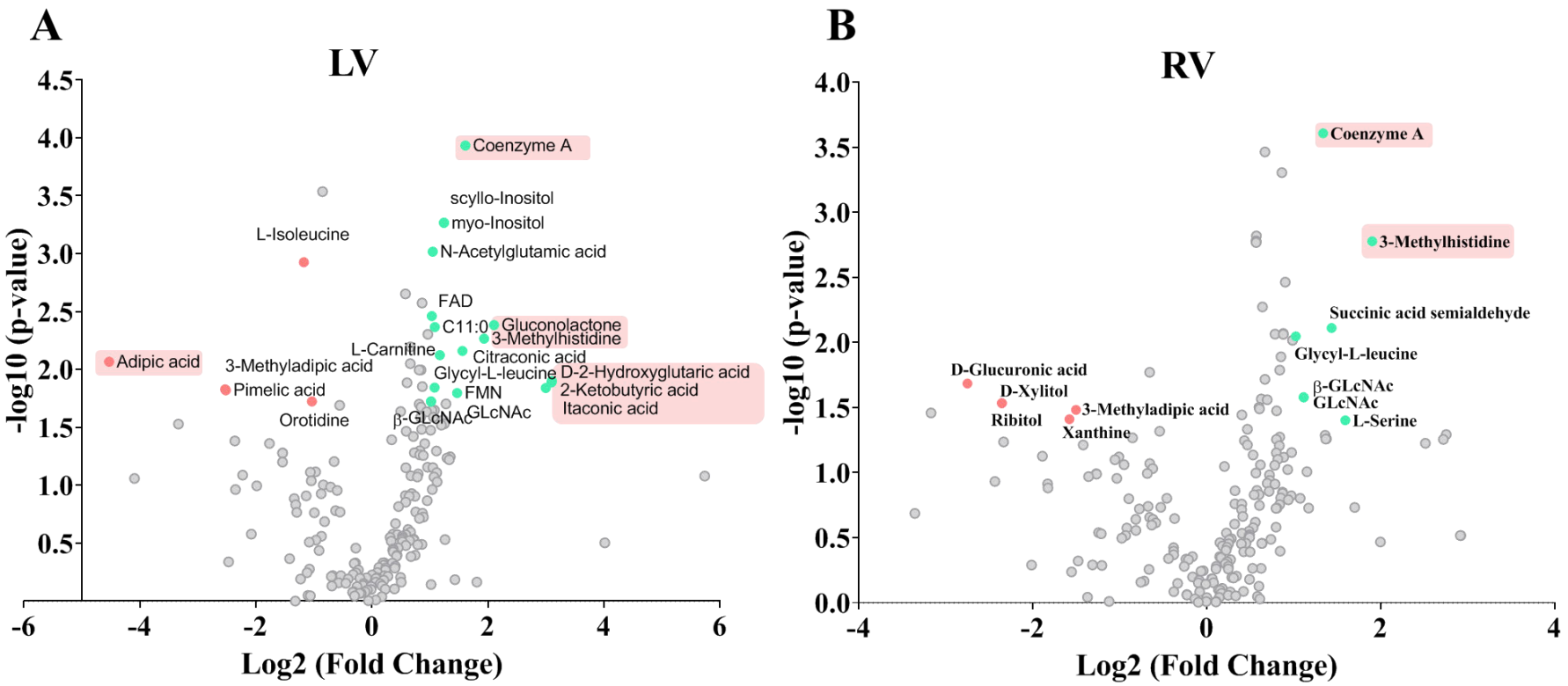

Figure 5.9. Volcano pot of significantly altered metabolites comparing BSD to BSD-Tx hearts for the left (A) and right ventricles (B). Green symbols represent metabolites downregulated in BSD-Tx hearts. Red symbols indicate metabolites upregulated in BSD-Tx hearts. Red highlighted metabolites indicate metabolites that were identified by both VP and SAM analysis. Grey symbols indicate metabolites not significantly altered between the two groups.

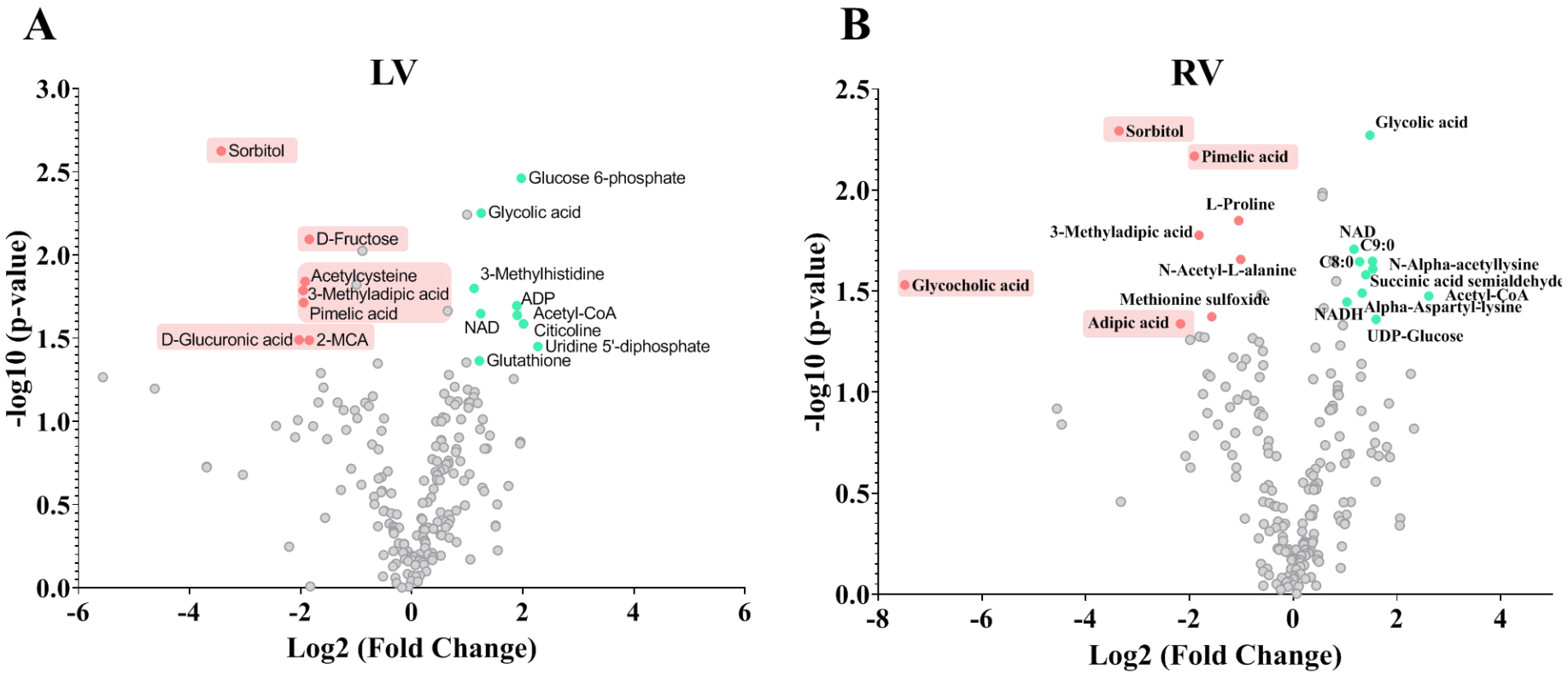

Figure 5.10. Volcano pot of significantly altered metabolites comparing SHAM to SH-Tx hearts for the left (A) and right ventricles (B). Green symbols represent metabolites downregulated in SH-Tx hearts. Red symbols indicate metabolites upregulated in SH-Tx hearts. Red highlighted metabolites indicate metabolites that were identified by both VP and SAM analysis. Grey symbols indicate metabolites not significantly altered between the two groups.

5.3 | Discussion

Peri-transplant cardiac metabolism is a poorly investigated area, yet has the potential to identify important, targetable pathological mechanisms. Presented here is the first preliminary metabolomics analysis of both BSD donor and subsequent transplanted hearts. Using a metabolomic approach, we have shown that donor BSD is characterised by accumulation of metabolites involved in protein turnover, amino-acid metabolism, oxidative stress, altered FAO, oxidative phosphorylation, propionate metabolism and the pentose phosphate pathway. This may suggest a hyper-catabolic state, which may be transferred during engraftment, potentially conferring an advantage over SHAM operated donors. Finally, post-HTx, there is a significant decline in metabolites involved in mitochondrial energetics, FAO, amino-acid metabolism and O-GlcNAc protein modifications.

5.3.1 | Metabolic consequences of donor BSD

Previous animal and human studies have consistently shown that post-BSD, HEPs are preserved [60, 114]. We have also shown preserved HEPs, alongside elevated coenzyme A and FMN, particularly in the RV. FMN is a component of mitochondrial NADH dehydrogenase (CI), acting as an electron carrier. Increased FMN may indicate higher CI activity, however as demonstrated in the previous chapter (pg. 121), CI activity post-BSD was unchanged compared to SHAM. This may be due to changes in mitochondrial morphology or content, which were corrected for in the mitochondrial respirometry experiments. In support of changes in mitochondrial dynamics, we also observed elevated coenzyme A, a product of citrate synthase activity, which would suggest higher TCA activity [326].

Coenzyme A is a well-known inhibitor of PDK, leading to the enhancement of glucose oxidation by increasing PDH activity [326]. We did not observe increases in glycolysis intermediates, however metabolites of neighbouring glycolytic pathways were enhanced. These were gluconolactone from the pentose phosphate pathway and sorbitol from the polyol pathway. Under normal and euglycaemic circumstances, both of these accessory pathways contributes minimally to glycolytic flux [327, 328]. However in hyperglycaemia, a consequence of BSD, the relative contributions of each pathway may increase due to a spillover effect or in response to the cellular milieu, i.e. ROS [329].

The pentose phosphate pathway is divided into an oxidative and a non-oxidative branch, and is becoming increasingly recognised as an important metabolic pathway in cardiac function [287]. The oxidative branch of the PPP generates 6-phosphogluconolactone and D-ribose 5-phosphate, important NADH generating reactions for the cytosol [328]. The oxidative PPP can be elevated in situations of oxidative stress and hyperglycaemia, both a consequence of donor BSD [330]. Elevated oxidative PPP and NADH acts to maintain the cytosolic glutathione pool in a reduced state [287, 328, 329]. However, in the previous chapter, we have shown that the GSH:GSSG ratio is decreased, indicating that oxidative PPP is insufficient to overcome the oxidative stress of BSD.

An additional glucose accessory pathway is the polyol pathway, the first step of which is production of sorbitol from glucose, catalysed by aldose reductase (ARase) [287]. The polyol pathway is believed to have both cardioprotective and proapoptotic actions [287]. The cardioprotective action mostly involves the antioxidant action of ARase, reducing lipid peroxidation [331]. The pro-apoptotic actions involve promotion of oxidative stress via utilisation of NADH, thus suppressing the glutathione pool and reduction of FA utilisation [327, 331]. Activation of the polyol pathway in the RV may predispose a higher oxidative state due to reductions in the cytosolic NADH pool and thus glutathione. A significant consequence of polyol activation is hyperosmotic stress, increasing oxidative stress, reducing Na^+/K^+ATPase activity leading to apoptosis [331]. Inhibiting aldose reductase activity has shown cardioprotective benefits in ischaemic and diabetic cardiomyopathies [332].

To further support higher oxidative stress post-BSD, we have also observed elevated levels of (R)-lipoic acid and methionine sulfoxide (MeS) (on a multivariate level). Methionine under situations of oxidative stress readily reacts with ROS to produced MeS [333]. The production of MeS can prohibit the formation of glutathione via S-adenosylmethionine and thus exacerbate oxidative stress [333]. MeS can be returned to the methionine pool, however this will be dependent on the activities of MeS reductases [333]. Lipoic acid is synthesised in the mitochondria and plays an important role as a potent antioxidant, quenching several forms of ROS and activating the endogenous production of glutathione [334, 335]. It is also crucial in aerobic metabolism, acting as an important cofactor within several 2-ketoacid dehydrogenases including, pyruvate dehydrogenase, α-ketoglutarate dehydrogenase, branched-chain

ketoacid dehydrogenase and 2-oxoadipate dehydrogenase [334, 336]. Elevated lipoic acid therefore, may also suggest that these enzymes are elevated post-BSD, thus increasing TCA capacity and mitochondrial NADH/$FADH_2$ turnover. In a feed forward mechanism, elevated mitochondrial function consequently may increase ROS production [141]. As stated in the previous chapter (pg. 130), this may be overcome by increasing mitochondrial proton leak, thereby alleviating ROS from an elevated oxidation rate [253].

Compared to SHAM donors we have observed an elevated level of the AAs N-acetylglutamic acid, L-proline, glycine, L-serine and acetyl-glycine (Fig 5.8). N-acetylglutamic acid is an essential metabolite in the urea cycle, however the heart lacks the full enzymatic suite for urea production and synthesis of N-acetylglutamic acid [337]. Therefore, elevated acetylglutamic acid levels may be due to higher protein breakdown supported by higher 3-methylhistidine, a marker for actin breakdown which cannot be metabolised and is excreted in the urine. Elevated AA content essentially has two fates, anaplerotic input into the TCA cycle or protein synthesis. Both pathways may be equally plausible in the context of BSD.

A hypercatabolic state appears to be supported by our data, evident by elevations in 2-methylhistidine, CoA, ROS and reductions in L-tryptophan post-BSD. As tryptophan cannot be metabolised by the heart, its activity is considered a marker of protein synthesis [291]. Therefore, a reduction in L-tryptophan, in the presence of elevated AAs may mean greater AA metabolism than incorporation into proteins. However, L-tryptophan is usually tracked over time to gauge the degree of protein synthesis [291]. We did not observe any evidence of elevated metabolic intermediates from anaplerotic TCA input from AAs, therefore a more thorough investigation into the fate of these elevated AAs is needed to determine the catabolic or anabolic state of the BSD heart.

FA metabolism may also be altered post-BSD, evidenced by higher octanoic (C8:0) and octadecanedoic acids (C18:0). Increases in long chain FAs (LCFA) (C18:0) suggests a disturbance in FA metabolism or an increase in LCFA uptake into the cell. Increases in circulating free FAs has been observed in animal models of BSD and human studies profiling patients with brain injury [44, 45]. As the majority of FA uptake is FAT/CD36-mediated, increased FA uptake may be due to enhanced transcriptional

regulation of FAT/CD36. The most significant regulators of FAO are peroxisome proliferator-activated receptor alpha (PPARα) and PPAR gamma coactivator 1 alpha (PGC1α). PPARα and PGC1α enhance mitochondrial FAO, but also peroxisomal β-oxidation [338]. The peroxisome is capable of chain shortening LCFAs, to medium chain FAs (MCFA), possibly as a protective mechanism to reduce mitochondrial uncoupling [339].

This may be evident by elevations in the FA C8:0 which is an MCFA with the unique property of not requiring membrane transport proteins for mitochondrial entry and subsequent β-oxidation [340]. In effect, this reduces FA accumulation and subsequent toxicity. Liepinsh and colleagues found that activation of peroxisomal FAO is cardioprotective in reperfusion injury [341]. This essentially reduces FA toxicity by redirecting FA flux from the classical CTP1-dependant to peroxisomal and mitochondrial-mediated pathways via PGC1α-PPARα activation [341].

Conversely, FA metabolism may also be downregulated and thus lead to an accumulation of MCFAs. This may be due to increases in 2-methylcitric acid which is usually attributed to propionic or methylmalonic acidemias, but may also accumulate from the conjugation of propionyl-CoA and TCA intermediate oxaloacetate catalysed by citrate synthase [342]. Enhancing propionate metabolism in the rat heart has shown increased 2-methylcitric acid content as well as significant mitochondrial CoA trapping [343]. In the same study, the authors also showed that this higher propionate flux induced CPT1-dependent and independent inhibition of FAO [343]. This is possibly due to cytosolic increases in malonyl-CoA (an inhibitor of CPT1) and consumption of mitochondrial CoA. A more thorough investigation into FA and lipid metabolism is warranted to further elucidate FA utilisation post-BSD.

To summarise, these data suggest that BSD induces metabolic alterations that persist at least 24 hrs after confirmation of brain death. These include higher glucose utilisation, possible decreases in FA utilisation, higher protein breakdown and subsequent AA accumulation, increased propionate metabolism and elevations in the mitochondrial metabolites FMN and CoA (Fig 5.11). As a consequence, this may increase oxidative stress, particularly in the RV, and thus lead to greater uncoupling of mitochondrial respiration, and enhance metabolic pathways involved in reducing ROS such as the pentose phosphate and polyol pathways. What remains unclear, is whether these metabolic

changes are; i) due to medical management of BSD post-confirmation, i.e. inotropic support and ii) the catabolic or anabolic nature of these changes. Regardless, these preliminary results warrant further investigation to elucidate aberrant metabolic pathways leading to donor heart dysfunction.

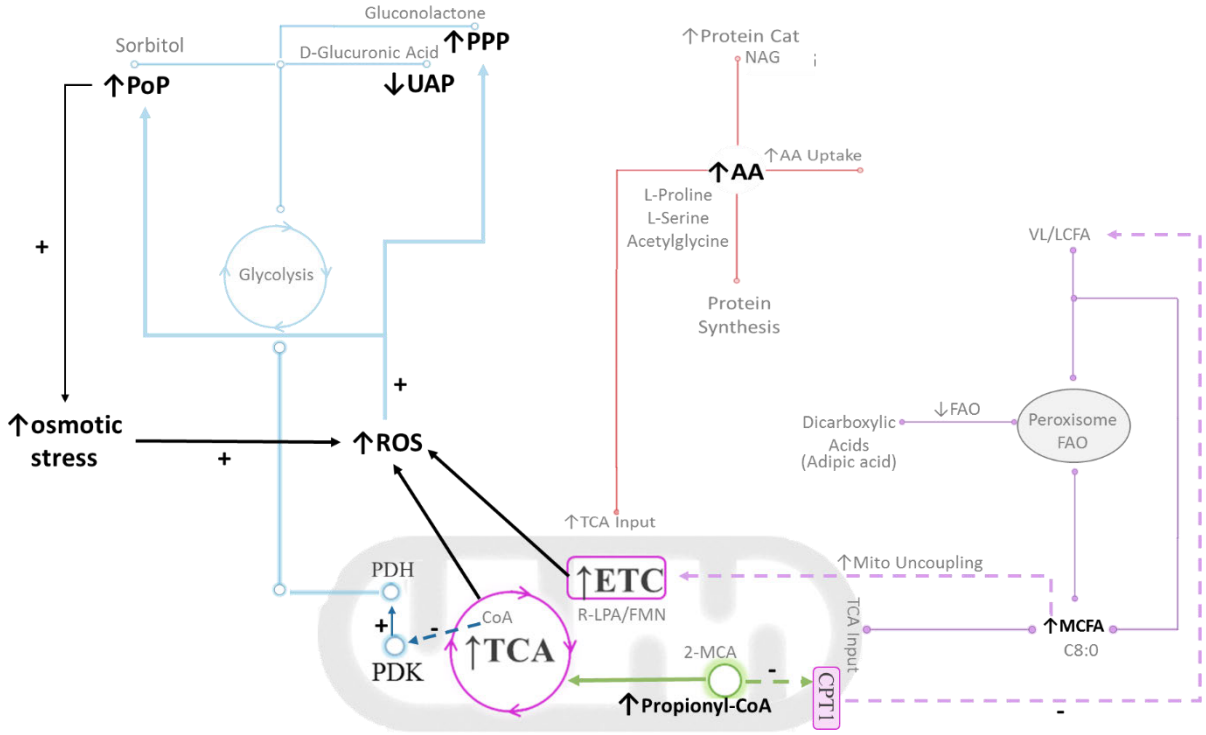

Figure 5.11. Summary of metabolomic profile of donor sheep hearts indicating the cardio-metabolic consequences of BSD. BSD was associated with an increase in metabolites involved in the PPP, PoP and AA metabolic pathways. This may increase anaplerotic input into the TCA thus increasing TCA activity and ETC activity. Increased MCFAs however may indicate deficiencies in mitochondrial FA transport thus activating peroxisome FAO increasing MCFAs which can diffuse into the mitochondria for subsequent β-oxidation. This FA transport inhibition may be the result of increased propionate metabolism potentially locking CPT1. PPP- pentose phosphate pathway, PoP- polyol pathway, UAP- uronic acid pathway, NAG- N-acetylglutamic acid, AA- amino acid, VLCFA- very long chain fatty acid, LCFA- long chian fatty acid, MCFA, medium chain fatty acid, TCA- tricarboxylic acid cycle, ROS- reactive oxygen species, PDH- pyruvate dehydrogenase, PDK- pyruvate dehydrogenase kinase, ETC- electron transport chain, 2-MCA- 2methylcitric acid, R-LPA- R-lipoic acid, FMN-flavin mononucleotide, FAO- fatty acid oxidation, FA- fatty acid.

5.3.2 | Metabolic Consequences of Transplantation

Firstly, the metabolic profile between BSD-Tx and SH-Tx were largely similar, implying transplantation alone provokes comparable metabolic alterations. The discrepancy in BSD-Tx-mediated metabolites may arise from the catabolism of i) proteins, ii) extracellular matrix components, iii) the cellular membrane and iv) pyrimidines. Alpha-aspartyl-lysine is a metabolite from the incomplete catabolism of proteins. Increased protein turnover may indicate elevated anaplerosis in order to maintain energetics post-CSS, via AA metabolism and TCA input. However, the donor heart (pre-HTx) also showed significant increases in protein turnover, as such, this may be a continued process carried forward from BSD injury.

Glycolic acid (GA) is considered a toxic renal metabolite, due mostly to its conversion to oxalic acid (OA), both of which are upregulated in the RV following BSD-Tx. Both GA and OA are end products of glyoxylate metabolism, derived most commonly from the breakdown of hydroxyproline [344]. Hydroxyproline is a major constituent of collagen and elastin fibres, the breakdown of which may contribute to the poor contractility observed both clinically and in this study (Chapter 3, pg. 77). Further, increases in glycerophosphocholine (GPC) suggest higher catabolism of phosphatidylcholine, the principle component of the cardiac sarcolemma [345]. Hatch and Choy showed that phosphatidylcholine biosynthesis can be reduced in episodes of hypoxia and reperfusion [346]. In effect, membrane degradation may lead to disturbances in electrophysiology, mitochondrial function and has been associated with reductions in β-AR density [347, 348].

Increases in GPC may also increase metabolic flux through the betaine pathway. Evidence supporting this comes from the increases in dimethylglycine and glycine. GPC can be broken down into choline and then betaine within the mitochondria [349]. Betaine may then be converted to dimethylglycine and subsequently sarcosine followed by glycine, a process that liberates $FADH_2$ for mitochondrial use [349]. Increasing glycine may also increase its input to the TCA to maintain energetics [349]. Another route glycine may take is the *de novo* synthesis of glutathione, which was elevated in the RV following BSD-Tx, compared to SH-Tx hearts [350]. Elevated glutathione may suggest a protective antioxidant mechanism of choline breakdown post-HTx, which is associated with the utilisation of BSD donor

hearts. Perhaps the heart is metabolically primed post-BSD, and therefore allows a unique physiological environment offering greater protection against CSS and reperfusion compared to SHAM donor hearts.

In BSD-Tx hearts, 3(β)-aminoisobutanoic acid (BAIBA) was elevated. BAIBA is the end-product of the catabolism of the pyrimidine thymine in the NADH consuming deamination reaction [351]. BAIBA has two fates within the cell, excretion or reduction to propionyl-CoA and subsequent formation of succinyl-CoA. Thus BAIBA may represent an alternate pathway to TCA input for ATP synthesis. BAIBA has also been implicated in the regulation of PCG1α-PPARα and AMPK pathways, decreasing insulin resistance and increasing FAO [351]. The exact fate of BAIBA cannot be determined, however in the presence of mitochondrial dysfunction, this may represent a terminal product of pyrimidine catabolism.

To specifically investigate metabolic carryover, we statistically interrogated the metabolic profile of the BSD heart compared to the transplanted BSD heart, and likewise for SHAM operated animals. Compared to their donor counterparts, transplanted hearts experienced significant decreases in metabolites involved in mitochondrial energetics. The upstream metabolic alterations differed between SHAM and BSD donor animals.

5.3.3 | Mitochondrial Energetics Post-Transplantation

The initial step in the TCA is the condensation reaction of oxaloacetate and acetyl-CoA to form citrate, releasing CoA [326]. As mentioned previously, CoA levels are elevated post-BSD compared to SHAM, however these levels are reduced post-HTx. When using SHAM donor hearts, acetyl-CoA levels are reduced post-HTx. Together, this suggests that when using SHAM donors, there is a decrease in TCA input from glycolysis, whereas using BSD donors, there is a reduction in TCA activity. In line with this hypothesis, we also observed reductions in succinic semialdehyde and precursor to succinic acid in both SH-Tx and BSD-Tx groups. Interestingly, for the BSD-Tx group, there was a significant reduction in 2-ketobutyric acid, an important metabolite involved in AA metabolism and subsequent input into the TCA cycle [352]. This would suggest a higher AA utilisation in BSD donor hearts but not in SHAM donor hearts. The previous univariate analysis between the two donor animals however revealed only

an accumulation of AAs and not their metabolites. This may be due to the higher TCA activity post-BSD, thus reducing TCA intermediates.

This post-HTx reduction in TCA activity in BSD-Tx hearts leads to a decrease in oxidised forms of NADH and $FADH_2$ implying mitochondrial dysfunction, further supported by reduced FMN content. However, the reduction in TCA input observed following SH-Tx resulted in reductions of both NAD+ and NADH. When considering the ratios of acetyl-CoA:CoA and NADH:NAD+, BSD-Tx is characterised by an increase in both, highlighting the mitochondria as an important regulator in BSD-Tx injury. These changes have been shown to inhibit PDH and enhance PDK, and thus may uncouple glycolysis and glucose oxidation [240, 289]. In SH-Tx, AcetylCoA:CoA ratios are increased with no change in $NADH:NAD^+$ (due to reductions in both), suggesting both upstream metabolic and mitochondrial dysfunction.

5.3.4 | Metabolism of Sugars Post-Transplantation

Prior to transplantation, BSD resulted in elevated levels of metabolites involved in parallel glucose pathways such as the PPP and polyol pathways. Following HTx, there was a reduction in the PPP intermediate gluconolactone as well as *myo*-inositol, *scyllo*-inositol, GLcNAc and β-N-acetylglucosamine (βGLcNAc) (Fig 5.12). However, D-glucuronic acid, ribitol and D-xylitol were elevated compared to pre-HTx. This suggests a depletion of the PPP pathway reducing the upstream metabolite gluconolactone with a build-up of the end-point pentitol metabolite ribitol from the non-oxidative PPP branch [353]. Increased D-glucuronic acid may act as an alternate route to producing D-xylulose-5, Phosphate (X5P), an intermediate of which is xylitol [328]. Production of X5P from glucuronic acid may then be metabolised via the PPP [354]. The pentitols ribitol and xylitol may also be oxidised via sorbitol dehydrogenase to produce oxidised pentoses D-ribulose and D-Xylulose, which after phosphorylation can be metabolised via the PPP [355].

Reductions in myocardial inositol levels may be due to decreased biosynthesis from glucose, or higher incorporation into the phosphoinositide cycle. In IRI, an immediate response is increased phosphoinositide 3-kinase (PI3K) pathway activation [356]. Activation of the PI3K pathway confers cell survival by reducing apoptosis via enhanced Akt/Protein Kinase B activity [357]. PI3K activation

is also associated with regulation of myocardial hypertrophy, contractility, electrophysiology and promotion of glucose uptake [358, 359]. Therefore, enhanced PI3K activity following BSD-Tx may reduce inositol levels and provide cardioprotection over SH-Tx, which showed no changes in post-HTx inositol levels. Importantly, univariate donor (pre-HTx) comparisons also showed no changes in myocardial inositol. This may be due to the higher β-AR stimulation of BSD injury and inotropic management, known to stimulate PI3K and thus reduce inositol levels [360], equivalent to SHAM levels.

Lastly, BSD-Tx was associated with reductions in GLcNAc and βGLcNAc. These amino sugar metabolites are especially important in O-linked-β-linked-N-acetylglucosamine (O-GlcNAc) post-translational protein modifications [361]. Reducing O-GLcNAc levels has been shown to sensitise the cell to oxidative stress and in models of IRI, increasing O-GLcNAc is cardioprotective [362]. No changes in GLcNAc levels were observed following SH-Tx (compared to SHAM donors), which may suggest donor BSD may influence O-GLcNAc, possibly as a consequence of glucose oversupply and spill-over described earlier. Indeed, this was observed in multivariate ANOVA with BSD hearts containing the highest level of UDP-GLcNAc compared to all other groups. UDP-GLcNAc is the precursor substrate donor used in glycosylation of protein serine and threonine residues [361]. This may suggest higher glucose flux through the hexosamine pathway post-BSD, thus increasing protein glycosylation which may or may not confer an advantage over SHAM donor hearts for CSS and reperfusion.

In further support of higher glucose availability from BSD donors, SH-Tx was associated with a reduction in G6P levels compared to pre-HTx. As previously stated, this may be associated with reduced TCA input as a consequence of upstream glycolysis deficiencies. SH-Tx hearts instead, showed elevated levels of sorbitol and D-fructose, metabolites of the pentose phosphate pathway. These metabolites, particularly sorbitol, are important osmoregulators and may promote hyperosmotic and oxidative stress following SH-Tx [327]. SH-Tx hearts were also associated with reductions in reduced glutathione, supporting higher oxidative stress. This may partly contribute to the worsened post-HTx function of SH-Tx compared to BSD-Tx (Chapter 2).

Interestingly, the HR group showed the highest level of sorbitol and MeS compared to all other groups. The HR group hearts were procured following establishment of CPB and therefore, may represent CPB-mediated metabolic alterations relevant to osmotic and oxidative stress [363, 364]. Myocardial ischaemia is inevitable peri-operatively, resulting in elevated oxidative stress which may enhance the PoP, thus contributing to the osmotic stress commonly observed. Strategies to reduce osmotic stress associated with CPB are usually focused on fluid management and increasing osmolarity of cardioplegic solutions [365, 366].

Collectively, it appears that BSD-Tx hearts contain higher levels of glucose metabolites divergent from glycolysis. This may be due to the uncoupling of glucose to glucose oxidation due to reductions in TCA activity and mitochondrial respiration. In effect, this may enhance the PI3K signalling pathway and GLcNAc post-translational modifications, possibly affording cardioprotection in the face of energetic compromise. These data highlight the mitochondria as a potentially important therapeutic target. SH-Tx however, is associated with reduced glycolysis and TCA input, and enhanced pentose phosphate pathway metabolism which may potentially lead to higher osmotic and oxidative stress. Further analysis specifically investigating the proteome is warranted in order to determine the fate of glycolytic intermediates and their cellular consequences post-HTx.

5.3.5 | Fatty Acid Metabolism Post-Transplantation

Regardless of the type of donor heart used, the changes in FA metabolism were similar post-HTx. These changes included decreases in the MCFAs C6:0 and C11:0 in BSD-Tx hearts and C8:0, C9:0 and C10:0 in SH-Tx hearts with increases in the dicarboxylic acids adipic acid, 3-methyladipic (multivariate) and pimelic acid (Fig 5.12). Additionally, SH-Tx hearts accumulated significant levels of the very long chain FA (VLCFA) behenic acid (C22:0). FA build-up as mentioned previously can lead to cardiotoxicity. To reduce this effect, production of dicarboxylic acids via omega-FAO (ω-FAO) in the endoplasmic reticulum is enhanced [341].

Thus the peroxisome may chain shorten VL/LCFAs to MCFAs via α-oxidation, and further chain shorten accumulated MCFAs to dicarboxylic acids via endoplasmic ω-FAO and peroxisome β-oxidation [338, 339]. Alternatively, reduced MCFAs may suggest a greater diffusion into the

mitochondria for β-oxidation independent of CPT1. However, in the presence of reduced TCA activity and mitochondrial dysfunction, this may not be likely. Peroxisomal FAO is regulated by PPARα/γ activity, which has been shown to have cardioprotective effects in the setting of IRI [341]. To clarify this, further studies will need to be conducted, focusing on lipid metabolism and the signalling involved in the context of transplantation. Reducing the peroxisomal formation of dicarboxylic acids and enhancing MCFA production may prove beneficial post-HTx. This must be coupled with improving mitochondrial utilisation of FAs, if indeed there is dysfunction at that level. A more thorough investigation into lipid signalling and FAO is warranted to completely understand the potential roles of altered FA metabolites.

5.3.6 | Amino Acid Metabolism Post-Transplantation

BSD-Tx was associated with reductions in several amino-acids compared to BSD. Glycyl-L-leucine (protein catabolism), L-serine and N-acetylglutamic acid (protein catabolism) are all reduced post-HTx (Fig 5.12). These amino-acids are referred to as glucogenic as they provide carbohydrate intermediates [291]. A post-HTx reduction in these amino-acids, in the presence of reduced 2-ketobutyric acid may indicate a decrease in amino-acid metabolism. Further, reductions in L-carnitine and L-acetylcarnitine were also observed in BSD-Tx hearts. Carnitine acts a cofactor in CPT1 activity and therefore, the reductions in carnitine may decrease mitochondrial FA transfer [227]. This may relate to the cytosolic increases in FAs, which are ultimately metabolised via the peroxisome in order to reduce FA-mediated uncoupling of mitochondria and toxicity. Reduced carnitine however, may also represent a greater incorporation into FA intermediates and therefore greater utilisation of FAs in BSD-Tx hearts.

There were no significant changes in post-HTx AA metabolism in the SHAM vs SH-Tx analysis aside from higher protein turnover markers in SHAM donor hearts. Due to this absence of AA changes and the significant upregulation in BSD and subsequent depletion post-HTx, it may be plausible that BSD is associated with higher AA flux which provides alternative fuel sources during CSS and HTx.

5.3.7 | Pyrimidine & Purine Breakdown Post-Transplantation

On a multivariate level, BAIBA was elevated in both BSD and BSD-Tx, but reduced in SH-Tx (Fig 5.12). This may support enhanced FAO as a consequence of BSD and an alternate source of TCA intermediates. This is then carried forward into CSS and reperfusion, potentially provoking cardioprotection. Increased xanthine, a product of purine breakdown was observed only in BSD-Tx hearts, promoting energetic compromise and higher oxidative stress [367, 368] (Fig 5.12). The degradation of ATP during ischaemia to xanthine has long been indicated in the generation of IRI via increased ROS production [367, 369]. Blocking the enzymatic conversion of hypoxyxanthine to xanthine using allopurinol has shown cardioprotection in settings of IRI and heart failure [370]. However, allopurinol use in heart transplantation is often complicated due to severe pharmacological interactions [371]. The use of allopurinol however, is often chronic and for the treatment of gout [371]. Short-term post-reperfusion allopurinol administration may prove beneficial in reducing ATP breakdown in the acute stages post-HTx.

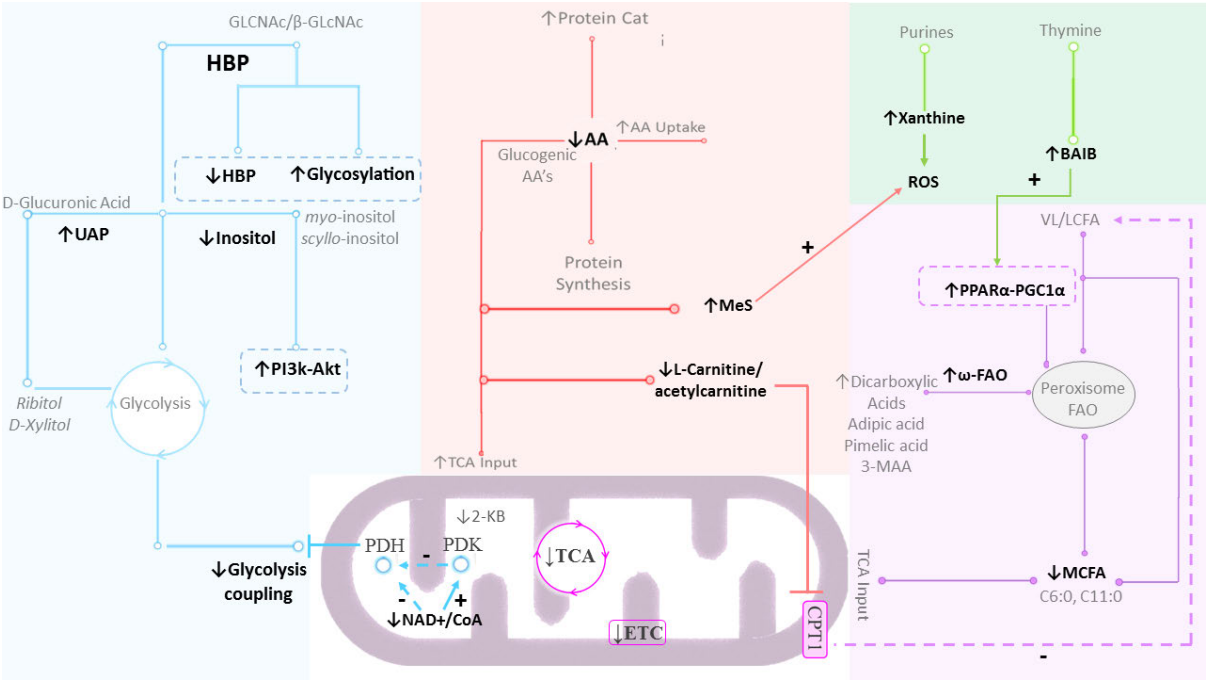

Figure 5.12. Summary of metabolomic profile of transplanted hearts indicating the cardio-metabolic consequences of transplantation from BSD donors. Transplantation is associated with reductions in metabolites involved in mitochondrial energetics which may block the coupling of glycolysis to glucose oxidation. An accumulation of glycolytic intermediates increases the production of d-glucuronic acid with a possible increase in protein glycosylation and PI3K signalling. Reductions in AA metabolism may decrease TCA anaplerosis, increase ROS and affect FAO via CPT1 inhibition. This may lead to enhanced ω-FAO leading to the accumulation of dicarboxylic acids. Further, increases in purine and pyrimidine metabolism may promote ROS and activate PPAR/PGC1α signalling. Dashed boxes indicate areas of further research. PPP- pentose phosphate pathway, PoP- polyol pathway, UAP- uronic acid pathway, NAG- N-acetylglutamic acid, AA- amino acid, VLCFA- very long chain fatty acid, LCFA- long chian fatty acid, MCFA, medium chain fatty acid, TCA- tricarboxylic acid cycle, ROS- reactive oxygen species, PDH- pyruvate dehydrogenase, PDK- pyruvate dehydrogenase kinase, ETC- electron transport chain, 2-MCA- 2methylcitric acid, R-LPA- Rlipoic acid, FMN-flavin mononucleotide, FAO- fatty acid oxidation, FA- fatty acid.

5.3.8 | Clinical Significance

For the BSD donor, the most significant metabolic changes are increased oxidative stress and glycolytic spillover. Therefore strategies that reduce oxidative stress or improve glycolysis and coupling to glucose oxidation may be advantageous to reduce the negative consequences of glucose spill over including osmotic and oxidative stress. In particular, reducing flux through the polyol pathway and formation of sorbitol can potentially reduce osmotic stress. This is highly relevant for CSS of the donor heart [372]. Reducing sorbitol concentration may in turn decrease cell oedema whilst the donor heart is in transit between donor and recipient. This can be achieved either by blocking aldose reductase or enhancing glycolysis [300, 372]. Inhibiting aldose reductase has been shown to reduce mitochondrial dysfunction, oxidative stress and improve contractile function in diabetic rat heart [287, 332]. However, a potential consequence of AR inhibition is enhanced protein glycation and formation of advanced glycation end products, which are associated with progression of diabetic cardiac dysfunction [287].

An alternative route to reduce sorbitol formation is to enhance glycolysis and coupling to glucose oxidation. Since ARase has a high affinity for glucose, and is therefore a poor substrate, funnelling glucose away from the polyol pathway reduces the bioavailability of glucose thereby alleviating sorbitol formation [373]. This can be achieved by inhibiting the PDK enzyme, thus increasing PDH activity. Dichloroacetate (DCA) is a classical PDK inhibitor with known clinical benefits on increasing glucose oxidation [290]. However, the use of DCA is precluded due to side effects and more significantly poor pharmacokinetics, requiring large frequent doses to achieve a clinical response [290]. New, more specific PDK inhibitors such as PS10 have shown improved increases in glucose oxidation over DCA [374].

In regard to post-HTx, the most significant metabolic alterations were reductions in mitochondrial energetics. This suggests that the most significant impact on cardiac function in the transplanted heart is at the level of the mitochondria. Several lines of evidence support this; i) reduced CoA levels, implying reduced TCA activity, ii) reduced NAD+ and FAD, implying poor NADH and $FADH_2$ turnover and iii) reduced FMN content, an important component in CI electron transport. Whether this mitochondrial dysfunction arises from CSS, as a consequence of transplantation itself or as a

combination of both should be clarified. Enhancing mitochondrial function, or increasing glycolytic coupling may improve cardiac dysfunction post-HTx and reduce glucose spill-over into pathways that may prove deleterious to cardiac performance.

Upstream changes in glucose and FA handling may also be relevant in post-HTx cardiac dysfunction. Particularly, the changes to glucose, sugar and FA metabolism in the transplanted heart are relevant to important cardioprotective pathways such as the PI3K-Akt/PKB, PPARα/γ and O-GLcNAc pathways [341, 362, 375]. Multi-Omic approaches should be employed to assess relevant signalling cascades implicated here.

5.3.9 | Limitations

Using this metabolomics approach we have essentially captured a 'snap shot' of metabolism. For the donor groups, this endpoint was clearly defined and consistent at 24 hrs post-BSD or SHAM. However, for the transplant groups, post-HTx monitoring times differed, with 25% of the HTx groups lasting only 2 hrs post-HTx. Although the differences in monitoring times between BSD-Tx and SH-Tx were statistically similar, time post-CPB may i) affect the metabolic profile and ii) add significant variation in the SH-Tx group, obscuring potentially relevant metabolic changes.

Additionally, this snapshot approach cannot definitively determine metabolic flux due to its dynamic nature. To do this radio- or isotopically labelled metabolites can be administered followed by mass spectrometry or magnetic resonance imaging. This would provide greater insight into the changes in metabolic pathways, and the fate of upstream metabolites as a consequence of transplantation.

Additionally, the heart contains a complex mixture of cell types, including 5 populations of ventricular cardiomyocyte distributed throughout the septum and ventricular walls [376]. These populations differ in nuclear enrichment of mitochondrial and metabolic genes and therefore vary in their workload efficiencies [376]. Indeed, Stöhr *et al*, found that regional kinetic energy differed between the base and the apex in working human hearts [377]. Consequently, by pooling regional samples, we may have obscured potentially relevant changes in regional ventricular metabolism and contributed to ventricular heterogeneity. To acquire a valid, high resolution signal from LC-MS/MS techniques, it was a

requirement to pool the biopsies to ensure a sufficient amount of tissue was present. Additionally, the biopsies reflected synonymous areas as those used for mitochondrial assessment and therefore made any conclusions more reliable as the tissue type and resultant pooling was similar. Regardless, future studies should specifically investigate the regional differences in both mitochondrial function and metabolism following BSD and HTx.

5.4 | Conclusion

Metabolism in the BSD and transplanted heart is rarely studied in the context of identifying pathophysiology. Rather, circulating metabolites are assessed for their applicability as biomarkers for diagnosis of graft dysfunction and/or acute rejection. This study aimed to utilise a metabolomic approach to investigate the metabolic profile of BSD and transplanted hearts. In summary, these data have shown significant alterations in cardio-metabolic function as a consequence of BSD and subsequent transplantation. BSD hearts are characterised by elevated TCA, anaplerotic input from AAs, and NADH turnover which in turn increases oxidative stress. BSD may also impact FAO in a CPT1-dependent manner. This may be overcome by increases in peroxisome FAO and utilisation of MCFAs.

Transplantation on the other hand, is characterised by significant metabolic impairment at the level of the mitochondria. This may result in increased glycolysis and glucose oxidation coupling, AA metabolism and FAO. Peroxisome and ω-FAO is enhanced thus, increasing the formation of "non-metabolisable" dicarboxylic acids. BSD-Tx was also characterised by enhanced purine and pyrimidine catabolism. These changes may activate signalling pathways including the PI3K, PCG1α-PPARα and glycosylation pathways. Collectively, these changes may contribute to the acute energy crisis and contractile dysfunction often observed post-HTx. Overall, these data highlight important aberrant metabolic functional changes which may be targetable. Improving the metabolic profile of the transplanted heart may improve cardiac function and thus patient outcomes. Further research is necessary to completely elucidate the fates of these alterations and realisation of therapeutic targets.

Chapter 6

General Discussion & Conclusions

Contents

6.0 | Introduction

End-stage heart failure is an increasing global problem, with HTx as an effective terminal treatment, alongside mechanical assist devices. Two significant limitations to 30-day mortality in the context of HTx are the poor supply of suitable donor hearts, and cardiac dysfunction post-procedure [8, 378]. Poor donor heart supply may originate from the deleterious consequences of donor BSD. As confirmed BSD is a requirement for organ donation, utilising this donor pool imposes a constraint on available donor hearts. BSD may also contribute to cardiac dysfunction often observed post-HTx. In this chapter, we will follow the clinical journey the donor heart travels, from donor BSD injury through to transplantation. During this discussion, data generated herein will be synthesised and used to help identify pathological mechanisms relevant to both the pre-transplant and post-transplanted hearts.

6.1 | Cardiovascular Consequences of donor BSD

HTx begins with the admission of a patient to the ICU or emergency department with severe brain injury. If non-amenable to treatment, BSD is usually queried and if confirmed, initiates the process of organ donation and retrieval. Over the last 5 years, time from admission to BSD confirmation in Australian centres was 41.5 hrs, and time from BSD to organ donation was 21.8 hrs, a total of 63.3 hrs [7]. In Chapter 2 we described a model of BSD that closely replicated this clinical scenario, particularly the time from BSD to organ donation. Replicating admission to BSD times is a logistical hurdle that could not be incorporated into the study design. However, increasing time from the initial brain (and cardiac) injury may have profound effects on the human donor heart. Specifically, longer times between brain death and heart retrieval may allow myocardial recovery from the initial BSD-mediated dysfunction. Jawitz et al, investigated 22, 960 donor-recipient pairs and found that retrievals extended to >42 hours from BSD were not associated with worse survival (HR 1.01, 95% CI 0.94-1.08) [379]. This finding was replicated in further studies suggesting a 1.5-2 day waiting period before heart retrieval is considered to allow for myocardial recovery [380, 381]. Despite this shortfall, the majority of other models replicating BSD and HTx only employ a 6 hr BSD duration and often no subsequent heterotropic

HTx, therefore accounting for only around 9% of the donor journey [39]. Our study encompasses a greater proportion of the average donor journey (~40% [24/63.3]) and is therefore comparatively more clinically relevant.

BSD initiation produced significant elevations in catecholamines, cTnI, haemodynamics and arrhythmias coinciding with the hyperdynamic phase of BSD also observed in both animal and human studies of BSD [40, 102, 103, 382]. This hyperactive phase was followed by the well documented hypodynamic phase associated with hypotension and poor contractility requiring high inotropic support. This is a common manifestation of BSD-mediated cardiac injury observed in clinical situations [159]. This hypodynamic phase is clinically important as this is the period in which the heart is assessed for medical suitability [378].

Consequently, more than 60% of these hearts are deemed unsuitable, half of which are on functional grounds [22]. It is this electrophysiological and contractile dysfunction that has driven decades of research into better understanding the mechanisms behind donor cardiac dysfunction. This thesis addressed several of these hypotheses and in most circumstances, represents the first empirical evidence directly assessing them in a clinically relevant model. Table 6.1 outlines the major BSD-mediated changes observed in this study, their possible causes and therapeutic potential.

BSD-mediated cardiac dysfunction is often likened to Tako-Tsubo cardiomyopathy, a catecholamine-induced contractile dysfunction [36]. This is due to the similarities in catecholamine profiles, regional hypokinesis, bi-ventricular contractile dysfunction and the reversibility in dysfunction. As such, contractility measured via echocardiography is a common feature in donor heart assessment. In particular, the LV ejection fraction (LVEF) is traditionally considered the most important surrogate variable, as LVEF can predict satisfactory post-HTx cardiac function [383]. However, recent data has shown equal 1-year survival post-HTx from donor hearts with LVEF<45% [384]. In our *in vitro* contractility experiments we did not observe reductions in LV force production, but rather reduced basal and maximum (-)-noradrenaline induced contractility in isolated right ventricular trabeculae.

A significant consideration in *in vitro* testing is the force measured from isolated trabeculae represents an idealised measure of contractility, as the measured contractile force is independent of loading conditions. Assessing cardiac contractility in this manner may explain why we observed no changes in LV force production post-BSD. Lower pre-load as a consequence of diabetes insipidus and reduced afterload due to loss of neurovascular tone both reduce contractility via the Frank-Starling and Anrep effects, respectively [13, 85]. Szabo showed that if loading conditions were kept constant, BSD-mediated cardiac dysfunction could be ameliorated [85]. Moreover, *ex vivo* donor heart testing has shown no obvious reductions in function compared to non-BSD hearts [221]. Left ventricular function post-BSD may then be determined by the degree of myocardial injury and recovery, and also the level of vasoactive treatment.

Table 6.1 Overview on significant findings following donor BSD compared to SHAM

	Parameter	Effect Compared to SHAM	Possible Causes	Therapeutic Potential
In vitro Muscle Mechanics	β_1-AR (-)-noradrenaline Sensitivity	↔	N/A	Alternative inotropic agents Enhance Ca^{2+} handling
	Contractility	↓	Poor Ca^{2+} handling catecholamine toxicity inotropic support	
	Diastolic Function	↑		
	Vascular Tone	↓		
Mitochondrial Respiration	LEAK	↑	↑ ROS production *Physiological uncoupling*	Decrease mitochondrial and cytosolic ROS production
	Complex I	↔		
	Complex II	↔		
	ROS	↑ (↓GSH:GSSG, ↑3-NT)		
Metabolism	CHO	↑ PPP and PoP	Hyperglycaemia Mitochondrial dysfunction ROS	Enhance glycolytic coupling ↓ propionate metabolism (2-MCA build-up) Inhibit PoP
	FAO	↓ FA transport	↑ propionate metabolism	
	AA	↑ AA utilisation	↑ adrenergic stimulation	
	ROS	↑ (R-lipoic acid, MeS)		

β_1-AR- beta 1 adrenoceptor, N/A – not applicable, Ca^{2+} - calcium, GSH:GSSG – reduced to oxidised glutathione ratio, ROS- reactive oxygen species, 3-NT- 3-nitrotyrosine modified proteins, PPP- pentose phosphate pathway, PoP- Polyol Pathway, FA- fatty acid, CHO- carbohydrate, FAO- fatty acid oxidation, AA- amino acid, MeS- methionine sulphate, 2-MCA- 2-methylcitric acid

However for the RV, reduced *in vitro* contractility suggests dysfunction at the level of the myocyte. Post-HTx RV function is particularly compromised, which may be due to mechanisms initiated by BSD. It is generally well accepted that BSD causes a reduction in β-AR sensitivity due to the large catecholamine release [8]. Data in support of this has shown increased β-ARR and GRK2 levels in 6 hr models of BSD [49, 60]. In this study, we did not see any functional desensitisation to noradrenaline 24 hrs post-BSD. Together, these data may suggest that the acute (within 6 hrs post-BSD) response to BSD is phosphorylation of β-ARs, inducing functional desensitisation. Whilst longer, more clinically relevant post-BSD time frames suggests a return to baseline sensitivity. This is especially important in regard to inotropic support.

Recently, high donor inotropic support has shown suitable post-HTx outcomes even in the presence of histological injury [215]. These data support the use of 'marginal' donor hearts, those hearts that don't meet traditional acceptance guidelines, in order to meet growing demand. Our data also support this notion, at least from a receptor sensitivity perspective. However, efficacy of noradrenaline at the β_1-AR is reduced, particularly for the RV. Therefore, use of β-AR agonists should be approached with caution. A significant factor that may affect β-AR-mediated contractility is Ca^{2+} handling.

We did not directly assess Ca^{2+} handling in this study, but did observe Ca^{2+}-associated changes. Specifically, the RV in BSD hearts more frequently showed increases in diastolic force *in vitro*. Poor cardiomyocyte relaxation may suggest Ca^{2+} overload, which in turn may be due to the use of sympathomimetic inotropic support. It may be prudent then, in a BSD donor to utilise non-sympathomimetic forms of inotropic support to enhance cardiac contractility and protect the heart from the negative effects of β-AR stimulation. There are a number of alternate inotropic agents that may be utilised to support contractility that may be advantageous in the setting of BSD [385, 386]. Table 6.2 summarises the advantages and disadvantages of each group of alternative agents. Supporting the donor heart for transplantation however has important ethical considerations, expanded on in section 6.1.2.

Table 6.2 Advantages and disadvantages of alternative non-sympathomimetic inotropic agents which may be useful in the context of HTx

Drug Class	Example	Advantage	Disadvantage
PDE-Inhibitors	Milrinone	Reduce catecholamine requirement	Potentiates arrhythmias
Ca^{2+} Sensitisers	Levosimendan	Reduce catecholamine requirement	Potentiates arrhythmias Diastolic dysfunction Energetic compromise
Myosin activator	Omecamtiv Mecarbil	↑ inotropy without Ca^{2+} changes ↑ cardiac efficiency	Diastolic dysfunction Potentially ↑ O_2 consumption
NHO Donors	Angeli's salt	Independent of β-AR signalling Enhances Ca^{2+} handling	Additive to oxidative stress
Ca^{2+} handling therapeutics	EF-hand Ca^{2+} binding motifs	Improves diastolic function Independent of β-AR signalling	Unknown

HNO- nitroxyl, Ca^{2+} - calcium, β-AR – beta-adrenoceptor

Another important factor in contractile function is efficient mitochondrial activity. We have observed significant RV mitochondrial uncoupling, albeit with preserved CI and CII respiratory capacities and membrane potential. This increase in uncoupling may be due to higher levels of ROS production, evidenced by increased 3-NT, MeS and a reduced GSH:GSSG ratio. Elevated ROS has been shown to induce higher proton leak, which in turn accelerates OXPHOS and proton leak through enhanced ANT levels [248, 250]. These actions function in a positive feedback loop to ultimately reduce ROS formation in a mechanism referred to as "uncoupling to survive" [253]. In turn this uncoupling may drive reductions in ATP production in a stimulated heart in order to reduce oxidative stress, at the expense of contractility.

Increased ROS production may also directly reduce cardiac contractility. NADH oxidases 1/4 (NOX1/4), catecholamine auto-oxidation and deamination, and mitochondrial respiration are all

important sources of cardiac ROS [264, 265]. This elevated ROS has been shown to activate ryanodine receptors and increase protein phosphatases, thereby reducing phospholamban activity and consequently SERCA activity [387]. ROS may act in a 'U-type' fashion, where low ROS is cardioprotective and high ROS is apoptotic [388, 389]. This may be dependent on the type of ROS produced, the subcellular localisation and the duration and strength of the ROS signal.

Further, we have shown using hiPSC-CMs that intense β-AR stimulation may increase the translocation of GRK2 to the mitochondria. This highlights an alternate pathway of elevated GRK2 observed in BSD studies [49]. Moreover, this translocation is ROS-dependent, activating the MAP-ERK pathway [61]. Our group has previously shown that ET-1 is elevated post-BSD [159]. ET-1 may also activate the MAP-ERK pathway thus potentially contribute to increased mitochondrial GRK2 [387]. The effect of mitochondrial GRK2 in cardiomyocytes is reductions in FA utilisation and increasing superoxide production [238].

In high resolution respirometry we did not observe conclusive evidence of FA utilisation at CI. CII-mediated oxygen consumption however was reduced, which may suggest a reduction in mitochondrial transport of FA's and as such, in our assay, mediate a substrate inhibition of CII. In support of a CPT1-mediated inhibition of FA transport, we have shown an increase in 2-MCA levels. 2-MCA is a by-product of propionate metabolism and has been shown to inhibit FA transport via production of malonyl-CoA. We did not observe any increases in malonyl-CoA, however this may due to the short 1.25 minute half-life [301].

Other metabolic changes post-BSD include possible increases in AA utilisation, evidence of higher TCA and ETC, activity and enhancement of neighbouring pathways of glycolysis. Enhanced AA metabolism supports the anaplerotic input of TCA intermediates to support the potential increase in TCA activity. Higher TCA activity is evidenced by increases in free CoA, R-lipoic acid and supported by the similarities in mitochondrial respiratory activity between BSD and SHAM. Physiological uncoupling, as mentioned, may functionally reduce the rate of OXPHOS in order to reduce oxidative stress.

This uncoupling-mediated 'break' on mitochondrial respiration in turn, may reduce the rate of mitochondrial glucose utilisation. In effect, this imposes a functional backflow through glycolysis and therefore, in conjunction with hyperglycaemia, increases flux through the PPP and PoP pathways. Both pathways are also upregulated by ROS in order to reduce further ROS formation [327, 354]. The PPP pathway is an important regulator of cytosolic NADH which acts to maintain the glutathione pool in a reduced state [328]. Therefore, its upregulation may have an anti-oxidative response. Upregulation of the PoP is recognised as an important pathological mechanism in diabetes, particularly retinopathy, kidney dysfunction and nephropathy [327, 331]. This can be attributed to the accumulation of sorbitol, as sorbitol induces significant osmotic stress. In the setting of transplantation this is particularly important for the next stage of transplantation, CSS.

In summary, in a clinically relevant model of donor BSD, we have shown significant cardiovascular alterations over several levels of cellular function. Specifically, we have shown that the RV of BSD donor hearts is mechanically compromised. This contractile dysfunction is not as a consequence of reductions in β-AR sensitivity. However the changes in contractility may be as a result of uncoupled mitochondrial respiration, due mostly to increases in oxidative stress. This elevated oxidative stress may arise from sympathomimetic inotropic support which in turn affects intracellular Ca^{2+} handling. Ultimately, this leads to altered glucose and fatty acid utilisation with a potential greater reliance on AA utilisation. Therapeutic potential exists for lowering ROS production and enhancing metabolic flux through glycolysis, possibly by targeting the mitochondria and alternate inotropic agents.

6.1.1 | Ethical Considerations

Employing medical management strategies to preserve donor heart function raises some important ethical questions. Any medical treatment of the potential organ donor falls into 2 categories, medically beneficial and non-beneficial. This depends on the degree of injury severity, where some patients may sustain considerable injury that any treatment is deemed non-beneficial.

Therefore, an important question to ask is, should treatment be administered with the intention of preserving the potential to donate?

Generally, guidelines recommend that donor organ optimisation should be employed where the patient's wishes to donate are clear [390]. Any decision on treatments should be made with full transparency with the treatment team, transplant team and the family [390, 391]. If the patient's wishes are not known, guidelines recommend stabilising treatments until the patient's wishes are determined [392]. Some however argue that treating in the absence of the patient's wishes are not in the best interest of the patient, and is therefore an unethical practice [392]. Employing the strategies outlined here may fall into an ethical grey zone. To overcome these potential issues, therapeutic strategies to enhance donor heart function may then be directed to post-explanation during organ storage and transport.

6.2 | Cold Static Storage

Organ preservation and transport is one of the most important periods in the journey the donor heart must travel. In this study, no assessment of cardiovascular function was undertaken during CSS, which represents a limitation in the understanding of peri-transplant cardiac dysfunction. The logistical issues with sampling during preservation added to an already logistically demanding project and therefore was not performed. Further, this project represents a subsection of a larger project employing a new strategy of organ preservation. This arm will include the utilisation of hypothermic machine perfusion system to provide the donor heart with sufficient oxygen and nutrients during heart preservation. The advent of machine perfusion systems comes from decades of research, identifying the ischaemic response to CSS as a considerable factor to poor post-HTx cardiac function.

This ischaemic response is also associated with energetic compromise and potentially mitochondrial uncoupling. This study indicates that higher oxidative stress, BSD-mediated mitochondrial uncoupling and higher levels of sorbitol are possibly transferred from the donor to organ preservation. CSS may then exacerbate oxidative stress and mitochondrial dysfunction due

to ischaemic damage. Higher sorbitol levels in the donor heart may also contribute to osmotic stress. This is dependent on the preservation solution used, with some solutions containing compounds (mannitol) which increase the osmolarity of the solution [107]. Reducing this pre-CSS donor profile, or specifically targeting BSD-mediated changes in the PPP and oxidative states may prove advantageous for post-HTx function.

6.3 | Cardiovascular Consequences of Transplantation

The final destination for the donor heart is transplantation, which consequently also represents a significant injury to the donor heart. In this study we have shown significant post-HTx cardiac dysfunction. This includes, arrhythmias, prolonged QTc, depressed MAP (<70 mmHg) and elevated cTnI. Interestingly, transplants utilising non-BSD hearts were associated with worse post-HTx function leading to early termination, <3 hrs post-CPB. These effects may be initiated by a lack of preconditioning and poor contractile, adrenergic, mitochondrial and metabolic function (Table 6.3).

In vitro contractility testing showed reduced RV contractility and a trend toward reduced LV contractility post-transplantation. RV dysfunction is a common clinical complication post-HTx and a significant contributor to 30-day mortality [221]. Donor BSD, ischaemic time, CPB and IRI are considered etiological factors predisposing the transplanted heart to RV failure [221]. Data presented in this thesis further support these mechanisms, with a particular focus on mitochondrial, metabolic and adrenergic involvement.

6.3.1 | Contribution of Donor BSD

BSD-mediated cardiac dysfunction frequently appears in predictive models of graft dysfunction. Recently, Barac *et al.*, reported similar post-HTx survival between a large cohort of traumatic brain injury (TBI) and non-TBI donors [393]. There are several major limitations with this study; TBI donor hearts presenting with significant LV dysfunction were not included, no data on time from injury to donation were assessed, and donors from haemorrhagic stroke were not analysed. The latter cohort of donors represents about half of all donor hearts in Australia [7].

The specific mechanisms that contribute to graft dysfunction, originating from BSD, are mostly unknown. RV dysfunction, for example, appears to originate in the BSD donor at the level of the myocyte. In particular, mitochondrial uncoupling due to an enhanced oxidative state may compromise the myocardium and decrease ischaemic tolerability. Ultimately, this leads to post-HTx ROS production and a bi-ventricular increase in mitochondrial uncoupling. Unexpectedly, BSD hearts may contain higher substrate availability over non-BSD hearts. In effect, this may actually confer a metabolic advantage over SHAM hearts and may be a mechanism by which BSD hearts performed better than SHAM. Therefore optimising substrate utilisation, by enhancing mitochondrial function may be advantageous.

Paradoxically, the 'catecholamine storm' may also provide a level of ischaemic preconditioning, accounting for the worse post-HTx outcomes observed with SHAM donor hearts. Adrenergic preconditioning, specifically β_1/β_2 agonism is hypothesised to augment PKC, PKA, p38-MAPK signalling and activate the reperfusion injury salvage kinase (RISK) pathway [167, 394]. Collectively, these responses are believed to be cardioprotective, improving functional recovery and reducing apoptotic injury from ischaemia [167, 394]. The early evidence of reduced donor cardiac dysfunction with sympatholytic strategies suffered from the limitations of short BSD duration and no subsequent transplantation [222]. Allowing the donor heart to recover from the catecholamine excess may also allow a level of preconditioning. It would be advantageous to specifically address adrenergic preconditioning and transplant outcomes, especially when considering the recent evidence showing high inotropic donor support is not associated with worse transplant outcomes [215].

6.3.2 | Contribution of Ischaemia & IRI

While the donor heart maintains β-AR sensitivity, post-HTx, β-AR sensitivity declines. This may arise from either CSS, or as a consequence of denervation [132, 202]. As the transplanted heart lacks a noradrenaline uptake 1 mechanism, this makes the myocardium hypersensitive to catecholamines [132]. However, combined with inotropic support, β-AR's become overstimulated and thus, may initiate desensitisation. This essentially compromises contractility,

but also renders sympathomimetic agents relatively ineffective. As with the donor, it may be advantageous to utilise alternate inotropic agents to support haemodynamics. Levosimendan for example, a Ca^{2+} sensitiser, has been successfully utilised in HTx to reduce catecholamine requirements and improve ventricular performance [220]. Further, 30-day mortality using levosimendan is improved, however long-term (1-3 years) survival was reduced [395]. It may be beneficial to utilise a combination of inotropic support in both the acute and chronic stages of transplantation, with the aim to reduce sympathomimetic requirement.

A significant contributor to poor contractility in this study is mitochondrial dysfunction. Our data coincide with previous data examining mitochondrial function in the context of IRI. This highlights IRI as one of the most important consequences in peri-transplant cardiac dysfunction. Specifically, we have shown increased oxygen wastage at CI, which may be consequence of reverse electron flow from CII, thus reducing membrane potential generation and increasing ROS production. This mitochondrial dysfunction imposes significant metabolic alterations, and vice versa.

Using metabolomics we have shown significant depletions in mitochondrial energetics which may reduce glycolytic flux, by substrate inhibition of PDH. This may lead to alterations in glycosylation and PI3K-Akt signalling, which may be cardioprotective or apoptotic depending on the direction of change [361, 375]. Depletions in amino-acid utilisation in the presence of reduced glycolytic flux decreases TCA input from supplementary metabolites, which may contribute to energetic crisis post-HTx. Reductions in L-carnitine for example, reduces mitochondrial transport of FA's, thus increasing metabolic inflexibility and creation of FA compounds that cannot be metabolised. The transplanted heart is in a heightened catabolic state, metabolising both purines and pyrimidines which further exacerbate oxidative stress and FAO dysfunction.

Targeting the mitochondria post-transplantation may be a promising therapeutic strategy to improve graft function. This may be achieved by mitochondrial specific antioxidants (e.g. MitoQ [396]), inhibitors of sites of electron leakage (e.g. inhibitors of the IQ site within CI [142]), or administration of isolated mitochondria [397]. In turn this may improve metabolic dysfunction

imposed by mitochondrial dysfunction, particularly substrate inhibition of PDH. Pharmacological enhancement of glucose oxidation or inhibition of FAO has also been shown to be cardioprotective in the setting of IRI [290].

Table 6.3 Overview on significant findings post-HTx in BSD-Tx compared to pre-HTx and HR controls.

	Parameter	Effect of BSD-Tx Compared to Controls	Possible Causes	Therapeutic Potential
In vitro Muscle Mechanics	β_1-AR NA Sensitivity	↓	Inotropic support, loss of NA uptake1 mechanism, CSS	Alternate inotropic agents
	Contractility	↓	↓ β_1-AR NA Sensitivity, IRI, catecholamine toxicity	
Mitochondrial Respiration	LEAK	↑	ROS, IRI, *potentially poor* Ca^{2+} *handling*	↓ Mitochondrial ROS production Mitochondrial transplant
	Complex I	↑		
	Complex II	↓		
	ROS	↑		
Metabolism	CHO	↑ Glycolytic uncoupling	ROS, IRI, Mitochondrial dysfunction	Reduce oxidative stress (allopurinol) Enhance glycolytic coupling Improve mitochondrial function
	FAO	↓ FA utilisation		
	AA	↓ AA utilisation		
	ROS	↑ oxidative stress (xanthine, MeS)		

NA- Noradrenaline, ROS- reactive oxygen species, MeS- methionine sulfoxide, IRI- ischaemia reperfusion injury

6.4 | Future Directions

Future investigation based on these data can be separated into two broad categories. Those that seek further clarification of the importance or interaction of other pathways involved in BSD and HTx, but contribute to contractile, mitochondrial and metabolic dysfunction and those targeted therapies during CSS or post-HTx. Hereafter describes multiple future investigations which logistically may be best performed in smaller animals to identify the most potent treatments before translation into larger animals and the human.

6.4.1 | Areas that require clarification

These data are focused on the isolated effects of BSD and HTx on cardiac contractility, mitochondrial function and metabolic regulation. In vivo contractile, mitochondrial and metabolic function is subject to numerous other stressors not directly examined here including, inflammation, hormonal changes and altered coagulation [11, 43, 66]. Although not in the scope of this study, it is appreciated that these factors can influence the translation of these data. The inflammatory effects in the context of HTx begin at BSD and subsequent cold ischaemia, activating the endothelium promoting cell death, permeability, and further release of cytokines [103, 398]. Upon reperfusion, these processes manifest as endothelial disruption, immune cell infiltration and cellular swelling post-HTx and potentiating PGD [103]. BSD and BSD-mediated elevations in IL-6 activates coagulation leading to augmented fibrin regulation, platelet activation and dysregulated von Willebrand factor, which may preclude the donor heart from heart retrieval and transplantation [100]. Further, mitochondrial function and the inflammatory cascade are intimately connected. Therefore, precipitating direct myocyte damage through cytokine signalling, mitochondrial dysfunction and vice versa mitochondrial dysfunction promoting inflammation. The full pathophysiological milieu post-BSD and HTx and the interconnectedness between these systems should be investigated further.

Additionally, pilot data using hIPSC-CM's has suggested a potential role for mitochondrial GRK2 contributing to mitochondrial and metabolic dysregulation following BSD. Further studies should determine to what degree this translocation occurs *in vivo* following both BSD and HTx. One important

mechanism that was not investigated in this study was Ca^{2+} handling. As adrenergic signalling appears to be important in both the donor and transplanted hearts, investigating how the myocardium is utilising Ca^{2+} may provide further insight into the deleterious consequences of BSD and transplantation. Istaroxime for example, is a promising luso-inotropic agent that inhibits the Na^{+}/K^{+}ATPase pump and increases SERCA activity [399]. Istaroxime administration for heart failure has been shown to improve haemodynamics without pro-arrhythmic or ischaemic side effects [399, 400]. Targeting potential aberrant Ca^{2+} handling in the context of transplantation may be beneficial.

6.4.2 | Targeted therapy

This study did not directly investigate the biochemical effects of CSS, however significant cardiac dysfunction was observed following this period. Based on this observation, it is apparent that significant cardiac dysfunction occurs during this time and as such CSS should remain a research priority. CSS is already an area of active research; however the ideal preservation solution remains elusive, interest has shifted toward mechanical perfusion systems which support metabolism, and reduce inflammation, oxidative stress and ischaemic damage. Given the potential ethical issues surrounding donor heart management prior to heart retrieval, it may be useful to treat the donor heart ex vivo in these perfusion systems with targeted therapies. These therapies may include decreasing mitochondrial ROS production via S3QEL's/ S1QEL's, preventing succinate build-up, and enhancing glycolytic coupling (trimetazidine) by reducing fatty acid build-up and use.

Post-HTx targeted therapies may include the use of non-adrenergic inotropes such as omecamtiv mecarbil or Ca^{2+} enhancers/sensitisers. Mitochondrial targets include reducing ROS production and perhaps replacing damaged mitochondria with a healthy population of either donor or recipient mitochondria, thus improving energetics. Metabolic dysfunction requires further functional assessment metabolic flux, but future research may employ therapeutics that enhance glycolytic coupling and strategies that reduce metabolites involved in oxidative stress.

6.4.3 | Potential role for mechanical support

Another interesting avenue to explore is mechanical unloading of potentially both the donor and post-transplanted heart. Mechanical unloading is achieved utilising mechanical devices such as ventricular assist devices (VAD), intra-aortic balloon pumps (IABP) and extracorporeal membrane oxygenation (ECMO) devices [386]. The aims of mechanical unloading are to reduce energetic demand and lower myocardial oxygen consumption. In doing so, unloading has several beneficial effects including, enhancing mitochondrial function, metabolism, adrenergic responsiveness, Ca^{2+} handling, improved coronary perfusion and electrophysiological function [401].

Mechanical devices have shown to be cardioprotective in the settings of ischaemic heart disease, lowering infarct size and improving mitochondrial function if applied prior to the ischaemic episode. ECMO utilisation to support RV graft dysfunction post-HTx can improve 30-day survival [221]. Extrapolating this cardioprotection in the setting of ischaemic injury and transplantation, to the heart donor may confer additional improvements to the availability of donor hearts. A significant hurdle to this hypothesis is the relatively high mortality, 50 – 70% in patients receiving ECMO treatment for cardiogenic shock [402]. An important consequence of donor BSD is loss of vasomotor tone. This essentially alters loading conditions on the heart, and as such reduces contractility and MAP. Medical management aims to restore MAP and correct loading conditions. Permissive hypodynamics however may allow a degree of mechanical unloading in the donor heart which may be beneficial. This strategy however, may come at the cost of end organ perfusion, which must be closely monitored.

Utilisation of mechanical devices for the donor heart as a bridge to transplantation may help to increase myocardial performance. This may have significant implications in cost of care and ethical implications regarding end of life treatment. For example, extending a patient's life via mechanical intervention for the sole purpose of preserving/improving heart function to benefit another patient. As mentioned, this method would have to be approached with a full understanding of the donors wishes. Coupling donor heart mechanical unloading to machine perfusion as an alternate preservation strategy may confer significant advantages to improving post-HTx cardiac function.

6.5 | Conclusion

Heart disease is the single leading cause of death globally, with one death every 28 minutes in Australia [403, 404]. Cardiac disease is projected to increase in conjunction with an ageing population. Despite a multimodal treatment approach, eventually heart disease progresses to end-stage heart failure. It is at this stage that the gold standard treatment is HTx. Transplantation however is still associated with cardiac complications leading to early mortality [15]. Prior to transplantation itself, a significant limitation is the poor availability of suitable donor hearts for an increasing demand. This shortage of donor hearts can be attributed to donor BSD.

This thesis addressed cardiovascular function in both the donor and post-transplanted hearts in a clinically relevant ovine model of HTx from BSD donors. Specifically, this study focussed on cardiac contractility, mitochondrial function and metabolism in an effort to explain cardiac compromise. The main findings identified by these experiments are as follows:

1. Donor BSD compromises specifically the RV, possibly due to catecholamine-mediated increases in ROS initiating mitochondrial uncoupling and metabolic dysfunction, thus predisposing the donor heart to further injury
2. Post-transplanted hearts are associated with;
    a. Considerable *in vitro* RV contractile dysfunction and decreased β_1-AR sensitivity to (-)-noradrenaline
    b. Significant mitochondrial dysfunction, most likely driven by IRI
    c. Higher oxidative stress, again driven by IRI
    d. Dysfunction in glucose, AA and FA metabolism, possibly due to mitochondrial dysfunction

Based on these results, it appears that donor oxidative stress and mitochondrial function are important determinants in BSD-mediated cardiovascular dysfunction. Post-transplantation however, the mitochondrial, oxidative, metabolic and adrenergic systems are significantly impaired. However, each of these deficiencies are targetable either by pharmacological or non-pharmacological means. By

highlighting these factors, it is expected that therapeutic strategies that target this dysfunction can increase both the quality and number of donor BSD hearts, and post-HTx cardiovascular outcomes.

6.6 | References

1. Lund, L.H. and G. Savarese, *Global Public Health Burden of Heart Failure.* Cardiac Failure Review, 2017. **03**(01).
2. Kolwicz, S.C., *An "Exercise" in Cardiac Metabolism.* Frontiers in Cardiovascular Medicine, 2018. **5**.
3. Aissaoui, N., M. Morshuis, H. Maoulida, J.-E. Salem, G. Lebreton, M. Brunn, et al., *Management of end-stage heart failure patients with or without ventricular assist device: an observational comparison of clinical and economic outcomes†.* European Journal of Cardio-Thoracic Surgery, 2018. **53**(1): p. 170-177.
4. Alba, A.C., E. Bain, N. Ng, M. Stein, K. O'Brien, F. Foroutan, et al., *Complications after Heart Transplantation: Hope for the best, but Prepare for the Worst.* International Journal of Transplantation Research and Medicine, 2016. **2**(2): p. 2:22.
5. Iyer, A., G. Kumarasinghe, M. Hicks, A. Watson, L. Gao, A. Doyle, et al., *Primary graft failure after heart transplantation.* J Transplant, 2011. **2011**: p. 175768.
6. Thajudeen, A., E.C. Stecker, M. Shehata, J. Patel, X. Wang, J.H. McAnulty, Jr., et al., *Arrhythmias after heart transplantation: mechanisms and management.* J Am Heart Assoc, 2012. **1**(2): p. e001461.
7. *ANZOD Registry, Annual Report, Section 3: Deceased Organ Donor Pathway*, A.a.N.Z.D.a.T. Registry, Editor. 2019.
8. Kobashigawa, J., A. Zuckermann, P. Macdonald, P. Leprince, F. Esmailian, M. Luu, et al., *Report from a consensus conference on primary graft dysfunction after cardiac transplantation.* J Heart Lung Transplant, 2014. **33**(4): p. 327-40.
9. *Annual Report, Section 7: Deceased Donor Heart Donation*, in *2018 Annual Report*, A.a.N.Z.D.a.T.R. (ANZOD), Editor. 2018: Adelaide, Australia.
10. *ANZOD Reistry. 2016 Annual Report, Appendix 1 Data Table.*, A.a.N.Z.D.a.T. Registry, Editor. 2016, Australia and New Zealand Dialysis and Transplant Registry: Adelaide, Australia.
11. Apostolakis, E., H. Parissis, and D. Dougenis, *Brain death and donor heart dysfunction: implications in cardiac transplantation.* J Card Surg, 2010. **25**(1): p. 98-106.
12. Ranasinghe, A.M. and R.S. Bonser, *Endocrine changes in brain death and transplantation.* Best Pract Res Clin Endocrinol Metab, 2011. **25**(5): p. 799-812.
13. Szabo, G., *Physiologic Changes After Brain Death.* The Journal of Heart and Lung Transplantation, 2004. **23**(9S): p. S223-S226.
14. Wybraniec, M.T., K. Mizia-Stec, and L. Krzych, *Neurocardiogenic injury in subarachnoid hemorrhage: A wide spectrum of catecholamin-mediated brain-heart interactions.* Cardiol J, 2014. **21**(3): p. 220-8.
15. McCartney, S.L., C. Patel, and J.M. Del Rio, *Long-term outcomes and management of the heart transplant recipient.* Best Pract Res Clin Anaesthesiol, 2017. **31**(2): p. 237-248.
16. Skorić, B., M. Čikeš, J.L. Maček, Ž. Baričević, I. Škorak, H. Gašparović, et al., *Cardiac allograft vasculopathy: diagnosis, therapy, and prognosis.* Croatian Medical Journal, 2014. **55**(6): p. 562-576.
17. Ruthirago, D., P. Julayanont, P. Tantrachoti, J. Kim, and K. Nugent, *Cardiac Arrhythmias and Abnormal Electrocardiograms After Acute Stroke.* The American Journal of the Medical Sciences, 2016. **351**(1): p. 112-118.
18. Koppikar, S., A. Baranchuk, J.C. Guzman, and C.A. Morillo, *Stroke and ventricular arrhythmias.* Int J Cardiol, 2013. **168**(2): p. 653-9.
19. Khush, K.K., R. Menza, J. Nguyen, B.A. Goldstein, J.G. Zaroff, and B.J. Drew, *Electrocardiographic characteristics of potential organ donors and associations with cardiac allograft use.* Circ Heart Fail, 2012. **5**(4): p. 475-83.

20. Christe, G., G. Hadour, M. Ovize, and R. Ferrera, *Brain death does not change epicardial action potentials and their response to ischemia-reperfusion in open-chest pigs.* J Heart Lung Transplant, 2006. **25**(7): p. 847-53.
21. *Chapter 7: Heart Donation Australia and New Zealand and Dialysis and Transplantation Registry*, in *Australian and New Zealand Orgain Donation Registry,*. 2016 Australian and New Zealand Orgain Donation Registry: Adelaide Australia.
22. *ANZOD Registry. (2018) Annual Report, Section 7: Deceased Donor Heart Donation.* Australia and New Zealand Dialysis and Transplant Registry: Adelaide, Australia.
23. *ANZOD Annual Report, Organs Retrieved*, A.a.N.Z.D.a.T.R. (ANZOD), Editor. 2009: Adelaide, Australia. p. 23-36.
24. *ANZOD Annual Report, Organs Retrieved*, A.a.N.Z.D.a.T.R. (ANZOD), Editor. 2010: Adelaide, Australia. p. 23-36.
25. *ANZOD Annual Report, Organs Retrieved*, A.a.N.Z.D.a.T.R. (ANZOD), Editor. 2011: Adelaide, Australia. p. 37-54.
26. *ANZOD Annual Report, Cardio-Thoracic Organ Donation*, A.a.N.Z.D.a.T.R. (ANZOD), Editor. 2012: Adelaide, Australia. p. 41-46.
27. *ANZOD Annual Report. Chapter 5 Organ Data*, A.a.N.Z.D.a.T.R. (ANZOD), Editor. 2013: Adelaide, Australia.
28. *ANZOD Annual Report, Chapter 5 Organ Data*, A.a.N.Z.D.a.T.R. (ANZOD), Editor. 2014: Adelaide, Australia.
29. *ANZOD Registry Report*, A.a.N.Z.D.a.T.R. (ANZOD), Editor. 2015: Adelaide, Australia.
30. *ANZOD Annual Report, Section 7 Deceased Donor Heart Donation*, A.a.N.Z.D.a.T.R. (ANZOD), Editor. 2017: Adelaide, Australia.
31. van Bree, M.D., Y.B. Roos, I.A. van der Bilt, A.A. Wilde, M.E. Sprengers, K. de Gans, et al., *Prevalence and characterization of ECG abnormalities after intracerebral hemorrhage.* Neurocrit Care, 2010. **12**(1): p. 50-5.
32. VanDer Bilt I., Hasan D., VanDenBrink R., Cramer M. J., VanDerJagt M., van Kooten F., et al., *Cardiac dysfunction after aneurysmal subarachnoid haemorrhage, relationship with outcome.* American Academy of Neurology, 2014. **25**(7): p. 847-53.
33. Dujardin K.S., McCully R.B., Wijdicks E.F.M., Tazelaar H.D., Seward J.B., McGregor C.G.A., et al., *Myocardial dysfunction associated with brain death: Clinical, echocardiographic and pathologic features.* The Journal of Heart Lung Transplantation, 2000. **20**: p. 350-57.
34. Frontera, J.A., A. Parra, D. Shimbo, A. Fernandez, J.M. Schmidt, P. Peter, et al., *Cardiac arrhythmias after subarachnoid hemorrhage: risk factors and impact on outcome.* Cerebrovasc Dis, 2008. **26**(1): p. 71-8.
35. Malik, A.N., B.A. Gross, P.M. Rosalind Lai, Z.B. Moses, and R. Du, *Neurogenic Stress Cardiomyopathy After Aneurysmal Subarachnoid Hemorrhage.* World Neurosurg, 2015. **83**(6): p. 880-5.
36. Berman, M., A. Ali, E. Ashley, D. Freed, K. Clarke, S. Tsui, et al., *Is stress cardiomyopathy the underlying cause of ventricular dysfunction associated with brain death?* J Heart Lung Transplant, 2010. **29**(9): p. 957-65.
37. Uvelin, A., J. Pejaković, and V. Mijatović, *Acquired prolongation of QT interval as a risk factor for torsade de pointes ventricular tachycardia: a narrative review for the anesthesiologist and intensivist.* Journal of Anesthesia, 2017. **31**(3): p. 413-423.
38. Herijgers P., Borgers M., and Flameng W., *The effect of brain death on cardiovscular function in rats. Part I. Is the heart damaged?* Cardiovascular Research, 1997. **38**: p. 98-106.
39. See Hoe, L.E., M.A. Wells, N. Bartnikowski, N.G. Obonyo, J.E. Millar, A. Khoo, et al., *Heart Transplantation From Brain Dead Donors.* Transplantation, 2020. **Publish Ahead of Print**.
40. Bugge, J.F., *Brain death and its implications for management of the potential organ donor.* Acta Anaesthesiol Scand, 2009. **53**(10): p. 1239-50.

41. Szabo, G., T. Hackert, G.A. Buhmann, C.F. Sebening, and S.H. Vahl, *Downregulation of myocardial contractility via intact ventriculo-arterial coupling in the brain dead donor.* European Journal of Cardio-Thoracic Surgery, 2001(20): p. 170-176.
42. Seguin C., Devaux Y., Grosjean S., Medhy Siaghy E., Mairose P., Zannad F., et al., *Evidence of functional myocardial ischaemia with myocardial dysfunction in brain-dead pigs.* Circulation, 2001. **104**(Suppl I): p. I197-I201.
43. Barklin, A., A. Larsson, C. Vestergaard, J. Koefoed-Nielsen, A. Bach, R. Nyboe, et al., *Does brain death induce a pro-inflammatory response at the organ level in a porcine model?* Acta Anaesthesiol Scand, 2008. **52**(5): p. 621-7.
44. Anthonymuthu, T.S., E.M. Kenny, and H. Bayir, *Therapies targeting lipid peroxidation in traumatic brain injury.* Brain Res, 2016. **1640**(Pt A): p. 57-76.
45. Drosatos, K. and P.C. Schulze, *Cardiac lipotoxicity: molecular pathways and therapeutic implications.* Curr Heart Fail Rep, 2013. **10**(2): p. 109-21.
46. Kolwicz, S.C., Jr., L. Liu, I.J. Goldberg, and R. Tian, *Enhancing Cardiac Triacylglycerol Metabolism Improves Recovery From Ischemic Stress.* Diabetes, 2015. **64**(8): p. 2817-27.
47. Oresic, M., J.P. Posti, M.H. Kamstrup-Nielsen, R.S. Takala, H.F. Lingsma, I. Mattila, et al., *Human Serum Metabolites Associate With Severity and Patient Outcomes in Traumatic Brain Injury.* EBioMedicine, 2016. **12**: p. 118-126.
48. Bittner H.B., Kendall S.W.H., Chen E.P., and Van Trigt P., *Endocrine changes and metabolic responses in a validated canine brain death model.* Journal Of Critical Care, 1995. **10**(2): p. 56-63.
49. Pandalai, P.K., J.M. Lyons, J.Y. Duffy, K.M. McLean, C.J. Wagner, W.H. Merrill, et al., *Role of the beta-adrenergic receptor kinase in myocardial dysfunction after brain death.* J Thorac Cardiovasc Surg, 2005. **130**(4): p. 1183-9.
50. Herijgers P., Nishimura Y., and Flameng W., *Endothelial Activation Through Brain Death?* J Heart Lung Transplant, 2004. **23**(9S): p. S234-S239.
51. Quintana-Quezada, R.A., I. Rajapreyar, A. Postalian-Yrausquin, Y.C. Yeh, S. Choi, B. Akkanti, et al., *Clinical Factors Implicated in Primary Graft Dysfunction After Heart Transplantation: A Single-center Experience.* Transplant Proc, 2016. **48**(6): p. 2168-71.
52. Li, J., I.E. Konstantinov, S. Cai, M. Shimizu, and A.N. Redington, *Systemic and myocardial oxygen transport responses to brain death in pigs.* Transplant Proc, 2007. **39**(1): p. 21-6.
53. Yeh, T., Jr., A.S. Wechsler, L. Graham, K.E. Loesser, D.A. Sica, L. Wolfe, et al., *Central sympathetic blockade ameliorates brain death-induced cardiotoxicity and associated changes in myocardial gene expression.* J Thorac Cardiovasc Surg, 2002. **124**(6): p. 1087-98.
54. Shivalkar, B., J. Van Loon, W. Wieland, T.B. Tjandra-Maga, B. M., C. Plets, et al., *Variable effects of explosive or gradual increase of intracranial pressure on myocardial structure and function.* Circulation, 1993. **87**: p. 230-239.
55. Garcia-Sainz J.A., Vazquez-Prado J., and Medina L de C., *a1-Adrenoceptors: function and phosphorylation.* European Journal of Pharmacology, 2000. **389**: p. 1-12.
56. Borea P.A., Amerini S., Masini I., Cerbai E., Ledda F., Mantelli L., et al., *B1- and B2-Adrenoceptors in Sheep Cardiac Ventricular Muscle.* Journal of Molecular and Cellular Cardiology, 1992. **24**: p. 753-764.
57. Najafi, A., V. Sequeira, D.W. Kuster, and J. van der Velden, *beta-adrenergic receptor signalling and its functional consequences in the diseased heart.* Eur J Clin Invest, 2016. **46**(4): p. 362-74.
58. Woo, A.Y. and R.P. Xiao, *beta-Adrenergic receptor subtype signaling in heart: from bench to bedside.* Acta Pharmacol Sin, 2012. **33**(3): p. 335-41.
59. Novitzky, D., A.G. Rose, and D.K. Cooper, *Injury of myocardial conduction tissue and coronary artery smooth muscle following brain death in the baboon.* Transplantation, 1988. **45**(5): p. 964-6.

60. Bittner, H.B., E.P. Chen, C.A. Milano, S.W.H. Kendall, R.B. Jennings, D.C. Sabiston, et al., *Myocardial β-Adrenergic Receptor Function and High-Energy Phosphates in Brain Death–Related Cardiac Dysfunction.* Circulation, 1995. **92**(9): p. 472-478.
61. Woodall, M.C., M. Ciccarelli, B.P. Woodall, and W.J. Koch, *G protein-coupled receptor kinase 2: a link between myocardial contractile function and cardiac metabolism.* Circ Res, 2014. **114**(10): p. 1661-70.
62. Van Trigt, P., H.B. Bittner, S.W. Kendall, and C.A. Milano, *Mechanisms of Transplant Right Ventricular Dysfunction.* Annals of Surgery, 1995. **221**(6): p. 666-676.
63. D' Amico T. A., Meyers C.H., Koutlas T. C., Peterseim D. S., D.C. Sabiston, Van Trigt P., et al., *Desensitization of myocardial b-adrenergic receptors and deterioration of left ventricular function after brain death.* The Journal of Thoracic and cardiovascular Surgery, 1995. **110**(3): p. 746-751.
64. White, M., R.J. Wiechmann, R.L. Roden, M.B. Hagan, M.M. Wollmering, J.D. Port, et al., *Cardiac beta-adrenergic neuroeffector systems in acute myocardial dysfunction related to brain injury. Evidence for catecholamine-mediated myocardial damage.* Circulation, 1995. **92**(8): p. 2183-9.
65. Arbour, R.B., *Early metabolic/cellular-level resuscitation following terminal brain stem herniation: implications for organ transplantation.* AACN Adv Crit Care, 2013. **24**(1): p. 59-78.
66. Floerchinger, B., R. Oberhuber, and S.G. Tullius, *Effects of brain death on organ quality and transplant outcome.* Transplant Rev (Orlando), 2012. **26**(2): p. 54-9.
67. Holzem, K.M., K.C. Vinnakota, V.K. Ravikumar, E.J. Madden, G.A. Ewald, K. Dikranian, et al., *Mitochondrial structure and function are not different between nonfailing donor and end-stage failing human hearts.* FASEB J, 2016. **30**(8): p. 2698-707.
68. Scheubel, R.J., M. Tostlebe, A. Simm, S. Rohrbach, R. Prondzinsky, F.N. Gellerich, et al., *Dysfunction of Mitochondrial Respiratory Chain complex I in Human Failing Myocardium Is Not Due to Disturbed Mitochondrial Gene Expression.* Journal of the American College of Cardiology, 2002. **40**(12): p. 2174-2181.
69. Sharov, V.G., A.V. Todor, N. Silverman, S. Goldstein, and H.N. Sabbah, *Abnormal mitochondrial respiration in failed human myocardium.* J Mol Cell Cardiol, 2000. **32**(12): p. 2361-7.
70. Sztark F, Thicoipe M, Lassie P, Petitjean ME, and Dabadie P, *Mitochondrial energy metabolism in brain-dead organ donors.* Ann Transplant, 2000. **4**: p. 41-44.
71. Ferrera, R., J. Bopassa, C. Rodriguez, G. Baverel, and M. Ovize, *High energy compound stability during experimental brain death.* Transplant Proc, 2006. **38**(7): p. 2285-6.
72. Stoica, S.C., D.K. Satchithananda, C. Atkinson, P.A. White, A.N. Redington, M. Goddard, et al., *The energy metabolism in the right and left ventricles of human donor hearts across transplantation.* Eur J Cardiothorac Surg, 2003. **23**(4): p. 503-512.
73. Zanier, E.R., T. Zoerle, M. Fiorini, L. Longhi, L. Cracco, A. Bersano, et al., *Heart-fatty acid-binding and tau proteins relate to brain injury severity and long-term outcome in subarachnoid haemorrhage patients.* Br J Anaesth, 2013. **111**(3): p. 424-32.
74. Furuhashi, M. and G.S. Hotamisligil, *Fatty acid-binding proteins: role in metabolic diseases and potential as drug targets.* Nat Rev Drug Discov, 2008. **7**(6): p. 489-503.
75. Oresic, M., J.P. Posti, M.H. Kamstrup-Nielsen, R.S.K. Takala, H.F. Lingsma, I. Mattila, et al., *Human Serum Metabolites Associate With Severity and Patient Outcomes in Traumatic Brain Injury.* EBioMedicine, 2016. **12**: p. 118-126.
76. Tonin, A.M., A.U. Amaral, E.N. Busanello, M. Grings, R.F. Castilho, and M. Wajner, *Long-chain 3-hydroxy fatty acids accumulating in long-chain 3-hydroxyacyl-CoA dehydrogenase and mitochondrial trifunctional protein deficiencies uncouple oxidative phosphorylation in heart mitochondria.* J Bioenerg Biomembr, 2013. **45**(1-2): p. 47-57.
77. Guzzardi, M.A. and P. Iozzo, *Fatty heart, cardiac damage, and inflammation.* Rev Diabet Stud, 2011. **8**(3): p. 403-17.

78. Neves, J.S., A.M. Leite-Moreira, M. Neiva-Sousa, J. Almeida-Coelho, R. Castro-Ferreira, and A.F. Leite-Moreira, *Acute Myocardial Response to Stretch: What We (don't) Know.* Front Physiol, 2015. **6**: p. 408.
79. Camici, P.G., G. d'Amati, and O. Rimoldi, *Coronary microvascular dysfunction: mechanisms and functional assessment.* Nat Rev Cardiol, 2015. **12**(1): p. 48-62.
80. Gutierrez, E., A.J. Flammer, L.O. Lerman, J. Elizaga, A. Lerman, and F. Fernandez-Aviles, *Endothelial dysfunction over the course of coronary artery disease.* Eur Heart J, 2013. **34**(41): p. 3175-81.
81. Szabo G., Buhmann V., Bahrle S., Vahl C.F., and Hagl S., *BRAIN DEATH IMPAIRS CORONARY ENDOTHELIAL FUNCTION.* Transplantation, 2001. **73**(11): p. 1846-48.
82. Oishi, Y., *Impairment of coronary flow reserve and left ventricular function in the brain-dead canine heart.* European Journal of Cardio-Thoracic Surgery, 2003. **24**(3): p. 404-410.
83. Oishi, Y., Y. Nishimura, Y. Tanoue, N. Kajihara, K. Imasaka, S. Morita, et al., *Endothelin-1 receptor antagonist prevents deterioration of left ventricular function and coronary flow reserve in brain-dead canine heart.* J Heart Lung Transplant, 2005. **24**(9): p. 1354-61.
84. Bohm, F. and J. Pernow, *The importance of endothelin-1 for vascular dysfunction in cardiovascular disease.* Cardiovasc Res, 2007. **76**(1): p. 8-18.
85. Szabo G., Hackert T., Buhmann V., Graf A., Vahl C.F., and Hagl S., *Downregulation of myocardial contractility via intact ventriculo-arterial coupling in the brian dead organ donor.* European Journal of Cardio-Thoracic Surgery, 2001. **20**: p. 170-176.
86. Novitzky, D., D.K.C. Cooper, Morrell D, and Isaacs S, *Change from Aerobic to Anaerobic Metabolism after Brain Death, and Reversal after Triiodothyronine Therapy.* Transplantation, 1988. **45**(1): p. 32-36.
87. Novitzky, D., Z. Mi, J.F. Collins, and D.K. Cooper, *Increased Procurement of Thoracic Donor Organs After Thyroid Hormone Therapy.* Semin Thorac Cardiovasc Surg, 2015. **27**(2): p. 123-32.
88. Hing, A.J., M. Hicks, S.R. Garlick, L. Gao, S.H. Kesteven, S.C. Faddy, et al., *The effects of hormone resuscitation on cardiac function and hemodynamics in a porcine brain-dead organ donor model.* Am J Transplant, 2007. **7**(4): p. 809-17.
89. Pingitore, A., G. Nicolini, C. Kusmic, G. Iervasi, P. Grigolini, and F. Forini, *Cardioprotection and thyroid hormones.* Heart Fail Rev, 2016. **21**(4): p. 391-9.
90. Marin-Garcia, J., *Thyroid hormone and myocardial mitochondrial biogenesis.* Vascul Pharmacol, 2010. **52**(3-4): p. 120-30.
91. James, S.R., A.M. Ranasinghe, R. Venkateswaran, C.J. McCabe, J.A. Franklyn, and R.S. Bonser, *The effects of acute triiodothyronine therapy on myocardial gene expression in brain stem dead cardiac donors.* J Clin Endocrinol Metab, 2010. **95**(3): p. 1338-43.
92. Macdonald, P.S., A. Aneman, D. Bhonagiri, D. Jones, G. O'Callaghan, W. Silvester, et al., *A systematic review and meta-analysis of clinical trials of thyroid hormone administration to brain dead potential organ donors.* Crit Care Med, 2012. **40**(5): p. 1635-44.
93. Rech, T.H., R.B. Moraes, D. Crispim, M.A. Czepielewski, and C.B. Leitao, *Management of the brain-dead organ donor: a systematic review and meta-analysis.* Transplantation, 2013. **95**(7): p. 966-74.
94. Buchanan, I.A. and V.A. Mehta, *Thyroid hormone resuscitation after brain death in potential organ donors: A primer for neurocritical care providers and narrative review of the literature.* Clin Neurol Neurosurg, 2018. **165**: p. 96-102.
95. Goarin JP., Cohen S., Riou B., Jacquens Y., Guesde R., Le Bret F., et al., *The Effects of Triiodothyronine on Hemodynamic Status and Cardiac Function in Potential Heart Donors.* Anesthesia and Analgesia, 1996. **83**: p. 41-47.
96. Schwartz I., Bird S., Lotz Z., Innes C.R., and Hickman R., *The influence of thyroid hormone replacement in a porcine model of brain death.* Transplantation, 1993. **55**(3): p. 474-476.

97. Robin A.N., Barouk J.D., Darnal E., Riou B., and Langeron O., *Free Cortisol and Accuracy of Total Cortisol Measurements in the Diagnosis of Adrenal Insufficiency in Brain-dead Patients.* Anesthesia, 2011. **115**(3): p. 568-74.
98. Marik p.E. and Zaloga G.P., *Adrenal Insufficiency In the Critically Ill: A New Look at an Old Problem.* Chest, 2002. **122**: p. 1784-1796.
99. Opdam, H.I., *Hormonal Therapy in Organ Donors.* Crit Care Clin, 2019. **35**(2): p. 389-405.
100. Meyfroidt, G., J. Gunst, I. Martin-Loeches, M. Smith, C. Robba, F.S. Taccone, et al., *Management of the brain-dead donor in the ICU: general and specific therapy to improve transplantable organ quality.* Intensive Care Med, 2019. **45**(3): p. 343-353.
101. Cohen J., Chernov K., Ben-Shimon O., and Singer P., *Management of the Brain-Dead, Heart-Beating Potential Donor.* The Israel Medical Association Journal, 2002. **4**: p. 243-246.
102. Gordon, J.K. and J. McKinlay, *Physiological changes after brain stem death and management of the heart-beating donor.* BJA Educ, 2012. **12**(5): p. 225-229.
103. Watts, R.P., O. Thom, and J.F. Fraser, *Inflammatory signalling associated with brain dead organ donation: from brain injury to brain stem death and posttransplant ischaemia reperfusion injury.* J Transplant, 2013. **2013**: p. 521369.
104. Stanzani, G., M.R. Duchen, and M. Singer, *The role of mitochondria in sepsis-induced cardiomyopathy.* Biochim Biophys Acta Mol Basis Dis, 2019. **1865**(4): p. 759-773.
105. Yeager, M.P., P.M. Guyre, and A.U. Munck, *Glucocorticoid regulation of the inflammatory response to injury.* Acta Anaesthesiol Scand, 2004. **48**(7): p. 799-813.
106. Schipper, D.A., K.M. Marsh, A.S. Ferng, D.J. Duncker, J.D. Laman, and Z. Khalpey, *The Critical Role of Bioenergetics in Donor Cardiac Allograft Preservation.* J Cardiovasc Transl Res, 2016. **9**(3): p. 176-83.
107. Anaya-Prado R. and Delgado-Vasquez J.A., *Scientific basis of organ preservation.* Current Opinion in Organ Transplantation, 2008. **13**: p. 129-134.
108. See, Y.P., R.D. Weisel, D.A.G. Mickle, K.H. Teoh, G.J. Wilson, L.C. Tumiati, et al., *Prolonged hypothermic cardiac storage for transplantation.* The Journal of Thoracic and Cardiovascular Surgery, 1992. **104**(3): p. 817-824.
109. Kay, L., Z. Daneshrad, V.A. Saks, and R. A., *Alteration in the control of mitochondrial respirtion by outer mitochondrial membrane and creatine during heart preservation.* Cardiovascular Research, 1997. **34**: p. 547-556.
110. Kuznetsov AV, Schneeberger S, Seiler R, Brandacher G, Mark W, Steurer W, et al., *Mitochondrial defects and heterogeneous cytochrome c release after cardiac cold ischemia and reperfusion.* Am J Physiol Heart Circ Physiol, 2003. **286**: p. H1633-H1641.
111. Scheiber, D., T. Jelenik, E. Zweck, P. Horn, H.P. Schultheiss, D. Lassner, et al., *High-resolution respirometry in human endomyocardial biopsies shows reduced ventricular oxidative capacity related to heart failure.* Exp Mol Med, 2019. **51**(2): p. 1-10.
112. Gnaiger E, Kuznetsov AV, Schneeberger S, Seiler R, Brandacher G, Steurer W, et al., *Mitochondria in the Cold*, in *Life in the Cold*, K.M. Heldmaier G., Editor. 2001, Springer, Berlin, Heidelberg.
113. Lemieux, H., S. Semsroth, H. Antretter, D. Hofer, and E. Gnaiger, *Mitochondrial respiratory control and early defects of oxidative phosphorylation in the failing human heart.* Int J Biochem Cell Biol, 2011. **43**(12): p. 1729-38.
114. Brandon Bravo Bruinisma GJ, Van de Kolk CWA, Nederhoff MGJ, Bredee JJ, Ruigork TJC, and Van Echteld CJA, *Brain Death–Related Energetic Failure of the Donor Heart Becomes Apparent Only During Storage and Reperfusion: An Ex Vivo Phosphorus-31 Magnetic Resonance Spectroscopy Study on the Feline Heart.* J Heart Lung Transplant, 2001. **20**: p. 996-1004.
115. Biagioli, B., S. Scolletta, L. Marchetti, A. Tabucchi, and F. Carlucci, *Relationships between hemodynamic parameters and myocardial energy and antioxidant status in heart transplantation.* Biomed Pharmacother, 2003. **57**(3-4): p. 156-162.

116. Minasian, S.M., M.M. Galagudza, Y.V. Dmitriev, A.A. Karpov, and T.D. Vlasov, *Preservation of the donor heart: from basic science to clinical studies.* Interact Cardiovasc Thorac Surg, 2015. **20**(4): p. 510-9.
117. Latchana, N., J.R. Peck, B. Whitson, and S.M. Black, *Preservation solutions for cardiac and pulmonary donor grafts: a review of the current literature.* J Thorac Dis, 2014. **6**(8): p. 1143-9.
118. Li, Y., S. Guo, G. Liu, Y. Yuan, W. Wang, Z. Zheng, et al., *Three Preservation Solutions for Cold Storage of Heart Allografts: A Systematic Review and Meta-Analysis.* Artif Organs, 2016. **40**(5): p. 489-96.
119. Ferng, A.S., D. Schipper, A.M. Connell, K.M. Marsh, S. Knapp, and Z. Khalpey, *Novel vs clinical organ preservation solutions: improved cardiac mitochondrial protection.* J Cardiothorac Surg, 2017. **12**(1): p. 7.
120. Wicomb W.N., Cooper D.K.C., Novitzky D., and Barnard C.N., *Cardiac Transplantation Following Storage of the Donor Heart by a Portable Hypothermic Perfusion System.* The Annals of Thoracic Surgey, 1984. **37**(3): p. 243-248.
121. Macdonald, P.S., H.C. Chew, M. Connellan, and K. Dhital, *Extracorporeal heart perfusion before heart transplantation: the heart in a box.* Curr Opin Organ Transplant, 2016. **21**(3): p. 336-42.
122. Van Caenegem, O., C. Beauloye, J. Vercruysse, S. Horman, L. Bertrand, N. Bethuyne, et al., *Hypothermic continuous machine perfusion improves metabolic preservation and functional recovery in heart grafts.* Transpl Int, 2015. **28**(2): p. 224-31.
123. Cobert, M.L., M.E. Merritt, L.M. West, C. Ayers, M.E. Jessen, and M. Peltz, *Metabolic characteristics of human hearts preserved for 12 hours by static storage, antegrade perfusion, or retrograde coronary sinus perfusion.* J Thorac Cardiovasc Surg, 2014. **148**(5): p. 2310-2315 e1.
124. Iyer, A., L. Gao, A. Doyle, P. Rao, J.R. Cropper, C. Soto, et al., *Normothermic ex vivo perfusion provides superior organ preservation and enables viability assessment of hearts from DCD donors.* Am J Transplant, 2015. **15**(2): p. 371-80.
125. Qin, G., T. Sjoberg, Q. Liao, X. Sun, and S. Steen, *Intact endothelial and contractile function of coronary artery after 8 hours of heart preservation.* Scand Cardiovasc J, 2016. **50**(5-6): p. 362-366.
126. Ardehali, A., F. Esmailian, M. Deng, E. Soltesz, E. Hsich, Y. Naka, et al., *Ex-vivo perfusion of donor hearts for human heart transplantation (PROCEED II): a prospective, open-label, multicentre, randomised non-inferiority trial.* The Lancet, 2015. **385**(9987): p. 2577-2584.
127. Baretti R., Debus B., Lin B-S., Weng Y-G., Pasic M., Hubler M., et al., *Arrhythmia post heart transplantation.* Applied Cardiopulmonary Pathophysiology, 2011. **15**: p. 256-271.
128. Chang, H.Y., L.W. Lo, A.N. Feng, M.C. Chiang, W.H. Yin, M.S. Young, et al., *Long-term follow-up of arrhythmia characteristics and clinical outcomes in heart transplant patients.* Transplant Proc, 2013. **45**(1): p. 369-75.
129. Pickham, D., K. Hickey, L. Doering, B. Chen, C. Castillo, and B.J. Drew, *Electrocardiographic abnormalities in the first year after heart transplantation.* J Electrocardiol, 2014. **47**(2): p. 135-9.
130. Moore, J.P., J.C. Alejos, G. Perens, S. Wong, and K.M. Shannon, *The corrected QT interval before and after heart transplantation.* Am J Cardiol, 2009. **104**(4): p. 596-601.
131. Yusuf, S., D. Phil, N. Dhalla, J. Wittes, A. Mitchell, and M. Yacoub, *Increased sensitivity of the denervated transplanted human heart to isoprenaline both before and after B-adrenergic blockade.* Circulation, 1987. **75**(4): p. 696-704.
132. Gilbert, E.M., C.C. Eiswirth, P.C. Mealey, P. Larrabee, C.M. Herrick, and M.R. Bristow, *Beta Adrenergic Supersensitivity of the Tx heart is presynaptic in origin.* Circulation, 1989. **79**: p. 344-349.

133. Hausenloy, D.J. and D.M. Yellon, *Myocardial ischemia-reperfusion injury: a neglected therapeutic target.* J Clin Invest, 2013. **123**(1): p. 92-100.
134. Gvozdjakova, A., J. Kucharska, S. Mizera, Z. Braunova, Z. Schreinerova, E. Schramekova, et al., *Coenzyme Q10 depletion and mitochondrial energy disturbances in rejection development in patients after heart transplantation.* BioFactors, 1999. **9**: p. 301-306.
135. Romero, E., E. Chang, E. Tabak, D. Pinheiro, J. Tallaj, S. Litovsky, et al., *Rejection-associated Mitochondrial Impairment After Heart Transplantation.* Transplant Direct, 2020. **6**(11): p. e616.
136. Scheiber, D., T. Jelenik, P. Horn, Schultheiss HP, D. Lassner, U. Boeken, et al., *Impaired myocardial mitochondrial function correlates with inflammatory cell burden in humans following heart transplantation.* Eur Heart J, 2017. **38Supp**: p. 11268.
137. Chouchani, E.T., V.R. Pell, A.M. James, L.M. Work, K. Saeb-Parsy, C. Frezza, et al., *A Unifying Mechanism for Mitochondrial Superoxide Production during Ischemia-Reperfusion Injury.* Cell Metab, 2016. **23**(2): p. 254-63.
138. Zhou, T., C.C. Chuang, and L. Zuo, *Molecular Characterization of Reactive Oxygen Species in Myocardial Ischemia-Reperfusion Injury.* Biomed Res Int, 2015. **2015**: p. 864946.
139. Wong, H.S., P.A. Dighe, V. Mezera, P.A. Monternier, and M.D. Brand, *Production of superoxide and hydrogen peroxide from specific mitochondrial sites under different bioenergetic conditions.* J Biol Chem, 2017. **292**(41): p. 16804-16809.
140. Brand, M.D., *The sites and topology of mitochondrial superoxide production.* Exp Gerontol, 2010. **45**(7-8): p. 466-72.
141. Brand, M.D., *Mitochondrial generation of superoxide and hydrogen peroxide as the source of mitochondrial redox signaling.* Free Radic Biol Med, 2016. **100**: p. 14-31.
142. Brand, M.D., R.L. Goncalves, A.L. Orr, L. Vargas, A.A. Gerencser, M. Borch Jensen, et al., *Suppressors of Superoxide-H2O2 Production at Site IQ of Mitochondrial Complex I Protect against Stem Cell Hyperplasia and Ischemia-Reperfusion Injury.* Cell Metab, 2016. **24**(4): p. 582-592.
143. Arakawa, K., H. Himeno, J. Kirigaya, F. Otomo, K. Matsushita, H. Nakahashi, et al., *Impact of n-3 polyunsaturated fatty acids in predicting ischemia/reperfusion injury and progression of myocardial damage after reperfusion in patients with ST-segment elevation acute myocardial infarction.* J Cardiol, 2015. **66**(2): p. 101-7.
144. Soderlund, C. and G. Radegran, *Immunosuppressive therapies after heart transplantation--The balance between under- and over-immunosuppression.* Transplant Rev (Orlando), 2015. **29**(3): p. 181-9.
145. Drake-Holland A.J., Van der Vusse G.J., Roemen T.H.M., Hynd J.W., Mansaray M., Wright Z.M., et al., *Chronic Catecholamine Depletion Switches Myocardium from Carbohydrate to Lipid Utilisation.* Cardiovascular Drugs and Therapy, 2001. **15**: p. 111-117.
146. Lin, F., Y. Ou, C.Z. Huang, S.Z. Lin, and Y.B. Ye, *Metabolomics identifies metabolite biomarkers associated with acute rejection after heart transplantation in rats.* Sci Rep, 2017. **7**(1): p. 15422.
147. Karimianpour, A. and A. Maran, *Advances in Coronary No-Reflow Phenomenon-a Contemporary Review.* Curr Atheroscler Rep, 2018. **20**(9): p. 44.
148. Stoica, S.C., M. Goddard, and S. Large, *The ednothelium in clinical cardiac transplantation.* Ann Thorac Surg, 2002. **73**: p. 1002-8.
149. Schramm, R., M.D. Menger, S. Kirsch, F. Langer, Y. Harder, J. Hamacher, et al., *The subepicardial microcirculation in heterotopically transplanted mouse hearts: an intravital multifluorescence microscopy study.* J Thorac Cardiovasc Surg, 2007. **134**(1): p. 210-7, 217 e1.
150. Koch, A., T.M. Bingold, J. Oberlander, F.-U. Sack, H.F. Otto, S. Hagl, et al., *Capillary endothelia and cardiomyocyte differ in vulnerability to ischemia/reperfusion during clinical heart transplantation.* European Journal of Cardio-Thoracic Surgery, 2001. **20**: p. 996-1001.

151. Tuuminen, R., S. Syrjala, R. Krebs, M.A. Keranen, K. Koli, U. Abo-Ramadan, et al., *Donor simvastatin treatment abolishes rat cardiac allograft ischemia/reperfusion injury and chronic rejection through microvascular protection.* Circulation, 2011. **124**(10): p. 1138-50.
152. Syrjala, S.O., A.I. Nykanen, R. Tuuminen, A. Raissadati, M.A. Keranen, R. Arnaudova, et al., *Donor Heart Treatment With COMP-Ang1 Limits Ischemia-Reperfusion Injury and Rejection of Cardiac Allografts.* Am J Transplant, 2015. **15**(8): p. 2075-84.
153. van den Hoogen, P., M.M. Huibers, J.P. Sluijter, and R.A. de Weger, *Cardiac allograft vasculopathy: a donor or recipient induced pathology?* J Cardiovasc Transl Res, 2015. **8**(2): p. 106-16.
154. *Ethical Guidelines for Organ Transplantation from Deceased Donors*, A.G.N.H.a.M.R. Council, Editor. 2016: Canberra.
155. *ANZOD Registry. 2018 annual Report, Section 3: Deceased Organ Donor Pathway.* , A.a.N.Z.D.a.T.R. (ANZOD), Editor. 2018: Adelaide, Australia.
156. Erasmus, M., A. Neyrink, M. Sabatino, and L. Potena, *Heart allograft preservation: an arduous journey from the donor to the recipient.* Curr Opin Cardiol, 2017.
157. Kadner, A., R.H. Chen, and A.D. H., *Heterotopic heart transplantation: experimental development and clinical experience.* European Journal of Cardio-Thoracic Surgery, 2000. **17**: p. 474-481.
158. Copeland, J. and H. Copeland, *Heterotopic Heart Transplantation: Technical Considerations.* Operative Techniques in Thoracic and Cardiovascular Surgery, 2016. **21**(3): p. 269-280.
159. Watts, R.P., I. Bilska, S. Diab, K.R. Dunster, A.C. Bulmer, A.G. Barnett, et al., *Novel 24-h ovine model of brain death to study the profile of the endothelin axis during cardiopulmonary injury.* Intensive Care Med Exp, 2015. **3**(1): p. 31.
160. Simonova, G., J.P. Tung, J.F. Fraser, H.L. Do, A. Staib, M.S. Chew, et al., *A comprehensive ovine model of blood transfusion.* Vox Sang, 2014. **106**(2): p. 153-60.
161. Bergenfeldt, H., J. Stehlik, P. Hoglund, B. Andersson, and J. Nilsson, *Donor-recipient size matching and mortality in heart transplantation: Influence of body mass index and gender.* J Heart Lung Transplant, 2017. **36**(9): p. 940-947.
162. DiVincenti L., Westcott R., and Lee C., *Sheep (Ovis aries) as a Model for Cardiovascular Surgery and Management before, during, and after cardiopulmonary Bypass.* Journal of the American Association for Laboratory Animal Science, 2014. **53**(5): p. 439-448.
163. Barnes, T.J., M.A. Hockstein, and C.S. Jabaley, *Vasoplegia after cardiopulmonary bypass: A narrative review of pathophysiology and emerging targeted therapies.* SAGE Open Med, 2020. **8**: p. 2050312120935466.
164. Hajjar, L.A., J.L. Vincent, F.R. Barbosa Gomes Galas, A. Rhodes, G. Landoni, E.A. Osawa, et al., *Vasopressin versus Norepinephrine in Patients with Vasoplegic Shock after Cardiac Surgery: The VANCS Randomized Controlled Trial.* Anesthesiology, 2017. **126**(1): p. 85-93.
165. Lambden, S., B.C. Creagh-Brown, J. Hunt, C. Summers, and L.G. Forni, *Definitions and pathophysiology of vasoplegic shock.* Crit Care, 2018. **22**(1): p. 174.
166. Chan, J.L., J.A. Kobashigawa, T.L. Aintablian, S.J. Dimbil, P.A. Perry, J.K. Patel, et al., *Characterizing Predictors and Severity of Vasoplegia Syndrome After Heart Transplantation.* Ann Thorac Surg, 2018. **105**(3): p. 770-777.
167. See Hoe, L.E., J.M. Schilling, A.R. Busija, K.J. Haushalter, V. Ozberk, M.M. Keshwani, et al., *Chronic beta1-adrenoceptor blockade impairs ischaemic tolerance and preconditioning in murine myocardium.* Eur J Pharmacol, 2016. **789**: p. 1-7.
168. Nakahira, K., S. Hisata, and A.M. Choi, *The Roles of Mitochondrial Damage-Associated Molecular Patterns in Diseases.* Antioxid Redox Signal, 2015. **23**(17): p. 1329-50.
169. Capote, L.A., R. Mendez Perez, and A. Lymperopoulos, *GPCR signaling and cardiac function.* Eur J Pharmacol, 2015. **763**(Pt B): p. 143-8.
170. Lymperopoulos, A., G. Rengo, and W.J. Koch, *Adrenergic nervous system in heart failure: pathophysiology and therapy.* Circ Res, 2013. **113**(6): p. 739-53.

171. Lucia, C.d., A. Eguchi, and W.J. Koch, *New Insights in Cardiac β-Adrenergic Signaling During Heart Failure and Aging.* Frontiers in Pharmacology, 2018. **9**: p. 904.
172. Goodwill, A.G., G.M. Dick, A.M. Kiel, and J.D. Tune, *Regulation of Coronary Blood Flow.* Compr Physiol, 2017. **7**(2): p. 321-382.
173. Vanhoutte, P.M., H. Shimokawa, M. Feletou, and E.H. Tang, *Endothelial dysfunction and vascular disease - a 30th anniversary update.* Acta Physiol (Oxf), 2017. **219**(1): p. 22-96.
174. Flacco, N., V. Segura, M. Perez-Aso, S. Estrada, J.F. Seller, F. Jimenez-Altayo, et al., *Different beta-adrenoceptor subtypes coupling to cAMP or NO/cGMP pathways: implications in the relaxant response of rat conductance and resistance vessels.* Br J Pharmacol, 2013. **169**(2): p. 413-25.
175. Zhao, Y., P.M. Vanhoutte, and S.W. Leung, *Vascular nitric oxide: Beyond eNOS.* J Pharmacol Sci, 2015. **129**(2): p. 83-94.
176. Tank, A.W. and D. Lee Wong, *Peripheral and central effects of circulating catecholamines.* Compr Physiol, 2015. **5**(1): p. 1-15.
177. Anwar, A.S.M.T. and J.-m. Lee, *Medical Management of Brain-Dead Organ Donors.* Acute and Critical Care, 2019. **34**(1): p. 14-29.
178. Han, C.C., Y. Ma, Y. Li, Y. Wang, and W. Wei, *Regulatory effects of GRK2 on GPCRs and non-GPCRs and possible use as a drug target (Review).* Int J Mol Med, 2016. **38**(4): p. 987-94.
179. Sheng, Y. and L. Zhu, *The crosstalk between autonomic nervous system and blood vessels.* Int J Physiol Pathophysiol Pharmacol, 2018. **10**(1): p. 17-28.
180. Lundberg, J.M., *Pharmacology of cotransmission in the autonomic nervous system: intergrative aspects on amines, neuropeptides, adenosine triphosphate, amino acids and nitric oxide.* Pharmacological Reviews, 1996. **48**(1): p. 113-178.
181. Moura, D., H. Pinheiro, M.Q. Paiva, and S. Guimaraes, *Prejunctional effects of angiotensin II and bradykinin in the heart and blood vessels.* Journal of Autonomic Pharmacology, 2000. **19**: p. 321-325.
182. Martin, D.S., E. Vogel, J. Freeling, and C. Reihe, *Activation of bradykinin-sensitive pericardial afferents increases systemic venous tone in conscious rats.* Auton Neurosci, 2020. **223**: p. 102624.
183. Chen, J.W., Y.S. Chen, N.H. Chi, S.C. Huang, H.Y. Yu, N.K. Chou, et al., *Risk factors and prognosis of patients with primary graft failure after heart transplantation: an Asian center experience.* Transplant Proc, 2014. **46**(3): p. 914-9.
184. Yamani, M.H., M.S. Lauer, R.C. Starling, C.E. Pothier, E.M. Tuzcu, N.B. Ratliff, et al., *Impact of donor spontaneous intracranial hemorrhage on outcome after heart transplantation.* Am J Transplant, 2004. **4**(2): p. 257-61.
185. Tsai, F., D. Marelli, J. Bresson, D. Gjertson, R. Kermani, J. Patel, et al., *Use of hearts transplanted from donors with atraumatic intracranial bleeds.* J Heart Lung Transplant, 2002. **21**: p. 623-628.
186. Yang Q., He G-W., Underwood M.J., and Yu C-M., *Cellular and molecular mechanisms of endothelial ischemia/ reperfusion injury: perspectives and implications for postischemic myocardial protection_YANG.pdf>.* American Journal of Resuscitation, 2016. **8**(2): p. 765-777.
187. Kaumann A. J., Hall J. A., Murray K. J., Wells F. C., and Brown M. J., *A comparison of the effects of adrenaline and noradrenaline on human heart: the role of β1-and β2-adrenoceptors in the stimulation of adenylate cyclase and contractile force.* European Heart Journal, 1989. **10(Suppl B)**: p. 29-37.
188. Molenaar P., Christ T., Hussain R. I., Engel A., Berk E., Gillette K. T., et al., *PDE3, but not PDE4, reduces β_1 - and β_2-adrenoceptor-mediated inotropic and lusitropic effects in failing ventricle from metoprolol-treated patient.* Br J Pharmacol, 2013. **169**(3): p. 528-538.
189. Molenaar P., Bartel S., Cochrane A., Vetter D., Jalali H., Pohlner P., et al., *Both β2- and β1-Adrenergic Receptors Mediate Hastened Relaxation and Phosphorylation of Phospholamban*

and Troponin I in Ventricular Myocardium of Fallot Infants, Consistent With Selective Coupling of β2-adrenergic receptors to Gs-Protein. Circulation, 2000. **102**: p. 1814-1821.
190. Dooley, L.M., E.A. Washington, A. Abdalmula, E.M. Tudor, W.G. Kimpton, and S.R. Bailey, *Endothelial Dysfunction in an Ovine Model of Collagen-Induced Arthritis.* Journal of Vascular Research, 2014. **51**(2): p. 90-101.
191. Kaumann A. J., Bartel S., Molenaar P., Sanders L., Burrell K., Vetter D., et al., *Activation of β2-Adrenergic Receptors Hastens Relaxation and Mediates Phosphorylation of Phospholamban, Troponin I, and C-Protein in Ventricular Myocardium From Patients With Terminal Heart Failure.* Circulation, 1999. **99**(1): p. 65-72.
192. Molenaar P., Christ T., Berk E., Engel A., Gillette K. T., Galindo-Tovar A., et al., *Carvedilol induces greater control of β2- than β1-adrenoceptor-mediated inotropic and lusitropic effects by PDE3, while PDE4 has no effect in human failing myocardium.* Naunyn-Schmiedeberg's Arch Pharmacolgy, 2014. **387**: p. 629-640.
193. Gauthier C., Leblais V., Kobzik L., Trochu J., Khandoudi N., Bril A., et al., *The Negative Inotropic Effect of b3-Adrenoceptor Stimulation Is Mediated by Activation of a Nitric Oxide Synthase Pathway in Human Ventricle.* The Journal of Clinical Investigation, 1998. **102**(7): p. 1377-1384.
194. Gauthier C., Tavernier G., Charpentier F., Langin D., and Le Marec H., *Functional b3-Adrenoceptor in the Human Heart.* The Journal of Clinical Investigation, 1996. **98**(2): p. 556-562.
195. Joseph, S.S., J.A. Lynham, P. Molenaar, A.A. Grace, W.H. Colledge, and A.J. Kaumann, *Intrinsic sympathomimetic activity of (-)-pindolol mediated through a (-)-propranolol-resistant site of the beta1-adrenoceptor in human atrium and recombinant receptors.* Naunyn Schmiedebergs Arch Pharmacol, 2003. **368**(6): p. 496-503.
196. Christ T., Molenaar P., Klenowski P. M., Ravens U., and K.A. J., *Human atrial b1L-adrenoceptor but not b3-adrenoceptor activation increases force and Ca2+ current at physiological temperature.* Br J Pharmacol, 2011. **162**(4): p. 823-839.
197. Mo, W., M.C. Michel, X.W. Lee, A.J. Kaumann, and P. Molenaar, *The beta3 -adrenoceptor agonist mirabegron increases human atrial force through beta1 -adrenoceptors: an indirect mechanism?* Br J Pharmacol, 2017. **174**(16): p. 2706-2715.
198. Green, B.A. and E.L. Frank, *Comparison of plasma free metanephrines between healthy dogs and 3 dogs with pheochromocytoma.* Vet Clin Pathol, 2013. **42**(4): p. 499-503.
199. Kromer, B.M. and J.R. Tippins, *Coronary artery constriction by the isoprostane 8-epi prostaglandin F2α.* British Journal of Pharmacology, 1996. **119**: p. 1276-1280.
200. Asp, M.L., J.J. Martindale, F.I. Heinis, W. Wang, and J.M. Metzger, *Calcium mishandling in diastolic dysfunction: Mechanisms and potential therapies.* Biochimica et Biophysica Acta (BBA) - Molecular Cell Research, 2013. **1833**(4): p. 895-900.
201. Liaudet, L., B. Calderari, and P. Pacher, *Pathophysiological mechanisms of catecholamine and cocaine-mediated cardiotoxicity.* Heart Fail Rev, 2014. **19**(6): p. 815-24.
202. Ji, X.F., W. Shuo, L. Yang, and C.S. Li, *Impaired beta-adrenergic receptor signalling in post-resuscitation myocardial dysfunction.* Resuscitation, 2012. **83**(5): p. 640-4.
203. Vettel, C., M.C. Hottenrott, R. Spindler, U. Benck, P. Schnuelle, C. Tsagogiorgas, et al., *Dopamine and lipophilic derivates protect cardiomyocytes against cold preservation injury.* J Pharmacol Exp Ther, 2014. **348**(1): p. 77-85.
204. Stadlbauer, V., P. Stiegler, P. Taeubl, M. Sereinigg, A. Puntschart, A. Bradatsch, et al., *Energy status of pig donor organs after ischemia is independent of donor type.* J Surg Res, 2013. **180**(2): p. 356-67.
205. Kaumann A. J. and Sanders L., *Both β1- and β2-adrenoceptors mediate catecholamine-evoked arrhythmias in isolated human right atrium.* Naunyn-Schmiedeberg's Arch Pharmacol 1993. **348**: p. 536-540.

206. Bers, D.M., *Cardiac sarcoplasmic reticulum calcium leak: basis and roles in cardiac dysfunction.* Annu Rev Physiol, 2014. **76**: p. 107-27.
207. Walweel, K., Y.W. Oo, and D.R. Laver, *The emerging role of calmodulin regulation of RyR2 in controlling heart rhythm, the progression of heart failure and the antiarrhythmic action of dantrolene.* Clin Exp Pharmacol Physiol, 2017. **44**(1): p. 135-142.
208. Tschope C., Koch M., Spillman F., Heringer-Walther S., Mochmann H., Stauss H., et al., *Upregulation of the cardiac bradykinin B2 receptors after myocardial infarction.* Immunopharmacology, 1999. **44**: p. 111-117.
209. Trabold, R., C. Eros, K. Zweckberger, J. Relton, H. Beck, J. Nussberger, et al., *The role of bradykinin B(1) and B(2) receptors for secondary brain damage after traumatic brain injury in mice.* J Cereb Blood Flow Metab, 2010. **30**(1): p. 130-9.
210. Albert-Weissenberger, C., S. Mencl, S. Hopp, C. Kleinschnitz, and A.L. Siren, *Role of the kallikrein-kinin system in traumatic brain injury.* Front Cell Neurosci, 2014. **8**: p. 345.
211. Stoica, S.C., D.K. Satchithananda, P.A. White, J. Parameshwar, A.N. Redington, and S.R. Large, *Noradrenaline Use in the Human Donor and Relationship with Load-Independent Right Ventricular Contractility.* Transplantation, 2004. **78**(8): p. 1193-1197.
212. Braulio, R., M.D. Sanches, A.L. Teixeira Junior, P.H. Costa, C. Moreira Mda, M.A. Rocha, et al., *Associated Clinical and Laboratory Markers of Donor on Allograft Function After Heart Transplant.* Braz J Cardiovasc Surg, 2016. **31**(2): p. 89-97.
213. Angleitner, P., A. Kaider, J. Gokler, R. Moayedifar, E. Osorio-Jaramillo, A. Zuckermann, et al., *High-dose catecholamine donor support and outcomes after heart transplantation.* J Heart Lung Transplant, 2018. **37**(5): p. 596-603.
214. Nixon, J.L., A.G. Kfoury, K. Brunisholz, B.D. Horne, C. Myrick, D.V. Miller, et al., *Impact of high-dose inotropic donor support on early myocardial necrosis and outcomes in cardiac transplantation.* Clin Transplant, 2012. **26**(2): p. 322-7.
215. Rosa Costanzo, M., *Don't worry, be happy with intravenous norepinephrine.* J Heart Lung Transplant, 2018. **37**(5): p. 572-574.
216. Rabin, J. and D.J. Kaczorowski, *Perioperative Management of the Cardiac Transplant Recipient.* Critical Care Clinics, 2019. **35**(1): p. 45-60.
217. Kansara, P. and J.A. Kobashigawa, *Management of heart transplant recipients: reference for primary care physicians.* Postgrad Med, 2012. **124**(4): p. 215-24.
218. Tevaearai, H.T., B.G. Walton, A.D. Eckhart, J.R. Keys, and W.J. Koch, *Donor heart contractile dysfunction following prolonged ex vivo preservation can be prevented by gene-mediated b-adrenergic signaling modulation.* European Journal of Cardio-Thoracic Surgery, 2002(22): p. 733-737.
219. Boucher, M., S. Nim, C. de Montigny, and G. Rousseau, *Alterations of beta-adrenoceptor responsiveness in postischemic myocardium after 72 h of reperfusion.* Eur J Pharmacol, 2004. **495**(2-3): p. 185-91.
220. Beiras-Fernandez, A., F.C. Weis, F. Kur, I. Kaczmarek, M. Schmoeckel, M. Weis, et al., *Primary graft failure and Ca2+ sensitizers after heart transplantation.* Transplant Proc, 2008. **40**(4): p. 951-2.
221. Mathew J and Dipchand AI, *Right Ventricular Dysfunction Post-Heart Transplantation*, in *Adaptation and Failure in Congenital and Acquired Heart Disease*. 2018, Springer International p. 193-216.
222. Cooper D. K., Novitzky D., and Wicomb W.N., *The pathophysiological effects of brain death on potential donor organs, with particular reference to the heart.* Annals of the Royal College of Surgeons of England, 1989. **71**: p. 261-266.
223. Couch, L.S. and S.E. Harding, *Takotsubo Syndrome: Stress or NO Stress?* JACC Basic Transl Sci, 2018. **3**(2): p. 227-229.
224. Zhou, B. and R. Tian, *Mitochondrial dysfunction in pathophysiology of heart failure.* J Clin Invest, 2018. **128**(9): p. 3716-3726.

225. Pascual, F. and R.A. Coleman, *Fuel availability and fate in cardiac metabolism: A tale of two substrates.* Biochim Biophys Acta, 2016. **1861**(10): p. 1425-33.
226. Lopaschuk, G.D. and J.R.B. Dyck, *Glycolysis Regulation.* 2005.
227. Lopaschuk, G.D., J.R. Ussher, C.D. Folmes, J.S. Jaswal, and W.C. Stanley, *Myocardial fatty acid metabolism in health and disease.* Physiol Rev, 2010. **90**(1): p. 207-58.
228. Murphy, M.P. and R.C. Hartley, *Mitochondria as a therapeutic target for common pathologies.* Nat Rev Drug Discov, 2018.
229. Osellame, L.D., T.S. Blacker, and M.R. Duchen, *Cellular and molecular mechanisms of mitochondrial function.* Best Practice & Research Clinical Endocrinology & Metabolism, 2012. **26**(6): p. 711-723.
230. Morelli, A.M., S. Ravera, D. Calzia, and I. Panfoli, *An update of the chemiosmotic theory as suggested by possible proton currents inside the coupling membrane.* Open Biology, 2019. **9**(4): p. 180221.
231. Lodish H., Berk A., Zipursky SL., Matsudaira P., Baltimore D., and Darnell J., *Section 16.2, Electron Transport and Oxidative Phosphorylation*, in *Molecular Cell Biology. 4th Edition*. 2000, W. H. Freeman: New York.
232. Perry, S.W., J.P. Norman, J. Barbieri, E.B. Brown, and H.A. Gelbard, *Mitochondrial membrane potential probes and the proton gradient: a practical usage guide.* Biotechniques, 2011. **50**(2): p. 98-115.
233. Rich P., *Chemiosmotic coupling: The cost of living.* Nature, 2003. **421**(6923).
234. Izem-Meziane, M., B. Djerdjouri, S. Rimbaud, F. Caffin, D. Fortin, A. Garnier, et al., *Catecholamine-induced cardiac mitochondrial dysfunction and mPTP opening: protective effect of curcumin.* Am J Physiol Heart Circ Physiol, 2012. **302**(3): p. H665-74.
235. Raisky, O., L. Gomez, L. Chalabreysse, O. Gateau-Roesch, J. Loufouat, F. Thivolet-Bejui, et al., *Mitochondrial permeability transition in cardiomyocyte apoptosis during acute graft rejection.* Am J Transplant, 2004. **4**(7): p. 1071-8.
236. Karwi, Q.G., G.M. Uddin, K.L. Ho, and G.D. Lopaschuk, *Loss of Metabolic Flexibility in the Failing Heart.* Front Cardiovasc Med, 2018. **5**: p. 68.
237. Chen, M., P.Y. Sato, J.K. Chuprun, R.J. Peroutka, N.J. Otis, J. Ibetti, et al., *Prodeath signaling of G protein-coupled receptor kinase 2 in cardiac myocytes after ischemic stress occurs via extracellular signal-regulated kinase-dependent heat shock protein 90-mediated mitochondrial targeting.* Circ Res, 2013. **112**(8): p. 1121-34.
238. Sato, P.Y., J.K. Chuprun, J. Ibetti, A. Cannavo, K. Drosatos, J.W. Elrod, et al., *GRK2 compromises cardiomyocyte mitochondrial function by diminishing fatty acid-mediated oxygen consumption and increasing superoxide levels.* J Mol Cell Cardiol, 2015. **89**(Pt B): p. 360-4.
239. Brandon Bravo Bruinsma GJ, Van de Kolk CWA, Nederhoff MGJ, Bredee JJ, Ruigork TJC, and C. Van Echteld, *Brain Death–Related Energetic Failure of the Donor Heart Becomes Apparent Only During Storage and Reperfusion: An Ex Vivo Phosphorus-31 Magnetic Resonance Spectroscopy Study on the Feline Heart.* The Journal of Heart and Lung Transplantation, 2000. **20**(9): p. 996-1004.
240. Gao Q., Deng H., Li H., Sun C., Sun Y., Wei B., et al., *Glycolysis and fatty acid β-oxidation, which one is the culprit of ischemic reperfusion injury?* International Journal of Clinical and Experimental Medicine, 2018. **11**(1): p. 59-68.
241. Gnaiger, E., *Mitochondrial Pathways and Respiratory Control. An Introduction to OXPHOS Analysis. 4th ed.* 2014: Mitochondr Physiol Network 19.12.
242. Chowdhury, S.R., J. Djordjevic, B.C. Albensi, and P. Fernyhough, *Simultaneous evaluation of substrate-dependent oxygen consumption rates and mitochondrial membrane potential by TMRM and safranin in cortical mitochondria.* Biosci Rep, 2015. **36**(1): p. e00286.
243. Perry, C.G., D.A. Kane, I.R. Lanza, and P.D. Neufer, *Methods for assessing mitochondrial function in diabetes.* Diabetes, 2013. **62**(4): p. 1041-53.

244. Park, S.Y., J.R. Gifford, R.H. Andtbacka, J.D. Trinity, J.R. Hyngstrom, R.S. Garten, et al., *Cardiac, skeletal, and smooth muscle mitochondrial respiration: are all mitochondria created equal?* Am J Physiol Heart Circ Physiol, 2014. **307**(3): p. H346-52.
245. Winkler-Stuck, K., E. Kirches, C. Mawrin, K. Dietzmann, H. Lins, C.W. Wallesch, et al., *Re-evaluation of the dysfunction of mitochondrial respiratory chain in skeletal muscle of patients with Parkinson's disease.* J Neural Transm (Vienna), 2005. **112**(4): p. 499-518.
246. Cheng, J., G. Nanayakkara, Y. Shao, R. Cueto, L. Wang, W.Y. Yang, et al., *Mitochondrial Proton Leak Plays a Critical Role in Pathogenesis of Cardiovascular Diseases.* Adv Exp Med Biol, 2017. **982**: p. 359-370.
247. Jastroch, M., A.S. Divakaruni, S. Mookerjee, J.R. Treberg, and M.D. Brand, *Mitochondrial proton and electron leaks.* Essays Biochem, 2010. **47**: p. 53-67.
248. Divakaruni, A.S. and M.D. Brand, *The regulation and physiology of mitochondrial proton leak.* Physiology (Bethesda), 2011. **26**(3): p. 192-205.
249. Bertero, E. and C. Maack, *Calcium Signaling and Reactive Oxygen Species in Mitochondria.* Circ Res, 2018. **122**(10): p. 1460-1478.
250. Correa, F., N. Pavon, M. Buelna-Chontal, N. Chiquete-Felix, L. Hernandez-Esquivel, and E. Chavez, *Calcium Induces Mitochondrial Oxidative Stress Because of its Binding to Adenine Nucleotide Translocase.* Cell Biochem Biophys, 2018. **76**(4): p. 445-450.
251. Halestrap A.P. and Brenner C., *The Adenine Nucleotide Translocase: A Central Component of the Mitochondrial Permeability Transition Pore and Key Player in Cell Death.* Current Medicinal Chemsitry, 2003. **10**: p. 1507-1525.
252. Giorgio, V., L. Guo, C. Bassot, V. Petronilli, and P. Bernardi, *Calcium and regulation of the mitochondrial permeability transition.* Cell Calcium, 2018. **70**: p. 56-63.
253. Brand MD, *Uncoupling to survive? The role of mitochondrial inefficiency in ageing.* Exp Gerontol, 2000. **35**: p. 811-820.
254. Monteagudo Vela, M., D. Garcia Saez, and A.R. Simon, *Current approaches in retrieval and heart preservation.* Ann Cardiothorac Surg, 2018. **7**(1): p. 67-74.
255. Chouchani, E.T., V.R. Pell, E. Gaude, D. Aksentijevic, S.Y. Sundier, E.L. Robb, et al., *Ischaemic accumulation of succinate controls reperfusion injury through mitochondrial ROS.* Nature, 2014. **515**(7527): p. 431-435.
256. Martin, J.L., A.S.H. Costa, A.V. Gruszczyk, T.E. Beach, F.M. Allen, H.A. Prag, et al., *Succinate accumulation drives ischaemia-reperfusion injury during organ transplantation.* Nat Metab, 2019. **1**: p. 966-974.
257. Ribas, V., C. Garcia-Ruiz, and J.C. Fernandez-Checa, *Glutathione and mitochondria.* Front Pharmacol, 2014. **5**: p. 151.
258. Galloway, C.A. and Y. Yoon, *Mitochondrial morphology in metabolic diseases.* Antioxid Redox Signal, 2013. **19**(4): p. 415-30.
259. Garbern, J.C. and R.T. Lee, *Mitochondria and metabolic transitions in cardiomyocytes: lessons from development for stem cell-derived cardiomyocytes.* Stem Cell Res Ther, 2021. **12**(1): p. 177.
260. Dai, D.F., M.E. Danoviz, B. Wiczer, M.A. Laflamme, and R. Tian, *Mitochondrial Maturation in Human Pluripotent Stem Cell Derived Cardiomyocytes.* Stem Cells Int, 2017. **2017**: p. 5153625.
261. Jung, G., G. Fajardo, A.J. Ribeiro, K.B. Kooiker, M. Coronado, M. Zhao, et al., *Time-dependent evolution of functional vs. remodeling signaling in induced pluripotent stem cell-derived cardiomyocytes and induced maturation with biomechanical stimulation.* FASEB J, 2016. **30**(4): p. 1464-79.
262. Wallace, D.C., W. Fan, and V. Procaccio, *Mitochondrial energetics and therapeutics.* Annu Rev Pathol, 2010. **5**: p. 297-348.

263. Farias, J.G., V.M. Molina, R.A. Carrasco, A.B. Zepeda, E. Figueroa, P. Letelier, et al., *Antioxidant Therapeutic Strategies for Cardiovascular Conditions Associated with Oxidative Stress.* Nutrients, 2017. **9**(9).
264. Deshwal, S., M. Di Sante, F. Di Lisa, and N. Kaludercic, *Emerging role of monoamine oxidase as a therapeutic target for cardiovascular disease.* Curr Opin Pharmacol, 2017. **33**: p. 64-69.
265. Deshwal, S., M. Forkink, C.H. Hu, G. Buonincontri, S. Antonucci, M. Di Sante, et al., *Monoamine oxidase-dependent endoplasmic reticulum-mitochondria dysfunction and mast cell degranulation lead to adverse cardiac remodeling in diabetes.* Cell Death Differ, 2018. **25**(9): p. 1671-1685.
266. Mayor, F., Jr., M. Cruces-Sande, A.C. Arcones, R. Vila-Bedmar, A.M. Briones, M. Salaices, et al., *G protein-coupled receptor kinase 2 (GRK2) as an integrative signalling node in the regulation of cardiovascular function and metabolic homeostasis.* Cell Signal, 2018. **41**: p. 25-32.
267. Santema, B.T., W. Ouwerkerk, J. Tromp, I.E. Sama, A. Ravera, V. Regitz-Zagrosek, et al., *Identifying optimal doses of heart failure medications in men compared with women: a prospective, observational, cohort study.* The Lancet, 2019. **394**(10205): p. 1254-1263.
268. Furiasse, N. and J.A. Kobashigawa, *Immunosuppression and adult heart transplantation: emerging therapies and opportunities.* Expert Rev Cardiovasc Ther, 2017. **15**(1): p. 59-69.
269. Zhang, C.X., Y. Cheng, D.Z. Liu, M. Liu, H. Cui, B.L. Zhang, et al., *Mitochondria-targeted cyclosporin A delivery system to treat myocardial ischemia reperfusion injury of rats.* J Nanobiotechnology, 2019. **17**(1): p. 18.
270. Cung, T.T., O. Morel, G. Cayla, G. Rioufol, D. Garcia-Dorado, D. Angoulvant, et al., *Cyclosporine before PCI in Patients with Acute Myocardial Infarction.* N Engl J Med, 2015. **373**(11): p. 1021-31.
271. Ikeda, G., T. Matoba, Y. Nakano, K. Nagaoka, A. Ishikita, K. Nakano, et al., *Nanoparticle-Mediated Targeting of Cyclosporine A Enhances Cardioprotection Against Ischemia-Reperfusion Injury Through Inhibition of Mitochondrial Permeability Transition Pore Opening.* Sci Rep, 2016. **6**: p. 20467.
272. Chiari P, Angoulvant D, Mewton N, Desebbe O, Obadia JF, Robin J, et al., *Cyclosporine protects the heart during aortic valve surgery.* Anesthesiology, 2014. **121**: p. 232-238.
273. La Monaca, E. and V. Fodale, *Effects of anesthetics on mitochondrial signaling and function.* Current Drug Safety, 2012. **7**: p. 126-139.
274. Murphy, G.S., J.W. Szokol, J.H. Marymont, M.J. Avram, and J.S. Vender, *Opioids and cardioprotection: the impact of morphine and fentanyl on recovery of ventricular function after cardiopulmonary bypass.* J Cardiothorac Vasc Anesth, 2006. **20**(4): p. 493-502.
275. Hsieh, V.C., E.J. Krane, and P.G. Morgan, *Mitochondrial Disease and Anesthesia.* Journal of Inborn Errors of Metabolism and Screening, 2017. **5**.
276. Colleoni, M., B. Costa, E. Gori, and A. Santagostino, *Biochemical characterization of the effects of the benzodiazepine, midazolam, on mitochondrial electron transfer.* Pharmacology & Toxicology, 1996. **78**: p. 69-76.
277. Nazari, A., S.S. Sadr, M. Faghihi, Y. Azizi, M.J. Hosseini, N. Mobarra, et al., *Vasopressin attenuates ischemia-reperfusion injury via reduction of oxidative stress and inhibition of mitochondrial permeability transition pore opening in rat hearts.* Eur J Pharmacol, 2015. **760**: p. 96-102.
278. Bordt, E.A., C.J. Smith, T.G. Demarest, S.D. Bilbo, and M.A. Kingsbury, *Mitochondria, Oxytocin, and Vasopressin: Unfolding the Inflammatory Protein Response.* Neurotox Res, 2019. **36**(2): p. 239-256.
279. Heather, L.C., C.A. Carr, D.J. Stuckey, S. Pope, K.J. Morten, E.E. Carter, et al., *Critical role of complex III in the early metabolic changes following myocardial infarction.* Cardiovasc Res, 2010. **85**(1): p. 127-36.

280. Fuentes-Antras, J., B. Picatoste, E. Ramirez, J. Egido, J. Tunon, and O. Lorenzo, *Targeting metabolic disturbance in the diabetic heart.* Cardiovasc Diabetol, 2015. **14**: p. 17.
281. Cotter, D.G., R.C. Schugar, and P.A. Crawford, *Ketone body metabolism and cardiovascular disease.* Am J Physiol Heart Circ Physiol, 2013. **304**(8): p. H1060-76.
282. Smolders, V.F., E. Zodda, P.H.A. Quax, M. Carini, J.A. Barbera, T.M. Thomson, et al., *Metabolic Alterations in Cardiopulmonary Vascular Dysfunction.* Front Mol Biosci, 2018. **5**: p. 120.
283. Stanley W.C., *Changes in cardiac metabolism: a critical step from stable angina to ischaemic cardiomyopathy.* European Heart Journal Supplements, 2001. **3**(Supplement O): p. O2-O7.
284. Fillmore, N., J. Mori, and G.D. Lopaschuk, *Mitochondrial fatty acid oxidation alterations in heart failure, ischaemic heart disease and diabetic cardiomyopathy.* Br J Pharmacol, 2014. **171**(8): p. 2080-90.
285. Houten, S.M., S. Violante, F.V. Ventura, and R.J. Wanders, *The Biochemistry and Physiology of Mitochondrial Fatty Acid beta-Oxidation and Its Genetic Disorders.* Annu Rev Physiol, 2016. **78**: p. 23-44.
286. Kolwicz, S.C., Jr. and R. Tian, *Glucose metabolism and cardiac hypertrophy.* Cardiovasc Res, 2011. **90**(2): p. 194-201.
287. Tran, D.H. and Z.V. Wang, *Glucose Metabolism in Cardiac Hypertrophy and Heart Failure.* J Am Heart Assoc, 2019. **8**(12): p. e012673.
288. Fillmore, N., J.L. Levasseur, A. Fukushima, C.S. Wagg, W. Wang, J.R.B. Dyck, et al., *Uncoupling of glycolysis from glucose oxidation accompanies the development of heart failure with preserved ejection fraction.* Mol Med, 2018. **24**(1): p. 3.
289. Mallet, R.T., *Pyruvate: Metabolic Protector of Cardiac Performance.* Proceedings of the Society for Experimental Biology and Medicine, 2008. **223**(2): p. 136-148.
290. Lopaschuk, G.D., *Metabolic Modulators in Heart Disease: Past, Present, and Future.* Can J Cardiol, 2017. **33**(7): p. 838-849.
291. Drake, K.J., V.Y. Sidorov, O.P. McGuinness, D.H. Wasserman, and J.P. Wikswo, *Amino acids as metabolic substrates during cardiac ischemia.* Exp Biol Med (Maywood), 2012. **237**(12): p. 1369-78.
292. Huang, Y., M. Zhou, H. Sun, and Y. Wang, *Branched-chain amino acid metabolism in heart disease: an epiphenomenon or a real culprit?* Cardiovasc Res, 2011. **90**(2): p. 220-3.
293. Novitzky D., *Novel Actions of Thyroid Hormone: The Role of Triiodothyronine in Cardiac Transplantation.* Thyroid, 1996. **6**(5): p. 531-536.
294. Kitai T., T. Tanaka, Terasaki M., Okamoto R., Ozawa K., Morikawa S., et al., *Energy Metabolism of the Heart and the Liver in Brain-Dead Dogs as Assessed by 31P NMR Spectroscopy.* Journal of Surgical Research, 1993. **55**: p. 599-606.
295. McConville, P., E.G. Lakatta, and R.G. Spencer, *Greater glycogen utilization during 1- than 2-adrenergic receptor stimulation in the isolated perfused rat heart.* Am J Physiol Endocrinol Metab, 2007. **293**(6): p. E1828-35.
296. Liemburg-Apers, D.C., P.H. Willems, W.J. Koopman, and S. Grefte, *Interactions between mitochondrial reactive oxygen species and cellular glucose metabolism.* Arch Toxicol, 2015. **89**(8): p. 1209-26.
297. Hartmann, C., P. Radermacher, M. Wepler, and B. Nussbaum, *Non-Hemodynamic Effects of Catecholamines.* Shock, 2017. **48**(4): p. 390-400.
298. Dujardin K S., McCully R B., Wijdicks E F M., Tazelaar H D., Seward J B., McGregor C G., et al., *Myocardial Dysfunction Associated with Brain Death: Clinical, Echocardiographic and Pathologic Features.* The Journal of Heart and Lung Transplantation, 2000. **20**(3): p. 350-357.
299. Hartmann, C., P. Radermacher, M. Wepler, and B. Nußbaum, *Non-Hemodynamic Effects of Catecholamines.* Shock, 2017. **48**(4): p. 390-400.
300. Apstein C.S., *Increased glycolytic substrate protection improves ischemic cardiac dysfunction and reduces injury.* American Heart Journal, 2000. **137**: p. S107-S114.

301. Ussher, J.R. and G.D. Lopaschuk, *The malonyl CoA axis as a potential target for treating ischaemic heart disease.* Cardiovasc Res, 2008. **79**(2): p. 259-68.
302. Jang, S., P. Gornicki, J. Marjanovic, E. Bass, T. P. Iurcotta, P. Rodriguez, et al., *Activity and structure of human acetyl-CoA carboxylase targeted by a specific inhibitor.* FEBS Letters, 2018. **592**(12): p. 2048-2058.
303. Shao, Y., B. Redfors, M. Stahlman, M.S. Tang, A. Miljanovic, H. Mollmann, et al., *A mouse model reveals an important role for catecholamine-induced lipotoxicity in the pathogenesis of stress-induced cardiomyopathy.* Eur J Heart Fail, 2013. **15**(1): p. 9-22.
304. Wallhaus T.R., Taylor M., DeGrado T.R., Russell D. C., Stank P., Nickles R. J., et al., *Myocardial Free Fatty Acid and Glucose Use After Carvedilol Treatment in Patients With Congestive Heart Failure.* Circulation, 2001. **103**: p. 2441-2446.
305. Nikolaidis L. A., Hentosz T., Doverspike A., Huerbin R., Stolarski C., Shen Y-T., et al., *Catecholamine stimulation is associated with impaired myocardial O2 utilization in heart failure.* Cardiovascular Research, 2002. **53**: p. 392-404.
306. Hue, L. and H. Taegtmeyer, *The Randle cycle revisited: a new head for an old hat.* Am J Physiol Endocrinol Metab, 2009. **297**(3): p. E578-91.
307. Guarini, G., A. Huqi, D. Morrone, P.F.G. Capozza, and M. Marzilli, *Trimetazidine and Other Metabolic Modifiers.* Eur Cardiol, 2018. **13**(2): p. 104-111.
308. Phuong H., Choi B. Y., Chong C. R., Raman B., and Horowitz D., *Can Perhexiline Be Utilized Without Long-Term Toxicity? A Clinical Practice Audit.* Therapeutic Drug Monitoring, 2016. **38**: p. 73-78.
309. Steggall, A., I.R. Mordi, and C.C. Lang, *Targeting Metabolic Modulation and Mitochondrial Dysfunction in the Treatment of Heart Failure.* Diseases, 2017. **5**(2).
310. Rosano, G.M. and C. Vitale, *Metabolic Modulation of Cardiac Metabolism in Heart Failure.* Card Fail Rev, 2018. **4**(2): p. 99-103.
311. Fagerholm V., Haaparanta M., and S. M., *α2-Adrenoceptor Regulation of Blood Glucose Homeostasis.* Basic & Clinical Pharmacology & Toxicology, 2011. **108**: p. 365-370.
312. Heather L. C., Catchpole A. F., Stuckey D. J., Cole M. A., Carr C. A., and Clarke K., *Isoproterenol induces in vivo functional and metabolic abnormalities: similar to those found in the infarcted rat heart.* Journal of Physiology and Pharmacology, 2009. **60**(3): p. 31-39.
313. Mangmool, S., T. Denkaew, S. Phosri, D. Pinthong, W. Parichatikanond, T. Shimauchi, et al., *Sustained betaAR Stimulation Mediates Cardiac Insulin Resistance in a PKA-Dependent Manner.* Mol Endocrinol, 2016. **30**(1): p. 118-32.
314. Mangmool, S., T. Denkaew, W. Parichatikanond, and H. Kurose, *beta-Adrenergic Receptor and Insulin Resistance in the Heart.* Biomol Ther (Seoul), 2017. **25**(1): p. 44-56.
315. Riddy, D.M., P. Delerive, R.J. Summers, P.M. Sexton, and C.J. Langmead, *G Protein-Coupled Receptors Targeting Insulin Resistance, Obesity, and Type 2 Diabetes Mellitus.* Pharmacol Rev, 2018. **70**(1): p. 39-67.
316. Lyon, A.R., P.S. Rees, S. Prasad, P.A. Poole-Wilson, and S.E. Harding, *Stress (Takotsubo) cardiomyopathy--a novel pathophysiological hypothesis to explain catecholamine-induced acute myocardial stunning.* Nat Clin Pract Cardiovasc Med, 2008. **5**(1): p. 22-9.
317. Li, Q., J.Y. Youn, and H. Cai, *Mechanisms and consequences of endothelial nitric oxide synthase dysfunction in hypertension.* J Hypertens, 2015. **33**(6): p. 1128-36.
318. Chandra, S., M.J. Romero, A. Shatanawi, A.M. Alkilany, R.B. Caldwell, and R.W. Caldwell, *Oxidative species increase arginase activity in endothelial cells through the RhoA/Rho kinase pathway.* Br J Pharmacol, 2012. **165**(2): p. 506-19.
319. Pernow, J. and C. Jung, *Arginase as a potential target in the treatment of cardiovascular disease: reversal of arginine steal?* Cardiovasc Res, 2013. **98**(3): p. 334-43.
320. Andrasi, T.B., N. Stumpf, and A. Blazovics, *Progressive development of renal vascular dysfunction in brain death implicates reversible alterations of nitric oxide metabolism.* Transplant Proc, 2011. **43**(5): p. 1495-502.

321. Christiansen, J.J., C.B. Djurhuus, C.H. Gravholt, P. Iversen, J.S. Christiansen, O. Schmitz, et al., *Effects of cortisol on carbohydrate, lipid, and protein metabolism: studies of acute cortisol withdrawal in adrenocortical failure.* J Clin Endocrinol Metab, 2007. **92**(9): p. 3553-9.
322. Sumner, L.W., A. Amberg, D. Barrett, M.H. Beale, R. Beger, C.A. Daykin, et al., *Proposed minimum reporting standards for chemical analysis Chemical Analysis Working Group (CAWG) Metabolomics Standards Initiative (MSI).* Metabolomics, 2007. **3**(3): p. 211-221.
323. Wu, Y. and L. Li, *Sample normalization methods in quantitative metabolomics.* J Chromatogr A, 2016. **1430**: p. 80-95.
324. Durbin B.P., Hardin J.S., Hawkins J.S., and Rocle D.M., *A variance-stabilizing transformation for gene-expression microarray data.* Bioinformatics, 2002. **18**(Supplementary 1): p. S105-S110.
325. Bartel, J., J. Krumsiek, and F.J. Theis, *Statistical Methods for the Analysis of High-Throughput Metabolomics Data.* Computational and Structural Biotechnology Journal, 2013. **4**(5): p. e201301009.
326. Pietrocola, F., L. Galluzzi, J.M. Bravo-San Pedro, F. Madeo, and G. Kroemer, *Acetyl coenzyme A: a central metabolite and second messenger.* Cell Metab, 2015. **21**(6): p. 805-21.
327. Yan, L.J., *Redox imbalance stress in diabetes mellitus: Role of the polyol pathway.* Animal Model Exp Med, 2018. **1**(1): p. 7-13.
328. Wamelink, M.M., E.A. Struys, and C. Jakobs, *The biochemistry, metabolism and inherited defects of the pentose phosphate pathway: a review.* J Inherit Metab Dis, 2008. **31**(6): p. 703-17.
329. Wende, A.R., M.K. Brahma, G.R. McGinnis, and M.E. Young, *Metabolic Origins of Heart Failure.* JACC Basic Transl Sci, 2017. **2**(3): p. 297-310.
330. Peoples, J.N.R., T. Maxmillian, Q. Le, S.M. Nadtochiy, P.S. Brookes, G.A. Porter, Jr., et al., *Metabolomics reveals critical adrenergic regulatory checkpoints in glycolysis and pentose-phosphate pathways in embryonic heart.* J Biol Chem, 2018. **293**(18): p. 6925-6941.
331. Tang, W.H., K.A. Martin, and J. Hwa, *Aldose reductase, oxidative stress, and diabetic mellitus.* Front Pharmacol, 2012. **3**: p. 87.
332. Ramasamy, R. and I.J. Goldberg, *Aldose reductase and cardiovascular diseases, creating human-like diabetic complications in an experimental model.* Circ Res, 2010. **106**(9): p. 1449-58.
333. Lee, B.C. and V.N. Gladyshev, *The biological significance of methionine sulfoxide stereochemistry.* Free Radic Biol Med, 2011. **50**(2): p. 221-7.
334. Solmonson, A. and R.J. DeBerardinis, *Lipoic acid metabolism and mitochondrial redox regulation.* J Biol Chem, 2018. **293**(20): p. 7522-7530.
335. Wollin S. D and J. P.J.H., *α-Lipoic Acid and Cardiovascular Disease.* Recent Advances in Nutritional Sciences, 2003(133): p. 3327-3330.
336. Quinlan, C.L., R.L. Goncalves, M. Hey-Mogensen, N. Yadava, V.I. Bunik, and M.D. Brand, *The 2-oxoacid dehydrogenase complexes in mitochondria can produce superoxide/hydrogen peroxide at much higher rates than complex I.* J Biol Chem, 2014. **289**(12): p. 8312-25.
337. Neill, M.A., J. Aschner, F. Barr, and M.L. Summar, *Quantitative RT-PCR comparison of the urea and nitric oxide cycle gene transcripts in adult human tissues.* Mol Genet Metab, 2009. **97**(2): p. 121-7.
338. Poirier, Y., V.D. Antonenkov, T. Glumoff, and J.K. Hiltunen, *Peroxisomal β-oxidation—A metabolic pathway with multiple functions.* Biochimica et Biophysica Acta (BBA) - Molecular Cell Research, 2006. **1763**(12): p. 1413-1426.
339. Westin, M.A., M.C. Hunt, and S.E. Alexson, *The identification of a succinyl-CoA thioesterase suggests a novel pathway for succinate production in peroxisomes.* J Biol Chem, 2005. **280**(46): p. 38125-32.
340. Schonfeld, P. and L. Wojtczak, *Short- and medium-chain fatty acids in energy metabolism: the cellular perspective.* J Lipid Res, 2016. **57**(6): p. 943-54.

341. Liepinsh E., Skapare E., Kuka J., Makrecka M., Cirule H., Vavers E., et al., *Activated peroxisomal fatty acid metabolism improves cardiac recovery in ischemia-reperfusion.* Naunyn-Schmiedeberg's Arch Pharmacolgy, 2013. **386**: p. 541-550.
342. Wongkittichote, P., N. Ah Mew, and K.A. Chapman, *Propionyl-CoA carboxylase - A review.* Mol Genet Metab, 2017. **122**(4): p. 145-152.
343. Wang, Y., B.A. Christopher, K.A. Wilson, D. Muoio, R.W. McGarrah, H. Brunengraber, et al., *Propionate-induced changes in cardiac metabolism, notably CoA trapping, are not altered by l-carnitine.* Am J Physiol Endocrinol Metab, 2018. **315**(4): p. E622-E633.
344. Matson E. and Reginato A. M., *Crystalline Disorders Associated With Renal Disease Including Oxalate Arthropathy*, in *Gout and Other Crystal Arthropathies*. 2012, Elsevier Saunders: Philadephia.
345. van der Veen, J.N., J.P. Kennelly, S. Wan, J.E. Vance, D.E. Vance, and R.L. Jacobs, *The critical role of phosphatidylcholine and phosphatidylethanolamine metabolism in health and disease.* Biochim Biophys Acta Biomembr, 2017. **1859**(9 Pt B): p. 1558-1572.
346. Hatch M. G. and Choy C P., *Effect of Hypoxia on Phosphatidylcholine Biosynthesis in the Isolated Hamster Heart.* Biochemistry Journal, 1990. **268**: p. 47-54.
347. Syme, C., S. Czajkowski, J. Shin, M. Abrahamowicz, G. Leonard, M. Perron, et al., *Glycerophosphocholine Metabolites and Cardiovascular Disease Risk Factors in Adolescents: A Cohort Study.* Circulation, 2016. **134**(21): p. 1629-1636.
348. Skuladottir G V., Schioth H B., and G. S., *Polyunsaturated fatty acids in heart muscle and alpha-adrenoceptor binding properties.* Biochimica et Biophysica Acta, 1993. **1178**: p. 49-54.
349. Wang, W., Z. Wu, Z. Dai, Y. Yang, J. Wang, and G. Wu, *Glycine metabolism in animals and humans: implications for nutrition and health.* Amino Acids, 2013. **45**(3): p. 463-77.
350. Lu, S.C., *Regulation of glutathione synthesis.* Mol Aspects Med, 2009. **30**(1-2): p. 42-59.
351. Tanianskii, D.A., N. Jarzebska, A.L. Birkenfeld, J.F. O'Sullivan, and R.N. Rodionov, *Beta-Aminoisobutyric Acid as a Novel Regulator of Carbohydrate and Lipid Metabolism.* Nutrients, 2019. **11**(3).
352. Zeng, H., R. Tong, W. Tong, Q. Yang, M. Qiu, A. Xiong, et al., *Metabolic Biomarkers for Prognostic Prediction of Pre-diabetes: results from a longitudinal cohort study.* Sci Rep, 2017. **7**(1): p. 6575.
353. Huck, J.H., B. Roos, C. Jakobs, M.S. van der Knaap, and N.M. Verhoeven, *Evaluation of pentitol metabolism in mammalian tissues provides new insight into disorders of human sugar metabolism.* Mol Genet Metab, 2004. **82**(3): p. 231-7.
354. Stincone, A., A. Prigione, T. Cramer, M.M. Wamelink, K. Campbell, E. Cheung, et al., *The return of metabolism: biochemistry and physiology of the pentose phosphate pathway.* Biol Rev Camb Philos Soc, 2015. **90**(3): p. 927-63.
355. Wolfgang M. and Auld D. S., *Purification and Characterization of Human Liver Sorbitol Dehydrogenase.* Biochemistry, 1987. **27**: p. 1622-1628.
356. Croze, M.L. and C.O. Soulage, *Potential role and therapeutic interests of myo-inositol in metabolic diseases.* Biochimie, 2013. **95**(10): p. 1811-27.
357. Song G., Ouyang G., and B. S., *The activation of Akt/PKB signaling pathway and cell survival.* Journal of cellular and molecular medicine, 2005. **9**(1): p. 59-71.
358. Manning, B.D. and A. Toker, *AKT/PKB Signaling: Navigating the Network.* Cell, 2017. **169**(3): p. 381-405.
359. Oudit, G.Y. and J.M. Penninger, *Cardiac regulation by phosphoinositide 3-kinases and PTEN.* Cardiovasc Res, 2009. **82**(2): p. 250-60.
360. Yang, J., Y. Liu, X. Fan, Z. Li, and Y. Cheng, *A pathway and network review on beta-adrenoceptor signaling and beta blockers in cardiac remodeling.* Heart Fail Rev, 2014. **19**(6): p. 799-814.
361. Bond, M.R. and J.A. Hanover, *A little sugar goes a long way: the cell biology of O-GlcNAc.* J Cell Biol, 2015. **208**(7): p. 869-80.

362. Ferron, M., M. Denis, A. Persello, R. Rathagirishnan, and B. Lauzier, *Protein O-GlcNAcylation in Cardiac Pathologies: Past, Present, Future.* Front Endocrinol (Lausanne), 2018. **9**: p. 819.
363. Young R., *Perioperative Fluid and Electrolyte Management in Cardiac Surgery A Review.* The Journal of ExtraCorporeal Technology, 2012. **44**: p. P20-P26.
364. Zakkar, M., G. Guida, M.S. Suleiman, and G.D. Angelini, *Cardiopulmonary bypass and oxidative stress.* Oxid Med Cell Longev, 2015. **2015**: p. 189863.
365. De Hert, S. and A. Moerman, *Myocardial injury and protection related to cardiopulmonary bypass.* Best Pract Res Clin Anaesthesiol, 2015. **29**(2): p. 137-49.
366. Aldemir, M., C. Karatepe, E.D. Bakı, G. Çarşanba, and E. Tecer, *Comparison of Plegisol and Modified ST Thomas Hospital Cardioplegic Solution in the Development of Ventricular Fibrillation after Declamping of the Aorta.* World Journal of Cardiovascular Surgery, 2014. **04**(10): p. 159-166.
367. Sagor, M.A., N. Tabassum, M.A. Potol, and M.A. Alam, *Xanthine Oxidase Inhibitor, Allopurinol, Prevented Oxidative Stress, Fibrosis, and Myocardial Damage in Isoproterenol Induced Aged Rats.* Oxid Med Cell Longev, 2015. **2015**: p. 478039.
368. Wang, Z.V., J. Ding, X. Luo, S. Zhang, G. Yang, Q. Zhu, et al., *Effect of Allopurinol on Myocardial Energy Metabolism in Chronic Heart Failure Rats After Myocardial Infarct.* International Heart Journal, 2016. **57**: p. 753-759.
369. Wu, M.Y., G.T. Yiang, W.T. Liao, A.P. Tsai, Y.L. Cheng, P.W. Cheng, et al., *Current Mechanistic Concepts in Ischemia and Reperfusion Injury.* Cell Physiol Biochem, 2018. **46**(4): p. 1650-1667.
370. Thanassoulis. G., Brophy J. M., Richard. H., and Pilote. L., *Gout, Allopurinol Use, and Heart Failure Outcomes.* Archives of Internal Medicine, 2010. **170**(15): p. 1358-1365.
371. Wluka. A., Ryna P. J., Miller A. M., Richardson. M., Bergin. P. J., Page. J. L., et al., *Post–cardiac transplantation gout incidence of therapeutic complications.* The Journal of Heart and Lung Transplantation, 2000. **19**: p. 951-956.
372. Galvez, A.S., J.A. Ulloa, M. Chiong, A. Criollo, V. Eisner, L.F. Barros, et al., *Aldose reductase induced by hyperosmotic stress mediates cardiomyocyte apoptosis: differential effects of sorbitol and mannitol.* J Biol Chem, 2003. **278**(40): p. 38484-94.
373. Lewko, B., E. Latawiec, A. Maryn, A. Barczynska, M. Pikula, M. Zielinski, et al., *Osmolarity and glucose differentially regulate aldose reductase activity in cultured mouse podocytes.* Exp Diabetes Res, 2011. **2011**: p. 278963.
374. Wu. C., Satapati. S., Gui. W., Wynn. R., Sharma. G., Lou. M., et al., *A novel inhibitor of pyruvate dehydrogenase kinase stimulates myocardial carbohydrate oxidation in diet-induced obesity.* Journal of Biological Chemistry, 2018. **293**(25): p. 9604-9613.
375. McLean, B.A., P.C. Kienesberger, W. Wang, G. Masson, P. Zhabyeyev, J.R. Dyck, et al., *Enhanced recovery from ischemia-reperfusion injury in PI3Kalpha dominant negative hearts: investigating the role of alternate PI3K isoforms, increased glucose oxidation and MAPK signaling.* J Mol Cell Cardiol, 2013. **54**: p. 9-18.
376. Litvinukova, M., C. Talavera-Lopez, H. Maatz, D. Reichart, C.L. Worth, E.L. Lindberg, et al., *Cells of the adult human heart.* Nature, 2020. **588**(7838): p. 466-472.
377. Stohr, E.J., J. Gonzalez-Alonso, I.N. Bezodis, and R. Shave, *Left ventricular energetics: new insight into the plasticity of regional contributions at rest and during exercise.* Am J Physiol Heart Circ Physiol, 2014. **306**(2): p. H225-32.
378. Kobashigawa, J., K. Khush, M. Colvin, M. Acker, A. Van Bakel, H. Eisen, et al., *Report From the American Society of Transplantation Conference on Donor Heart Selection in Adult Cardiac Transplantation in the United States.* Am J Transplant, 2017. **17**(10): p. 2559-2566.
379. Jawitz, O.K., V. Raman, Y.D. Barac, J. Anand, C.B. Patel, R.J. Mentz, et al., *Influence of donor brain death duration on outcomes following heart transplantation: A United Network for Organ Sharing Registry analysis.* J Thorac Cardiovasc Surg, 2020. **159**(4): p. 1345-1353 e2.

380. Dimarakis, I., N.R. Banner, S. Rushton, H.S.E. Wong, M. Berman, N. Howell, et al., *The interval between brainstem death and cardiac assessment influences the retrieval of hearts for transplantation.* Eur J Cardiothorac Surg, 2018. **53**(6): p. 1135-1143.
381. Venkateswaran, R.V., J. Lannon, E. Wong, M. Berman, N. Howell, J. Payne, et al., *The Interval between Brain Stem Death and Cardiac Assessment Influences the Retrieval of Hearts for Transplantation.* The Journal of Heart and Lung Transplantation, 2016. **35**(4): p. S218.
382. Venkateswaran, R.V., J.S. Ganesh, J. Thekkudan, R. Steeds, I.C. Wilson, J. Mascaro, et al., *Donor cardiac troponin-I: a biochemical surrogate of heart function.* Eur J Cardiothorac Surg, 2009. **36**(2): p. 286-92; discussion 292.
383. Dorent, R., E. Gandjbakhch, C. Goeminne, F. Ivanes, L. Sebbag, F. Bauer, et al., *Assessment of potential heart donors: A statement from the French heart transplant community.* Arch Cardiovasc Dis, 2018. **111**(2): p. 126-139.
384. Chen, C.W., M.H. Sprys, A.C. Gaffey, J.J. Chung, K.B. Margulies, M.A. Acker, et al., *Low ejection fraction in donor hearts is not directly associated with increased recipient mortality.* J Heart Lung Transplant, 2017. **36**(6): p. 611-615.
385. Maack, C., T. Eschenhagen, N. Hamdani, F.R. Heinzel, A.R. Lyon, D.J. Manstein, et al., *Treatments targeting inotropy.* Eur Heart J, 2018.
386. See Hoe, L.E., N. Bartnikowski, M.A. Wells, J.Y. Suen, and J.F. Fraser, *Hurdles to Cardioprotection in the Critically Ill.* Int J Mol Sci, 2019. **20**(15).
387. Perjés, Á., A.M. Kubin, A. Kónyi, S. Szabados, A. Cziráki, R. Skoumal, et al., *Physiological regulation of cardiac contractility by endogenous reactive oxygen species.* Acta Physiologica, 2012: p. n/a-n/a.
388. Hekimi, S., Y. Wang, and A. Noe, *Mitochondrial ROS and the Effectors of the Intrinsic Apoptotic Pathway in Aging Cells: The Discerning Killers!* Front Genet, 2016. **7**: p. 161.
389. Antonucci, S., J.F. Mulvey, N. Burger, M. Di Sante, A.R. Hall, E.C. Hinchy, et al., *Selective mitochondrial superoxide generation in vivo is cardioprotective through hormesis.* Free Radic Biol Med, 2019. **134**: p. 678-687.
390. Shemie, S.D., C. Simpson, J. Blackmer, S. MacDonald, S. Dhanani, S. Torrance, et al., *Ethics Guide Recommendations for Organ-Donation-Focused Physicians: Endorsed by the Canadian Medical Association.* Transplantation, 2017. **101**(5S Suppl 1): p. S41-S47.
391. MacDonald, S.I. and S.D. Shemie, *Ethical Challenges and the Donation Physician Specialist: A Scoping Review.* Transplantation, 2017. **101**(5S Suppl 1): p. S27-S40.
392. Littlejohns S., Bontoft H., Littlejohns P., Richardson J., and Robertson A., *Legal and ethical implications of NICE guidance aimed at optimising organ transplantation after circulatory death.* Clinical Medicine, 2013. **13**(4): p. 340-343.
393. Barac, Y.D., O.K. Jawitz, J. Klapper, J. Schroder, M.A. Daneshmand, C. Patel, et al., *Heart Transplantation Survival and the Use of Traumatically Brain-Injured Donors: UNOS Registry Propensity-Matched Analysis.* J Am Heart Assoc, 2019. **8**(17): p. e012894.
394. Salie, R., J.A. Moolman, and A. Lochner, *The role of beta-adrenergic receptors in the cardioprotective effects of beta-preconditioning (betaPC).* Cardiovasc Drugs Ther, 2011. **25**(1): p. 31-46.
395. Beiras-Fernandez, A., F. Kur, I. Kaczmarek, P. Frisch, M. Weis, B. Reichart, et al., *Levosimendan for primary graft failure after heart transplantation: a 3-year follow-up.* Transplant Proc, 2011. **43**(6): p. 2260-2.
396. Dare, A.J., A. Logan, and K. Saeb-Parsy, *The mitochondria-targeted anti-oxidant MitoQ decreases ischemia-reperfusion injury in a murine syngeneic heart transplant model.* The Journal of Heart Lung Transplantation, 2015. **34**(11): p. 1471-1480.
397. Kaza, A.K., I. Wamala, I. Friehs, J.D. Kuebler, R.H. Rathod, I. Berra, et al., *Myocardial rescue with autologous mitochondrial transplantation in a porcine model of ischemia/reperfusion.* J Thorac Cardiovasc Surg, 2017. **153**(4): p. 934-943.

398. Frye, C.C., A.I. Bery, D. Kreisel, and H.S. Kulkarni, *Sterile inflammation in thoracic transplantation.* Cell Mol Life Sci, 2021. **78**(2): p. 581-601.
399. Ferrandi, M., P. Barassi, F. Tadini-Buoninsegni, G. Bartolommei, I. Molinari, M.G. Tripodi, et al., *Istaroxime stimulates SERCA2a and accelerates calcium cycling in heart failure by relieving phospholamban inhibition.* Br J Pharmacol, 2013. **169**(8): p. 1849-61.
400. Aditya, S. and A. Rattan, *Istaroxime: A rising star in acute heart failure.* J Pharmacol Pharmacother, 2012. **3**(4): p. 353-5.
401. Fu, X., A. Segiser, T.P. Carrel, H.T. Tevaearai Stahel, and H. Most, *Rat Heterotopic Heart Transplantation Model to Investigate Unloading-Induced Myocardial Remodeling.* Front Cardiovasc Med, 2016. **3**: p. 34.
402. Fernando, S.M., D. Qureshi, P. Tanuseputro, E. Fan, L. Munshi, B. Rochwerg, et al., *Mortality and costs following extracorporeal membrane oxygenation in critically ill adults: a population-based cohort study.* Intensive Care Med, 2019. **45**(11): p. 1580-1589.
403. *Australian Bureau of Statistics 2019, Causes of Death 2018, cat. no. 3303.0.* September Ischaemic heart disease or Coronary Heart Disease accounted for the second highest number of years of potential life lost (68,532). It has both the highest number of deaths and the highest number of premature deaths (more than 6,000) 2018.
404. *Australian Bureau of Statistics 2018, National Health Survey 2017-18, Data customised using TableBuilder 3 Australian Bureau of Statistics 2019, Causes of Death 2018, cat. no. 3303.0.* September 4 Australian Institute of Health and Welfare 2019, National Hospital Morbidity Database (NHMD), 2018